Thermal Properties and Depth Profile Studies on Polymer-Polymer-Solvent Coatings

Ph.D. Thesis

Submitted in the partial fulfillment of the requirement for the Degree of

DOCTOR OF PHILOSOPHY

by

JYOTI SHARMA

(Registration No. 901609005)

Under the supervision of

Dr. Raj Kumar Arya
Associate Professor
Department of Chemical Engineering
Dr. B.R. Ambedkar NIT
Jalandhar

Dr. Sanjeev Kumar Ahuja
Associate Professor
Department of Chemical Engineering
Thapar Institute of Engineering &Technology
Patiala

SCHOOL OF CHEMISTRY & BIOCHEMISTRY
THAPAR INSTITUTE OF ENGINEERING & TECHNOLOGY
PATIALA, PUNJAB-147004, INDIA
JANUARY 2020

Dedicated to

My Parents (Shri. Durga Dutt Sharma &

Smt. Meena Dutt Sharma)

Certificate

This is to certify that the thesis entitled "**Thermal Properties and Depth Profile Studies on Polymer-Polymer-Solvent Coatings**" being submitted by Ms. Jyoti Sharma (Regn No. 901609005) in fulfillment of the requirement for the award of the Degree of Doctor of Philosophy in the School of Chemistry and Biochemistry, Thapar Institute of Engineering & Technology, Patiala, is a record of candidate's own independent and original research work carried out by her under our supervision and guidance. The material embodied in the thesis has not been submitted in part or full to any other University or Institute for the award of any degree.

22-01-2020

Dr. Raj Kumar Arya

Associate Professor
Department of Chemical Engineering
Dr. B.R. Ambedkar NIT,
Jalandhar-144011 Punjab, India

22/01/2020

Dr. Sanjeev Kumar Ahuja

Associate Professor
Department of Chemical Engineering
T.I.E.T Patiala-147004
Punjab, India

Declaration

I, hereby, declare that the present work in the thesis entitled "**Thermal Properties and Depth Profile Studies on Polymer-Polymer-Solvent Coatings**" in the fulfillment of the requirement for the award of the Degree of Doctor of Philosophy in the School of Chemistry and Biochemistry, Thapar Institute of Engineering & Technology, Patiala, is authentic record of my own work carried out under the supervision of Dr. Raj Kumar Arya (Associate Professor, Department of Chemical Engineering, Dr. B.R. Ambedkar National Institute of Technology, Jalandhar, India) and Dr. Sanjeev Kumar Ahuja (Associate Professor, Department of Chemical Engineering, Thapar Institute of Engineering & Technology, Patiala, India). The material embodied in the thesis has not been submitted in part or full to any other University or Institute for the award of any degree in India or Abroad.

January 22, 2020

Sharma

Jyoti Sharma

(Regn No. 901609005)

Acknowledgements

It is great opportunity to me to thank my supervisors Dr. Raj Kumar Arya and Dr. Sanjeev Kumar Ahuja for their invaluable guidance, consistent encouragement, support, and help in each and every step of my Ph.D. work. They have treated me like their own child and guided me so well in the professional as well as in the personal field. They have been always approachable to clarify my doubts despite their busy schedules. It has been a great experience to work under their guidance, and to learn from their research expertise.

I would like to thank to my mother, Mrs. Meena Dutt Sharma, father, Mr. Durga Dutt Sharma, and brother, Mr. Vishal Sharma for their love and support in my life and especially during this time period. They have been there for me and I am thankful for everything they have helped me to achieve.

I gratefully acknowledge the SERB-DST, New Delhi, India, for research grant (EEQ/2016/0000165). I am also thankful to my doctoral committee members Prof. (Dr) Bonamali Pal, Prof. (Dr) Satnam Singh, and Dr. Puneet Sharma for their encouragement, constructive criticism and inspirations. I would like to extend my thanks to SAI Labs, Thapar Institute of Engineering & Technology, Patiala, for SEM analysis, and SMITA Lab IIT, Delhi, and IIT, Bombay for conducting confocal Raman spectroscopy analysis.

I would like to thank Mr. Aadil Bathla, who helped me a lot in analyzing the SEM images and other important softwares. I learned a lot from him through our scholarly interactions. I also want to extend my thanks to Ms. Vanshita Goel. I am so thankful to have all these people in my life. Addition to this, I am thankful to the persons who knowingly and unknowingly helped me during the successful completion of this work.

Sharma

January 22, 2020

Jyoti Sharma

(901609005)

Abstract

The designing of the multi-polymer-solvent coatings is done by single thick layer and layer-by-layer techniques in order to minimize the residual solvent. The average concentrations of the polymers and solvent, change in coating thickness with time have been calculated from the gravimetric weight loss data. In the case of poly(styrene)-(poly(methyl methacrylate)-tetrahydrofuran (PS-PMMA-THF) and poly(styrene)-poly(methyl methacrylate)-toluene system, (PS-PMMA-TOL) the doubling the poly(styrene) mass fraction does not change the mass transfer mechanism within these coatings. However, doubling the poly(methyl methacrylate) mass fraction changes the mass transfer mechanism very significantly which leads to very slow diffusion process within these coatings.

In case of poly(styrene)- poly(methyl methacrylate)-ethylbenzene (PS-PMMA-EB), doubling of both the polymer mass fraction does not change the mass transfer mechanism within these coatings. However, the drying time is much higher as compared to the other two systems, that is poly(styrene)- poly(methyl methacrylate)-tetrahydrofuran, and poly(styrene)- poly(methyl methacrylate)-toluene coatings.

The effect of change of polymer and solvent has been studied. PMMA has been replaced by amorphous PEG to study the effect of its mass fraction on the residual solvent and morphology of the coatings. The results indicate that the single thick layer technique should be used to minimize the residual solvent in the coatings studied herein. However, these coatings are taking longer time to dry as compared to the layer-by-layer technique. Hence, higher energy demands for the drying operation.

The morphological studies of poly(styrene)-poly(ethylene glycol)-chlorobenzene films have been performed using scanning electron microscopy. The average diameter of the holes present in the coatings decreased from 7.68 mm to 3.74 mm with the increase in the polymer content from 5% to 10%. The solvent played a major role in forming ordered porous polymer films. Asymmetric membrane formed at different concentrations of the ternary system. The effects of various parameters

like polymer mass fraction, initial film thickness, and technique of application on the pore size and uniformity have been studied. Membrane type coating is observed at different concentrations of the ternary system.

The effect of molecular weight on the residual solvent, change in coating thickness, and polymer and solvent concentration of the coatings have been investigated in the case PS-PMMA-EB coatings. The molecular weight of poly(styrene) has a significant effect on the residual solvent as compared to the molecular weight of poly(methyl methacrylate). The residual solvent and coating thickness are lowest in the case of higher molecular weight of PS.

The effect of molecular weight of polymers on the glass transition temperature and morphological behavior of the coatings have been investigated over a broad range of molecular weights of polystyrene (35000, 192000, 280000 and 350000), and poly(methyl methacrylate) (120000, 350000 and 996000) in ethylbenzene. The prepared coating are analyzed by their glass transition temperatures (T_g) using differential scanning calorimetry, and their morphological behavior using scanning electron microscopy. The molecular weight of PS has shown significant effect on the glass transition temperature, and coating morphology.

The concentrations of the solvent and polymer have been measured inside dried poly(styrene)-poly(methyl methacrylate)- tetrahydrofuran coatings using confocal laser Raman spectroscopy. The PS-THF and PMMA-THF binary calibration plots have been used to determine the concentrations of ternary coatings. This study also substantiates that the concentrations of PS, PMMA, and THF change in the same manner as has been computed from their gravimetric studies. The distribution of the polymers is not in equal proportion from the substrate to the top. The percentage of PS is higher on the top as compared to PMMA.

Table of Contents

List of Figures

List of Tables

Nomenclature

$\frac{dx}{dt}$	The slope of moisture content vs. time graph at a particular time.
$\frac{\hat{V}_{FH}}{\gamma}$	Free-volume parameter.
χ_{ij}	Interaction parameter species i with respect to j
ϕ_i	Volume fraction of component i
V_i	Molar volume of the polymer i
ϕ_i	Volume fraction of the component i
k	Boltzmann constant
$g(\phi_i)$	free energy of homogeneous solution
ϕ_i	Volume fraction of component i
k_i	Flexibility constant for the polymer
l	Length of monomer unit
v_i	Volume occupied by a molecule of type i
m	Degree of polymerization
N_i	Degree of polymerization of polymer i
$\bar{x}$	Mean of diameter of the holes in the coating,
ϕ_i	Volume fraction of species i
T_g^{bulk}	Glass transition temperature of the bulk polymer
A	Area of drying surface
c	Concentration (g/cm^3)
D	Mutual diffusion coefficient (cm^2/s)
d	Depth of focus within the sample from surface of the sample
D_{0i}	Pre-exponential factor
m	Mass
M_p	Molecular weight of monomer
M_w	Molecular weight

N	Rate of drying
n	Number of holes
N_A	Avogadro's number
NA	Numerical aperture of the objective used
s	Standard deviation
t	Time (s)
V^*_j	Specific critical hole-free volume of a component of *j*
W_s:	Weight of solids
x_i	Diameter of the one hole
z	Distance (cm)
γ	Overlap factor
ξ	The ratio of molar volumes of the solvent and the polymer jumping units
CLB	Chlorobenzene
DSC	Differntial Scanning Calorimetry
EB	Ethylbenzene
PEG	Poly(ethylene glycol)
PMMA	Poly(methyl methacrylate)
PS	Poly(styrene)
SEM	Scanning Electron Microscopy
THF	Tetrahydrofuran
TOL	Toluene

List of Publications

1. **Jyoti Sharma**, Sanjeev Ahuja, Raj Kumar Arya, 'Depth profile study of poly(styrene) – poly(methyl methacrylate) – tetrahydrofuran Coatings, Progress in Organic coatings, 134 (2019) 297-302.
2. **Jyoti Sharma**, Sanjeev Ahuja, Raj Kumar Arya, 'Effect of molecular weight on residual solvent and other parameters in polymer-polymer-solvent coatings: Poly(Styrene)-poly(methyl methacrylate)-ethylbenzene system', Progress in Organic coatings, 134 (2019) 119–125
3. **Jyoti Sharma**, Sanjeev Ahuja, Raj Kumar Arya, 2019, "Effect of Molecular Weight on Morphology and Thermal Properties of Poly(Styrene)-Poly(Methyl Methacrylate)-Ethylbenzene Coatings", Progress in Organic Coatings, 132 (2019) 468-474.
4. **Jyoti Sharma**, Sanjeev Ahuja and Raj Kumar Arya, Experimental designing of polymer− polymer—solvent coatings: Poly (styrene)—poly (ethylene glycol)—chlorobenzene coatings, Progress in Organic Coatings, 128 (2019) 181-195.
5. **Jyoti Sharma**, Sanjeev Ahuja and Raj Kumar Arya, Drying induced phase separation in poly (styrene)–poly (ethylene glycol)–chlorobenzene system, Journal of Porous Materials, (2018) 1-15.
6. **Jyoti Sharma**, Raj Kumar Arya, Sanjeev Ahuja and Chitresh Kumar Bhargava, Residual solvent study in polymer− polymer—solvent coatings: Poly (styrene)—poly (methyl methacrylate)—tetrahydrofuran coatings, Progress in Organic Coatings, 113 (2017) 200-206.
7. **Jyoti Sharma**, Kshitij Tewari, and Raj Kumar Arya, Free volume theory of diffusion in polymer(s) – solvent(s) system – a review, Progress in Organic Coatings, 111 (2017) 83-92.
8. Anubhav Prashar, **Jyoti Sharma**, Sanjeev Ahuja, Avinash Chandra, Raj Kumar Arya, 2019, "Quaternary Polymeric Coating An Alternative to Minimize the Use of Single Solvent: Poly(methyl methacrylate) – Ethylbenzene – Toluene – Acetone System", Progress in Organic Coatings, Accepted on 12 March 2019.

9. Anubhav Parashar, **Jyoti Sharma**, Sanjeev Ahuja and Raj Kumar Arya, Quaternary polymeric coating as an alternative to minimize the use of costly solvents in binary coatings, Progress in Organic Coatings, 127 (2019) 319-329.
10. Ishita Sharma, **Jyoti Sharma**, Sanjeev Ahuja, and Raj Kumar Arya, 2018, Optimization of sodium dodecyl sulphate loading in poly (vinyl alcohol)-water coatings, Progress in Organic Coatings, 127 (2019) 401-407.
11. Daisy Sharma, **Jyoti Sharma**, Raj Kumar Arya, Sanjeev Ahuja and Shekhar Agnihotri, Surfactant enhanced drying of waterbased poly(vinyl alcohol) coatings, Progress in Organic Coatings, 125 (2018) 443-452.
12. Aman Pathania, **Jyoti Sharma**, Raj Kumar Arya, and Sanjeev Ahuja, Effect of crosslinked polymer content on drying of binary polymer—solvent coatings, Progress in Organic Coatings, 114 (2018) 78–89.
13. Harleen Kaur, **Jyoti Sharma**, Divyansh Jindal, Raj Kumar Arya, Sanjeev Ahuja and Shashi Bhushan Arya, Crosslinked polymer doped binary coatings for corrosion protection, Progress in Organic Coatings, 125 (2018) 32–39.

Conferences and Workshops

- Presented paper titled ‘Residual solvent study in polymer− polymer—solvent coatings: poly (styrene)—poly (ethylene glycol)—chlorobenzene coatings’ in 8TH PACT National workshop, HBTU Kanpur, 2018.
- Participated in joint workshop on ‘Recent advancement in thermal analysis techniques (DSC, TGA, DTA, STA, TMA), 15th September 2018 at IIT Delhi.
- Paper presented on ‘Gravimetric studies on the effect of molecular weight on poly(styrene)-poly(methyl methacrylate)-ethylbenzene coatings’ in 71st annual session of Indian Chemical Engineering Congress-CHEMCON 2018 at NIT Jalandhar as oral presentation.

Chapter 1

Introduction

In this era, tremendous advancements have been made in the field of polymer engineering and technology that have enhanced the versatility of the polymeric materials ranging from household to industrial applications. Polymer films find applications like magnetic tapes, storage devices, semiconductors, micro devices, optical fibers, membranes and filters, multiphase gels, functional films, drug release and encapsulation, biomedical films, protective polymeric films, and decorative films [1-10].

Coatings are prepared using polymers and are applied using thinners. Different combinations of thinners are used to dilute the polymeric solution to get a smooth and uniform coating. These coatings can be made from one polymer, or more than one polymer dissolved in one or more solvents. Solvents must be cheap, environmentally friendly and capable for easy recovery from the coating without involving anomalies such as cracks, wrinkles, blisters etc. [11]. The production anomalies can be controlled by minimizing the residual solvent.

Controlling the drying rate is useful in reducing the residual solvent specifically for food packaging films, and also to achieve good mechanical properties to get defect free coating, the residual solvent in the polymeric coating can be mathematically minimized by the use of a proper diffusion model and then by implementing the obtained operating condition in the production of the film. The diffusion of a solvent in the polymeric matrix is studied using free volume theory. Polymeric films can be prepared by several techniques such as solution casting [12], spin coating [13, 14], drop casting [15], dip casting [16] and film casting [17]. These techniques are described in the following section.

1.1 Film Preparation Methods

a) Solution Casting Method

It is the basic and simplest coating technique for polymeric films. Polymeric resins are immersed in volatile solvent(s) to get a homogeneous solution having low viscosity. The solution may either be spread on a substrate or cast into a mold. The substrate can be static or mobile in a batch or continuous process, respectively. This type of coating is used for making medical and optical films, and sheet forming for electronic application. This technique is highly useful in getting uniform film with high optical clarity [12].

b) Spin Coating Method

Spin coating technique also helps in producing thin uniform films. A drop of polymer solution is placed on the top of the substrate [13, 14]. The solution is subjected a centrifugal force with the rotation of the substrate. The thickness of the film reduces with time. In this technique, the drying is faster than the solution casting method. Gas separation membranes and photovoltaic field effect transistors are produced using this technique. A very high amount of solution is wasted due to the centrifugal action. The coating thickness in this technique is not uniform. The coatings prepared by this technique are thicker at the edges and thinner at the centre.

c) Drop Casting Method

This method is used for preparing small and accurate coatings and very small amount of solution is used. In this method, solution is poured on the substrate and allowed to dry without any spreading. It leads to inconsistent drying and non uniform film, which are thinner at the edges but thicker near the center. It is used for making expensive polymeric semiconductors that have poor solubility [15].

d) Dip Casting Method

These are mainly used for anti corrosive coatings. The substrate is immersed into the solution and then drawn out at certain speed to obtain a uniform coating. The thickness of the film is more at the bottom than at the top. It is used for tool handles, cleaning rubbers, balloons, and plastic caps.

e) Film Casting Method

This method is implemented to get thin sheets from viscous melts. The material is extruded and sent to a rotating chill roll, where it gets cooled and solidified. Separators for Li-ion batteries and optical devices for flat panel displays are prepared using this method [17].

1.2 Drying of Coatings

Drying is a unit operation to remove solvent from the wet coating. The coatings are wet when they are casted, and are dried to get a final product. Coatings may either be dried at ordinary conditions or subjected to intense drying conditions like heating or impinging the jet of air. Drying is a complex phenomenon involving both heat and mass transfer.

During the drying, physical and chemical transformation may occur, which causes changes in the product quality. This affects the heat and mass transfer mechanisms. Shrinkage, crystallization, puffing, skinning, and glass transition may accompany the process. Chemical transformations in odor, texture, color, or other properties of solid may accompany drying [18].

Some salient features of the drying operation are as follows:

a. Product size can range from a few microns to tens of centimeters.
b. Heat may be transferred by different modes.
c. Drying times can be from seconds to months.
d. Production speed can be required up to 1000m/s.
e. Production capacity has a wide variation.
f. Product porosity may vary over a wide range.
g. Drying temperatures range from below the triple point to above the critical point of the liquid.

Industrial coatings are dried in dryers. Different drying conditions like the temperature on top and bottom and air flows are maintained in different zones of dryers to get a desired coating without any defects. Over 85% of the industrial dryers are of the convective type with hot air or direct combustion gases as the drying medium. In multi zone dryers, the coatings are dried in a continuous manner, wherein the top and bottom air flow rates, temperature and residence time are varied to achieve the minimum residual solvent.

1.2.1 Importance of drying

The liquid content of a dried substance varies from product to product. The product that contains no liquid is known as bone dry. In general, dryness is a relative term, and drying means merely reducing the moisture content from an initial value to some acceptable final value.

Several reasons for carrying out the drying operation are following:

a. For reducing transportation cost.
b. For purifying product especially in crystallization to remove solvent adhering through the crystal.
c. Making the material more suitable for handling and storage.
d. For preventing corrosion, arising due to the presence of moisture.
e. For preparing films for different applications like protective and decorative purposes.

1.2.2 Drying rate

The drying rate is calculated from the slope of the moisture content vs. time data. The moisture content is expressed as the amount of moisture per unit weight (dry or wet). The typical drying rate curve as shown in Figure 1.1 will have a warming up period, a constant rate period, and a falling rate period. From point (A, B) to C is the warming up period, where the temperature of the solid is equal to the temperature of the gas stream, and the drying rate is increasing. From point C to D is the constant rate period, where moisture evaporates from the surface of the solid into the surrounding atmosphere and continues till a particular value of moisture content. This moisture content is known as critical moisture content after that the drying rate starts falling. The falling rate period is shown from point D to E. From point E to F is also the part of falling rate period but in this the inner moisture is also coming out of the surface and evaporates and saturation occurs at this point and is known as equilibrium moisture content. The moisture content that corresponds to point C is known as critical moisture content. The moisture content that corresponds to point E is the equilibrium moisture content. The rate of drying is given by

$$N = \frac{-W_s}{A} \times \frac{dx}{dt} \tag{1.1}$$

where N: rate of drying, W_s: weight of solids, A: area of drying surface, $\frac{dx}{dt}$: the slope of moisture content vs. time graph at a particular time.

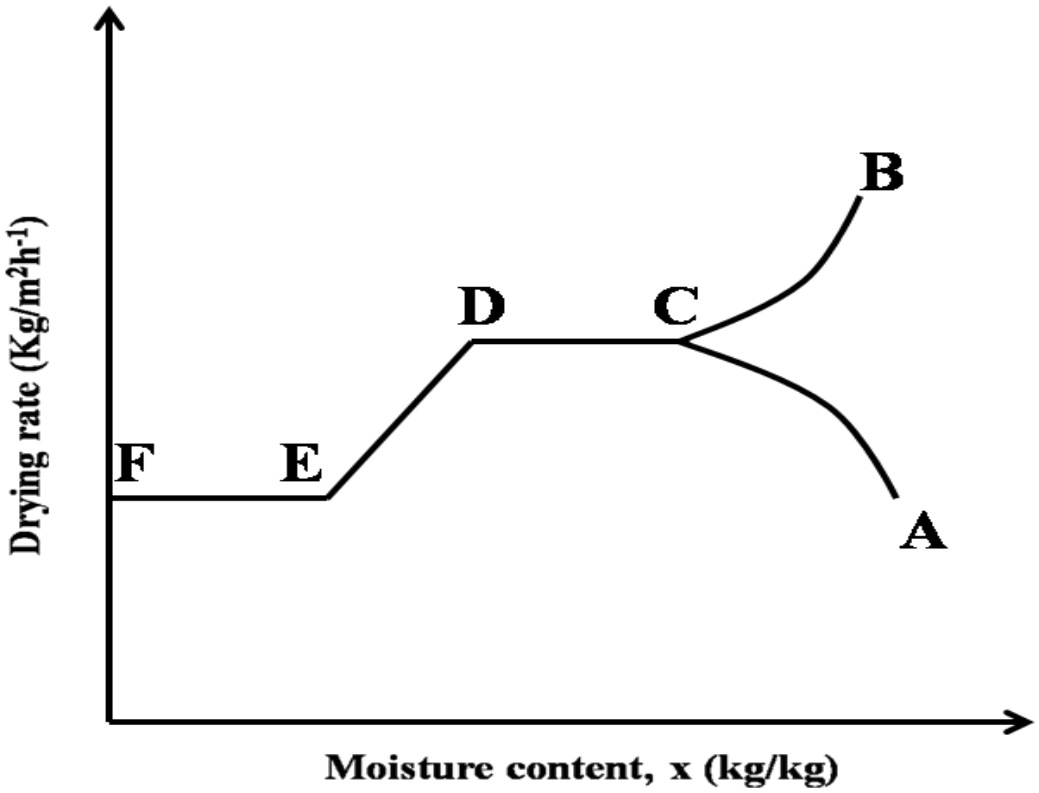

Figure 1.1: Drying rate vs. moisture content.

1.3 Diffusion in Polymeric Coatings

The removal of moisture from the polymeric coating is governed by the diffusion of solvent inside the coating. The transport phenomenon is controlled by the diffusion step. Transport of moisture within the solid may occur by liquid diffusion/vapor diffusion/Knudsen diffusion. In the liquid diffusion, the wet solid is at a temperature below the boiling point of the liquid. In the vapor diffusion, the liquid vaporizes within the material. In the knudsen diffusion, the drying takes place at very low temperatures and pressures.

The transport phenomenon of drying is generally governed by the Fick's first law of diffusion. According to this law, the flux of a paticular component at a location is equal to the diffusion coefficient times the concentration gradient. The rate of change of concentration with time is given by the Fick's second law of diffusion:

$$\frac{\partial c}{\partial t} = \frac{\partial}{\partial z}\left(D \frac{\partial c}{\partial z} \right) \tag{1.2}$$

where c: concentration (g/cm^3), D: mutual diffusion coefficient (cm^2/s), t: time (s), z: distance (cm).

The diffusion of penetrant in polymeric system is studies using free volume theory. Vrentas and Duda [19, 20] free volume theory is generally used to predict molecular diffusion in polymeric coatings. This theory is based on the availability of free volume within the coating. The self-diffusion coefficients are calculated using this theory. This theory is well-applicable for polymer – solvent coatings [11, 21-26], and the extension of this theory to polymer – solvent – solvent systems has also been reported [27, 28]. The self-diffusion coefficient in ternary polymeric system is given by:

$$D_i = D_{0i} \exp\left(-\frac{\left(\sum_{j=1}^{3} \omega_j \hat{V}_j^* \frac{\xi_{i3}}{\xi_{j3}} \right)}{\frac{\hat{V}_{FH}}{\gamma}} \right) \tag{1.3}$$

where V^*_j: specific critical hole-free volume of a component of j, ω_j: mass fraction of the component j, D_{0i}: pre-exponential factor, γ: overlap factor, ξ: the ratio of molar volumes of the solvent and the polymer jumping units, $\frac{\hat{V}_{FH}}{\gamma}$: free-volume parameter.

For polymer – solvent – solvent coatings, several models [29-32] have been developed using Bearman's friction factor theory [33], which relate the chemical potential to the self-diffusion coefficient. The real coatings are the solutions of more than one polymer. However, very less work has been done in the field of polymer – polymer – solvent coatings. Various models have been reported in the literature to predict chemical potential and free energy of polymer – polymer – solvent systems. These models can be used to predict the self – diffusion coefficient in polymer – polymer – solvent coatings, and, hence, the drying behavior of such coatings.

1.4 Confocal Raman Spectroscopy

The Raman spectroscopy is known to be a very useful tool for the study of small samples without any deformation of the samples. However, no resolution can be attained without the confocal arrangement in the Raman spectrometer because the light is collected equally from each plane in the sample. Due to its very good spatial resolution in lateral as well as optical axis of the microscope, the confocal Raman spectroscopy helps in various applications. Some of these applications are the study of thin layers that are buried in a matrix of another material, and multilayer foils or fiber composite materials. This also helps in the study of the properties of the material as a function of depth within the films. The ability to measure the concentration profiles within the coatings with a resolution of 1-2 μm is provided by the confocal arrangement attached to the Raman spectrometer [34].

1.5 Rationale of the Study

In the literature, plenty of data are available related to the drying of binary polymeric coatings, multicomponent polymeric coatings having one polymer and two solvents, and especially their residual solvent minimization, phase separation, designing of industrial dryers, etc. Vrentas and Duda free volume theory [19, 20] predicts the drying behavior of binary coatings with a high degree of accuracy [11, 21-23, 35]. For the ternary polymer – solvent – solvent coatings, several diffusion models are available to calculate the diffusion coefficient in polymer – solvent – solvent coatings [29-32] which are being tested with the experimental data [36].

However, there is no literature available regarding the residual solvent study, depth profiling of solvent and polymer during the course of drying, optimum drying parameter to reduce the residual solvent content, and glass transition temperature of the film in the area of polymer-polymer-solvent coatings.

This work envisages performing extensive experimental work to reduce the residual solvent content in polymer – polymer – solvent coatings, prepared using solution casting method. The depth profiling data is useful in magnetic devices,

storage devices, and optical devices, which motivates us to do the depth profiling of the coating using confocal Raman spectroscopy.

1.6 Objectives of the Present Work

The ultimate aim of the study is to minimize the residual solvent within the polymer – polymer – solvent coatings, study the thermal properties and coating composition. In most of the coating formulations, harmful organic solvents are being used. Proper designing will reduce the use of such solvents and will reduce the impact on the environment. In industrial units, the coatings are dried in the dryers for faster delivery of the finished product. Proper drying conditions reduce the energy consumption with better product quality of the finished product. Based on the literature survey, the following objectives are planned:

- Experimental design of polymer – polymer – solvent coatings to minimize the residual solvent.
- Thermal analysis of polymer – polymer – solvent coatings.
- Depth profile study of prepared coatings using confocal Raman spectroscopy.

1.7 Selection of Systems

The selection of polymer (1) –polymer (2) –solvent (1) is done based on the following two criteria:

- **Each system must be thermodynamically compatible in order to get homogeneous polymeric solutions**.

For the present study, PS-PMMA-THF, PS-PMMA-EB, PS-PMMA-TOL and PS-PEG-CLB systems are chosen. Solvent selection is being done based on solubility parameters as per the procedure develop by Hansen [37]. In this method, a spherical analysis was considered in which the center of sphere has values of δ_d, δ_p, δ_h of polymer. The values of δ_d, δ_p, δ_h of selected polymers and solvents are given in Table 1.1. δ_{dP}, δ_{pP}, and δ_{hP}, are the values of dispersion, polar, and hydrogen boding Hansen solubility parameters for polymer, and δ_{dS}, δ_{pS}, and δ_{hS}, are the values of dispersion, polar, and hydrogen boding solubility parameters for solvent.

The interaction radius for the polymer is defined as R_o as the radius of sphere. For good solvents, the distance between solvent and polymer is defined as R_a and must be less than R_o. The value of R_a can be calculated using following expression:

$$R_a = \sqrt{4 \times (\delta_{d_P} - \delta_{d_S})^2 + (\delta_{p_P} - \delta_{p_S})^2 + (\delta_{h_P} - \delta_{h_S})^2} \qquad (1.4)$$

The values of solubility parameters for selected polymers and solvents are given in Table 1.2. The values of R_o for poly(styrene),poly(methyl methacrylate) and poly(ethylene glycol) are 12.7**,** 8.96, and 18.38 [38, 39]. The calculated values of R_a and R_a/R_o are given in Table 2. All the selected polymer – solvent combinations come out to be miscible because ratio of R_a/R_o is less than 1 as per Hansen criteria.

Table 1.1: Solubility parameters of selected solvents and polymers.

S. No.	**Polymer/Solvent**	**Dispersion solubility, δ_d, MPa$^{1/2}$**	**Polar solubility, δ_p, MPa$^{1/2}$**	**Hydrogen bonding, δ_h, MPa$^{1/2}$**
1.	Poly(styrene)	21.3	5.7	4.3[37]
2.	Poly(methyl methacrylate)	17.7	6.7	6.2[37]
3.	Poly(ethylene glycol)	17.0	10.7	8.9 [40]
4.	Ethylbenzene	17.8	0.6	1.4[37]
5.	Toluene	18	1.4	2[37]
6.	Chlorobenzene	17.4	9.4	0 [41]
7.	Tetrahydrofuran	16.81	5.73	7.98 [42]

Table 1.2: The calculated values of interaction radius for different polymer – solvent systems.

S. No.	**Polymer – Solvent**	**R_a**	**R_a/R_0**
1.	Poly(styrene) – toluene	8.20	0.64
2.	Poly(styrene) – ethylbenzene	9.13	0.71
3.	Poly(styrene) – tetrahydrofuran	9.70	0.76
4.	Poly(styrene) – chlorobenzene	9.64	0.75
5.	Poly(methyl methacrylate) – toluene	6.55	0.73
6.	Poly(methyl methacrylate) – ethylbenzene	7.76	0.86
7.	Poly(methyl methacrylate) – tetrahydrofuran	2.69	0.30
8.	Poly(ethylene glycol)-chlorobenzene	9.02	0.49

- Each polymer and solvent must have at least one distinct characteristic Raman peak at different wave number in order to analyze the depth profiling data.

Based on the above two criteria the following four systems were selected for the present study.

i. Poly(styrene) (PS)–poly (methyl methacrylate) (PMMA)–tetrahydrofuran (THF),
ii. Poly(styrene) (PS)–poly (methyl methacrylate) (PMMA)-ethylbenzene (EB),
iii. Poly(styrene) (PS) –poly (methyl methacrylate) (PMMA)- toluene (TOL), and
iv. Poly(styrene) (PS) – poly(ethylene glycol) (PEG)- chlorobenzene (CLB).

Raman spectra of PS, PMMA, PEG, THF, EB, TOL, CLB and PS-PMMA-THF are given in Figure 1.2 to 1.9, respectively. As noted above, the characteristic peaks have been selected in such a way that they are not present in the other two components of the mixture. For example, in the case of PS-PMMA-THF system, the characteristic peak of PS, PMMA, and THF are at 1002.15 cm^{-1}, 812.545 cm^{-1}, and 914.113 cm^{-1}, respectively. The selected peaks are not overlapping with each other. Therefore, there ternary Raman spectra can be characterized using these peaks during depth profiling study. The selected Raman peaks of all the four selected systems are given in Table 1.1.

As described above, there are different methods of preparation of coatings such as solution casting [12], spin coating [13, 14], drop casting [15], dip casting [16] and film casting [17]. In the present study, the solution casting method is selected to prepare the polymeric coatings due to easy control of thickness at micron level. Figure 1.10 shows schematic of the solution casting technique and the procedure for conducting the experiments. Polymer – polymer – solvent solutions were made by dissolving the known amount of polymers and solvent in leach proof bottles. These solution bottles were manually shaken for several weeks to get a homogeneous polymer-solvent solution. Single thin films were prepared using these solutions by solution casting technique. A known amount of solution was transferred using micropipette into stainless steel circular sample holder having the depth of 2000 μm and diameter of 12.24 mm. The mass of film was recorded as a function of time by

means of Precisa analytical weighing balance having an accuracy of ± 0.0001g. The readings were taken until steady state was reached.

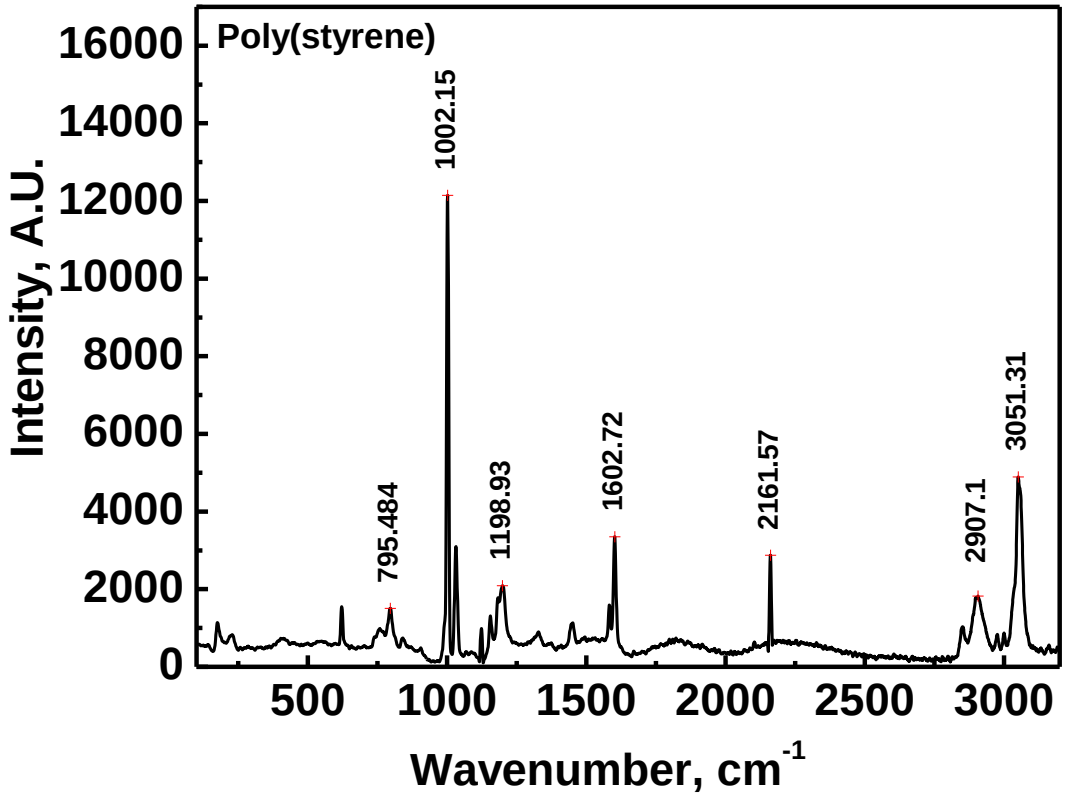

Figure 1.2: Raman spectra of poly(styrene).

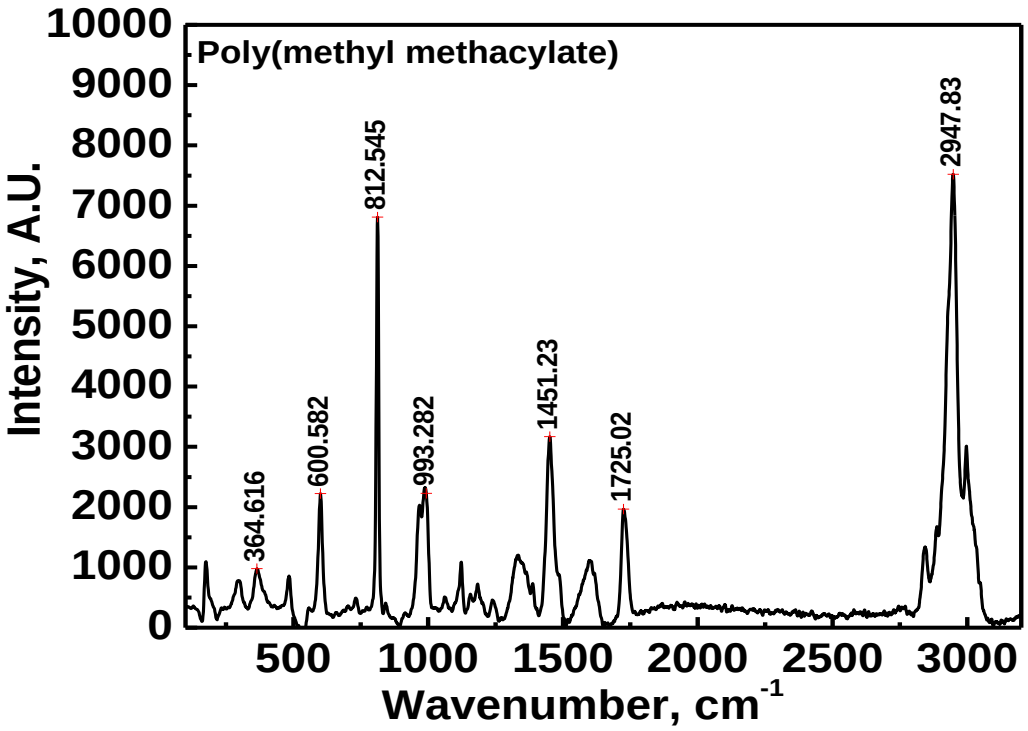

Figure 1.3: Raman spectra of poly (methyl methacrylate).

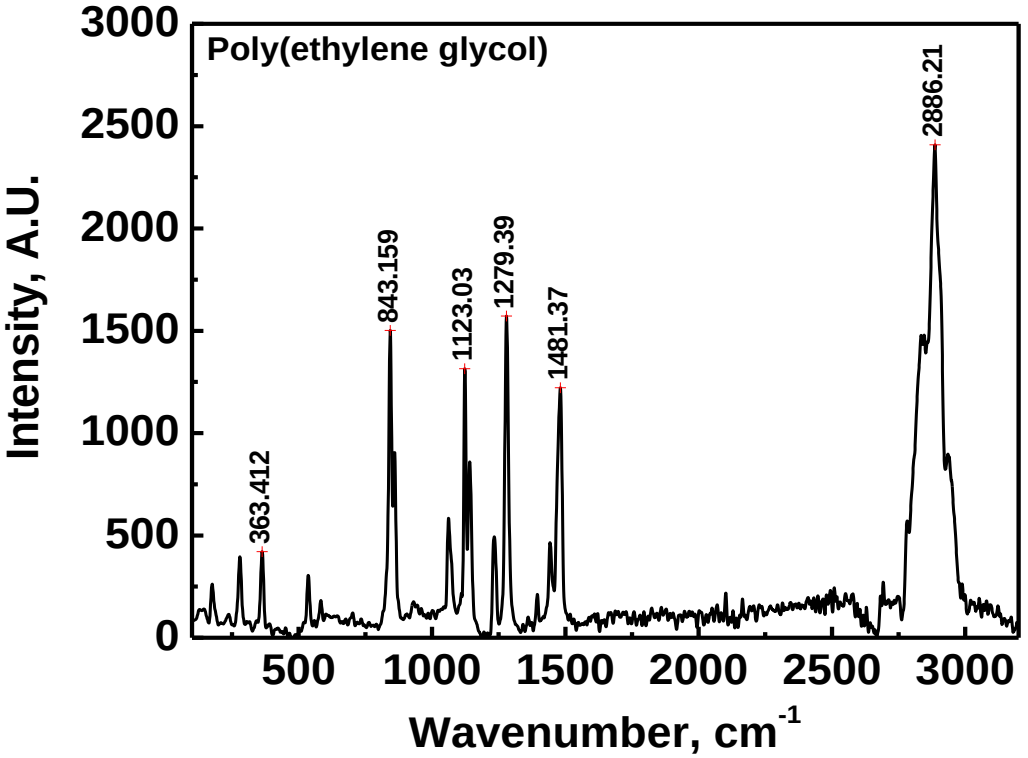

Figure 1.4: Raman spectra of poly (ethylene glycol).

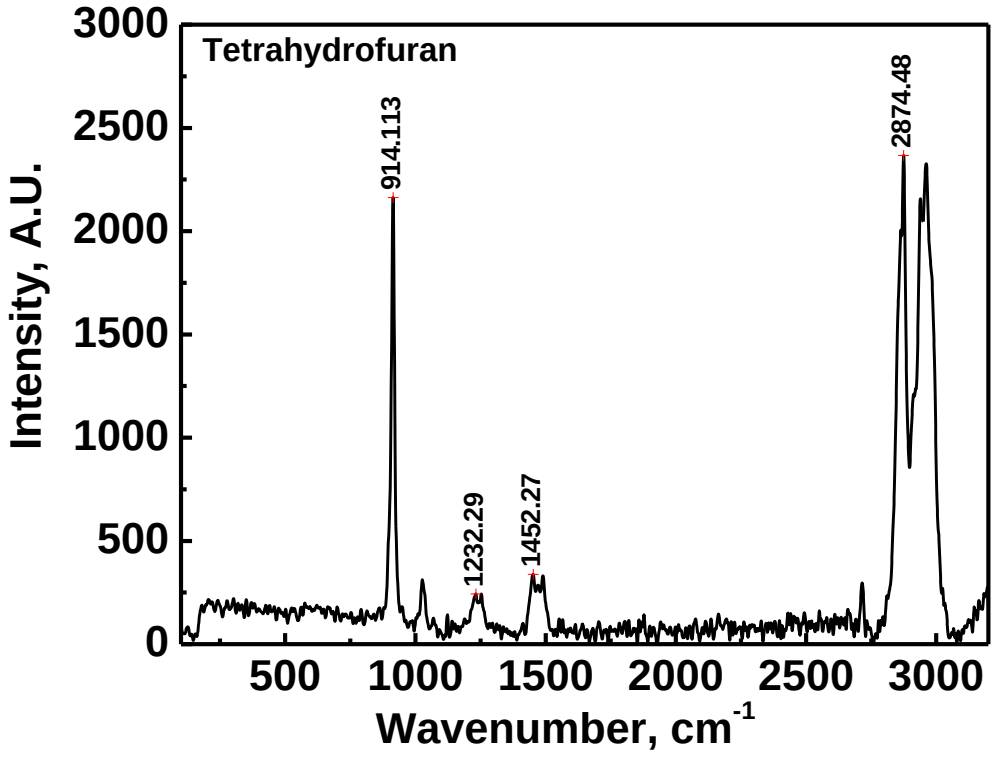

Figure 1.5: Raman spectra of tetrahydrofuran.

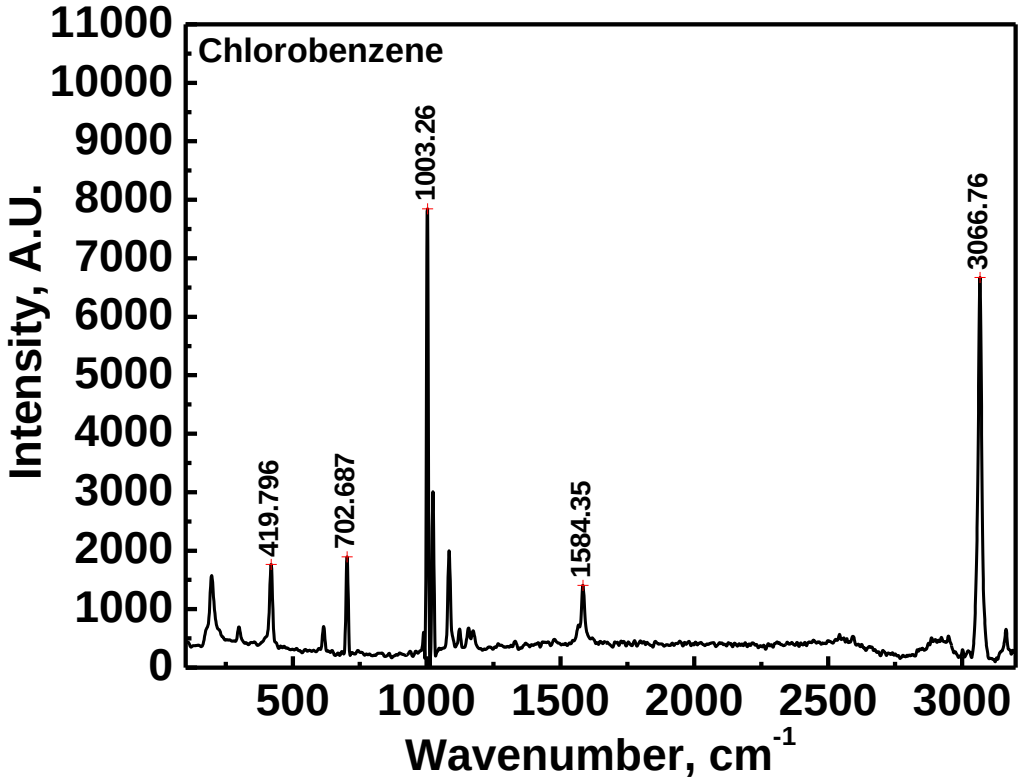

Figure 1.6: Raman spectra of chlorobenzene.

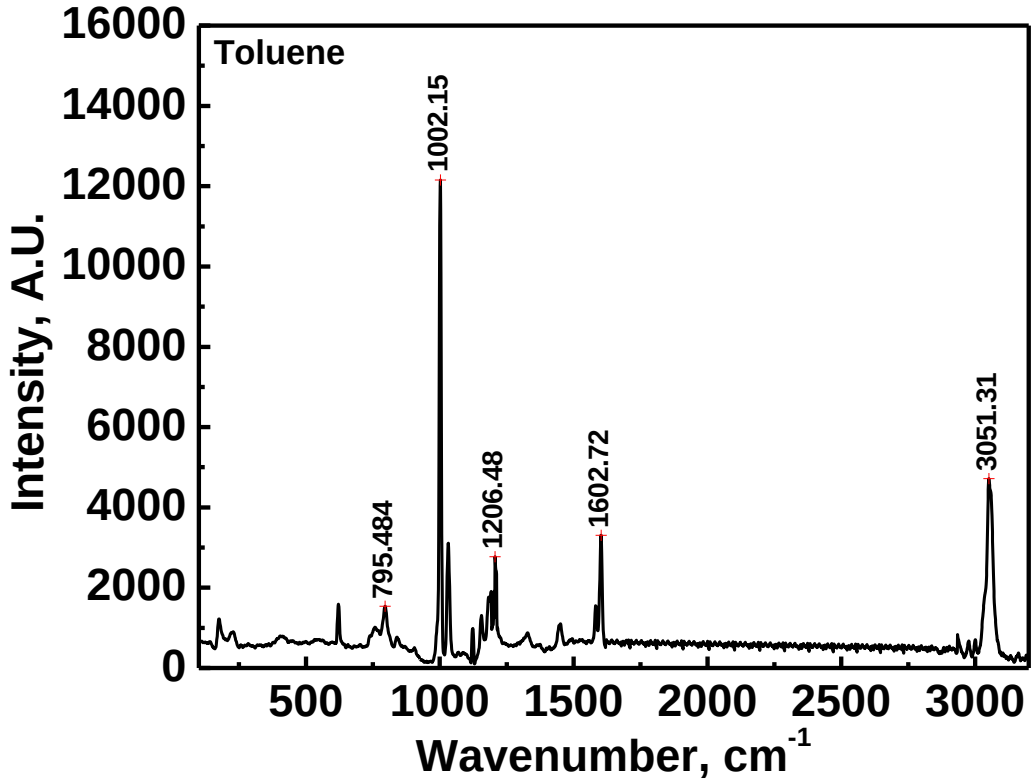

Figure 1.7: Raman spectra of Toluene.

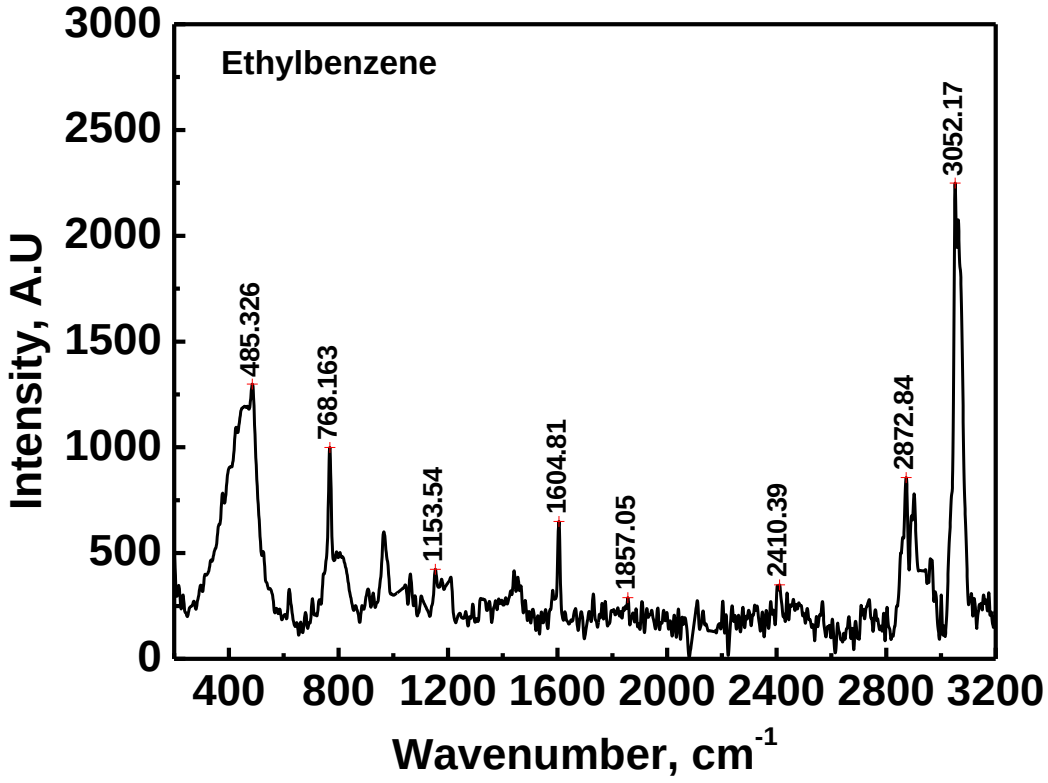

Figure 1.8: Raman spectra of ethylbenzene.

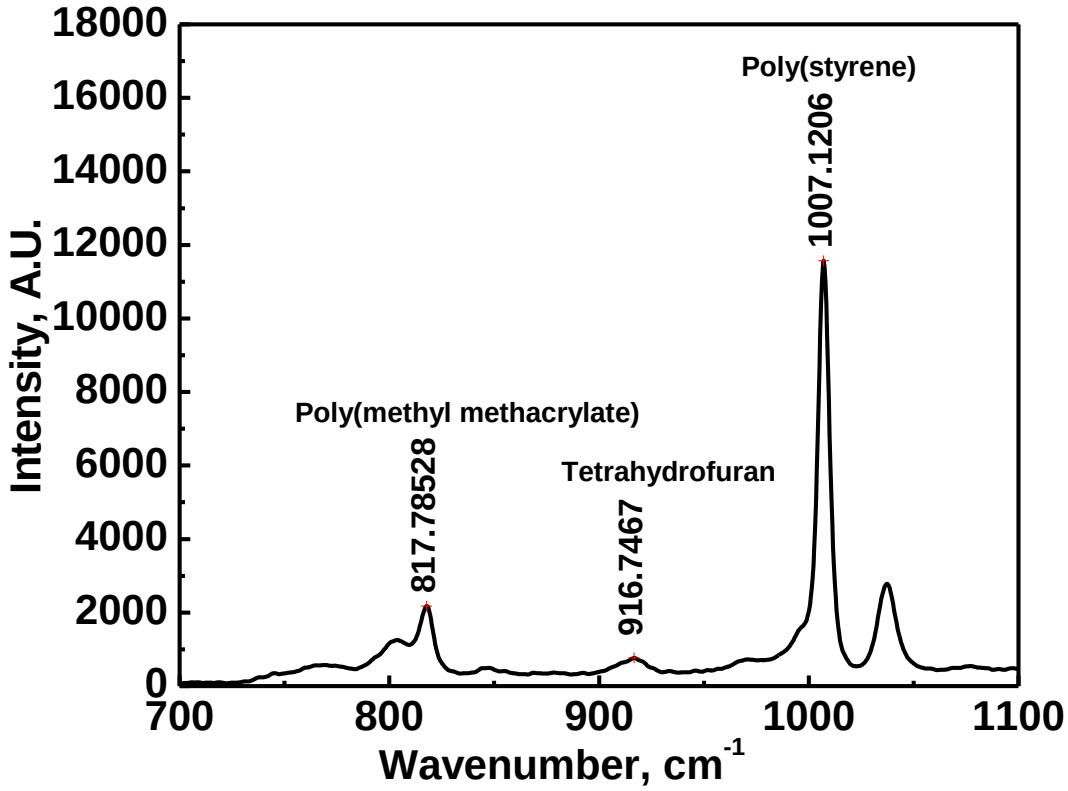

Figure 1.9: Raman spectra of PS-PMMA-THF system.

Table 1.3: Selected Raman characteristics peaks for various polymer (1) – polymer (2) – solvent systems.

System Name	Species	Raman peak, cm^{-1}
PS-PMMA-THF	PS	1002.15
	PMMA	812.545
	THF	914.113
PS-PMMA-EB	PS	1002.15
	PMMA	812.545
	EB	768.163
PS-PMMA-TOL	PS	2161.57
	PMMA	1725.02
	TOL	1206.48
PS-PEG-CLB	PS	1602.72
	PEG	843.159
	CLB	702.687

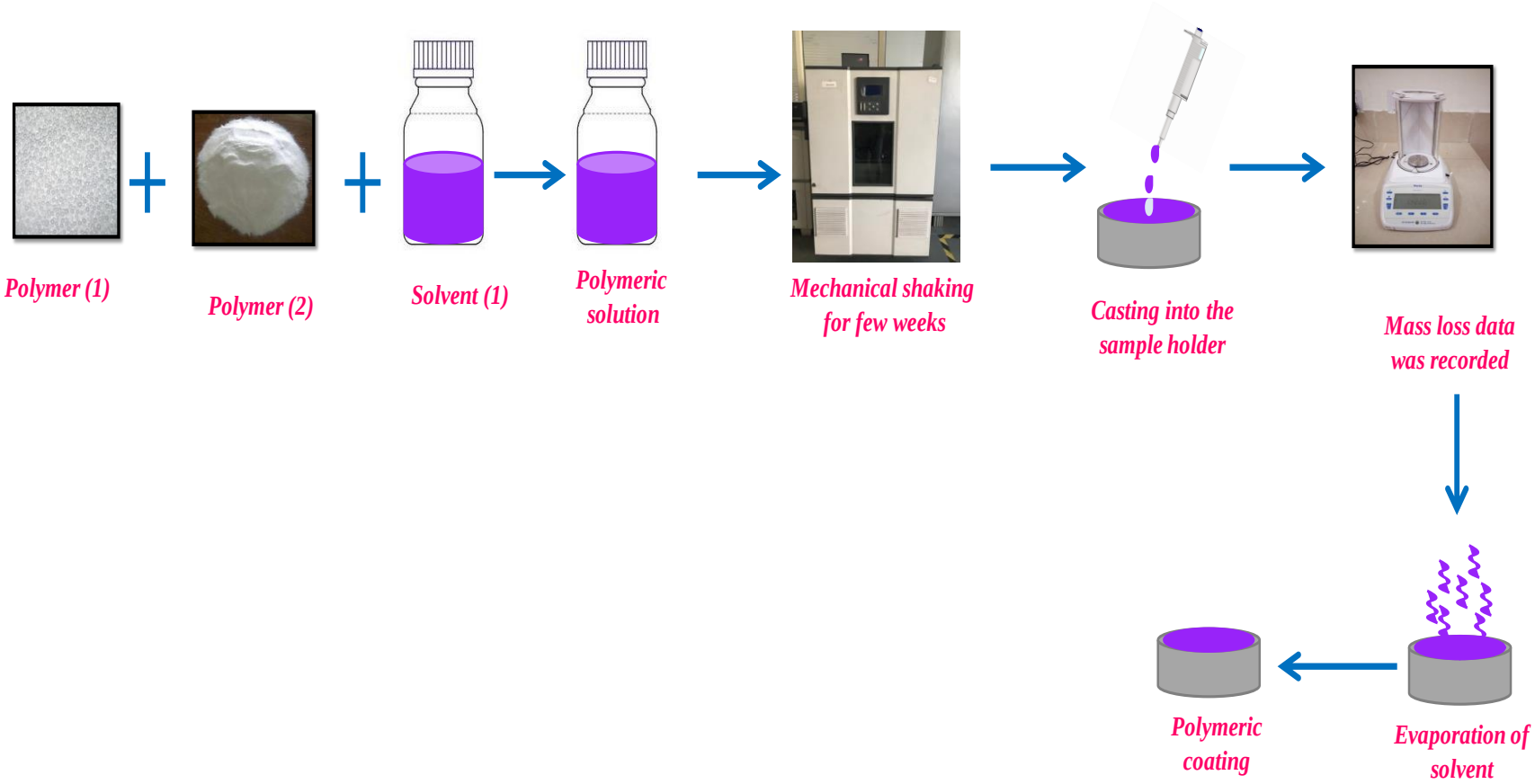

Figure 1.9: Schematic representation of the solution casting technique.

1.8 Organization of the Thesis

The thesis entitled '**Thermal Properties and Depth Profile Studies on Polymer-Polymer-Solvent Coatings**' is divided into the following seven chapters.

Chapter 1.

This chapter includes a brief introduction about the polymeric coatings and their applications and scope in different fields. Different types of coatings such as binary: polymer-solvent, and ternary: polymer (1)-polymer (2)-solvent or polymer-solvent (1)-solvent (2), and their methods of preparation are also highlighted in this part.

Chapter 2.

This chapter discusses the residual solvent study of the polymer-polymer-solvent system and is divided into three parts. In the residual solvent study of PS-PMMA-THF system, PS-PMMA-TOL system, and PS-PMMA-EB system are given in part A, B, and C respectively.

Chapter 3.

In this chapter, residual solvent study of PS-PEG-CLB system is carried out to see the effect of change of polymer and solvent. Here PMMA is replaced by PEG and CLB is selected as a solvent.

Chapter 4.

This chapter includes the morphological behavior of the prepared coating of the PS-PEG-CLB system using scanning electron microscopy (SEM). The coatings prepared from single thick layer and layer-by-layer techniques were analyzed by SEM. The outcomes from the drying induced phase separated coatings are discussed in this chapter.

Chapter 5.

This chapter gives a detailed discussion about another selected system that is poly(styrene)-poly(methyl methacrylate)-ethylbenzene. The gravimetric study on the effect of molecular weight of the polymers has been discussed in this chapter.

Chapter 6.

This chapter gives the detailed discussion about poly(styrene)-poly(methyl methacrylate)-ethylbenzene. The effect of molecular weight of both the polymers on the morphological behavior and the calorimetric study of the coatings are discussed in this chapter.

Chapter 7.

In this chapter, confocal Raman spectroscopy has been used to measure the depth dependent concentration profiles of polymers and solvent in dried PS-PMMA-THF coating. The Raman spectra at various positions from the substrate were collected till the surface and converted into concentration using binary calibration curves.

Chapter 8.

This chapter briefly concludes the results of the overall study of the polymer-polymer-solvent coatings of different selected systems.

References

[1] C. Panayiotou, J. Vera, Thermodynamics of polymer–polymer–solvent and block copolymer–solvent systems I. Experimental measurements, Polymer Journal, 16 (1984) 89-102.

[2] C. Panayiotou, J. Vera, Thermodynamics of Polymer–Polymer–Solvent and Block Copolymer–Solvent Systems II. Theoretical Treatment of Data with the Nonrandom New Flory Theory, Polymer Journal, 16 (1984) 103-112.

[3] A. Clark, Direct analysis of experimental tie line data (two polymer–one solvent systems) using Flory–Huggins theory, Carbohydrate Polymers, 42 (2000) 337-351.

[4] V.V. Krongauz, Diffusion in polymers dependence on crosslink density, Journal of Thermal Analysis And Calorimetry, 102 (2010) 435-445.

[5] T. Nguyen, X. Gu, M. Vanlandingham, E. Byrd, R. Ryntz, J.W. Martin, Degradation modes of crosslinked coatings exposed to photolytic environment, Journal of Coatings Technology and Research, 10 (2013) 1-14.

[6] S. Al Akhrass, R.-V. Ostaci, Y. Grohens, E. Drockenmuller, G. Reiter, Influence of progressive cross-linking on dewetting of polystyrene thin films, Langmuir, 24 (2008) 1884-1890.

[7] V. Carias, J. Wang, R. Toomey, Poly (N-isopropylacrylamide) cross-linked coatings with phototunable swelling, Langmuir, 30 (2014) 4105-4110.

[8] S.C. George, S. Thomas, Transport phenomena through polymeric systems, Progress in Polymer Science, 26 (2001) 985-1017.

[9] R. Wanchoo, A. Thakur, A. Sweta, Viscometric and rheological behaviour of chitosan-hydrophilic polymer blends, Chemical and biochemical engineering quarterly, 22 (2008) 15-24.

[10] M. Pramanik, S.K. Srivastava, B.K. Samantaray, A.K. Bhowmick, Rubber–clay nanocomposite by solution blending, Journal of Applied Polymer Science, 87 (2003) 2216-2220.

[11] R.K. Arya, Measurement of concentration profiles in thin film binary polymer-solvent coatings using confocal Raman spectroscopy: Free volume model validation, Drying technology, 32 (2014) 992-1002.

[12] U. Siemann, Solvent cast technology–a versatile tool for thin film production, Scattering Methods and the Properties of Polymer Materials, (2005) 307-316.

[13] W.W. Flack, D.S. Soong, A.T. Bell, D.W. Hess, A mathematical model for spin coating of polymer resists, Journal of Applied Physics, 56 (1984) 1199-1206.

[14] P. Mokarian-Tabari, M. Geoghegan, J. Howse, S. Heriot, R. Thompson, R. Jones, Quantitative evaluation of evaporation rate during spin-coating of polymer blend films: Control of film structure through defined-atmosphere solvent-casting, The European Physical Journal E, 33 (2010) 283-289.

[15] H. Li, J. Mei, A.L. Ayzner, M.F. Toney, J.B.-H. Tok, Z. Bao, A simple droplet pinning method for polymer film deposition for measuring charge transport in a thin film transistor, Organic Electronics, 13 (2012) 2450-2460.

[16] H. Kaur, J. Sharma, D. Jindal, R.K. Arya, S.K. Ahuja, S.B. Arya, Crosslinked polymer doped binary coatings for corrosion protection, Progress in Organic Coatings, 125 (2018) 32-39.

[17] T.I. Burghelea, H.J. Grieß, H. Münstedt, An in situ investigation of the draw resonance phenomenon in film casting of a polypropylene melt, Journal of Non-Newtonian Fluid Mechanics, 173 (2012) 87-96.

[18] A.S. Mujumdar, S. Devahastin, Fundamental principles of drying, in: Mujumdar's Practical Guide to Industrial Drying: Principles, Equipment and New Developments, Exergex, Brossard, Canada, 2000, pp. 1-22.

[19] J. Vrentas, J. Duda, Diffusion in polymer—solvent systems. I. Reexamination of the free-volume theory, Journal of Polymer Science: Polymer Physics Edition, 15 (1977) 403-416.

[20] J. Vrentas, J. Duda, Diffusion in polymer–solvent systems. II. A predictive theory for the dependence of diffusion coefficients on temperature, concentration, and molecular weight, Journal of Polymer Science: Polymer Physics Edition, 15 (1977) 417-439.

[21] R.A. Yapel, A physical model of the drying of coated films, in, University of Minnesota, USA, Minneapolis, 1988.

[22] S. Alsoy, J. Duda, Drying of solvent coated polymer films, Drying Technology, 16 (1998) 15-44.

[23] S. Alsoy, Predicting drying in multiple-zone ovens, Industrial & engineering chemistry research, 40 (2001) 2995-3001.

[24] W. Schabel, P. Scharfer, M. Kind, Measurement and Simulation of Concentration Profiles During Drying of Thin Films with Help of Confocal-Micro-Raman Spectroscopy, Chemie Ingenieur Technik, 75 (2003) 1105-1106.

[25] W. Schabel, P. Scharfer, M. Muller, I. Ludwig, M. Kind, Measurement and simulation of concentration profiles in the drying of binary polymer solutions, Chemie Ingenieur Technik, 75 (2003) 1336-1344.

[26] P. Scharfer, W. Schabel, M. Kind, Modelling of alcohol and water diffusion in fuel cell membranes—experimental validation by means of in situ Raman spectroscopy, Chemical Engineering Science, 63 (2008) 4676-4684.

[27] R.K. Arya, M. Vinjamur, Measurement of concentration profiles using confocal Raman spectroscopy in multicomponent polymeric coatings—model validation, Journal of Applied Polymer Science, 128 (2013) 3906-3918.

[28] D. Siebel, P. Scharfer, W. Schabel, Prediction of diffusion in a ternary solvent–solvent–polymer blend by means of binary diffusion data: Comparison of experimental data and simulative results, Journal of Applied Polymer Science, (2016).

[29] S. Alsoy, J.L. Duda, Modeling of multicomponent drying of polymer films, AIChE journal, 45 (1999) 896-905.

[30] M. Dabral, L. Francis, L. Scriven, Drying process paths of ternary polymer solution coating, AIChE journal, 48 (2002) 25-37.

[31] P.E. Price, I.H. Romdhane, Multicomponent diffusion theory and its applications to polymer-solvent systems, AIChE journal, 49 (2003) 309-322.

[32] J.M. Zielinski, B.F. Hanley, Practical friction-based approach to modeling multicomponent diffusion, AIChE journal, 45 (1999) 1-12.

[33] R.J. Bearman, On The Molecular Basis Of Some Current Theories Of Diffusion, The Journal of Physical Chemistry, 65 (1961) 1961-1968.

[34] W. Schabel, I. Ludwig, M. Kind, Measurements of concentration profiles in polymeric solvent coatings by means of an inverse confocal micro Raman spectrometer—Initial results, Drying Technology, 22 (2004) 285-294.

[35] D. Siebel, P. Scharfer, W. Schabel, Determination of Concentration-Dependent Diffusion Coefficients in Polymer–Solvent Systems: Analysis of Concentration Profiles Measured by Raman Spectroscopy during Single

Drying Experiments Excluding Boundary Conditions and Phase Equilibrium, Macromolecules, 48 (2015) 8608-8614.

[36] D. Siebel, P. Scharfer, W. Schabel, Prediction of diffusion in a ternary solvent–solvent–polymer blend by means of binary diffusion data: Comparison of experimental data and simulative results, Journal of Applied Polymer Science, 133 (2016).

[37] C.M. Hansen, The Three Dimensional Solubility Parameter, Danish Technical: Copenhagen, 14 (1967).

[38] C.M. Hansen, Hansen solubility parameters: a user's handbook, CRC press, 2002.

[39] T. Kitak, A. Dumičić, O. Planinšek, R. Šibanc, S. Srčič, Determination of solubility parameters of ibuprofen and ibuprofen lysinate, Molecules, 20 (2015) 21549-21568.

[40] C. Özdemir, A. Güner, Solubility profiles of poly (ethylene glycol)/solvent systems, I: Qualitative comparison of solubility parameter approaches, European Polymer Journal, 43 (2007) 3068-3093.

[41] D.H. Pashley, F.R. Tay, R.M. Carvalho, F.A. Rueggeberg, K.A. Agee, M. Carrilho, A. Donnelly, F. García-Godoy, From dry bonding to water-wet bonding to ethanol-wet bonding. A review of the interactions between dentin matrix and solvated resins using a macromodel of the hybrid layer, American Journal of Dentistry, 20 (2007) 7.

[42] Y. Jang, T. Hirai, Solvent-induced phase-inversion and electrical actuation of dielectric copolymer films, Materials Sciences and Applications, 2 (2011) 187.

Chapter 2

Residual Solvent Study

The residual solvent study of polymer-polymer-solvent coatings are studied in this chapter. The three selected systems, that is, PS-PMMA-THF, PS-PMMA-EB, and PS-PMMA-TOL are discussed in Part 2A, Part 2B, and Part 2C, respectively.

2.1 Introduction

Polymeric coatings have numerous applications like magnetic tapes, storage devices, optical fiber, membrane and filters, multiphase gels, function films, protective films, and decorative films, etc [1-3]. These coating are made up of one polymer or more than one polymer dissolved in one solvent and/or more than one solvent. Scott [4] studied the incompatibility of a few high polymers in a solution of common solvent in which each polymer is completely soluble. This incompatibility gives rise to phase separation or inhomogeneous solution which may or may not be desirable. The homogeneous solution is formed when the total concentration of both polymers is less than a threshold value [5].

Figure 2.1 shows a schematic of the drying of polymer – polymer – solvent coating. The mass of coating will start falling as soon as the coating is made due to evaporation of the solvent into the surrounding air. The mass transfer will take place from the top of the coating into the surrounding air and there will be no mass transfer from the bottom side due to the impermeable substrate. In the beginning, the mass transfer is purely convective due availability of reasonably high amount of solvent present in the coating – air interface. The convective mass transfer can be controlled by percentage saturation of surrounding air, its temperature, and flow rate. During the course of drying, the solvent level at top of the coating falls down and drying becomes internally controlled due to the diffusion process within the coating. The diffusion is a slow process, and, hence, the drying rate starts decreasing.

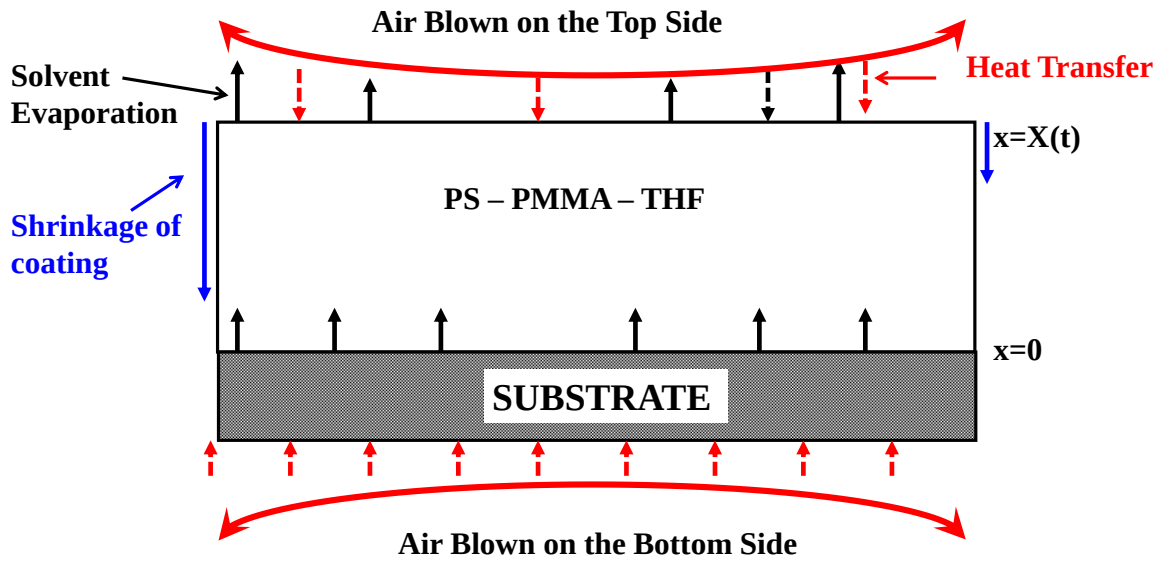

Figure 2.1: Schematic of polymer – polymer – solvent coating.

Thermodynamics of polymeric solution is complicated phenomena. It is very well explained by Flory-Huggins theory [6]. This theory relates Gibbs free energy to concentration of polymer(s) and solvent(s). Based on this, Favre et al. [7] had developed several expressions for chemical potential in polymeric solutions. Vrentas and Duda [8, 9] free volume theory is generally used to predict molecular diffusion in polymeric systems. This theory is based on the availability of free volume within the system which relates the self and mutual diffusion coefficients to free volume available for diffusion, composition of species and jumping units of polymer(s) and solvent(s). Later on Vrentas et al. [10] given the expression to calculate the jumping units. Several diffusion models (Alsoy and Duda [11], Zielinski and Hanley [12] , Dabral [13] in binary and ternary polymeric solutions were developed using Bearman's friction factor theory [14]. Price and Romdhane [15] had developed a generalized model for polymeric coatings using Bearman's friction factor theory.Self-diffusion coefficients were calculated using this theory. This theory is well-applicable for polymer – solvent system [16-22] and has also been tested for polymer – solvent – solvent systems [23].

For polymer – solvent – solvent systems, several models [11, 12, 24, 25] have been developed using Bearman's friction factor theory [26] which related chemical potential to the self-diffusion coefficient. For polymer – polymer – solvent systems

various models are available to calculate the chemical potential or free energy of the system and these can be used to develop the diffusion model for such systems.

Scott [4] studied the phase equilibria in high molecular weight polymer – polymer – solvent systems. He found that the role of solvent is not only in diluting the polymers but to decrease the interaction energy of the polymers. He suggested that osmotic pressures can be used to find the polymer – polymer interaction parameter which is very crucial in polymer – polymer – solvent systems. He stated that the polymer – polymer interaction parameter is due to heat contribution while the polymer – solvent interaction parameter will have a significant contribution from the entropy because the solvent only decreases the critical solution temperature. His study suggests that in the case of like polymers of same chemical nature the polymer – polymer interaction parameter will be nearly negligible and the solution would be compatible and homogeneous. He had given the following expression of partial molar free energies as:

$$\frac{\Delta\bar{F}_0}{RT} = \ln\phi_0 + \left(1-\frac{1}{m_1}\right)\phi_1 + \left(1-\frac{1}{m_2}\right)\phi_2 + \chi_{10}\phi_1^2 + \chi_{20}\phi_1^2 + \left(\chi_{10}+\chi_{20}-\chi_{12}\right)\phi_1\phi_2 \qquad (2.1)$$

$$\frac{\Delta\bar{F}_1}{RT} = \ln\phi_1 + \left(1-m_1\right)\phi_0 + \left(1-\frac{m_1}{m_2}\right)\phi_2 + m_1\left[\chi_{10}\phi_0^2 + \chi_{12}\phi_2^2 + \left(\chi_{10}+\chi_{12}-\chi_{20}\right)\phi_0\phi_2\right] \qquad (2.2)$$

$$\frac{\Delta\bar{F}_2}{RT} = \ln\phi_2 + \left(1-m_2\right)\phi_0 + \left(1-\frac{m_2}{m_1}\right)\phi_1 + m_2\left[\chi_{20}\phi_0^2 + \chi_{12}\phi_1^2 + \left(\chi_{20}+\chi_{12}-\chi_{20}\right)\phi_0\phi_1\right] \qquad (2.3)$$

where χ_{10}: polymer 1 and solvent interaction constant, χ_{20}: polymer 2 and solvent interaction constant, χ_{12}: polymer 1 and polymer 2 interaction constant, $m_i = \frac{V_i}{V_{i0}}$: degree of polymerization of polymer i, V_i: molar volume of the polymer i, V_{i0}: molar volume of one submolecule of the polymer i, ϕ_i: volume fraction of component i, subscript $i = 0,1,\text{and}\,2$: for solvent, polymer 1 and polymer 2 respectively.

Saeki [27] developed a semiempirical expression to calculate the partial entropy of mixing of polymer – polymer – solvent systems. He had considered the effect of polymer flexibility in the development. The polymer flexibility constant k is equal to zero for flexible polymers and greater than zero for semi flexible polymers. The expressions for the partial entropy of mixing are given by:

$$\frac{\Delta S_{M,0}}{k} = -\ln\phi_0 + (a-1) + \ln\frac{a}{a+b} + b + k_1\phi_1^2 \ln\frac{\frac{1}{r_1} + k_1(1-\phi_1)}{a+b} + k_2\phi_2^2 \ln\frac{\frac{1}{r_2} + k_2(1-\phi_2)}{a+b} \tag{2.4}$$

$$\frac{\Delta S_{M,1}}{r_1 k} = -\frac{1}{r_1}\ln\phi_1 + \left(a - \frac{1}{r_1}\right) + \frac{1}{r_1}\ln\frac{a\left[1 + k_1 r_1(1-\phi_1)\right]}{a+b} + b - k_1(1-\phi_1) + k_1(1-\phi_1)^2 \ln\frac{\frac{1}{r_1} + k_1(1-\phi_1)}{a+b} + k_2\phi_2^2 \ln\frac{\frac{1}{r_2} + k_2(1-\phi_2)}{a+b} \tag{2.5}$$

$$\frac{\Delta S_{M,2}}{r_2 k} = -\frac{1}{r_2}\ln\phi_2 + \left(a - \frac{1}{r_2}\right) + \frac{1}{r_2}\ln\frac{a\left[1 + k_2 r_2(1-\phi_2)\right]}{a+b} + b - k_2(1-\phi_2) + k_2(1-\phi_2)^2 \ln\frac{\frac{1}{r_2} + k_2(1-\phi_2)}{a+b} + k_1\phi_1^2 \ln\frac{\frac{1}{r_1} + k_1(1-\phi_1)}{a+b} \tag{2.6}$$

$$a = \phi_0 + \frac{\phi_1}{r_1} + \frac{\phi_2}{r_2},\ b = k_1\phi_1(1-\phi_1) + k_2\phi_2(1-\phi_2) \tag{2.7}$$

where ϕ_i: volume fraction of the component i, k_i: flexibility constant for the polymer, r_i: number of segments in the polymer i, k: Boltzmann constant, subscripts, $0, 1, \text{and } 2$: solvent, polymer 1, and polymer 2 respectively.

Ariyapadi and Nauman [28] developed the free energy expressions of inhomogeneous polymer – polymer – solvent system without considering the entropy contribution.

$$\Delta G_{mixing} = \left[\int g\left(\phi_1, \phi_2, ...\phi_n\right) + \sum_{i=1}^{n} K_i \left(\nabla \phi_i\right)^2 + \sum_{j \succ i} \sum_{i=1}^{n} K_{ij} \left(\nabla \phi_i\right)\left(\nabla \phi_j\right) \right] dV \tag{2.8}$$

$$R_{Gi}^2 = \frac{N_i l^2}{6},\ K_i = \frac{1}{6} R_{Gi}^2 \chi_{is},\ K_{ij} = \frac{1}{6}\left[R_{Gi}^2 \chi_{is} + R_{Gj}^2 \chi_{js} - \left(R_{Gi}^2 + R_{Gj}^2\right)\chi_{ij} \right] \tag{2.9}$$

In another paper, Ariyapadi and Nauman [29] developed the expression to calculate the free energy of the polymer – polymer – solvent system using mean field approach. This expression contains both the enthalpic and entropy contribution to the free energy of the system.

$$\Delta G_{\text{Total mixing}} = \int_V \left[\Delta g + \frac{K_1}{2}\left(\nabla \phi_1\right)^2 + K_{12}\left(\nabla \phi_1\right)\left(\nabla \phi_2\right) + \frac{K_2}{2}\left(\nabla \phi_2\right)^2 \right] dV \tag{2.10}$$

$$K_1 = \frac{R_{G1}^2}{3}\left[\chi_{1s} + \left(\frac{1}{N_1}\frac{1}{\phi_1} + \frac{1}{\phi_s} \right) \right],\ K_1 = \frac{R_{G1}^2}{3}\left[\chi_{1s} + \left(\frac{1}{N_1}\frac{1}{\phi_1} + \frac{1}{\phi_s} \right) \right] \tag{2.11}$$

$$K_{12} = \frac{R_{G1}^2}{6}\left(\chi_{1s} - \chi_{12} + \frac{1}{N_1}\frac{1}{\phi_s} \right) + \frac{R_{G2}^2}{6}\left(\chi_{2s} - \chi_{12} + \frac{1}{N_2}\frac{1}{\phi_s} \right) \tag{2.12}$$

In yet another paper, Ariyapadi and Nauman [30] developed another expression for enthalpy of mixing to calculate the free energy of inhomogeneous polymer – polymer – solvent system. This model worked well for all concentration fluctuations. They had not considered the volume change on mixing due to the negligible contribution of the volume change in the total enthalpy of mixing. Hence, the enthalpy of mixing was just equal to the change in internal energy. Moreover, they had also not considered the contribution of entropy gradient on the free energy and gave the following expression:

$$\Delta G_{\text{Total mixing}} = \int_V \Delta g dV + \int_V \sum_{n=1}^{\infty} (-1)^{n-1} \left[\frac{(K_1)_n}{2} \left(\nabla^{2n} \phi_1 \right) + B_n \left(\nabla^n \phi_1 \right) \left(\nabla^n \phi_2 \right) + \frac{(K_2)_n}{2} \left(\nabla^{2n} \phi_2 \right) \right] dV \tag{2.13}$$

where Δg : The Flory – Huggins expression for free energy of homogeneous polymer – polymer system and given by:

$$\Delta g = \frac{1}{m} \left[\phi_1 \ln \phi_1 + (1-\phi_1) \ln (1-\phi_1) \right] + \chi_{12} \phi_1 (1-\phi_1) \tag{2.14}$$

$$B_n = -\frac{\Omega_{13} + \Omega_{23} - \Omega_{12}}{2(2n+1)!}, \qquad (K_1)_n = -\frac{\Omega_{13}}{(2n+1)!}, \qquad (K_2)_n = -\frac{\Omega_{23}}{(2n+1)!}$$

$$\Omega_{13} = \frac{W_{11} \left(l_{11}^2 \right)_n}{v_1^2} + \frac{W_{33} \left(l_{33}^2 \right)_n}{v_3^2} - \frac{2W_{13} \left(l_{13}^2 \right)_n}{v_1 v_3},$$

$$\Omega_{23} = \frac{W_{22} \left(l_{22}^2 \right)_n}{v_2^2} + \frac{W_{33} \left(l_{33}^2 \right)_n}{v_3^2} - \frac{2W_{23} \left(l_{23}^2 \right)_n}{v_2 v_3}$$

$$\Omega_{12} = \frac{W_{11} \left(l_{11}^2 \right)_n}{v_1^2} + \frac{W_{22} \left(l_{22}^2 \right)_n}{v_2^2} - \frac{2W_{12} \left(l_{12}^2 \right)_n}{v_1 v_2},$$

For polymer – solvent, $\left(l_{ij}^2 \right)_n = \prod_{k=1}^{n} \left(\frac{2k+1}{3} \right) R_{Gi}^2$

For, polymer – polymer, $\left(l_{ij}^2 \right)_n = \prod_{k=1}^{n} \left(\frac{2k+1}{3} \right) \left(R_{Gi}^2 + R_{Gj}^2 \right)$

where $g(\phi_i)$: free energy of homogeneous solution, n: number of polymers, l: length of monomer unit, ϕ_i: volume fraction of component i, N_i: degree of polymerization of polymer i, $\Delta g = \frac{\text{free energy of mixing}}{kT}$, χ_{i3}: Flory-Huggins interaction parameter for polymer i and solvent, subscript s: solvent, v_i: volume occupied by a molecule of type i, m: degree of polymerization, ϕ_i: volume fraction of species i.

Lipatov et al. [31] studied the effect of concentration on the interaction parameter in polymer – polymer – solvent system. They studied the poly(styrene) – poly(butyl methacrylate) – carbon tetra chloride system. They found that the polymer – polymer interaction does change for small change in poly(butyl methacrylate) concentration. However, this interaction parameter decreased with more increase in poly(butyl methacrylate) concentration. They had also studied the mobility of solution during addition of another polymer and did not notice any change as compared to binary solutions of individual solutions.

Hong and Burns [32] studied the compatibility of poly(styrene) – poly(methyl methacrylate) – benzene system. They studied the effect of temperature and molecular weight of polymers on the compatibility. In their work, the polydispersity ratio was in the range of 1.55 to 4.7. They found significant change in phase separation with a change in average molecular weight of polymers. They had also found that the solution will phase separate at a lower total mass fraction of polymers at a higher temperature while the mass fraction of each polymer was equal. They had not found any increase in polymer compatibility by lowering the molecular weight of polymers at elevated temperatures.

Clark [3] developed computation solution scheme for generating the tie line data for polymer – polymer – solvent system. They found that Flory – Huggins theory was not able the predict phase behavior of the system studied. They found that the theoretical predictions based on the interaction parameters calculated at one condition are not accurate for another condition due to change in molecular weight and hence

the phase behavior of the system. They developed following equations for chemical potential in homogenous polymer – polymer – solvent systems:

$$\frac{\Delta\mu_1}{RT} = \ln\phi_1 + \left(1-\frac{1}{P_2}\right)\phi_2 + \left(1-\frac{1}{P_3}\right)\phi_3 + (1-\phi_1)(\chi_{12}\phi_2 + \chi_{13}\phi_3) - \chi_{23}\phi_2\phi_3$$
$$\frac{\Delta\mu_2}{RT} = \ln\phi_2 + \left(1-\frac{1}{P_2}\right)\phi_1 + \left(1-\frac{P_2}{P_3}\right)\phi_3 + P_2(1-\phi_2)(\chi_{12}\phi_1 + \chi_{23}\phi_3) - P_2\chi_{13}\phi_1\phi_3 \qquad (2.15)$$
$$\frac{\Delta\mu_3}{RT} = \ln\phi_3 + (1-P_3)\phi_1 + \left(1-\frac{P_3}{P_2}\right)\phi_2 + P_3(1-\phi_3)(\chi_{13}\phi_1 + \chi_{23}\phi_2) - P_3\chi_{12}\phi_1\phi_2$$

where P_2 and P_3: polymers molecular weight parameters, ϕ_i: volume fraction of the component i, χ_{ij}: interaction parameter species i and j.

Panayiotou and Vera [1] calculated the Flory-Huggins interaction parameters for several polymer – polymer – solvent systems. They found the solution compatibility increases with increase in the concentration of polymer in case poly(styrene) – poly(vinyl methyl ether) – benzene system at $25\,^{o}C$ which was opposite of the earlier published literature [33]. They suggested that such results can come due to change in molecular weights and due to nearly equal free energies of the equilibrium and nonequilibrium states.

2.2 Material and Methods

Poly(styrene) (PS) having density 1.05 g cm^{-3} and molecular weight 192000 (Sigma Aldrich, Germany), poly(methyl methacrylate) (PMMA) having density 1.18 g cm^{-3} and molecular weight 120000 (Sigma Aldrich, Germany), tetrahydrofuran (THF) having density 0.8892 g cm^{-3} and molecular weight 72.11, ethylbenzene (EB) having density 0.866 g cm^{-3} and molecular weight 106.17, and toluene (TOL) having density 0.867 g cm^{-3} and molecular weight 92.14 (Spectrochem, India). Polymer – polymer – solvent solutions were made by dissolving measured amounts of polymers and solvent in leach proof bottles. These solution bottles were manually shaken for several weeks to get homogeneous polymer- solvent solutions. Single thin films were prepared using these solutions by the solution casting technique. A known amount of

solution was transferred using micropipette into stainless steel circular sample holder having the depth of 2000 μm and diameter of 12.24 mm. The mass of film was recorded as a function of time using Precisa analytical weighing balance having the accuracy of ± 0.0001g. The readings were taken until steady state was reached. The thickness was calculated by dividing the volume of the coating by cross section of the sample holder. The volume of the coating was calculated by adding the volumes of polymers and solvent respectively. From initial mass percentage of each species, the mass of each polymer is known. The mass of solvent at any time will be total mass of the coating minus the mass of polymers. The volume of each specie was calculated as mass divided by the density of the specie. The mass of corresponding species divided by the volume of the coating will give the average concentration of the species under consideration. All experiments were performed without any air flow at a temperature of about 25ºC for which heat transfer coefficient comes out to be $8.36\ \mathrm{W.m^{-2}.K^{-1}}$.

Sample calculation procedure is given below. For a given system PS-PMMA-THF, Let the mass of PS-PMMA-THF solution is 0.5g having 5.2% PS, 6.25% PMMA and 88.55% solvent, respectively.

$$\text{Mass of PS, } M_{PS} = m \times \frac{5.2}{100} \Rightarrow 0.5 \times \frac{5.2}{100} = 0.026g$$

$$\text{Mass of PMMA, } M_{PMMA} = m \times \frac{6.25}{100} \Rightarrow 0.5 \times \frac{6.25}{100} = 0.031g$$

$$Mass\ of\ THF, M_{THF} = m - M_{PS} - M_{PMMA} \Rightarrow 0.5 - 0.026 - 0.031 = 0.443g$$

$$\text{Volume of PS-PMMA-THF, } V_{PSPMMATHF} = \frac{M_{PS}}{\text{Density of PS}} + \frac{M_{PMMA}}{\text{Density of PMMA}} + \frac{\mathrm{M_{THF}}}{\text{Density of THF}}$$

$$= \frac{0.026\ \mathrm{g}}{1.04\ \mathrm{g\,cm^{-3}}} + \frac{0.031\ \mathrm{g}}{1.18\ \mathrm{g\,cm^{-3}}} + \frac{0.443\ \mathrm{g}}{0.889\ \mathrm{g\,cm^{-3}}}$$

$$= 0.549\ cm^3$$

$$\text{Concentration of PS, } C_{PS} = \frac{M_{PS}}{V_{PSPMTHF}} \Rightarrow \frac{0.026}{0.549} = 0.047\ g\,cm^{-3}$$

$$\text{Concentration of PMMA, } C_{PMMA} = \frac{M_{PS}}{V_{PSPMTHF}} \Rightarrow \frac{0.031}{0.549} = 0.056\ g\,cm^{-3}$$

$$\text{Concentration of THF, } C_{PS} = \frac{M_{THF}}{V_{PSPMTHF}} \Rightarrow \frac{0.443}{0.549} = 0.806\ g\,cm^{-3}$$

$$\text{Residual solvent (\%)} = \frac{\text{Instantaneous } M_{THF}}{\text{Initial } M_{THF}} \times 100 \Rightarrow \frac{0.443}{0.443} \times 100 = 100\%$$

$$\text{The cross-sectional area of the substrate} = \pi\left(\frac{d}{2}\right)^2 = \left(\frac{22}{7}\right) \times \left[\frac{\left(\frac{12.24}{10}\right)}{2}\right]^2 = 1.1771 \text{ cm}^2$$

$$\text{Non-dimensional coating thickness} = \frac{0.466\ cm}{0.466\ cm} = 1$$

Part 2A. Residual Solvent Study in PS-PMMA-THF System

2.3 Results and Discussion

Figure 2.2a shows the average concentrations of poly(styrene) (PS), poly(methyl methacrylate) (PMMA), and tetrahydrofuran (THF) with time. PS, PMMA, and THF mass percentage in the beginning were 5.2%, 6.25%, and 88.55% respectively. Figure 2.2b shows the coating thickness and percentage residual solvent remaining with time in the same system. The initial coating thickness and solvent percentage were 935 μm and 88.55% respectively. The residual solvent is decreasing very rapidly in the beginning due to the low enthalpy of vaporization of the tetrahydrofuran. The fall in residual solvent is linear up to 405 s and by that time 76.93% of the solvent has been removed. This linear trend shows that the external mass transfer is dominating and drying is externally controlled. After this, there is a very slow decrease in the residual solvent with time. The residual solvent content at 1651 s, 2986 s, 4306 s, and 6902 s are 9.38%, 8.04%, 7.85%, and 7.38% respectively. The coating thickness at 1651 s, 2986 s, 4306 s, and 6902 s are 166 μm, 155 μm, 153 μm and 149 μm, respectively. There is very less change in coating thickness and residual solvent content from 4306 s to 6902 s. These data show that the mass transfer has become very slow due to the slow diffusion of solvent within the coating. The diffusion coefficient is a very strong function of the mass fraction of solvent within the coating [8, 9].

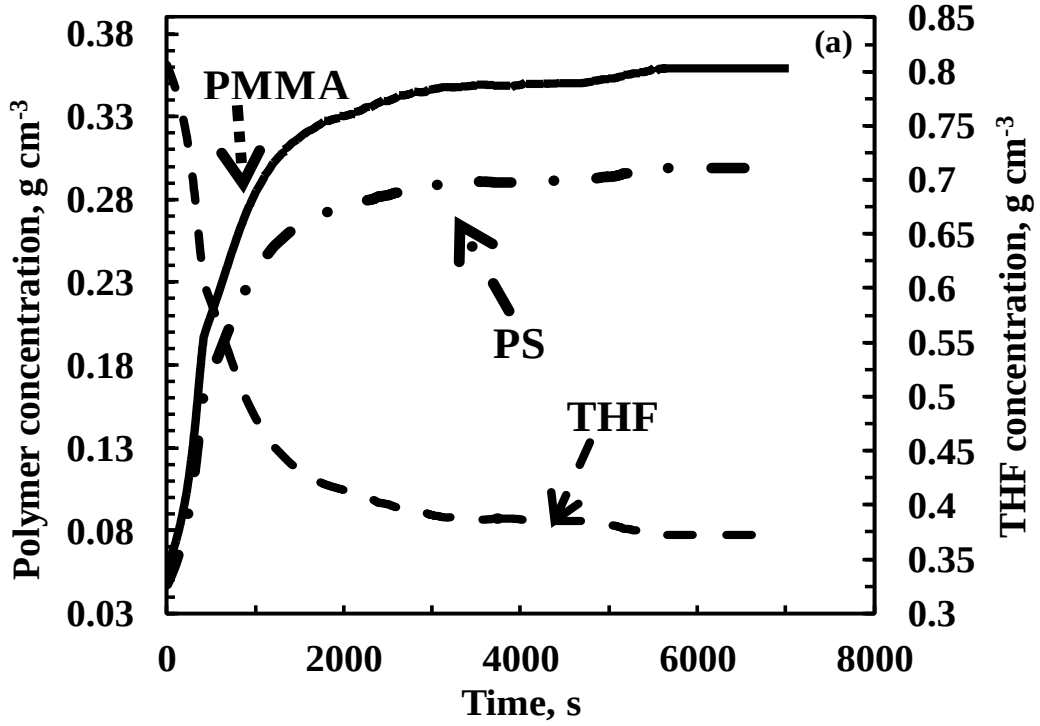

Figure 2.2(a): Average concentration of solvent and polymers with time in PS-PMMA-THF coating. PS, PMMA, and THF were 5.2 %, 6.25%, and 88.55% respectively, initial thickness of coating and temperature were: 935 microns and 25 ˚C respectively.

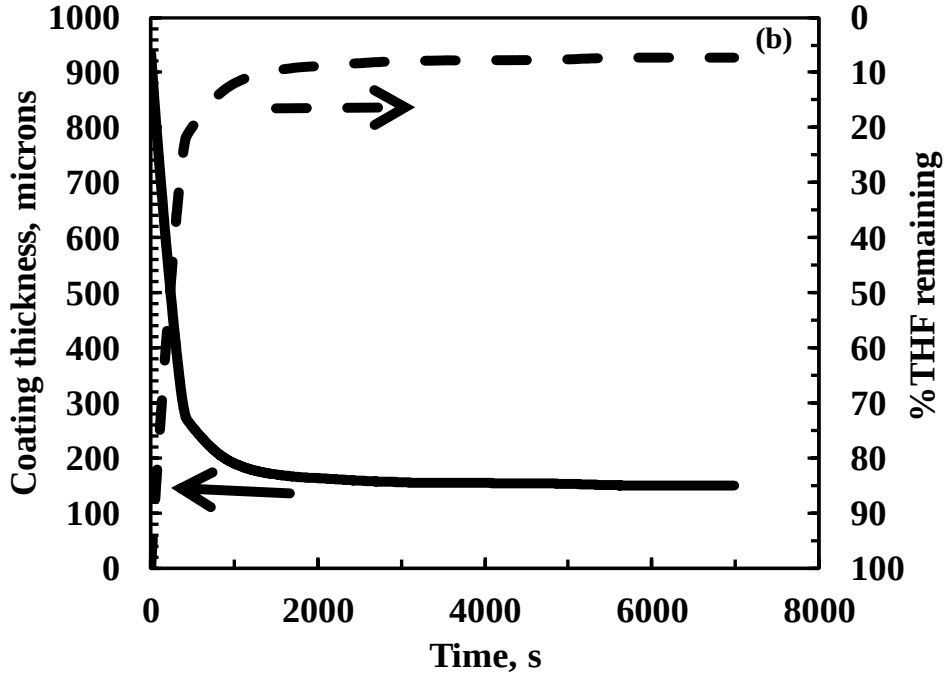

Figure 2.2(b): Coating thickness and % THF remaining with time in PS-PMMA-THF coating. PS, PMMA, and THF were 5.2 %, 6.25%, and 88.55% respectively, initial thickness of coating and temperature were: 935 microns and 25 ˚C respectively.

Figure 2.3a shows the concentration of PS, PMMA, and THF with time coating having 10.74% PS, 5.11% PMMA, and 84.15% THF, and 913 μm thickness in the beginning. Figure 2.3b shows the coating thickness and percentage residual within the coating with time. The drying trend, in this case, is similar to that of the previous coating having 5.2% PS, 6.25% PMMA, 88.55%THF, and 935 μm thickness. The residual solvent and coating thickness at 360 s, 1116 s, 2116 s, 2706 s, 3246 s and 4312 s are 20.57%, 9.29%, 6.96%, 6.31%, 5.96% and 5.72%, and 285 μm, 196 μm,178 μm, 173 μm, 170 μm and 168 μm, respectively. The drying trend is linear up to 360 s. The drying is almost over by 2706 s because after that there is no appreciable change in the residual solvent content for the very long time period, i.e., the residual solvent left after 4312 s is 5.72%.

The comparison of results obtained by coating having 10.74% PS, 5.11% PMMA, and 84.15% THF, and 913 μm thickness in the beginning with the 5.2% PS, 6.25% PMMA, 88.55%THF, and 935 μm thickness in the beginning show that drying in both the coatings is externally controlled for nearly same time interval (0 to 360 s or 405 s). At the end of the externally controlled zone, the residual solvent content left in the coatings is 5.72% and 7.38%, respectively. In these two cases, the initial poly(styrene) mass percentage was changed from 5.2% to 10.74% while poly(methyl methacrylate) mass fraction was nearly constant. These results show that doubling the mass fraction of poly(styrene) does not affect the drying trend of the coating and hence the drying mechanism as shown in Figure 2.4. The residual solvent left in the second system after the externally controlled zone is almost equal to the first system. The ultimate solvent left in the first and the second systems are 7.38% and 5.72%, respectively. It shows that the diffusion of solvent in the second system is slightly higher as compared to the first system, which could be due to the change in the polymer- solvent thermodynamics. The drying mechanism can be altered if there is some change in chemical potential and glass transition temperature. This shows that the glass transition temperature of these two systems remains nearly same which is the function of solvent content within the coating [34, 35] since the THF percentage in the beginning is 84.15% or 88.55%. The polymer – polymer – solvent system would go to phase separation whenever the total polymer percentage is around 30% in case of high molecular weight $\left(\approx 10^5\right)$ polymers [4]. Hence, these systems will remain

homogenous for sufficiently long drying time. The interaction between different polymer molecules gives the enthalpic contribution, however, the connectivity of monomer units within the polymer gives rise to entropic contribution [29]. The combinatorial term is very important in the study of thermodynamics of polymer – polymer – solvent systems [27] and it does not exist for the systems with small molecules [29].

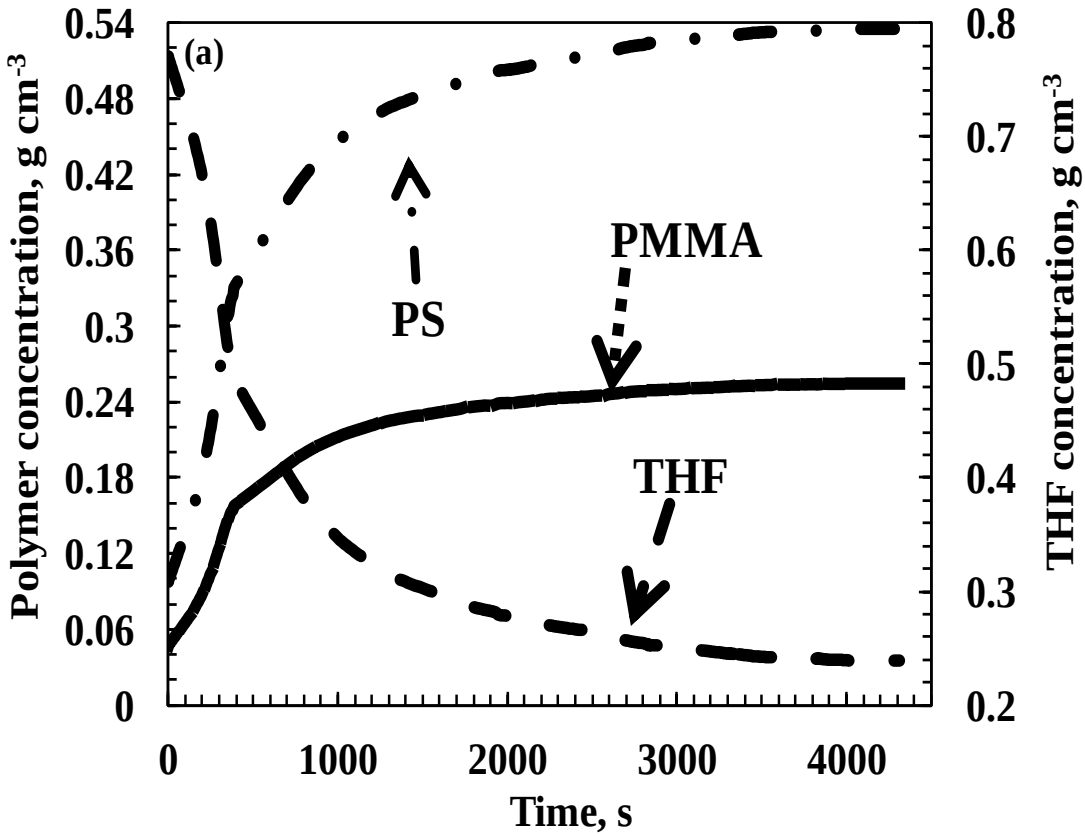

Figure 2.3(a): Average concentration of solvent and polymers with time in PS-PMMA-THF coating. PS, PMMA, and THF were 10.74 %, 5.11%, and 84.15% respectively, initial thickness of coating and temperature were: 913 microns and 25 ˚C respectively.

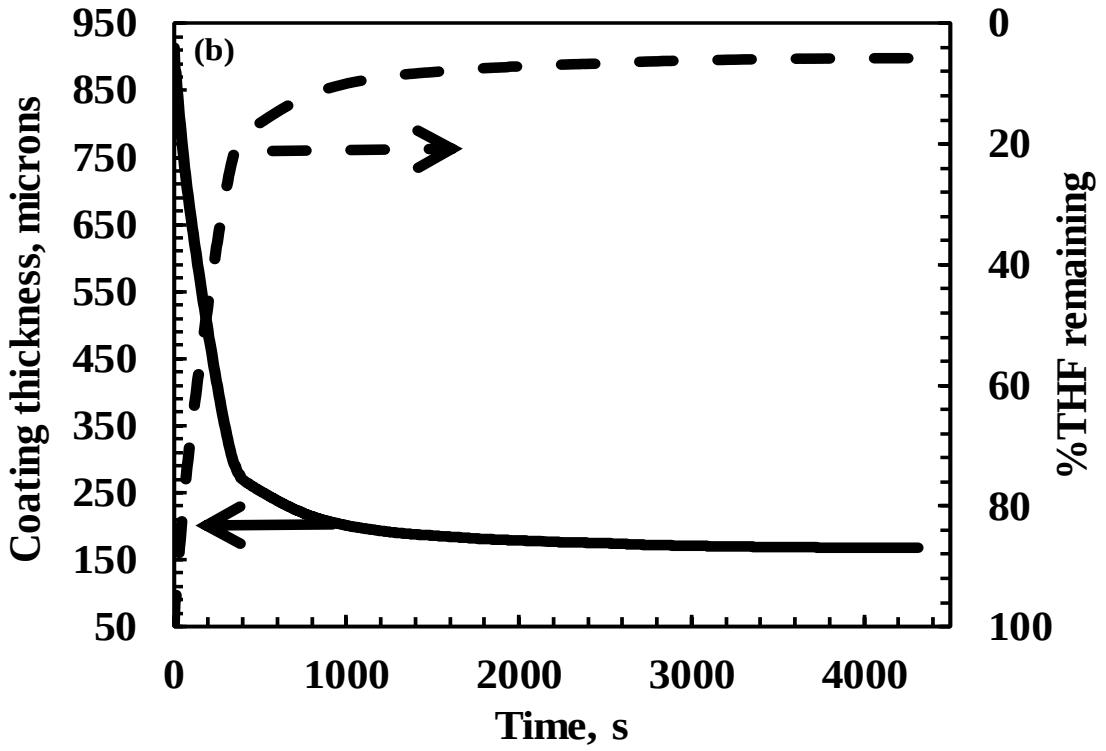

Figure 2.3(b): Coating thickness with time and % THF remaining with time in PS-PMMA-THF coating. PS, PMMA, and THF were 10.74 %, 5.11%, and 84.15% respectively, initial thickness of coating and temperature were: 913 microns and 25 ˚C respectively.

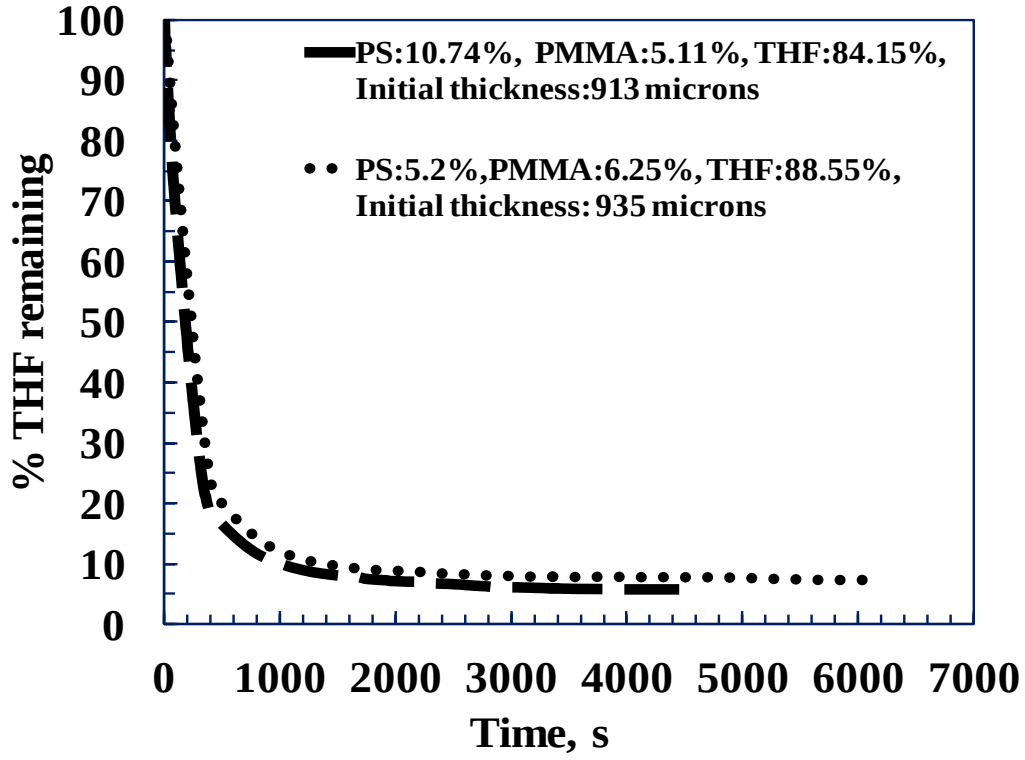

Figure 2.4: Residual solvent vs time in PS-PMMA-THF system of different concentration.

Figure 2.5a shows the average concentration of polymers and solvent in PS – PMMA – THF coating having 10.19% PS, 10.29% PMMA, 79.52% THF, and 909 µm thickness in the beginning. Figure 2.5b shows the change in coating thickness and residual solvent content with time in this coating. At 315 s, 1215 s, 2610 s, 4686 s, 6246 s and 7851 s, the residual solvent are 34.02%, 12.8%, 7.15%, 6.12%, 5.68%, and 5.27% and coating thickness are: 412 µm, 253 µm, 210 µm, 202 µm, 199 µm, and 196 µm, respectively. These results shows that the effect of polymer content on residual solvent is negligible, however the drying time taken for the system having doubled polymer mass fraction is longer. This shows that the diffusion of the solvent is slow for a longer time period and these coatings remain rubbery for a sufficiently longer time as compared to low polymer content coating.

Linear and exponential drying zones can be seen in Figure 2.5a & Figure 2.5b. The first zone is linear, i.e., externally controlled. The second zone is exponential in shape i.e., the diffusion controlled. Beginning from 100%, the residual solvent content at the end of the first zone (315 s) is 34.02% and at the end of second zone (1215 s) is 12.8%. The solvent removed in each zone is 66% and 62% respectively. These percentages are calculated based on initial percentage solvent in the beginning of each zone. From 1215 s to 2620 s (Δt=1395 s), the change in residual solvent content is 5.65%, however the change in residual solvent content during 2610 s to 4686 s (Δt=2076 s) and 4686 s to 7851 s (Δt=3165 s) is 0.44% and 0.41% respectively. This is a clear indication of the diffusion controlled drying mechanism from 315 s onwards.

Figures 2.6a & 2.6b (PS: 10.19%, PMMA: 10.29%, THF: 79.52%, Thickness: 909 µm) and Figures 2.2a & 2.2b (PS: 5.2%, PMMA: 6.25%, THF: 88.55%, Thickness: 935 µm) show similar drying trends. The profiles in Figure 2.6a & 2.6b are plateau off at the end of 4801 s which is significantly higher than the time of Figure 2.2a & 2.2b i.e, 2896 s. It shows that doubling the mass fraction of both the polymers does not affect the glass transition temperature of the coating but decreases the diffusion mass transfer significantly. These results are in agreement with free volume theory [8, 9]. The diffusion coefficient changes by orders of magnitude due to change in the mass fraction of the polymer [36]. However, these findings show

independency of diffusion coefficient in the systems up to 20% polymer mass fraction which may be due to some change in thermodynamics or phase separation at later stage of drying which results in nearly same residual solvent in systems with half polymer mass fraction as can be seen in Table 2.1, row 1 and row 3.

Figure 2.6a shows the average concentration of polymers and solvent in PS – PMMA – THF coating having 5.08% PS, 10.19% PMMA, 84.73% THF, and 1196 µm thickness in the beginning. Figure 2.6b shows the change in coating thickness and residual solvent content with time in this coating. At 490 s, 1260 s, 2661 s, 4626 s, 6467 s and 7851 s, the residual solvent are 28.93%, 12.75%, 5.14%, 3.25%, 2.76% and 2.67% and coating thickness are: 452 µm, 283 µm, 203 µm, 183 µm, 178 µm and 177 µm, respectively. After 490s, the residual solvent decreases very slowly with the time. These results show that doubling the mass fraction of PMMA does affect the drying trend of the coating and it shows that the diffusion of solvent in this system is slightly higher as compared to the other three systems which could be due to the change in the polymer solvent thermodynamics. On comparing systems (PS: 10.74%, PMMA: 5.11%, THF: 84.15%, Thickness: 913 µm) and (PS: 5.08%, PMMA: 10.19%, THF: 84.73%, Thickness: 1196 µm), the ultimate residual solvent left in the coating were 5.27% and 2.67%, respectively, and its comparison is shown in Figure 2.7

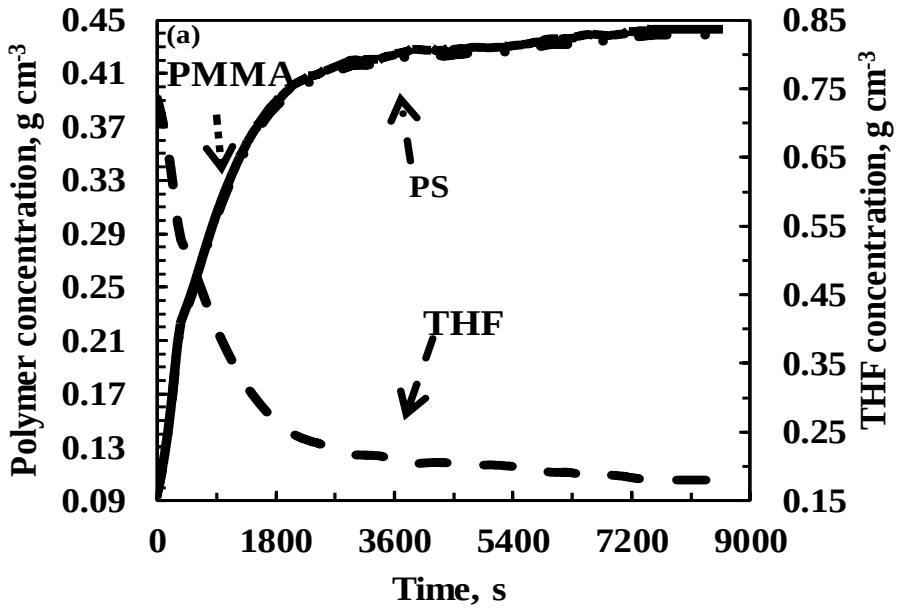

Figure 2.5(a): Average concentration of solvent and polymers with time in PS-PMMA-THF coating. PS, PMMA, and THF were 10.19 %, 10.29% and 79.52% respectively, initial thickness of coating and temperature were: 909 microns and 25 ˚C respectively.

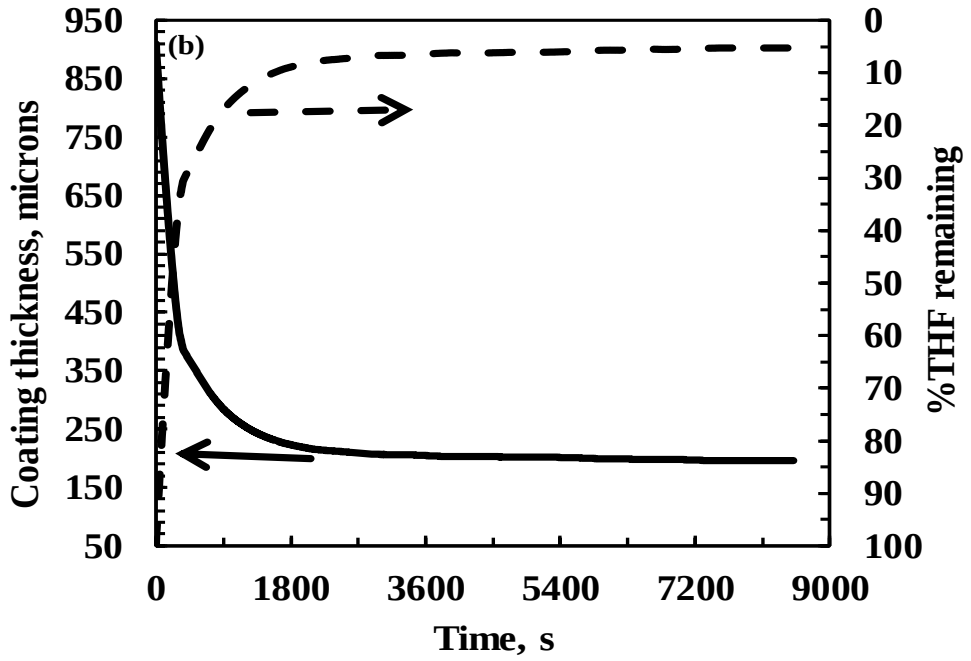

Figure 2.5(b): Coating thickness with time and % THF remaining with time in PS-PMMA-THF coating. PS, PMMA, and THF were 10.19 %, 10.29% and 79.52% respectively, initial thickness of coating and temperature were: 909 microns and 25 ˚C respectively.

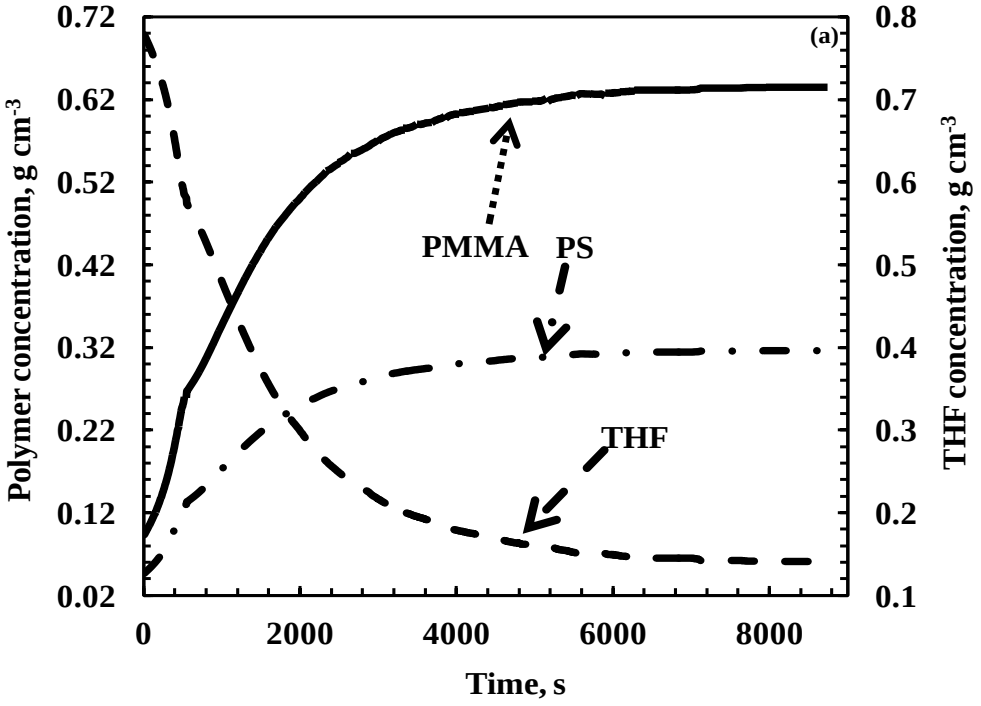

Figure 2.6 (a): Concentration of solvent and polymers with time. (b): Coating thickness and % THF remaining with time in PS-PMMA-THF coating. PS, PMMA, and THF were 5.08%, 10.19% and 84.73% respectively, initial thickness of coating and temperature were: 1196 microns and 25 ˚C respectively.

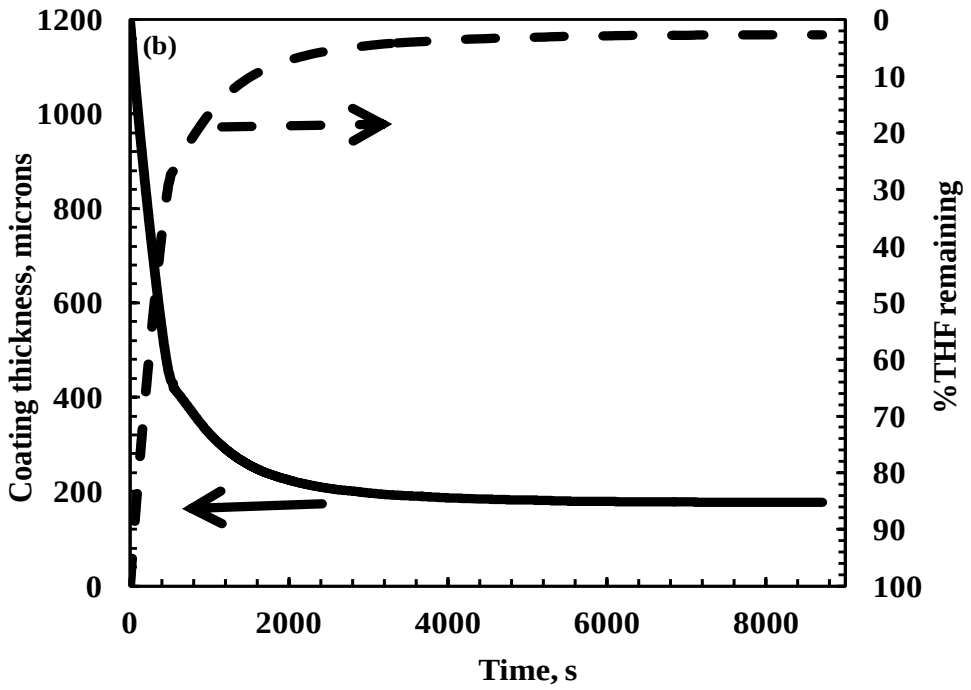

Figure 2.6 (b): Coating thickness and % THF remaining with time in PS-PMMA-THF coating. PS, PMMA, and THF were 5.08%, 10.19% and 84.73% respectively, initial thickness of coating and temperature were: 1196 microns and 25 ˚C respectively.

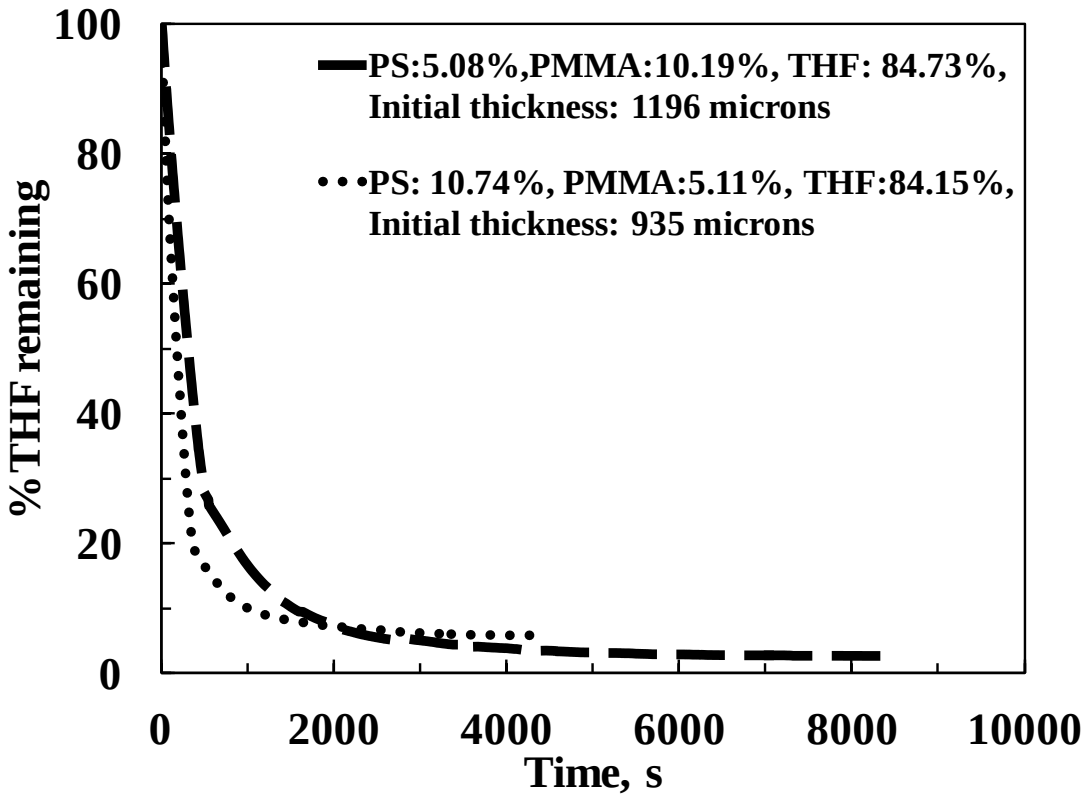

Figure 2.7: Residual solvent vs time in PS-PMMA-THF system of different concentration.

The summary of residual solvent and coating thickness in various systems studied in this work is given in Table 2.1. Doubling the mass fraction of poly(styrene) from 5.2% to 10.74% has decreased the residual solvent from 7.38% to 5.72% as can be seen in Table 2.1, row 1 and 2. Doubling the mass fraction of PMMA from 6.25% to 10.19% has tremendously decreased the residual solvent from 7.38% to 2.67% as shown in Table 2.1, row 1 and row 4. Doubling the mass fractions of poly(styrene) from 5.2% to 10.19% and PMMA from 6.25% to 10.29% has decreased the residual solvent from 7.38% to 5.27% as shown in Table 2.1, row 1 and 3. However, doubling the mass fraction of PMMA from 5.11% to 10.29% has not affected the residual solvent in 10% PS systems as can be seen in Table 2.1, row 2 and 3.

Table 2.1: Summary of polymer-polymer-solvent systems prepared.

S.No	PS (%)	PMMA (%)	THF (%)	Initial Thickness (microns)	Final Thickness microns)	Residual solvent (%)
1.	5.2	6.25	88.55	935	149	7.38
2.	10.74	5.11	84.15	913	168	5.72
3.	10.19	10.29	79.52	909	196	5.27
4.	5.08	10.19	84.73	1196	177	2.67

2.4 Conclusions

The residual solvent content in the poly(styrene)–poly(methyl methacrylate) – tetrahydrofuran coatings has not changed appreciably by changing the poly(styrene) content. The drying mechanism in the coating studied is not a strong function of poly(styrene). The change in poly(methyl methacrylate) mass fraction slowed down the drying process and the coatings are taking very long time to dry. However, the residual solvent content reduced to very low value by doubling the PMMA mass fractions in nearly 5% PS systems. The thermodynamics of this system is a strong function of the poly(methyl methacrylate) mass fraction. However, no change in residual solvent was observed by doubling the PMMA mass fraction in systems having 10% PS.

Arya and Vinjamur [23] reported the simulation as well as experimental results in case of PS-*p*-xylene –THF system and found that drying behavior was completely different whenever the concentration of any solvent was low and none of the drying models were able the predict the actual drying behavior. Similar results are obtained here too. The initial weight fraction of PMMA is not able the affect the amount of residual solvent as far as PS is high, i.e., around 10%. However, the affect of PMMA mass fraction was very significant in case of low PS mass fraction, i.e., 5%. This could be due to high dependency of polymer – polymer interaction in dilute solution. Moreover, PS is more glassy and brittle in nature as compared to PMMA which is in favor of low residual solvent whenever PS composition is low as compared to PMMA.

Part 2B. Residual Solvent Study in PS-PMMA-TOL System

2.5 Results and Discussion

The coatings of initially homogeneous poly(styrene) – poly(methyl methacrylate) – toluene system have been discussed in this section of the chapter. Figure 2.8a shows the average concentrations of poly(styrene) (PS), poly(methyl methacrylate) (PMMA), and toluene (TOL) with time. PS, PMMA, and TOL mass percentage in the beginning were 4.99 %, 5.04%, and 89.97%, respectively. Figure 2.8b shows the coating thickness and percentage residual solvent remaining with time in the same system. The initial coating thickness was 881 μm. The fall in residual solvent is linear up to 2051 s and by that time 89.02% of the solvent has been removed. This linear trend shows the external mass transfer is dominating and drying is externally controlled. After this, there is a very slow decrease in the residual solvent with time. The ultimate residual solvent that is permanently trapped in the coating is 6.64%.

Figure 2.9a shows the concentration of PS, PMMA, and TOL with time coating having 5.08% PS, 10.11% PMMA, and 84.81% TOL, and 896 μm thickness

in the beginning. Figure 2.9b shows the coating thickness and percentage residual within the coating with time. The drying trend, in this case, is similar to that of a previous coating having 4.99% PS, 5.04% PMMA, 89.97% TOL, and 881 μm thickness. The drying trend is linear up to 3311 s. The drying is almost over by 4861 s because after that there is no appreciable change in the residual solvent content for the very long time period i.e. residual solvent left after 6467 s is 4.23%.

Figure 2.10a shows the concentration of PS, PMMA, and TOL with time coating having 10.06% PS, 5.03% PMMA, and 84.91% TOL, and 951 μm thickness in the beginning. Figure 2.10b shows the coating thickness and percentage residual within the coating with time. The drying trend is linear up to 3111 s. The drying is almost over by 4517 s because after that there is no appreciable change in the residual solvent content for the very long time period i.e. residual solvent left after 6392 s is 9.04%.

Figure 2.11a shows the concentration of PS, PMMA, and TOL with time coating having 9.93% PS, 9.94% PMMA, and 80.14% TOL, and 931 μm thickness in the beginning. Figure 2.11b shows the coating thickness and percentage residual within the coating with time. There is a rapid decrease in the residual solvent percentage in the beginning due to high evaporation rate. A constant period is followed in the initial phase of drying. The linear trend is upto 3162 s, and by that time 83.64% of the solvent has been removed. The ultimate solvent evaporated very slowly at the end of the drying and the ultimate residual solvent left in the coating was 8.65%. Table 2.2 represents the summarized drying data of the PS-PMMA-TOL.

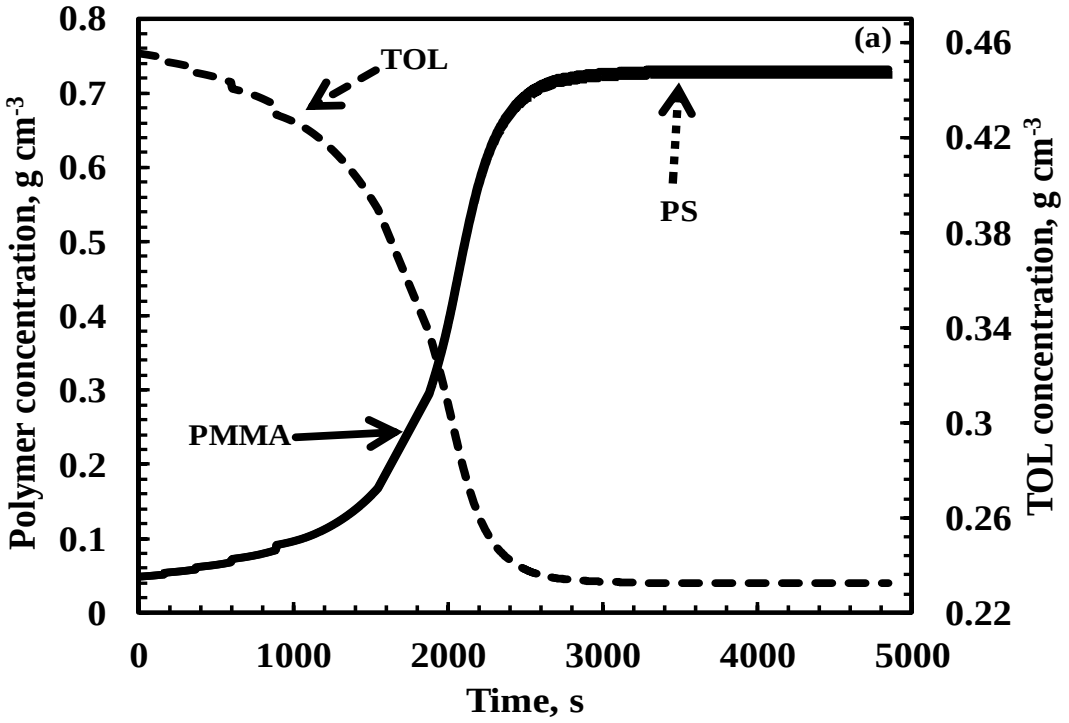

Figure 2.8 (a): Average concentration of solvent and polymers with time. in PS-PMMA-TOL coating. PS, PMMA, and TOL were 4.99 %, 5.04%, and 89.97% respectively. Initial thickness of coating and temperature were: 881 microns and 25˚C, respectively.

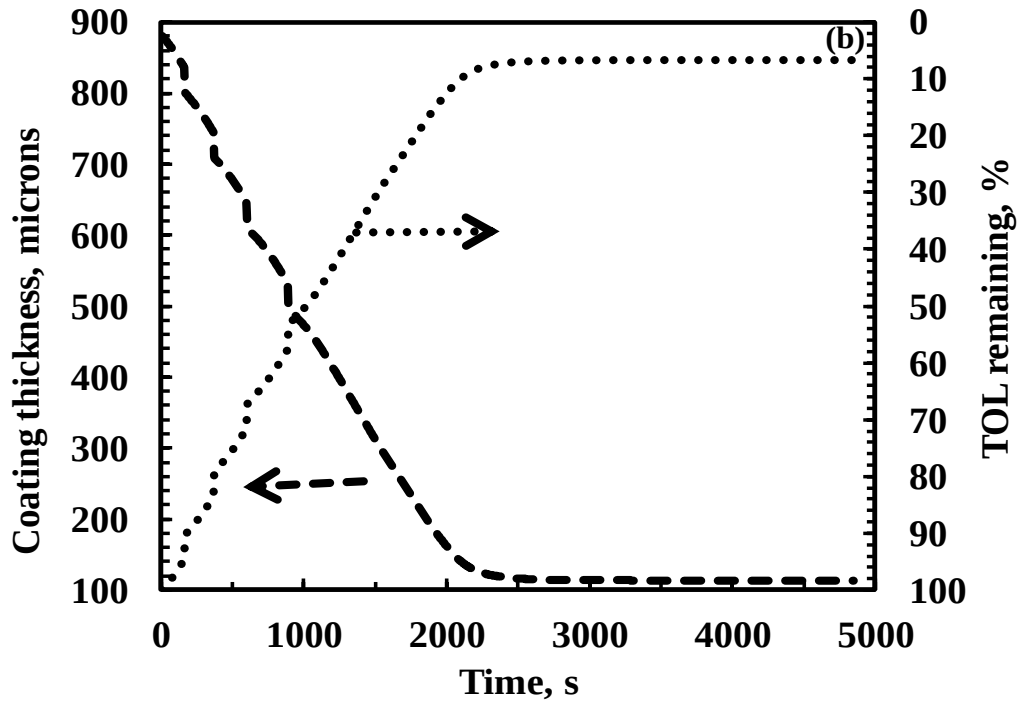

Figure 2.8 (b): Coating thickness and % TOL remaining with time in PS-PMMA-TOL coating. PS, PMMA, and TOL were 4.99 %, 5.04%, and 89.97% respectively. Initial thickness of coating and temperature were: 881 microns and 25 ˚C, respectively.

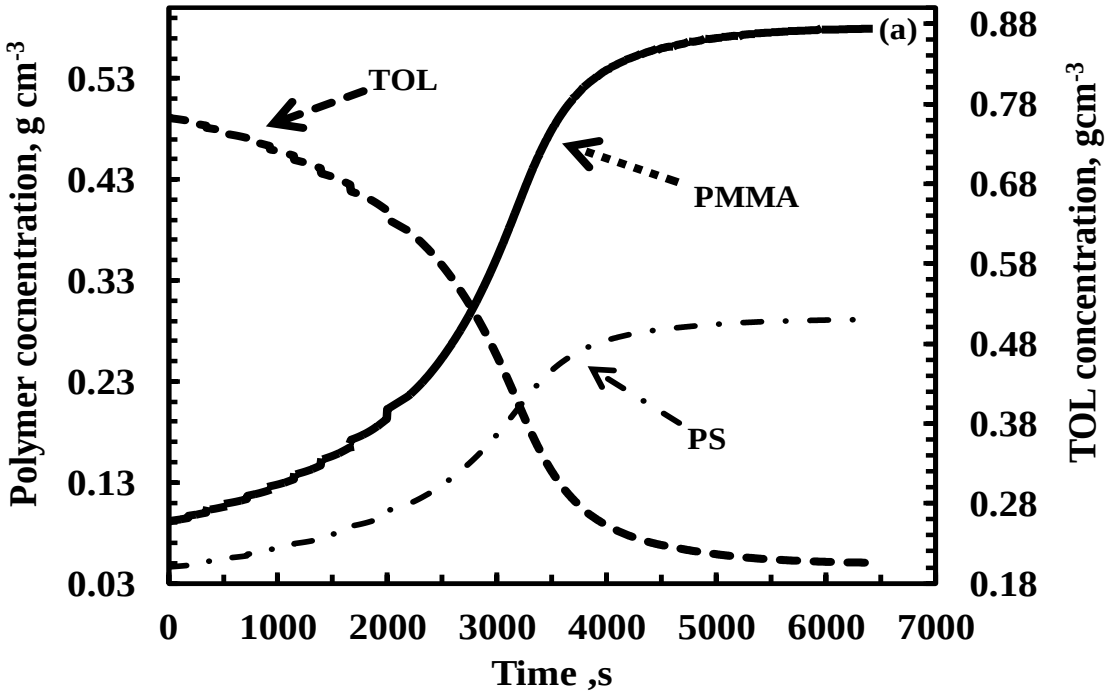

Figure 2.9(a): Average concentration of solvent and polymers with time in PS-PMMA-TOL coating. PS, PMMA, and TOL were 5.08%, 10.11%, and 84.81% respectively. Initial thickness of coating and temperature were: 896 microns and 25°C, respectively.

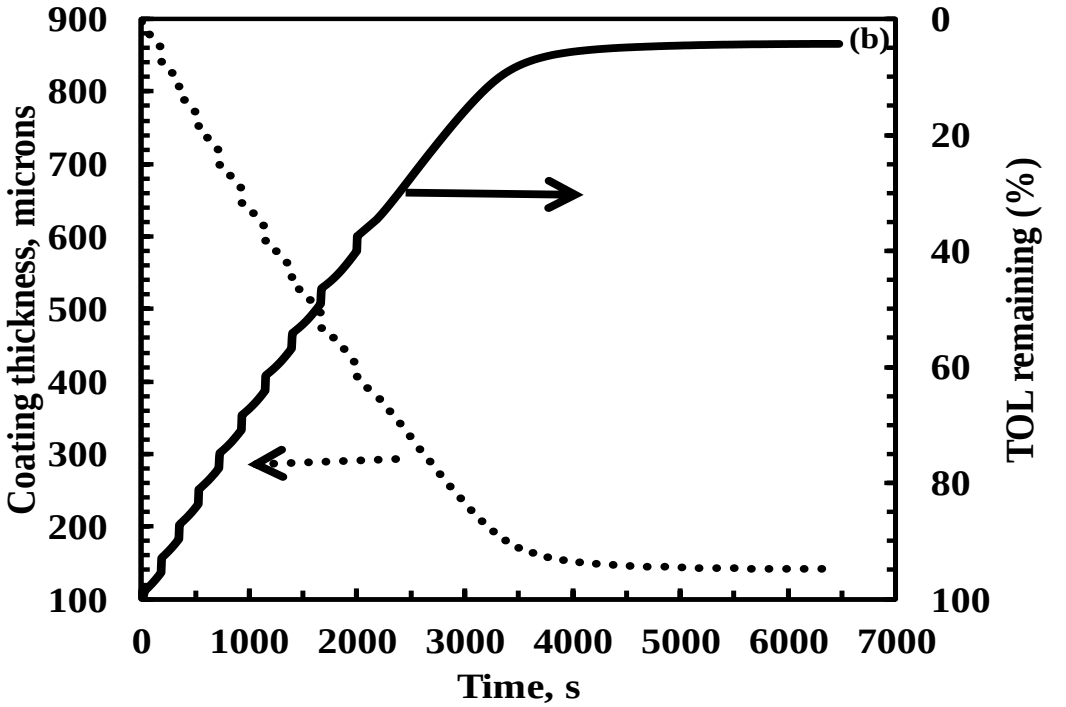

Figure 2.9(b): Coating thickness and % TOL remaining with time in PS-PMMA-TOL coating. PS, PMMA, and TOL were 5.08%, 10.11%, and 84.81% respectively. Initial thickness of coating and temperature were: 896 microns and 25°C, respectively.

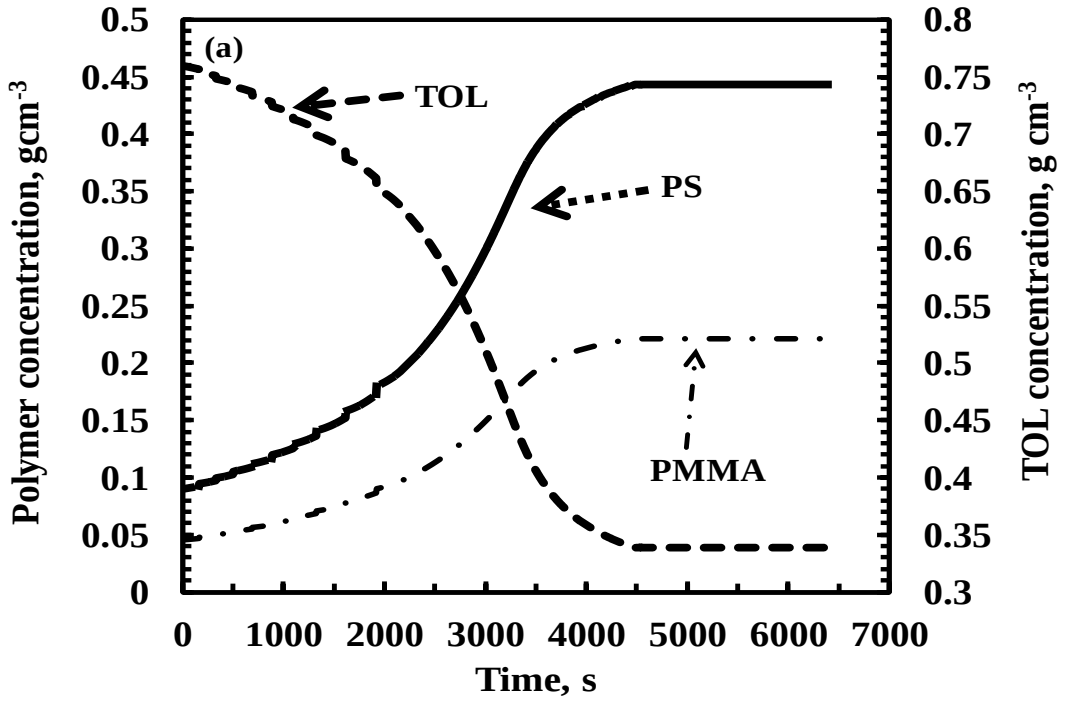

Figure 2.10(a): Average concentration of solvent and polymers with time in PS-PMMA-TOL coating. PS, PMMA, and TOL were 10.06%, 5.03%, and 84.91% respectively. Initial thickness of coating and temperature were: 951 microns and 25˚C, respectively.

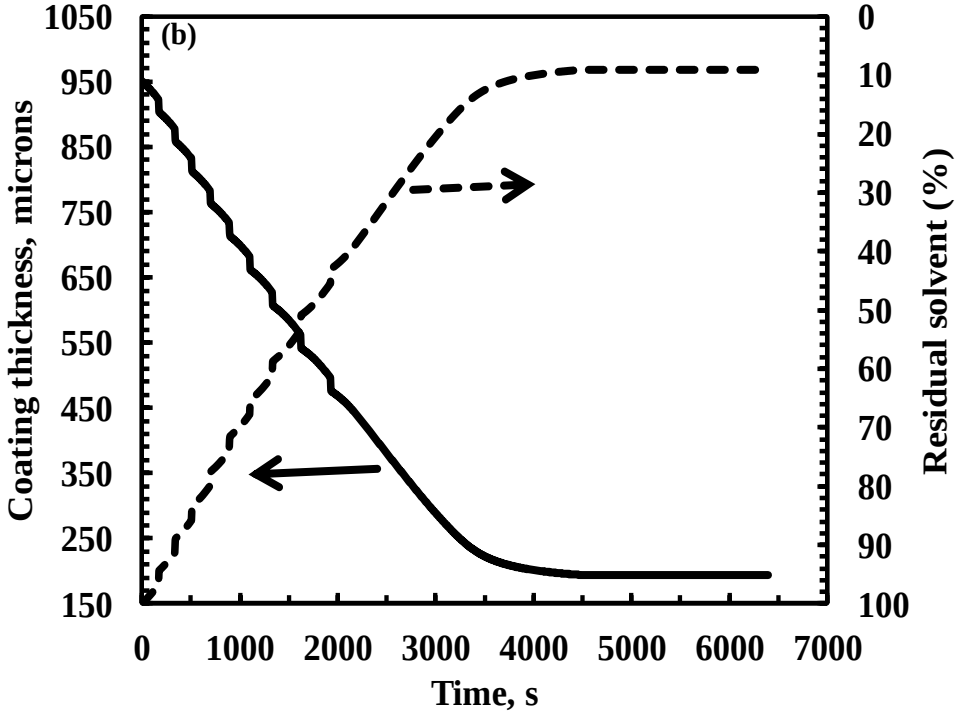

Figure 2.10(b): Coating thickness and % TOL remaining with time in PS-PMMA-TOL coating. PS, PMMA, and TOL were 10.06%, 5.03%, and 84.91% respectively. Initial thickness of coating and temperature were: 951 microns and 25 ˚C, respectively.

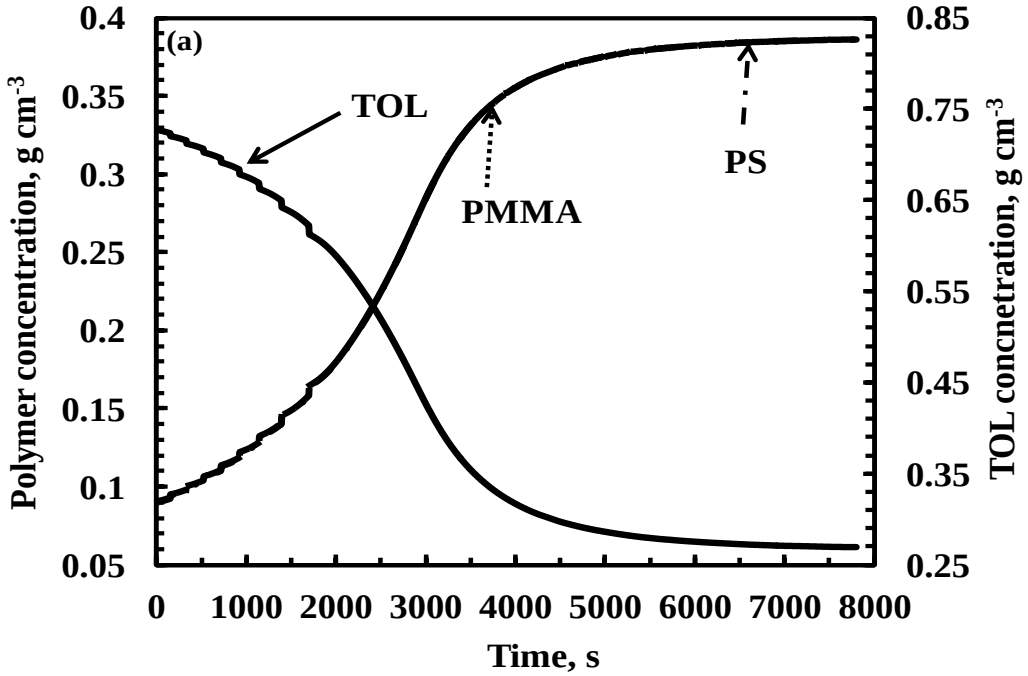

Figure 2.11(a): Average concentration of solvent and polymers with time in PS-PMMA-TOL coating. PS, PMMA, and TOL were 9.93%, 9.94%, and 80.14% respectively. Initial thickness of coating and temperature were: 931 microns and 25˚C, respectively.

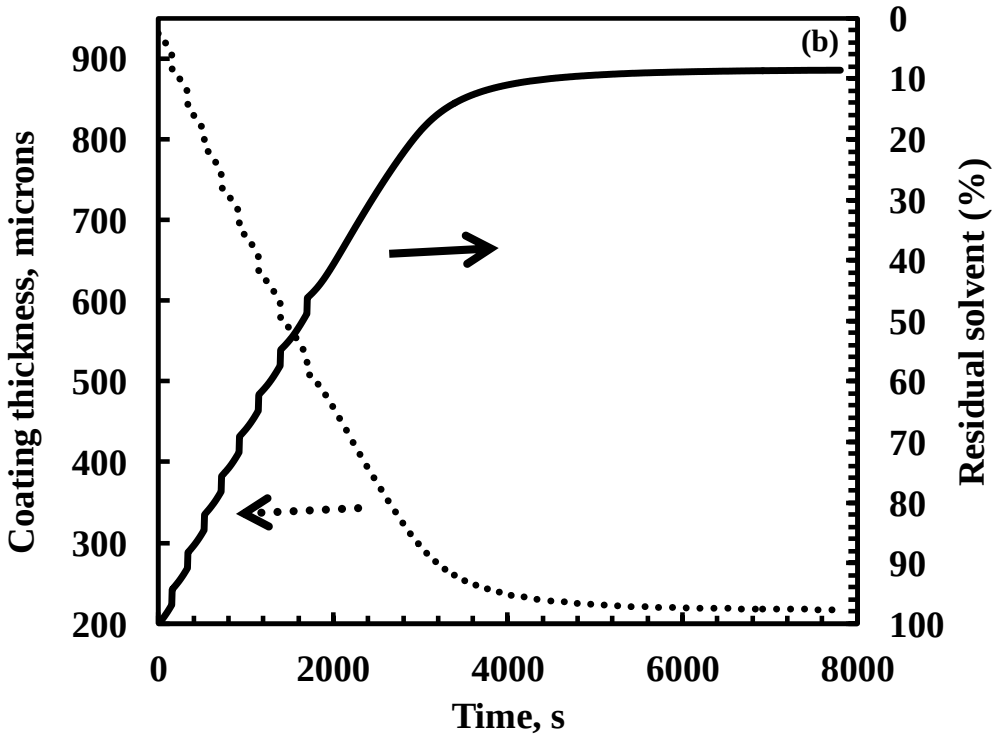

Figure 2.11(b): Average concentration of solvent and polymers with time. (b): Coating thickness and % TOL remaining with time in PS-PMMA-TOL coating. PS, PMMA, and TOL were 9.93%, 9.94%, and 80.14% respectively. Initial thickness of coating and temperature were: 931 microns and 25˚C, respectively.

Table 2.2: Summarized drying data of the PS-PMMA-TOL coatings.

S.No	PS (%)	PMMA (%)	TOL (%)	Initial Thickness (microns)	Final Thickness (microns)	Residual Solvent (%)
1.	4.99	5.04	89.97	881	114	6.64
2.	10.06	5.03	84.91	951	148	9.04
3.	9.93	9.94	80.14	931	217	8.65
4.	5.08	10.11	84.81	896	141	4.23

2.6 Conclusions

The residual solvent content in the PS-PMMA-TOL coatings followed the same trend as in the case of PS-PMMA-THF coating. This system also has not changed appreciably by changing the poly(styrene) content. The change in poly(methyl methacrylate) mass fraction slow down the drying process and coatings are taking very long time to drying. The thermodynamics of this system is a strong function of the poly(methyl methacrylate) mass fraction.

Part 2C. Residual solvent study in PS-PMMA-EB System

2.7 Results and Discussion

The coatings of initially homogeneous poly(styrene)-poly(methyl methacrylate)-ethylbenzene system have been discussed in this section of the chapter. Figure 2.12a shows the average concentrations of poly(styrene) (PS), poly(methyl methacrylate) (PMMA), and ethylbenzene (EB) with time. PS, PMMA, and EB mass percentage in the beginning were 5.01 %, 5.2%, and 89.79% respectively. Figure 2.12b shows the coating thickness and percentage residual solvent remaining with time in the same system. The initial coating thickness was 1225 μm. The fall in residual solvent is linear up to 20754 s and by that time 94.01% of the solvent has been removed. After this, there is a very slow decrease in the residual solvent with

time. The ultimate residual solvent that is permanently trapped in the coating is 4.52%.

Figure 2.13a shows the concentration of PS, PMMA, and EB with time coating having 4.96% PS, 10.05% PMMA, and 84.99% TOL, and 1210 µm thickness in the beginning. Figure 2.13b shows the coating thickness and percentage residual within the coating with time. The drying trend is linear up to 155371 s. The ultimate residual solvent that is permanently trapped in the coating is 3.18%. By doubling the PMMA concentration, the ultimate residual solvent is not much changed as compared to the previous case, but drying is bit faster than the previous case with same concentration of the polymer.

Figure 2.14a shows the concentration of PS, PMMA, and EB with time coating having 10.14% PS, 5.12% PMMA, and 84.74% EB, and 1207 µm thickness in the beginning. Figure 2.14b shows the coating thickness and percentage residual within the coating with time. The drying trend is linear up to 14362 s, and by that time 85.53% of the solvent has been removed. The ultimate solvent evaporated very slowly at the end of the drying and the ultimate residual solvent left in the coating was 3.30%.

Figure 2.15a shows the concentration of PS, PMMA, and EB with time coating having 10.37% PS, 10.23% PMMA, and 79.40% EB, and 1181 µm thickness in the beginning. Figure 2.15b shows the coating thickness and percentage residual within the coating with time. The linear trend is upto 13734 s, and by that time 88.66% of the solvent has been removed. The ultimate solvent evaporated very slowly at the end of the drying and the ultimate residual solvent left in the coating was 4.75%.

The drying time is significantly affected in this case. The coatings are taking more drying time, approximately 20,000 s, which is almost four times the previous two systems that is PS-PMMA-THF and PS-PMMA-TOL. The coatings are taking more drying time, approximately 20,000 s which is almost four times the previous two systems that is PS-PMMA-THF and PS-PMMA-TOL. This could be due to the low glass transition of coatings than the other two systems, which results in the higher

drying time than the other two ternary systems. The summarized drying data of this system is shown in Table 2.3.

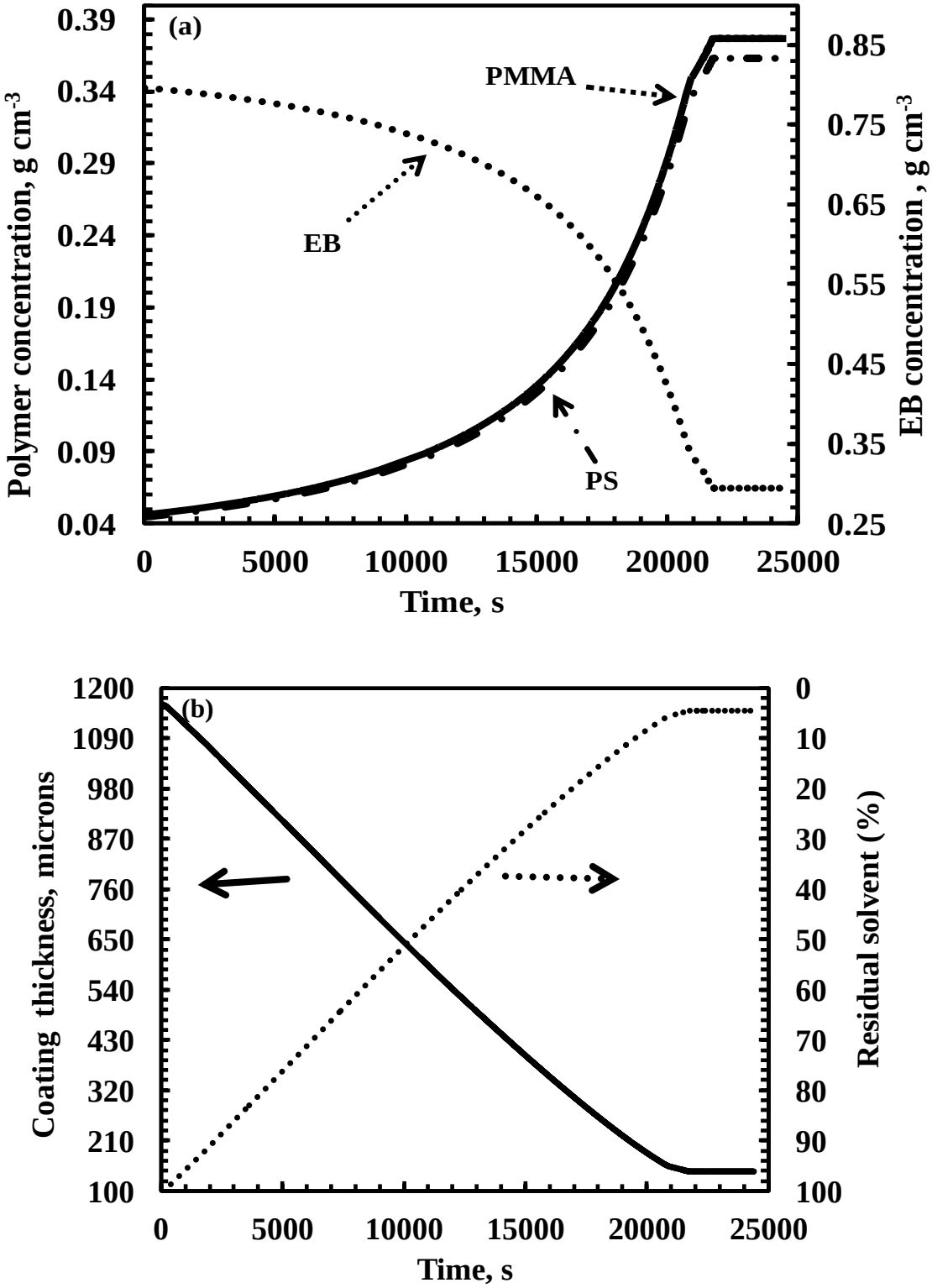

Figure 2.12(a): Average concentration of solvent and polymers with time. (b): Coating thickness and residual solvent with time in PS-PMMA-EB coating. PS, PMMA, and EB were 5.01%, 5.2%, and 89.79% respectively. Initial thickness of coating and temperature were: 1225 microns and 25 °C, respectively.

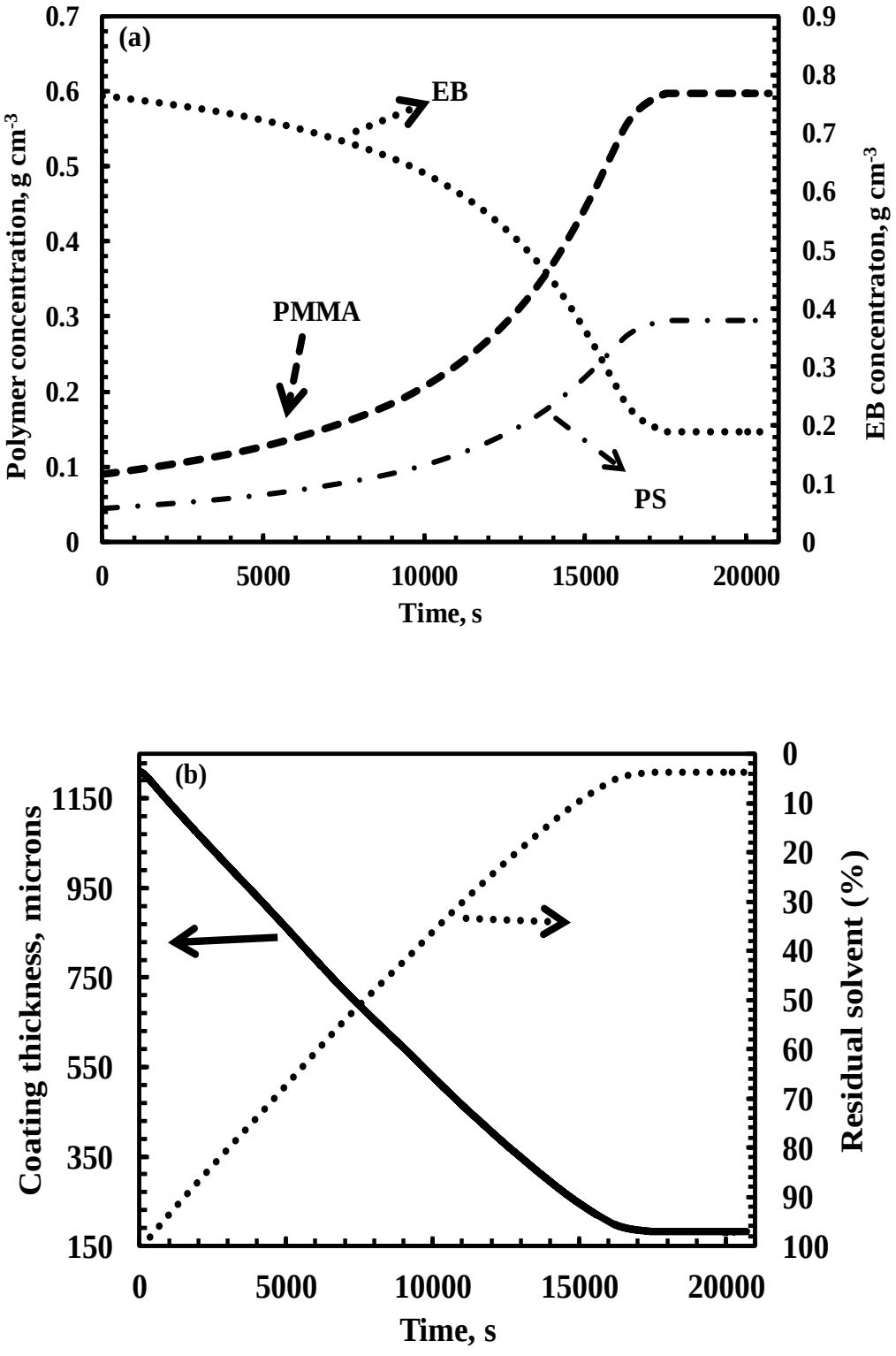

Figure 2.13(a): Average concentration of solvent and polymers with time. (b): Coating thickness and residual solvent with time in PS-PMMA-EB coating. PS, PMMA, and EB were 4.96%, 10.05%, and 84.99% respectively. Initial thickness of coating and temperature were: 1210 microns and 25 °C, respectively.

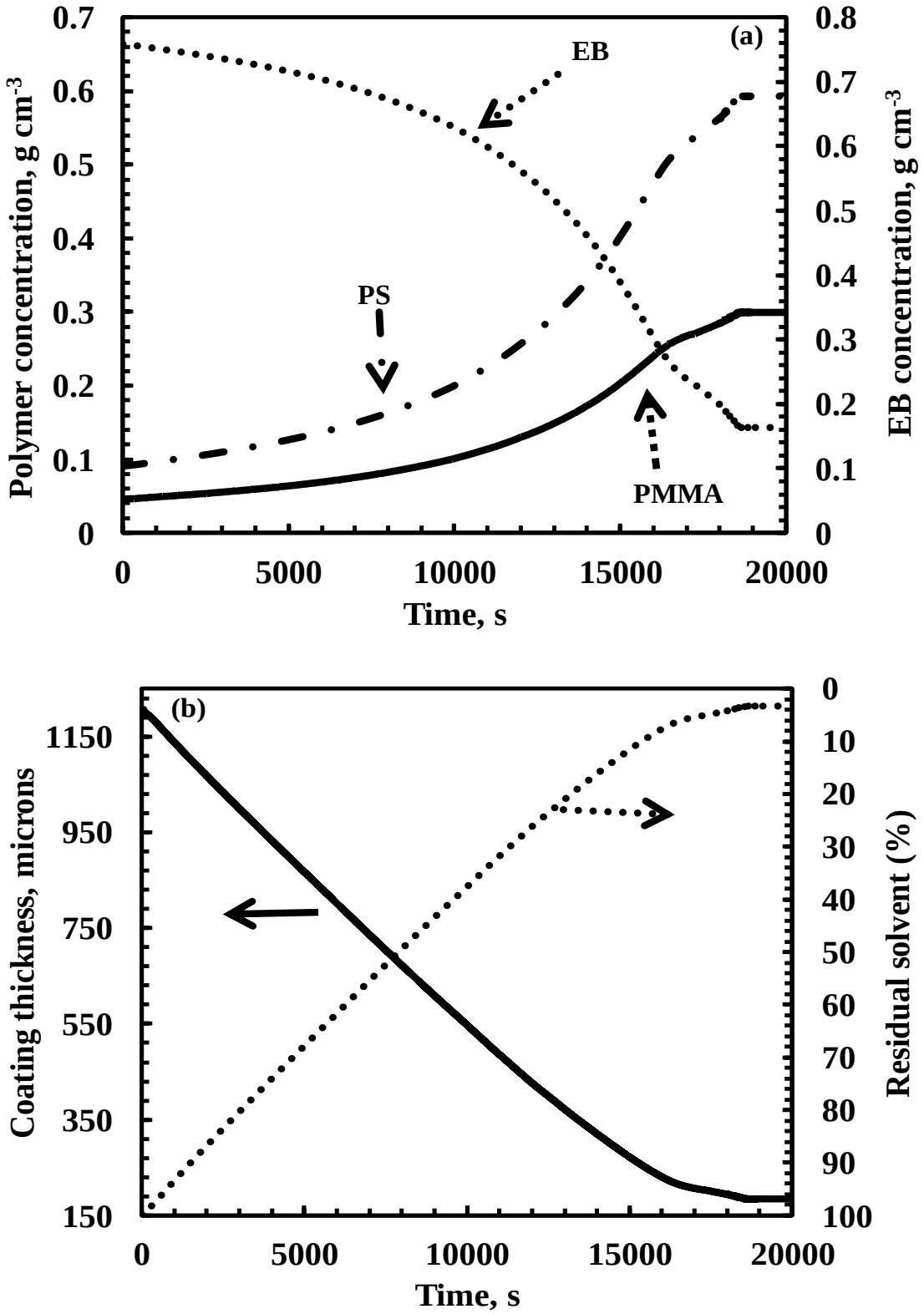

Figure 2.14(a): Average concentration of solvent and polymers with time. (b): Coating thickness and residual solvent with time in PS-PMMA-EB coating. PS, PMMA, and EB were 10.14%, 5.12%, and 84.74% respectively. Initial thickness of coating and temperature were: 1207 microns and 25 °C, respectively.

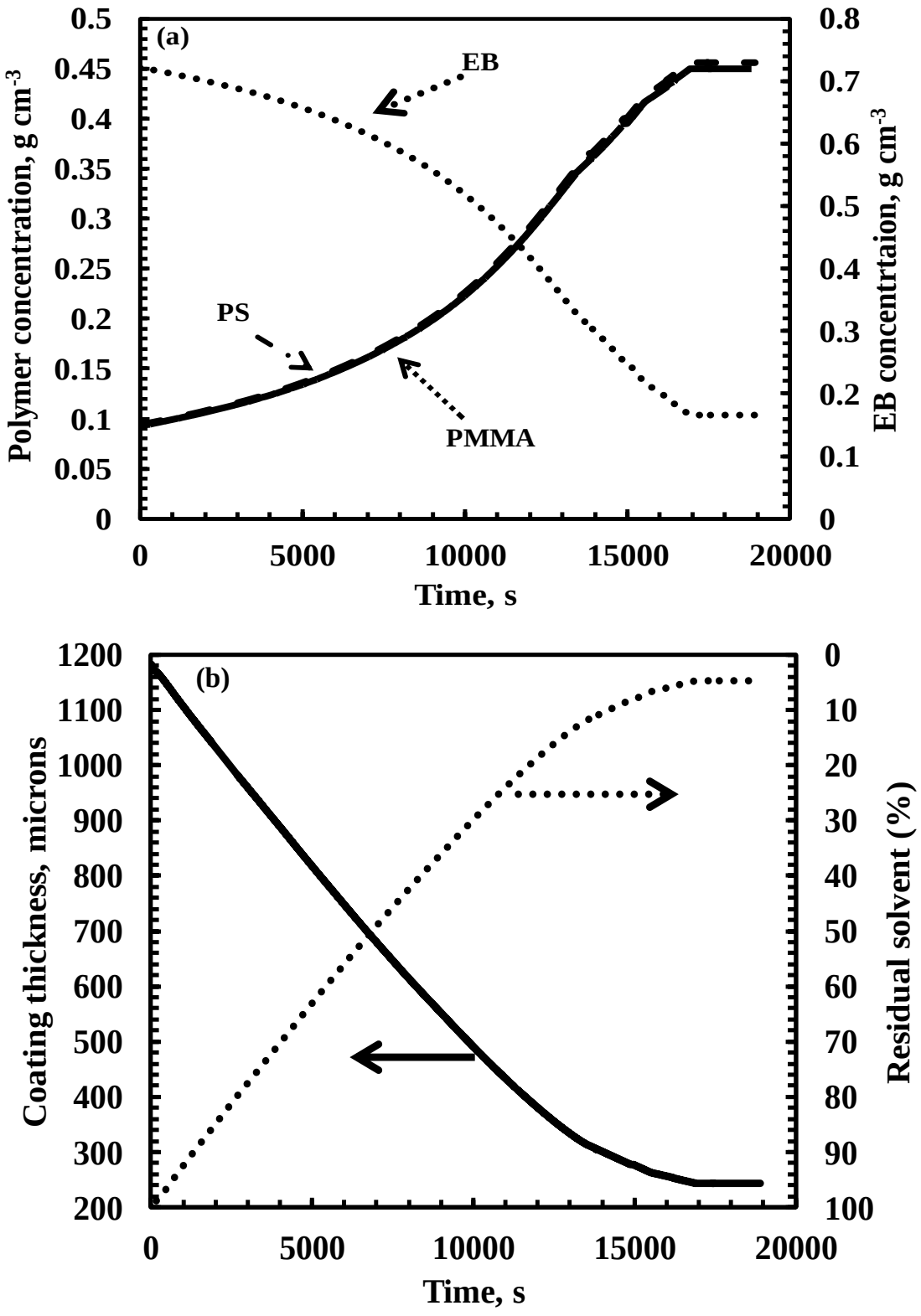

Figure 2.15(a): Average concentration of solvent and polymers with time. (b): Coating thickness and residual solvent with time in PS-PMMA-EB coating. PS, PMMA, and EB were 10.37%, 10.23%, and 79.4% respectively. Initial thickness of coating and temperature were: 1181 microns and 25 °C, respectively.

Table 2.3: Summarized drying data of the PS-PMMA-EB coatings.

S.No	PS (%)	PMMA (%)	EB (%)	Initial Thickness (microns)	Final Thickness (microns)	Residual Solvent (%)
1.	5.01	5.2	89.79	1225	150	4.52
2.	10.14	5.12	84.74	1207	185	3.30
3.	10.37	10.23	79.4	1181	244	4.75
4.	4.96	10.05	84.99	1210	177	3.18

2.8 Conclusions

The residual solvent content in PS-PMMA-EB does not change with the mass fraction of both the polymers. However, the coatings are taking more drying time, approximately 20,000 s, which is almost four times than the previous two systems that is PS-PMMA-THF and PS-PMMA-TOL. This could be due to the low glass transition of coatings than the other two systems.

References

[1] C. Panayiotou, J. Vera, Thermodynamics of polymer–polymer–solvent and block copolymer–solvent systems I. Experimental measurements, Polymer journal, 16 (1984) 89-102.

[2] C. Panayiotou, J. Vera, Thermodynamics of Polymer–Polymer–Solvent and Block Copolymer–Solvent Systems II. Theoretical Treatment of Data with the Nonrandom New Flory Theory, Polymer journal, 16 (1984) 103-112.

[3] A. Clark, Direct analysis of experimental tie line data (two polymer–one solvent systems) using Flory–Huggins theory, Carbohydrate polymers, 42 (2000) 337-351.

[4] R.L. Scott, The thermodynamics of high polymer solutions. V. Phase equilibria in the ternary system: polymer 1—polymer 2—solvent, The Journal of Chemical Physics, 17 (1949) 279-284.

[5] G. He, J. Yang, X. Zheng, Q. Wu, L. Guo, M. Zhang, X. Chen, Entanglement and phase separation in hyperbranched polymer/linear polymer/solvent ternary blends, Polymer Testing, 31 (2012) 182-190.

[6] P.J. Flory, Thermodynamics of high polymer solutions, The Journal of Chemical Physics, 9 (1941) 660-660.

[7] E. Favre, Q. Nguyen, R. Clement, J. Neel, Application of Flory-Huggins theory to ternary polymer-solvents equilibria: A case study, European polymer journal, 32 (1996) 303-309.

[8] J. Vrentas, J. Duda, Diffusion in polymer—solvent systems. I. Reexamination of the free-volume theory, Journal of Polymer Science: Polymer Physics Edition, 15 (1977) 403-416.

[9] J. Vrentas, J. Duda, Diffusion in polymer–solvent systems. II. A predictive theory for the dependence of diffusion coefficients on temperature, concentration, and molecular weight, Journal of Polymer Science: Polymer Physics Edition, 15 (1977) 417-439.

[10] J. Vrentas, J. Duda, H.C. Ling, Self-diffusion in polymer-solvent-solvent systems, Journal of Polymer Science: Polymer Physics Edition, 22 (1984) 459-469.

[11] S. Alsoy, J.L. Duda, Modeling of multicomponent drying of polymer films, AIChE journal, 45 (1999) 896-905.

[12] J.M. Zielinski, B.F. Hanley, Practical friction-based approach to modeling multicomponent diffusion, AIChE journal, 45 (1999) 1-12.

[13] M. Dabral, Solidification of coatings: theory and modeling of drying, curing and microstructure growth, 1999, Ph.D. Thesis, University of Minnesota, Minnepolis, MN, USA.

[14] R.J. Bearman, On the molecular basis of some current theories of diffusion1, The Journal of Physical Chemistry, 65 (1961) 1961-1968.

[15] I. Hadj Romdhane, P.E. Price, C.A. Miller, P.T. Benson, S. Wang, Drying of glassy polymer films, Industrial & engineering chemistry research, 40 (2001) 3065-3075.

[16] R.A. Yapel, A physical model of the drying of coated films, in, University of Minnesota, USA, Minneapolis, 1988.

[17] S. Alsoy, J. Duda, Drying of solvent coated polymer films, Drying Technology, 16 (1998) 15-44.

[18] S. Alsoy, Predicting drying in multiple-zone ovens, Industrial & engineering chemistry research, 40 (2001) 2995-3001.

[19] W. Schabel, P. Scharfer, M. Kind, Measurement and Simulation of Concentration Profiles During Drying of Thin Films with Help of Confocal-Micro-Raman Spectroscopy, Chemie Ingenieur Technik, 75 (2003) 1105-1106.

[20] W. Schabel, P. Scharfer, M. Muller, I. Ludwig, M. Kind, Measurement and simulation of concentration profiles in the drying of binary polymer solutions, Chemie Ingenieur Technik, 75 (2003) 1336-1344.

[21] P. Scharfer, W. Schabel, M. Kind, Modelling of alcohol and water diffusion in fuel cell membranes—experimental validation by means of in situ Raman spectroscopy, Chemical Engineering Science, 63 (2008) 4676-4684.

[22] R.K. Arya, Measurement of concentration profiles in thin film binary polymer-solvent coatings using confocal Raman spectroscopy: Free volume model validation, Drying Technology, 32 (2014) 992-1002.

[23] R.K. Arya, M. Vinjamur, Measurement of concentration profiles using confocal Raman spectroscopy in multicomponent polymeric coatings—model validation, Journal of Applied Polymer Science, 128 (2013) 3906-3918.

[24] M. Dabral, L. Francis, L. Scriven, Drying process paths of ternary polymer solution coating, AIChE journal, 48 (2002) 25-37.

[25] P.E. Price, I.H. Romdhane, Multicomponent diffusion theory and its applications to polymer-solvent systems, AIChE journal, 49 (2003) 309-322.

[26] R.J. Bearman, On The Molecular Basis Of Some Current Theories Of Diffusion, The Journal of Physical Chemistry, 65 (1961) 1961-1968.

[27] S. Saeki, Correlation between the combinatory entropy of polymer and ideal liquid solutions: 2. Ternary polymer-polymer-solvent and binary polymer-polymer systems, Polymer, 34 (1993) 4118-4122.

[28] M. Ariyapadi, E. Nauman, Free energy of an inhomogeneous polymer-polymer-solvent system, Journal of Polymer Science Part B: Polymer Physics, 27 (1989) 2637-2646.

[29] M. Ariyapadi, E. Nauman, Gradient energy parameters for polymer–polymer–solvent systems and their application to spinodal decomposition in true ternary systems, Journal of Polymer Science Part B: Polymer Physics, 28 (1990) 2395-2409.

[30] M.V. Ariyapadi, E.B. Nauman, Free energy of an inhomogeneous polymer–polymer–solvent system. II, Journal of Polymer Science Part B: Polymer Physics, 30 (1992) 533-538.

[31] Y. Lipatov, V. Chornaya, A. Nesterov, T. Todosiichuk, Concentration dependence of thermodynamic interaction parameters in a polymer-polymer-solvent system, Polymer Bulletin, 12 (1984) 49-53.

[32] S.D. Hong, C. Burns, Compatibility of polystyrene and poly (methyl methacrylate) in benzene. Effects of molecular weight and temperature, Journal of Applied Polymer Science, 15 (1971) 1995-2006.

[33] T. Kwei, T. Nishi, R. Roberts, A study of compatible polymer mixtures, Macromolecules, 7 (1974) 667-674.

[34] T. Chow, Glass transition temperature of polymer-diluent systems, Ferroelectrics, 30 (1980) 139-145.

[35] T. Chow, Molecular interpretation of the glass transition temperature of polymer-diluent systems, Macromolecules, 13 (1980) 362-364.

[36] S.-U. Hong, Prediction of polymer/solvent diffusion behavior using free-volume theory, Industrial & engineering chemistry research, 34 (1995) 2536-2544.

Chapter 3

Effect of Coating Application Technique on Residual Solvent

Most works studied the binary combinations of PS and PMMA in different solvents such as THF, TOL, etc. However, PS-PEG-CLB system has not been much reported in the literature. Therefore, this system has been selected to study the coating application techniques that is, layer-by-layer and single thick layer.

3.1 Introduction

Polymeric coatings have a wide application in photographic films, synthetic fibres, magnetic media, optical fibres, decorative films, and storage devices [1-4]. Surface coatings consists of guide coat, prime coat, topcoat, and final repair for the protective and decorative materials in white powdered or liquid form to the substrates [5].

Coatings are made from polymer dissolved in solution and casted onto substrate to get uniform defect-free coatings. Polymer solutions of multipolymer-solvent system help in improving rheological properties, and also affect the solubility of solutions. The films produced from multi component systems have significant importance in printing and coating applications [6]. More than one component in the film leads to the coupling of the mass and momentum transport by means of surface tension gradients or viscosity [7].

Solution coatings are made from non-volatile components such as polymers, surfactants or colloidal particles, while the volatile components evaporate and result into polymeric films left over on to the substrates. Using dryers or ovens, these coatings are then dried under quiescent conditions with or without air flow [8].

Being the most important step, drying converts the rubbery state of the coating into the glassy state. It is considered as the last and quality-controlling step of the polymeric film production, which determines the final structure and altere the properties of the coatings. To avoid the possible defects due to improper drying, like cracks, blisters, blissing, phase separations, etc. a well controlled drying process is to be followed. Solidification of wet film in the course of drying can be done by the removal of solvents (i.e, crystalisation, vitrification, gelation) or by reactions (i.e radiation curing or polymerization) [9]. Drying is governed by the transportation and removal of solvent within and from the coating, respectively, which in turn affects the properties of the film, crystallinity of the polymer, and physicomechanical properties of the film [10]. The nature of the polymer changes during the course of drying which can affect the drying process and the mass transfer rate too. Drying process slows down with the increase in the crystallinity of polymeric solutions.

There are several methods for drying of coatings such as controlled drying, thermal drying, condensation drying, etc. The quality of the polymeric films can be controlled by maintaining the required drying conditions. There are many research groups working on the reduction of residual solvent to obtain the minimal-defect or defect-free coatings [8, 11-13].

Diffusion is the phenomenon that is responsible for the transport of solvent in the polymer-solvent system. Mass and heat transfers are the simultaneous processes occuring in the overall drying process. The multi-component mass and heat transport occur in various procedures such as membrane manufacturing, coating processing, and polymerization reactions. Heat transport regulates the temperature profile and the mass transport helps in determining the composition dependent material properties such as surface tension and viscosity. Diffusion is known to be the rate controlling step in the polymer(s)-solvent(s) systems during transportation, which takes place within the polymeric coatings, whereas ‘evaporation’ controls the mass transport from the coating into the surrounding air/gases. Diffusion coefficient varies with the solvent concentration falls in the case of polymeric coating. As the drying proceeds, the concentration of the solvent at the exposed surface drops. Hence, the drying rate falls steadily. This period is called the falling rate period [14]. Diffusion also influences the residual solvent as well as the drying characteristics of the coating [15].

Siebel et al. [15] studied the binary solutions of poly(vinyl acetate) in methanol and toluene using inverse micro Raman spectroscopy over a wide range of concentrations. They stated that the experimental data deviated from the literature data, and that was highest at the bottom of the films of both the binary systems, due to a strong dependence of the diffusion coefficient. At the beginning of the drying procedure, the diffusion coefficient was estimated to be higher than 10^{-10} m^2/s. The calculated data was more accurately fitted with the literature data for the PVAc-toluene system than for the PVAc-Methanol system, since toluene is less volatile in nature than methanol.

Very recently, Sharma et al. [16] discussed about the free volume theory which was used by different researches that calculated the diffusion coefficient and discussed about the diffusion in the polymeric systems. They also concluded that Vrentas and Duda free volume theory is the most successful theory for predicting the diffusion coefficient of the polymer-solvent, polymer-solvent-solvent, and crosslinked polymer-solvent systems.

Arya et al. [17] studied the concentration profiles of binary coatings of poly(methyl methacrylate)-ethylbenzene and p-xylene-poly(styrene) systems using confocal raman spectroscopy and identified the area of increased value for solvent concentration. They concluded that in poly(methyl methacryalte)-ethylbenzene system, there was no steep concentration gradients due to the high diffusion of ethylbenzene, and these were different from the Fickian diffusion profile.

Pham et al. [7] developed a model for drying of multi-component thin films, that is polymer-surfactant-water system on the substrates with topography. Their results indicate that the substrate topography gives rise to non-uniform evaporation along the interface, which results in a non-uniform film where the film above the substrate crests was thinner than the film above the valleys. It was also shown that the thermal and surfactant Marangoni flows tend to amplify this non-uniformity.

Velega et al. [18] studied the drying behavior of two multi-component oral films based on hydroxypropyl methyl cellulose (amorphous) - poly(vinyl alcohol) (semicrystalline)- deionised water by using the Hill equation. Half maximal time (τ)

was successfully explained at the Fickian and non-Fickian stages. Their results showed the enhancement in the drying rate after the half maximal time with decrease in temperature. The drying rate first decreased with increase in temperature and then leveled off. There was two stage diffusion of the solvent. The initial drying rate followed the Fickian diffusion rules, and the later followed the non Fickian diffusion.

Yan et al. [19] worked on the layer-by-layer (LBL) technique for two coatings, namely polyethylenimine (PEI)-α zirconium phosphate (ZrP) and polyethylenimine (PEI)- ammonium polyphosphate(APP)-deionised water, and deposited them on ramie fabrics. Their thermogravimetric analysis (TGA), microscale combustion calorimeter (MCC), and vertical flame test (VFT) analysis advocated the LBL coatings since it enhanced the flame retardancy of the ramie fabrics. The system of PEI-ZrP coated inside and PEI-APP coated outside proved to be effective and provided good flame retardancy.

There is not much significant work reported in the field of polymer-polymer-solvent coatings. In the present study, poly(styrene) (PS)- poly(ethylene glycol) (PEG) – chlorobenzene (CLB) system has been selected to understand the drying mechanism. Coatings were designed through the layer-by-layer and single-layer methods to minimize the residual solvent to get the desired thickness. Multilayer and single thick layer coatings were designed to reduce the residual solvent. Solvent casting method was used to make thin films. Drying experiments were performed under quiescent condition without any air flow. The effect of coating methods on the coating thickness was discussed in detail. Hence, this study can help us choose the better method for minimizing the residual solvent and making perfect glassy films.

3.2 Materials and Methods

Poly(styrene) (PS) having density 1.05 g cm^{-3} and molecular weight 192000 and Poly(ethylene glycol)-6000 **(**Molecular weight: 5,000-7,000, density: 1.2 g cm^{-3}) (Sigma Aldrich, Germany). Chlorobenzene (Molecular weight: 112 g/mol, density: 1.11 g cm^{-3}) was supplied by Spectrochem, India. PS-PEG-CLB solution was prepared from a measured amount of PS and PEG in CLB. The solution was shaken in

a mechanical shaker for two days, followed by manually shaking for about 4-5 times a day for one week to get a homogeneous polymeric solution. Solution casting method was used to get a uniform and thin film. Micropipette was used to pour the polymeric solution into circular sample holder having different depth (2000 µm and 4000 µm) and diameters (12.24 mm and 14.65 mm). Some amount of the solution always got stuck to the microtip, which affected its initial thickness every time. Figure 3.1 shows the schematic of the preparation of coating using single thick layer and layer-by-layer technique.

Four different solutions of PS-PEG-CLB were prepared having 5.05 wt% (PS)- 4.98 wt% (PEG)- 89.97 wt% (CLB), 5.05 wt% (PS)-10.04 wt% (PEG) -84.91 wt% (CLB), 10.06 wt% (PS)- 5.13 wt% (PEG)- 84.81 wt% (CLB), and 10.01 wt% (PS)- 9.96 wt% (PEG)- 80.02 wt% (CLB). The gravimetric data was recorded with time using semi micro analytical weighing balance (Precisa ES225SM-DR) having an accuracy of ±0.0001g. Data were recorded till no further significant change in the mass with respect to time was observed. All experiments were performed by maintaining the temperature at 8 ˚C without any air flow.

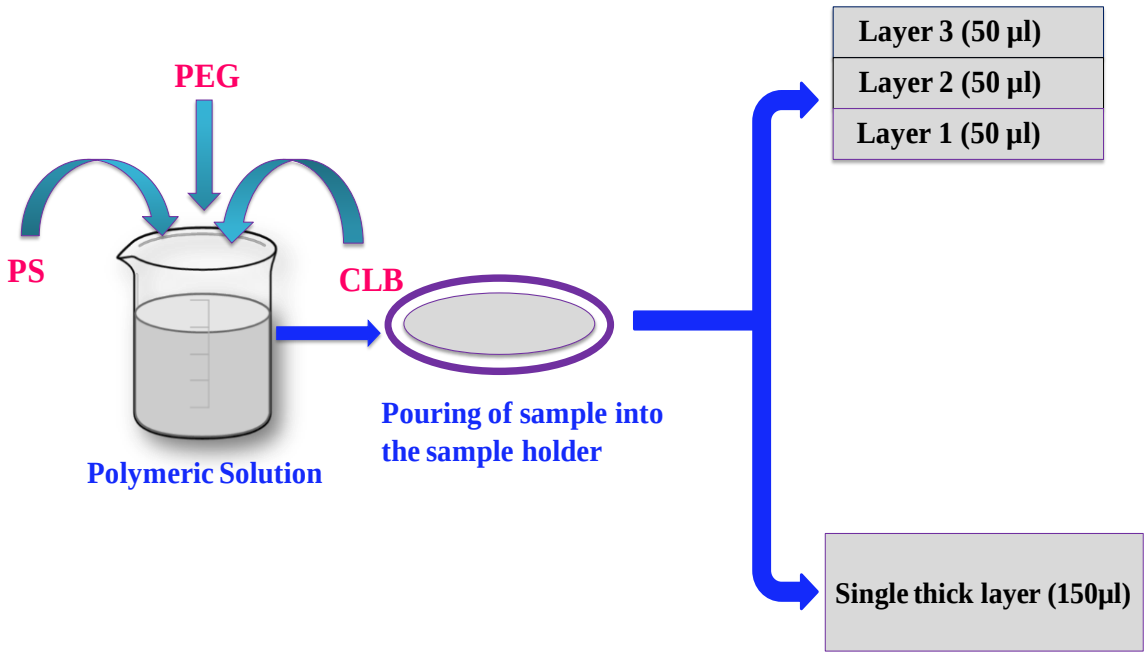

Figure 3.1: Pictorial representation of the LBL technique and a single thick layer of equal volume

In the layer-by-layer method, 50 µl of the prepared solution of a particular concentration was first poured into the sample holder. Its mass-loss data was recorded until a plateau reached. The resulting solution was left to dry for 1 week to get the first ultimate dried layer. The second layer was obtained in the same manner by drying the same solution of the same volume over the first dried layer. The same applies to the third layer. This procedure was then repeated for the 75 µl volume of the same concentration solution. The same procedure was followed for all the four different concentrations.

In the single thick layer method, the drying procedure was same. However, 150 µl of the solution was transferred into the sample holder in one go and not stage wise. The same applies to the second case wherein 225 µl solution was used.

3.3 Results and Discussion

3.3.1 PS (5.05 %) - PEG (4.98%) - CLB (89.97%) Coatings

Figure 3.2 shows the percentage residual CLB with time in PS-PEG-CLB coatings having PS (5.05%), PEG (4.98%), and CLB (89.97%) of a 50 µl solution of each layer, and a single thick layer of 150 µl. There is a rapid decrease in the residual solvent percentage in the beginning due to high evaporation rate. A constant rate period is followed in the initial phase of drying. The linear trend in the dried layers 1, 2, 3, and single thick layer is upto 5072 s, 4952 s, 4317 s, and 18091 s, and by that time 93.6%, 81.82%, 86.06% and 82.18% of the solvent has been removed, respectively. The ultimate solvent evaporated very slowly at the end of the drying and the ultimate residual solvent left in the layers 1, 2, 3, and single thick layer are 3.97%, 8.3%, 5.65%, and 12.8%, respectively. In the single thick layer, the drying is externally controlled. It shows that the diffusion in the single thick layer solution is higher as compared to the layer-by-layer solution. This could be due to the change in the polymer-polymer-solvent thermodynamics. The values of the overall residual solvent trapped inside the coatings are listed in the Table 3.1.

Figures 3.3a and 3.3b show the evolution of the coating thickness and non-dimensional coating thickness of the layer-by-layer and single thick layer coatings of PS-PEG-CLB having PS (5.05%), PEG (4.98%) and CLB (89.97%) in a 50 µl solution of each layer, and a single thick layer of 150 µl, respectively. Non dimensional thickness is defined as the ratio of instantaneous thickness to initial thickness. As shown in Figure 3.2, the single thick layer coating is taking more time as compared to the LBL coatings due to larger amount of solvent present in the coatings. Single thicker layer coating thickness of 150 µl is reduced to 271 µm in 20706 s starting from the initial thickness of 1260 µm. Layer 1, layer 2, and layer 3 in the LBL assembly are reduced to 51 µm, 71 µm, and 49 µm from their initial thickness of 377 µm, 407 µm, and 326 µm in 6882 s, 7297 s, and 5752 s, respectively.

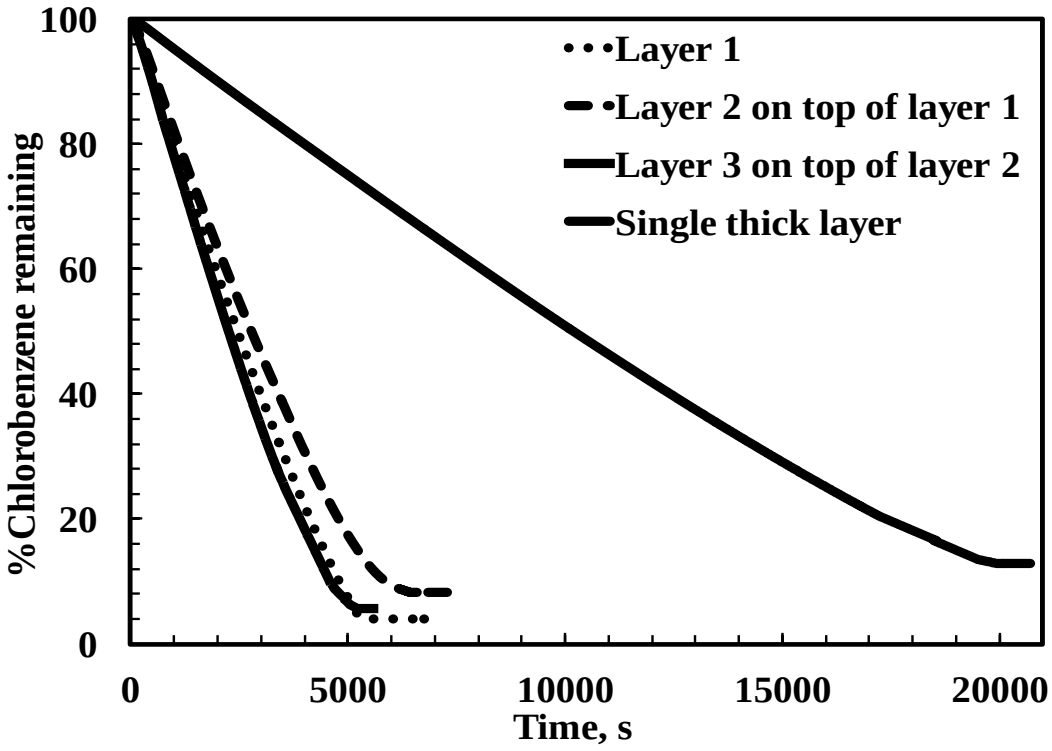

Figure 3.2: Residual solvent percentage with time in poly(styrene), poly(ethylene glycol) and chlorobenzene: 5.05 wt%, 4.98 wt% and 89.97 wt%, respectively of 50 µl injected volume at 8 ˚C.

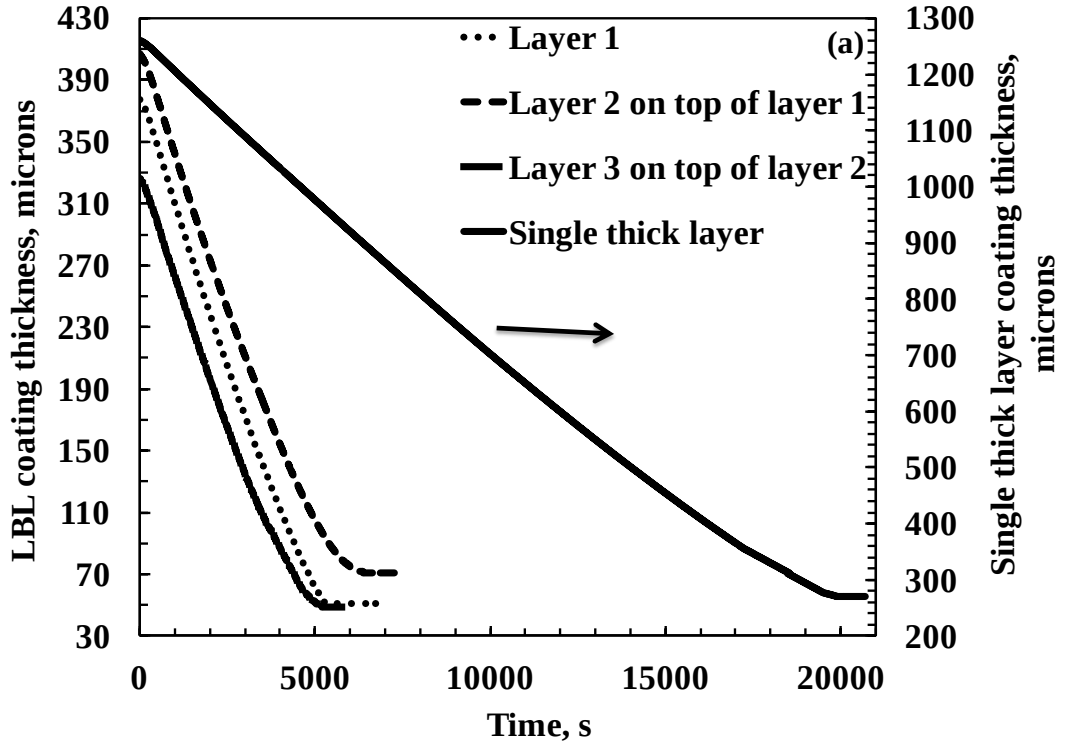

Figure 3.3 (a): Layer-by-layer coating thickness and single-layer coating thickness with time in poly(styrene), poly(ethylene glycol) and chlorobenzene: 5.05 wt%, 4.98 wt% and 89.97 wt%, respectively of 50 µl injected volume at 8 ˚C.

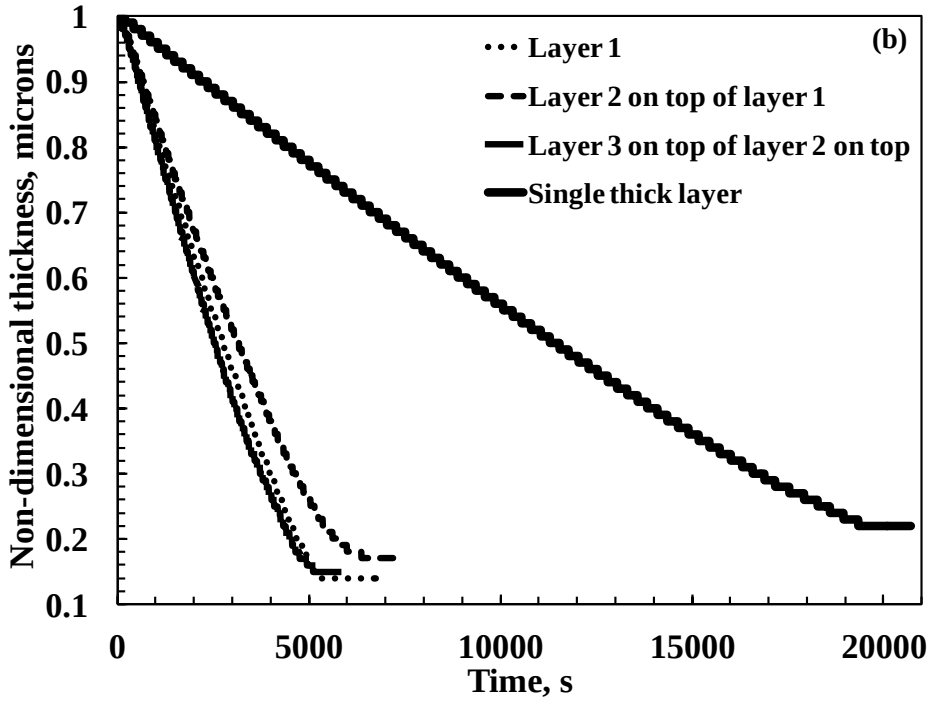

Figure 3.3 (b): Non-dimensional coating thickness with time in poly(styrene), poly(ethylene glycol) and chlorobenzene: 5.05 wt%, 4.98 wt% and 89.97 wt%, respectively of 50 µl injected volume at 8 ˚C.

Figure 3.4b shows the average concentration of poly(ethylene glycol) with time. It represents that the polymer concentration starts increasing with time due to the evaporation of chlorobenzene from the coating. In layer 1, layer 2, layer 3, and single thick layer coatings, the concentration of the polymer increases exponentially up to 5268 s, 5042 s, 5877 s, and 18741 s respectively, for the coatings having initial thickness of 377 µm, 407 µm, 326 µm, and 1260 µm respectively, and then plateaus off. The final concentration of PEG in layer 1, layer 2, layer 3 and single thick layer coating were 0.409 g cm^{-3}, 0.317 g cm^{-3}, 0.368 g cm^{-3}, and 0.25 g cm^{-3} for the coatings having initial concentration 0.055 g cm^{-3}, 0.055 g cm^{-3}, 0.055 g cm^{-3}, and 0.055 g cm^{-3}, respectively.

Figure 3.5 represents the percentage residual solvent of chlorobenzene with time having PS (5.05%), PEG (4.98%), and CLB (89.97%) of a 75 µl solution of each layer, and a single thick layer, that is, 225 µl. A constant period is followed in the initial phase of drying. The falling period in the dried layers 1, 2, 3, and single thick layer is up to 6132 s, 4158 s, 4358 s and 19748 s, and by that time 85.66%, 72.45%, 78.17%, and 85.7%, of the solvent has been removed, respectively. The ultimate residual solvent left in the layers 1, 2, 3, and single thick layer are 6.75%, 12.22%, 15.9%, and 11.69%, respectively. It also shows the same trend as in the Figure 3.2 corresponding to the case of 50 µl injected volume. The residual solvent was higher in the layer-by-layer assembly as compared to the single thick layer.

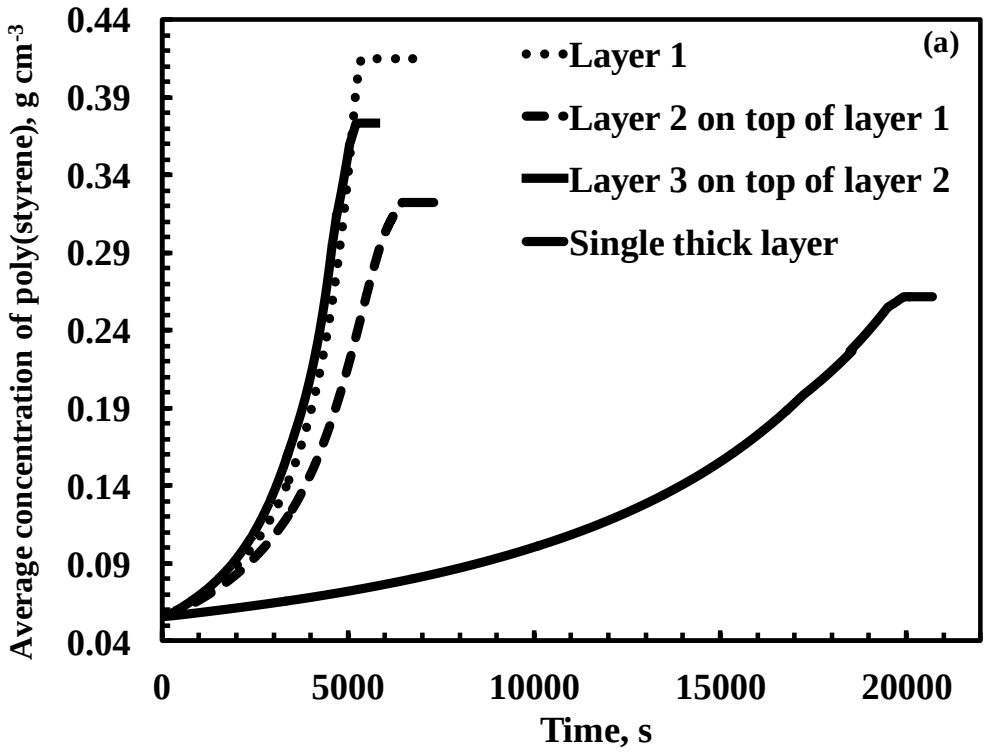

Figure 3.4(a): Average concentration of poly(styrene) with time in poly(styrene)-poly(ethylene glycol)-chlorobenzene: 5.05 wt%, 4.98 wt% and 89.97 wt%, respectively of 50 µl injected volume at 8 ˚C.

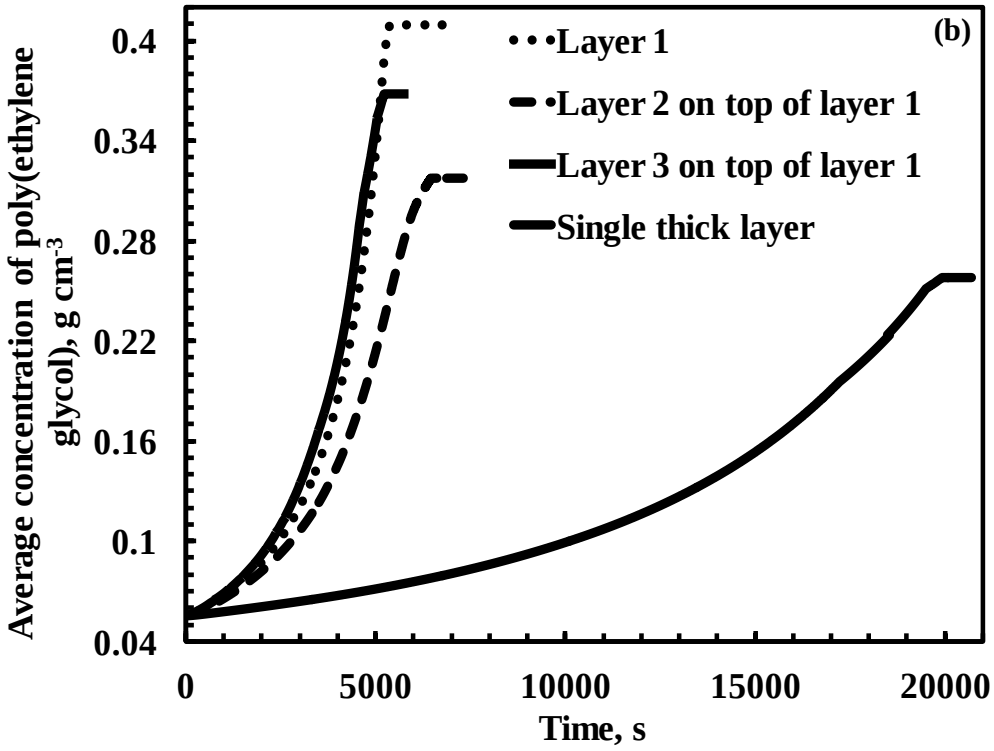

Figure 3.4(b): Average concentration of poly(ethylene glycol) with time in poly(styrene)- poly(ethylene glycol)-chlorobenzene: 5.05 wt%, 4.98 wt% and 89.97 wt%, respectively of 50 µl injected volume at 8 ˚C.

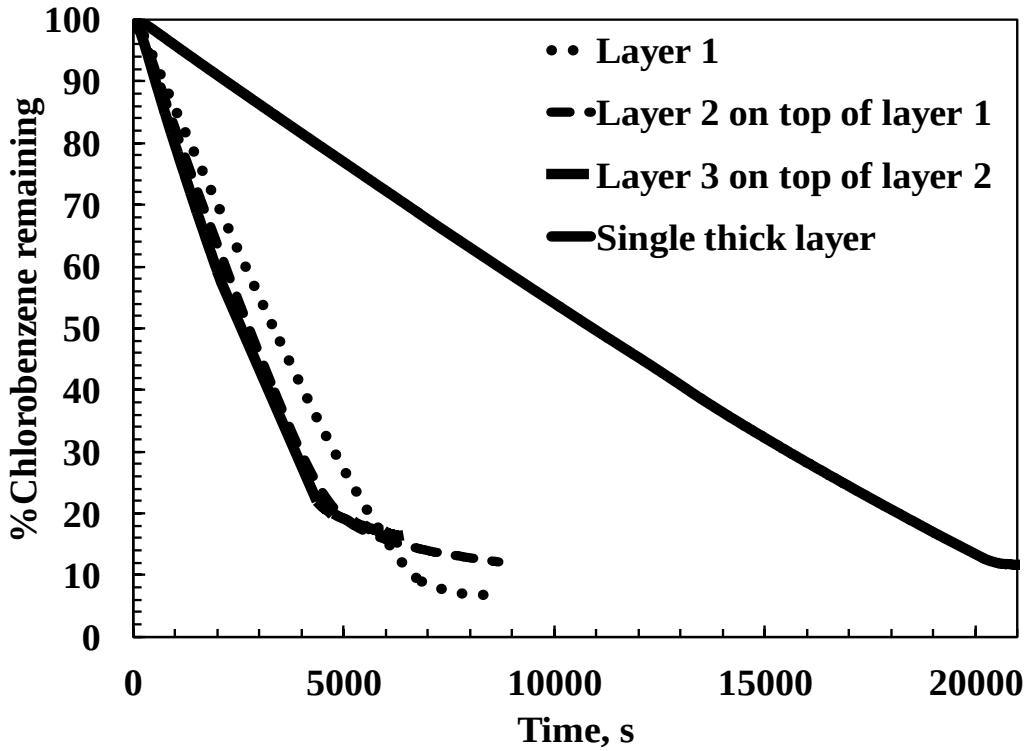

Figure 3.5: Percentage residual chlorobenzene with time in coating having poly(styrene), poly(ethylene glycol) and chlorobenzene: 5.05 wt%, 4.98 wt% and 89.97 wt%, respectively of 75 µl injected volume at 8 ˚C.

Figures 3.6a and 3.6b show the evolution of coating thickness and non-dimensional coating thickness of the layer-by-layer and single thick layer coatings of PS-PEG-CLB having PS (5.05%), PEG (4.98%) and CLB (89.97%) in a 75 µl solution of each layer and a single thick layer of 225 µl. As also shown in the Figure 3.2, the thicker coatings are taking more time as compared to the thinner coating due to larger amount of solvent present in the coatings. Single coating thickness of 225 µl is reduced to 276 µm in 21568 s starting from an initial thickness of 1349 µm. Layer 1, layer 2, and layer 3 in the LBL assembly is reduced to 109 µm, 119 µ, and122 µm, starting from an initial thickness of 678 µm, 570 µm, and 503 µm, respectively in 8728 s, 8680 s and 6489 s. It can be seen that the total thickness of the layer-by-layer assembly is more than the single thick layer.

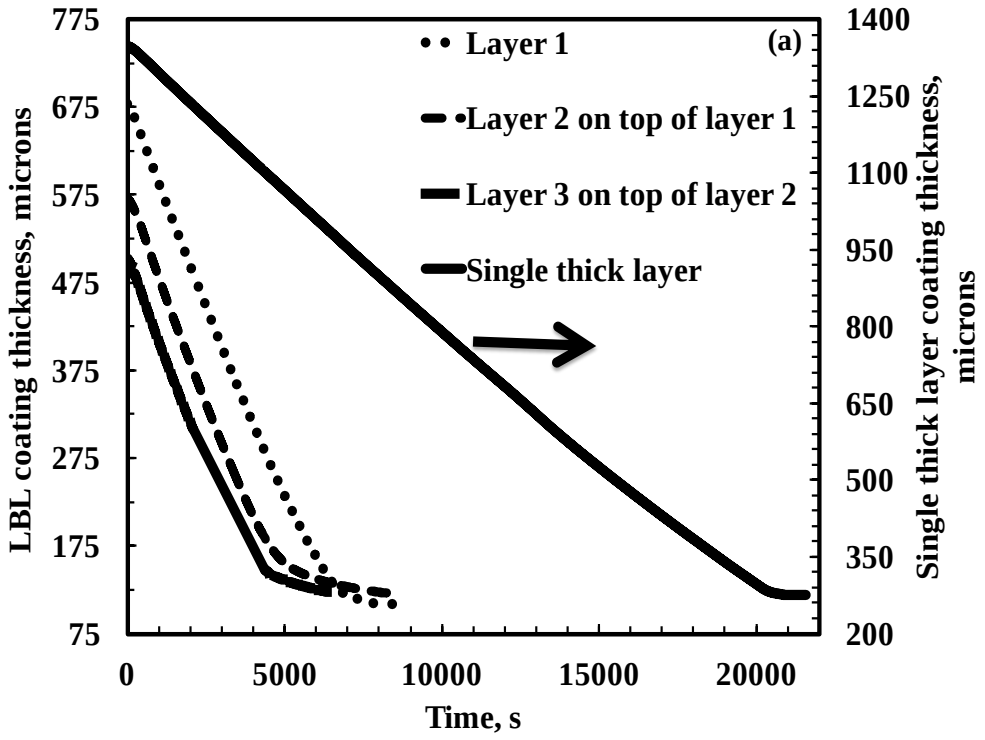

Figure **3.6 (a):** Layer-by-layer coating thickness and single-layer coating thickness with time in poly(styrene), poly(ethylene glycol) and chlorobenzene: 5.05 wt%, 4.98 wt% and 89.97 wt%, respectively of 75 µl injected volume at 8 ˚C.

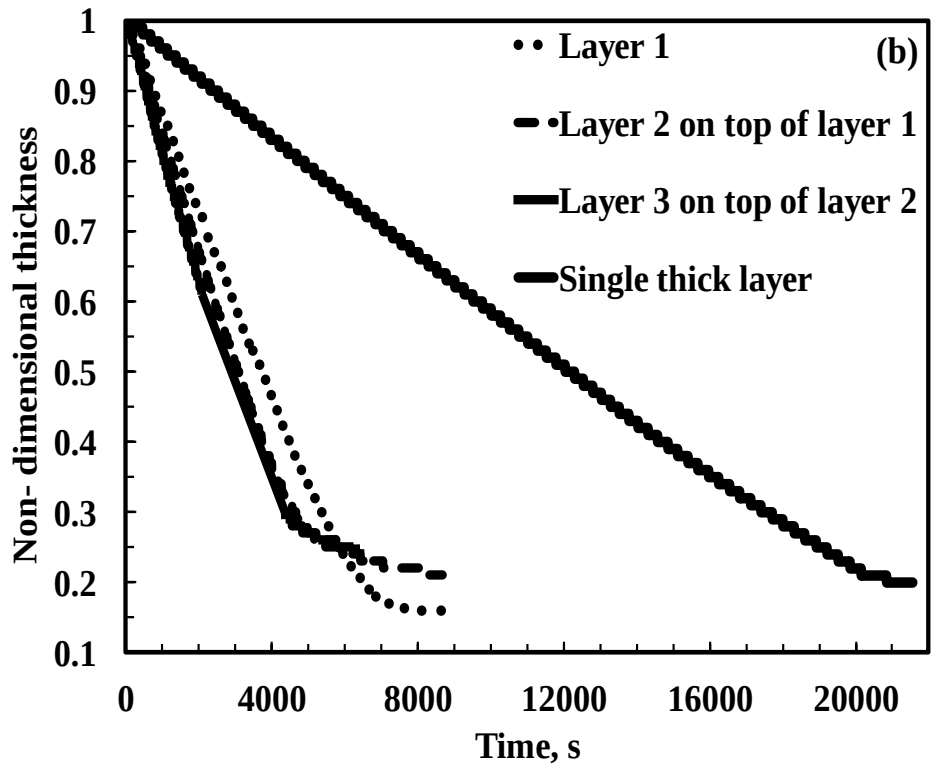

Figure **3.6 (b).** Non-dimensional coating thickness with time in poly(styrene), poly(ethylene glycol) and chlorobenzene: 5.05 wt%, 4.98 wt% and 89.97 wt%, respectively of 75 µl injected volume at 8 ˚C.

Figure 3.7a shows the average concentration of poly(styrene) with time. It represents that the polymer concentration starts increasing with time due to evaporation of chlorobenzene from the coating. In layer 1, layer 2, layer 3, and single thick layer coatings, the concentration of the polymer increases exponentially up to 7503 s, 5813 s, 5253 s, and 20008 s, respectively starting from an initial thickness of 678 µm, 570 µm, 503 µm, and 1349 µm, respectively and then plateaus off. The final concentration of PS in layer 1, layer 2, layer 3, and single thick layer coating were 0.350 g cm^{-3}, 0.267 g cm^{-3}, 0.231 g cm^{-3}, and 0.274 g $cm^{-3}$for coatings having initial concentration 0.056 g cm^{-3}, 0.056 g cm^{-3}, 0.056 g cm^{-3}, and 0.056 g cm^{-3}, respectively.

Figure 3.7b shows the average concentration of poly(ethylene glycol) with time. It represents that the polymer concentration start increasing with time due to the evaporation of chlorobenzene from coating. In layer 1, layer 2, layer 3, and single thick layer coatings, the concentration of the polymer increases exponentially up to 7693 s, 5948 s, 5393 s, and 20143 s, respectively, of coatings having initial thickness of 377 µm, 407 µm, 326 µm, and 1260 µm respectively and then plateaus off. The final concentration of PEG in layer 1, layer 2, layer 3, and single thick layer coatings were 0.345 g cm^{-3}, 0.264 g cm^{-3}, 0.228 g cm^{-3}, and 0.279 g cm^{-3} for coatings having initial concentration 0.055 g cm^{-3}, 0.055 g cm^{-3}, 0.055 g cm^{-3}, and 0.055 g cm^{-3}, respectively.

3.3.2 PS (5.05 %) - PEG (10.04%) - CLB (84.91%) Coatings

Figure 3.8 shows the percentage residual CLB with time in PS-PEG-CLB coatings having PS (5.05%), PEG (10.04%), and CLB (84.91%) of a 50 µl solution of each layer, and a single thick layer of 150 µl. The linear falling trend in the dried layer 1, 2, 3, and single thick layer is upto 5157 s, 6868 s, 5806 s, and 10279 s and by that time 86.61%, 88.4%, 89.31% and 87.9% of solvent has been removed, respectively. The ultimate residual solvent left in the layers 1, 2, 3 and single thick layer are 9.72%, 6.73%, 6.58%, and 9.83%, respectively.

Figure 3.9a and 3.9b show the evolution of the coating thickness and non-dimensional coating thickness of layer-by-layer and single thick layer coatings of PS-

PEG-CLB having PS (5.05%), PEG (10.04%), and CLB (84.91%) of a 50 µl solution of each layer and a single thick layer of 150 µl. As shown in the Figure 3.6 that thicker coatings is taking more time as compared to the thinner coating due to larger amount of solvent present in the coatings. Single coating thickness of 150 µl is reduced to 141 µm in 11929 s from its initial thickness of 613 µm. Layer 1, layer 2 and layer 3 in LBL assembly are reduced to 93 µm, 94 µm, 93 µm from their initial thicknesses of 406 µm, 462 µm, and 459 µm, in 6117 s, 8418 s, and 7592 s, respectively.

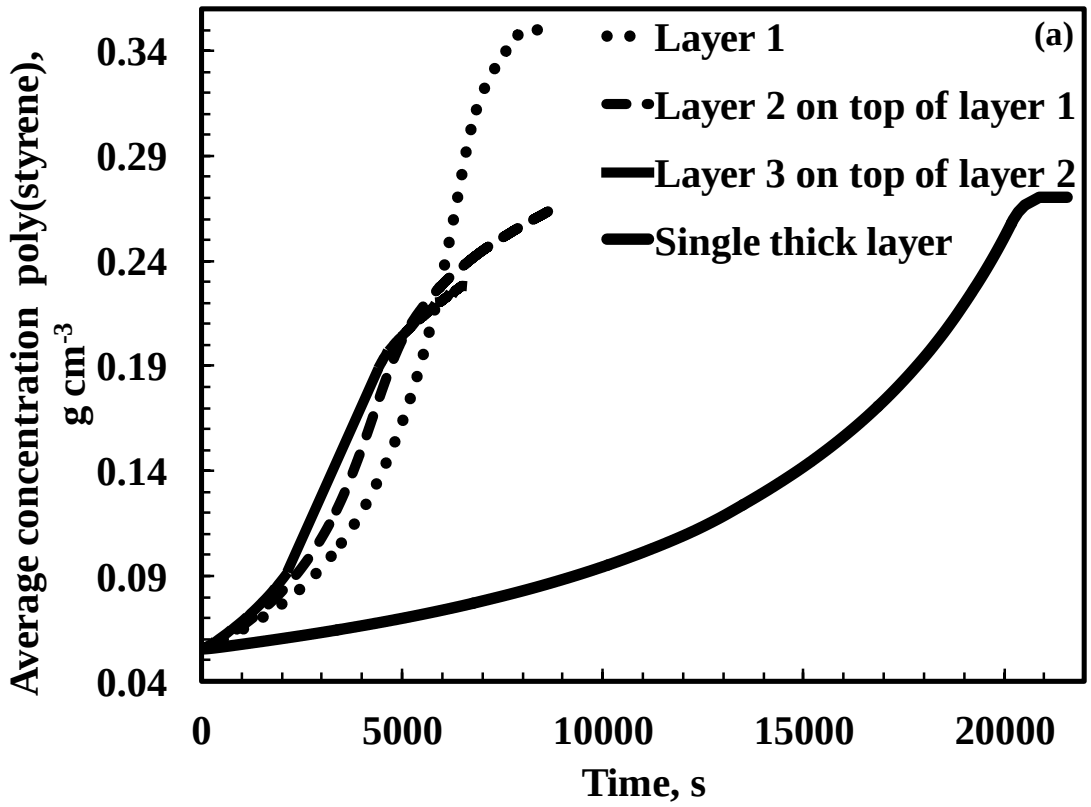

Figure 3.7(a): Average concentration of poly(styrene) with time in poly(styrene)-poly(ethylene glycol)-chlorobenzene: 5.05 wt%, 4.98 wt% and 89.97 wt%, respectively of 75 µl injected volume at 8 ˚C.

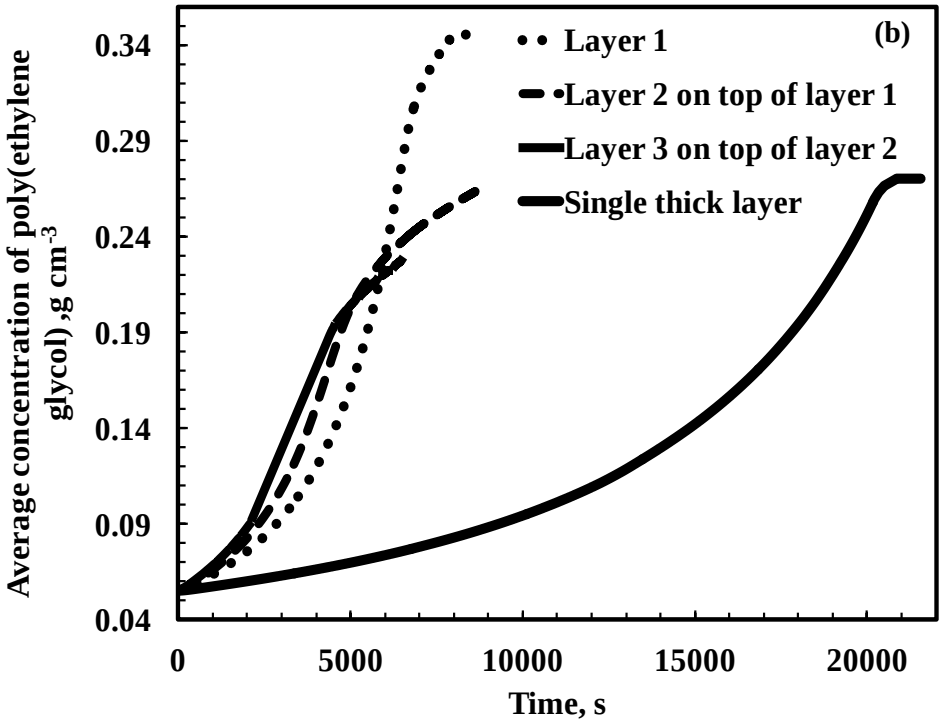

Figure 3.7(b): Average concentration of poly(ethylene glycol) with time in poly(styrene)- poly(ethylene glycol)-chlorobenzene: 5.05 wt%, 4.98 wt% and 89.97 wt%, respectively of 75 µl injected volume at 8 ˚C.

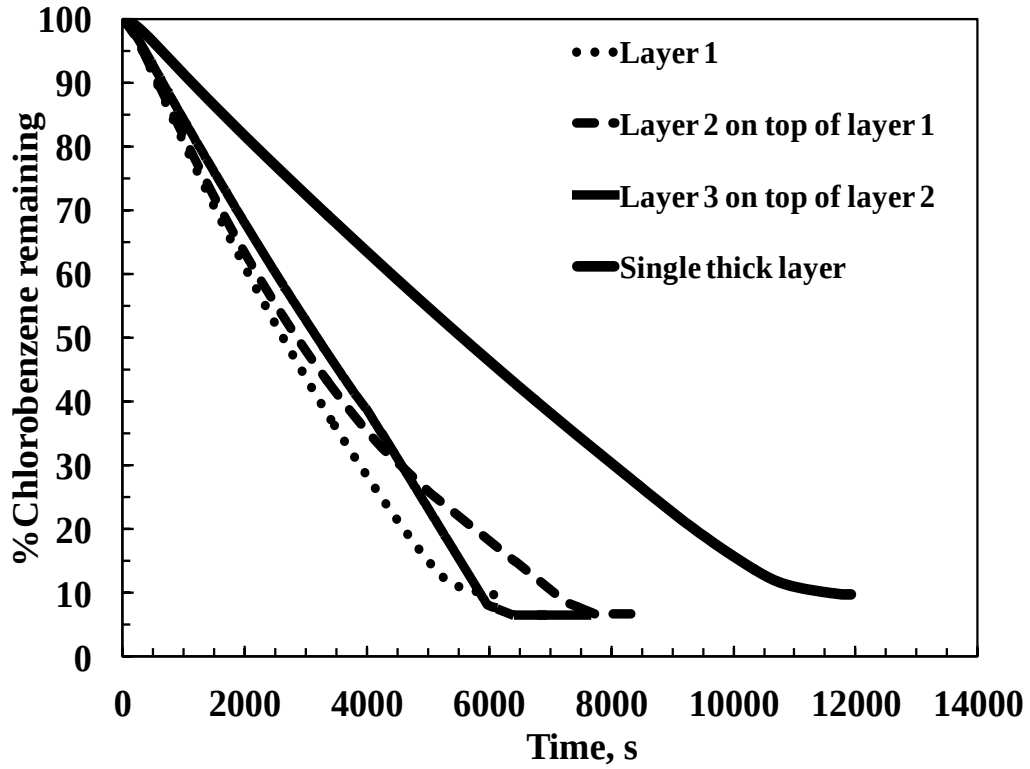

Figure 3.8: Percentage residual chlorobenzene with time in coating having poly(styrene), poly(ethylene glycol) and chlorobenzene: 5.05 wt%, 10.04 wt% and 84.91 wt%, respectively of 50 µl injected volume at 8 ˚C.

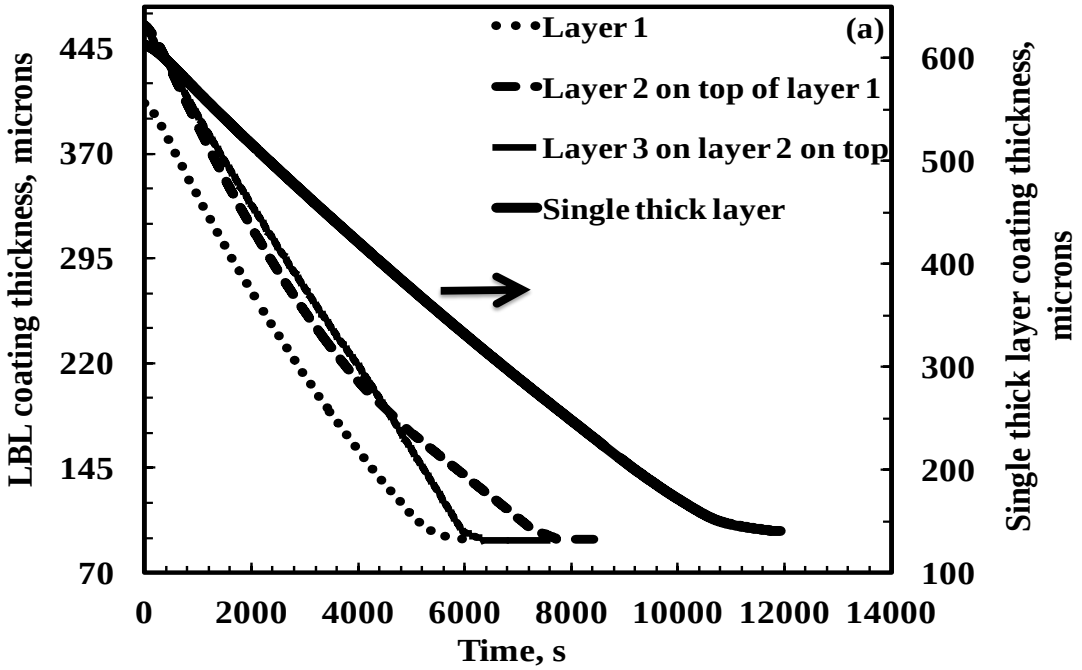

Figure 3.9(a): Layer-by-layer coating thickness and single-layer coating thickness with time in poly(styrene), poly(ethylene glycol) and chlorobenzene: 5.05 wt%, 10.04 wt% and 84.91 wt%, respectively of 50 µl injected volume at 8 ˚C.

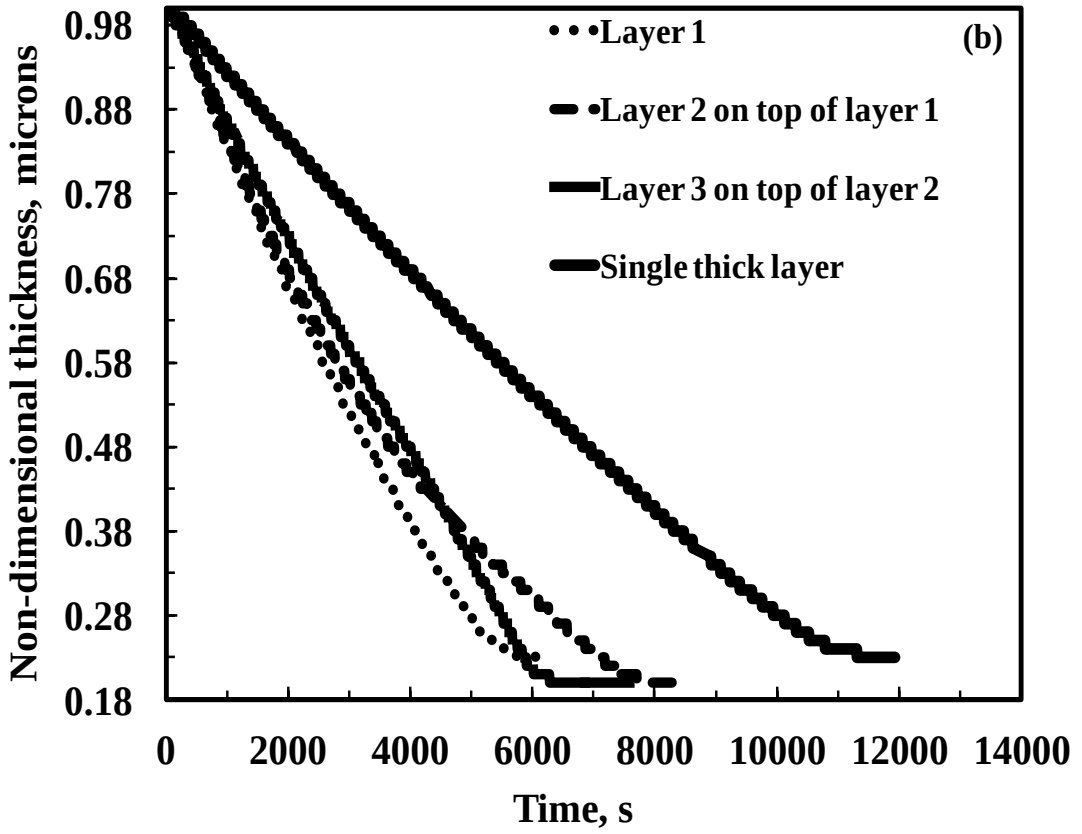

Figure 3.9 (b). Non-dimensional coating thickness with time in poly(styrene), poly(ethylene glycol) and chlorobenzene: 5.05 wt%, 10.04 wt% and 84.91 wt%, respectively of 50 µl injected volume at 8 ˚C.

Figure 3.10a shows the average concentration of poly(styrene) with time. It represents that the polymer concentration start increasing with time due to the evaporation of chlorobenzene from coating. In layer 1, layer 2, layer 3, and single thick layer coatings, the concentration of the polymer increases exponentially up to 5432 s, 7268 s, 5946 s, and 10549 s, respectively, for the coatings having initial thickness of 406 µm, 462 µm, 459 µm and 613 µm respectively, and then plateaus off. The final concentration of PS in layer 1, layer 2, layer 3, and single thick layer coatings were 0.245 g cm^{-3}, 0.276 g cm^{-3}, 0.278 g $cm^{-3}$and 0.244 g cm^{-3} for the coatings having initial concentration 0.056 g cm^{-3}, 0.056 g cm^{-3}, 0.056 g cm^{-3}, and 0.056 g cm^{-3} respectively.

Figure 3.10b shows the average concentration of poly(ethylene glycol) with time. It represents that the polymer concentration start increasing with time due to the evaporation of chlorobenzene from the coating. In layer 1, layer 2, layer 3, and single thick layer coatings, the concentration of the polymer increases exponentially up to 5482 s, 5926 s, 7188 s, and 10604 s, respectively for the coatings having initial thickness of 406 µm, 462 µm, 459 µm, and 613 µm respectively, and then plateaus off. In case of the single thick layer the concentration of polymer has not reached to the constant value, it is due to the slow drying of this coating. However, this coating is dried for a very long time which is almost double of other coating. The final concentration of PEG in layer 1, layer 2, layer 3, and single thick layer coating were 0.488 g cm^{-3}, 0.549 g cm^{-3}, 0.552 g cm^{-3}, and 0.486 g cm^{-3} for the coatings having initial concentration 0.11 g cm^{-3}, 0.11 g cm^{-3}, 0.11 g cm^{-3}, and 0.055 g cm^{-3} respectively.

Figure 3.11 shows the percentage residual CLB with time in PS-PEG-CLB coatings having PS (5.05%), PEG (10.04%), and CLB (84.91%) of a 75 µl solution of each layer, and a single thick layer of 225 µl. There is a rapid decrease in the residual solvent percentage in the beginning due to high evaporation rate. A constant period is followed in the initial phase of drying. The falling period in the dried layer 1, 2, 3 and single thick layer is upto 6102 s, 6983 s, 7058 s, and 19246 s and by that time 83.52%, 86.65%, 84.72%, and 86.07%, of the solvent has been removed, respectively. The ultimate residual solvent left in the layers 1, 2, 3, and single thick are 11.89%, 8.1%, 9.81%, and 10.88%, respectively.

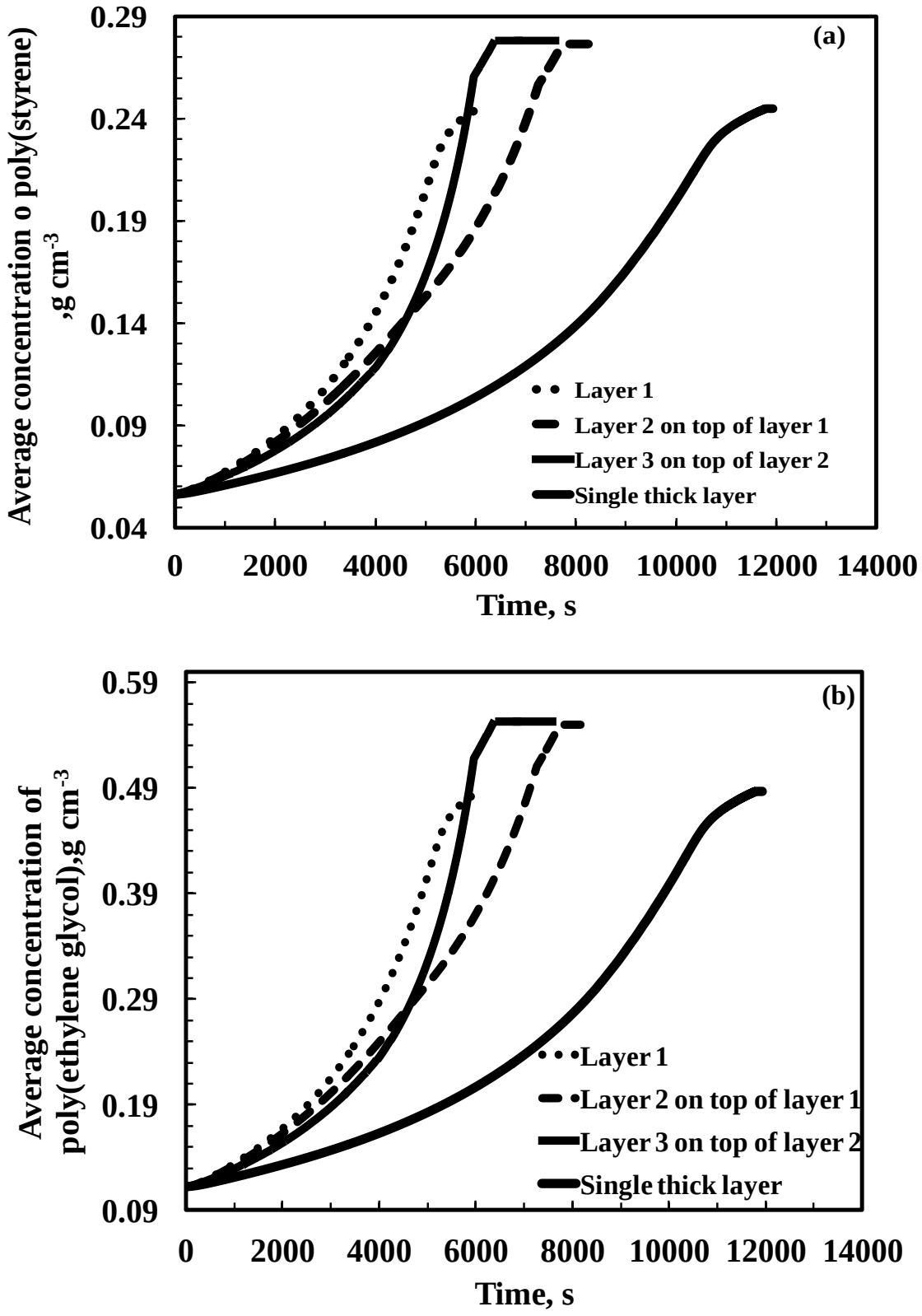

Figure 3.10(a): Average concentration of poly(styrene) with time. **(b).** Average concentration of poly(ethylene glycol) with time in poly(styrene)- poly(ethylene glycol)-chlorobenzene: 5.05 wt%, 10.04 wt% and 84.91 wt%, respectively of 50 µl injected volume at 8°C.

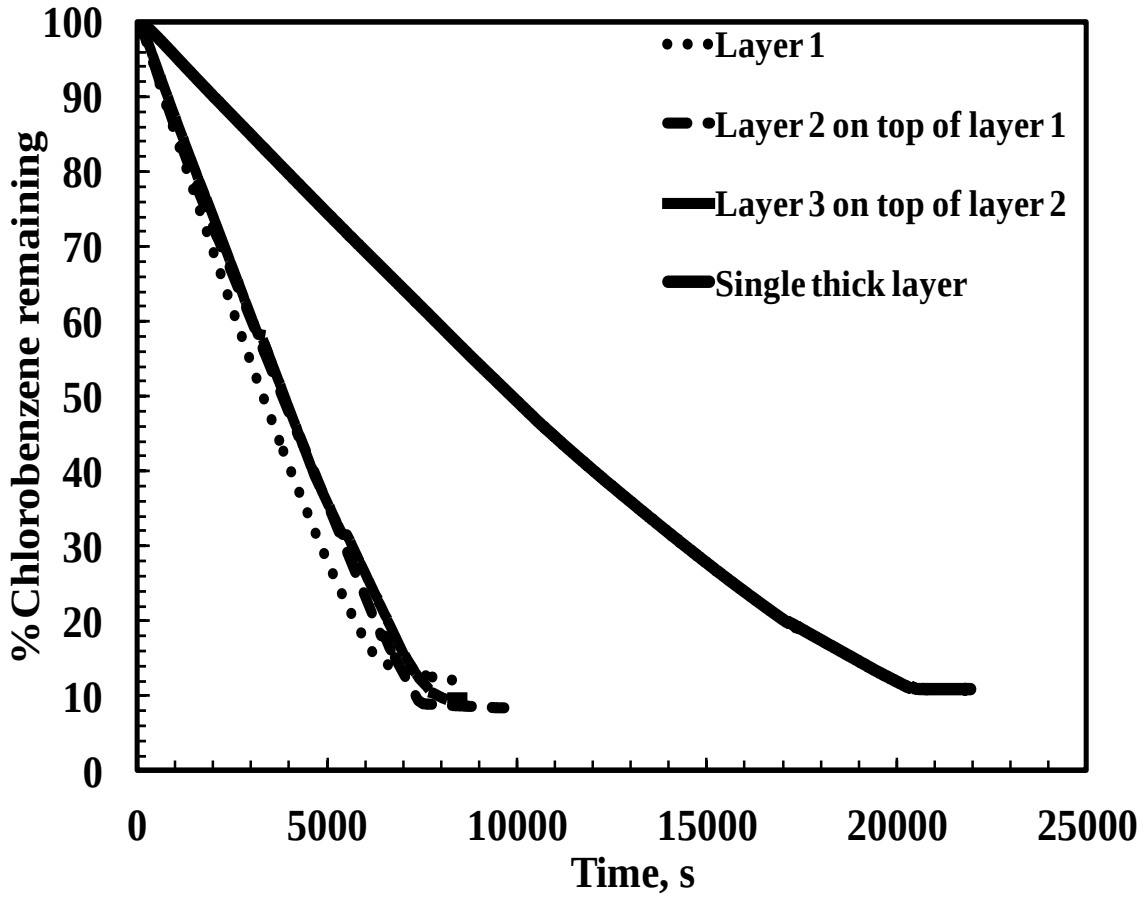

Figure 3.11: Percentage residual chlorobenzene with time in coating having poly(styrene), poly(ethylene glycol) and chlorobenzene: 5.05 wt%, 10.04 wt% and 84.91 wt%, respectively of 75 µl injected volume at 8 ˚C.

Figures 3.12a and 3.12b shows evolution of the coating thickness and non-dimensional coating thickness of layer-by-layer coating and single thick layer of PS-PEG-CLB having PS (5.05%), PEG (10.04%), and CLB (84.91%) of a 75µl solution of each layer and a single thick layer of 225 µl, respectively. In this case also, as shown in the Figure 3.6, that single thick layer coating is taking more time as compared to the LBL coating due to larger amount of solvent present in the coatings which is similar to 50 µl of injected volume case. Single coating thickness of 225 µl is reduced to 318 µm in 21956 s from its initial thickness of 1327 µm. Layer 1, layer 2 and layer 3 in the LBL assembly are reduced to 103 µm, 87 µm, 108 µm from their initial thicknesses of 416 µm, 402 µm, and 468 µm in 8558 s, 9674 s, and 8443 s, respectively.

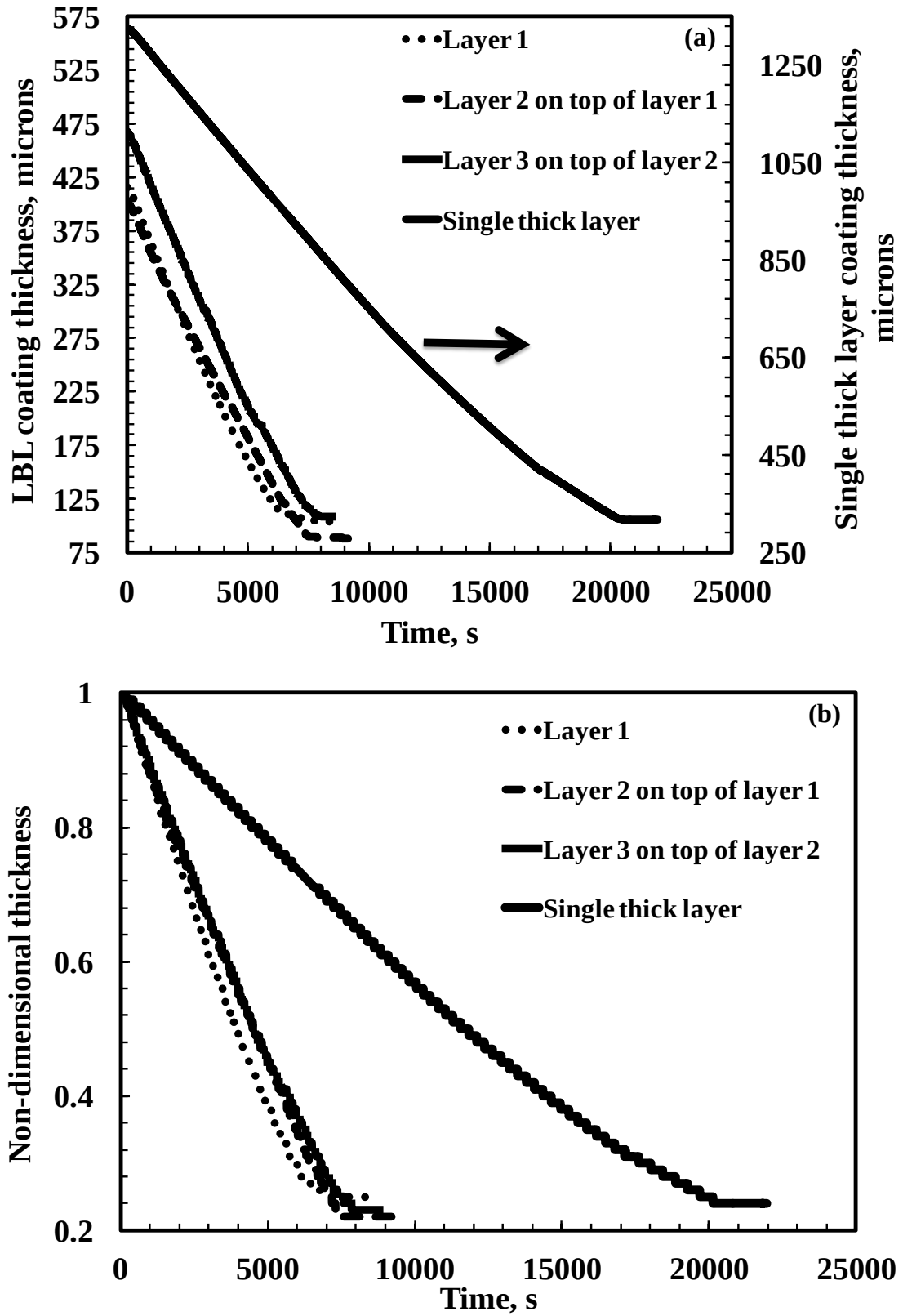

Figure 3.12 (a): Layer-by-layer coating thickness and single-layer coating thickness with time **(b).** Non dimensional thickness with time in poly(styrene), poly(ethylene glycol) and chlorobenzene: 5.05 wt%, 10.04 wt% and 84.91 wt%, respectively of 75 µl injected volume at 8 °C.

Figure 3.13a shows the average concentration of poly(styrene) with time. It represents that the polymer concentration start increasing with time due to the evaporation of chlorobenzene from coating. In layer 1, layer 2, layer 3, and single thick layer coatings, the concentration of the polymer increases exponentially up to 6617 s, 7324 s, 7758 s, and 19916 s, respectively for the coatings having initial thickness of 416 µm, 402 µm, 468 µm, and 1327 µm, respectively, and then plateaus off. The final concentration of PS in layer 1, layer 2, layer 3, and single thick layer coatings were 0.227 g cm^{-3}, 0.257 g cm^{-3}, 0.244 g cm^{-3}, and 0.235 g cm^{-3} for the coatings having initial concentration 0.056 g cm^{-3}, 0.056 g cm^{-3}, 0.056 g cm^{-3}, and 0.056 g cm^{-3}, respectively.

Figure 3.13b shows the average concentration of poly(ethylene glycol) with time. It represents that the polymer concentration start increasing with time due to the evaporation of chlorobenzene from coating. In layer 1, layer 2, layer 3, and single thick layer coatings, the concentration of the polymer increases exponentially up to 6432 s, 7379 s, 7843 s, and 20021 s, respectively, for the coatings having initial thickness of 416 µm, 402 µm, 468 µm, and 1327 µm, respectively, and then plateaus off. The final concentration of PEG in layer 1, layer 2, layer 3 and single thick layer coatings were 0.451 g cm^{-3}, 0.512 g cm^{-3}, 0.486 g cm^{-3}, and 0.468 g cm^{-3} for the coatings having initial concentration 0.11 g cm^{-3}, 0.11 g cm^{-3}, 0.11 g cm^{-3}, and 0.11 g cm^{-3}, respectively.

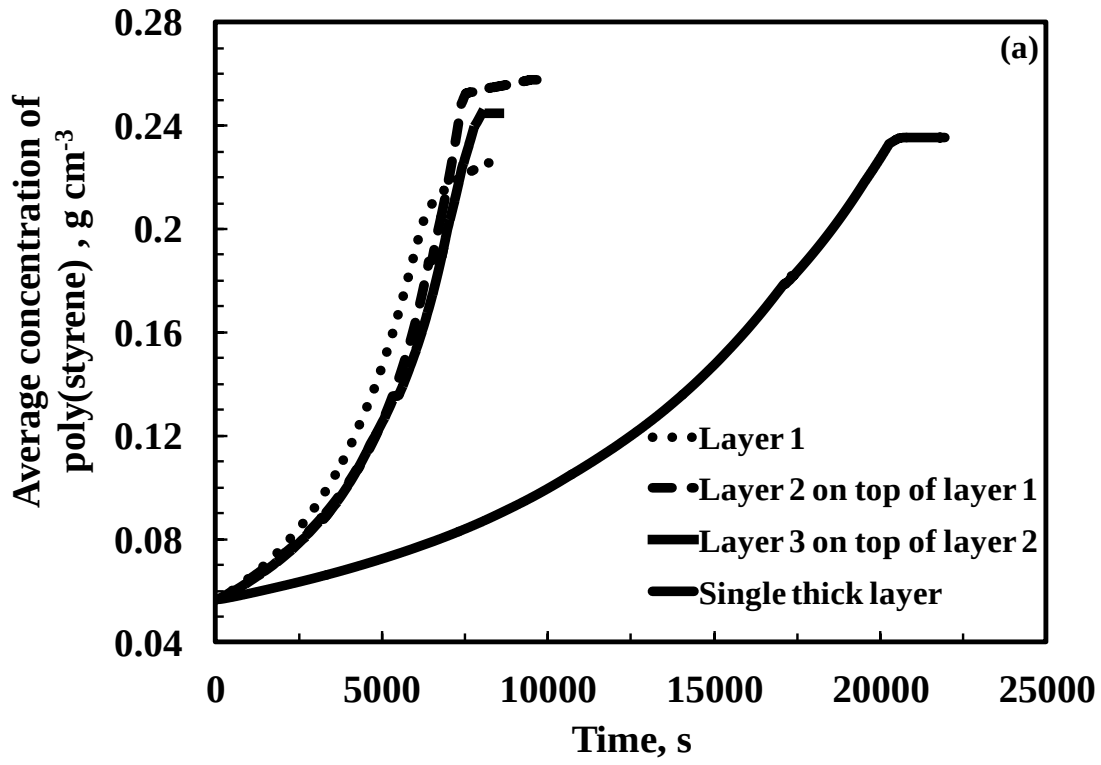

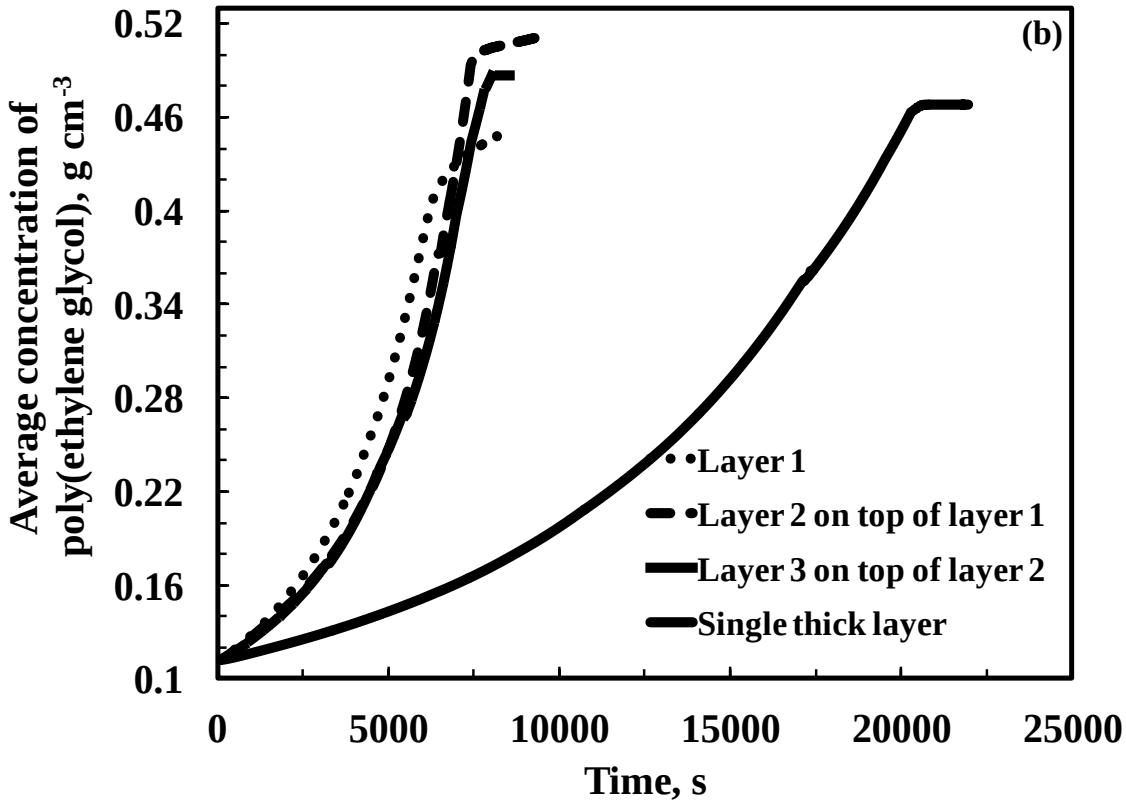

Figure 3.13 (a): Average concentration of poly(styrene) with time. **(b)** Average concentration of poly(ethylene glycol) with time in poly(styrene)- poly(ethylene glycol)-chlorobenzene: 5.05 wt%, 10.04 wt% and 84.91 wt%, respectively of 75 µl injected volume at 8 °C.

3.3.3 PS (10.06%) - PEG (5.13%) - CLB (84.81%) Coatings

Figure 3.14 shows the percentage residual CLB with time in PS-PEG-CLB coatings having PS (10.06%), PEG (5.13%), and CLB (84.81%) of a 50 µl solution of each layer, and a single thick layer of 150 µl. The falling period in the dried layer 1, 2, 3 and single thick layer is upto 3937 s, 3516 s, 3732 s, and 12761 s and by that time the solvent removed is 89.05%, 82.04%, 74.38%, and 84.37%, respectively. The ultimate residual solvent left in the layer 1, 2, 3, and single thick layer are 8.33%, 13.39%, 12.86%, and 8.1%, respectively. This system has more viscous solution due to the more mass fraction of the poly(styrene) content that leads to the more percentage of residual solvent in each layer of the coating. Hence, the residual solvent minimization is favored in thicker coatings [11].

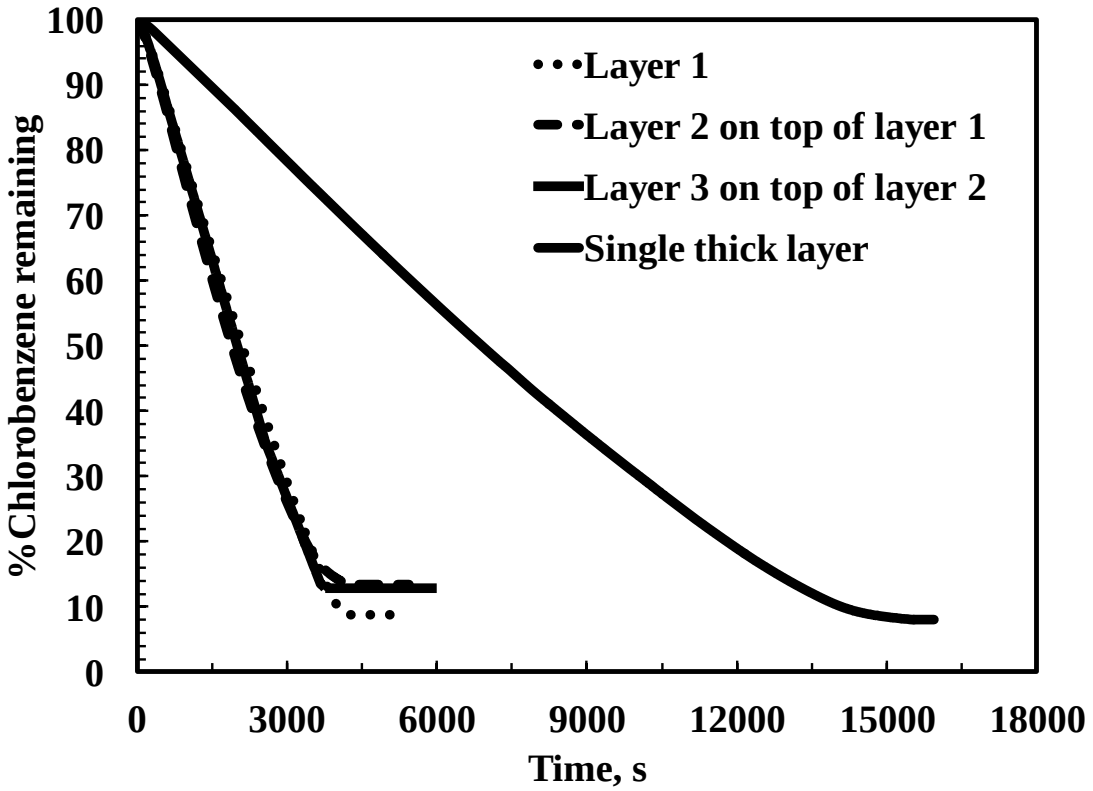

Figure 3.14: Percentage residual chlorobenzene with time in coating having poly(styrene), poly(ethylene glycol) and chlorobenzene: 10.06 wt%, 5.31 wt% and 84.81 wt%, respectively of 50µl injected volume at 8 °C.

Figure 3.15a and 3.15b shows the evolution of the coating thickness and non-dimensional coating thickness of layer-by-layer coating and single thick layer of PS-PEG-CLB having PS (10.06%), PEG (5.31%), and CLB (84.81%) of a 50 µl solution of each layer, and a single thick layer of 150 µl. As shown in the Figure 3.10, that single thick layer coatings will take more time as compared to the LBL coating due to larger amount of the solvent present in the coatings. Single coating thickness of 150 µl is reduced to 209 µm in 15941 s from its initial thickness of 946 µm. Layer 1, layer 2, layer 3 in LBL assembly are reduced to 47 µm, 57 µm, 50 µm from their initial thicknesses of 206 µm, 215 µm, and 192 µm in 5237 s, 5437 s, and 5888 s, respectively.

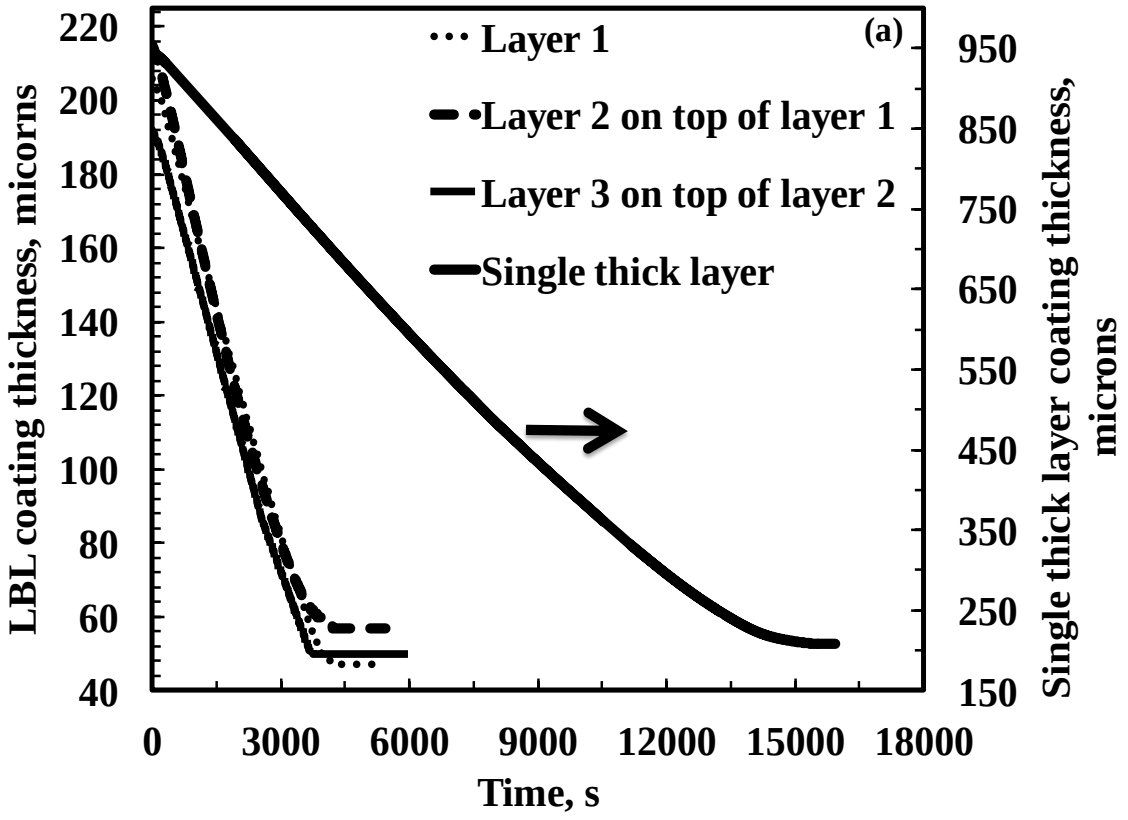

Figure 3.15 (a): Layer-by-layer coating thickness and single-layer coating thickness with time in poly(styrene), poly(ethylene glycol) and chlorobenzene: 10.06 wt%, 5.31 wt% and 84.81 wt%, respectively of 50 µl injected volume at 8 °C.

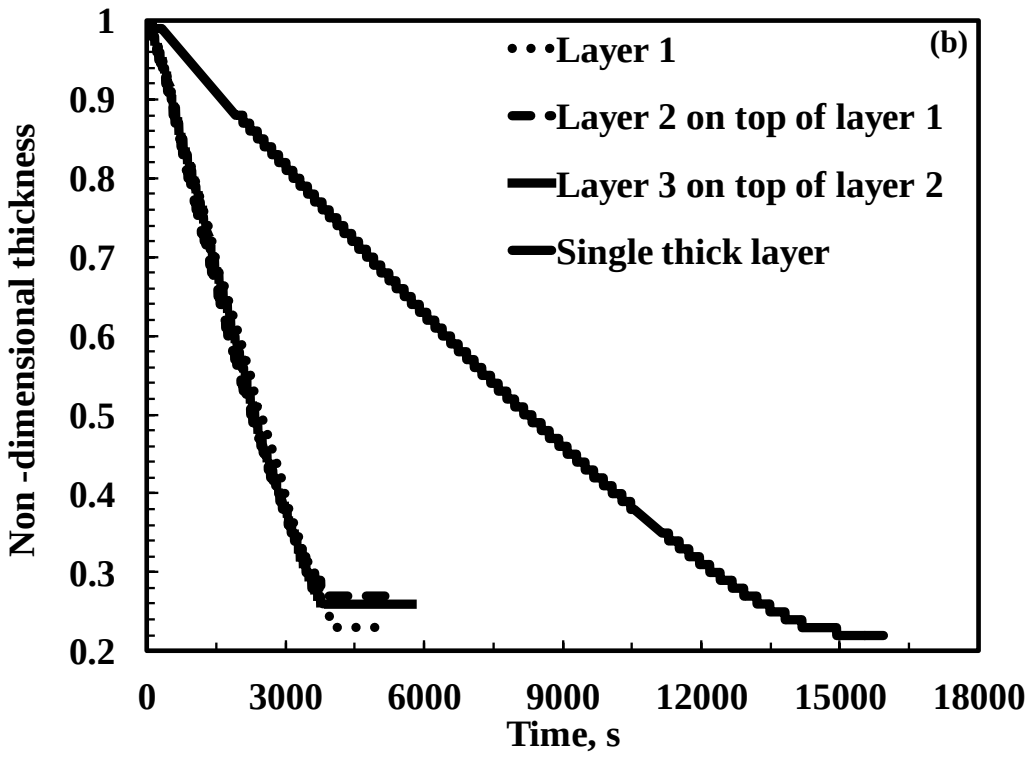

Figure 3.15 (b): Non-dimensional coating thickness with time in poly(styrene), poly(ethylene glycol) and chlorobenzene: 10.06 wt%, 5.31 wt% and 84.81 wt%, respectively of 50 µl injected volume at 8 °C.

Figure 3.16a shows the average concentration of poly(styrene) with time. It represents that the polymer concentration start increasing with time due to the evaporation of chlorobenzene from coating. In layer 1, layer 2, layer 3, and single thick layer coatings, the concentration of the polymer increases exponentially up to 4117 s, 3781 s, 3662 s, and 14196 s respectively, for the coatings having initial thickness of 206 µm, 215 µm, 192 µm, and 946 µm, respectively and then plateaus off. The final concentration of PS in layer 1, layer 2, layer 3 and single thick layer coatings were 0.489 g cm^{-3}, 0.418 g cm^{-3}, 0.425 g cm^{-3}, and 0.501 g cm^{-3} for the coatings having initial concentration 0.11 g cm^{-3}, 0.11 g cm^{-3}, 0.11 g cm^{-3}, and 0.11 g cm^{-3}, respectively.

Figure 3.16b shows the average concentration of poly(ethylene glycol) with time. It represents that the polymer concentration start increasing with time due to the evaporation of chlorobenzene from coating. In layer 1, layer 2, layer 3, and single thick layer coatings, the concentration of the polymer increases exponentially up to 4092 s, 3911 s, 3677 s, and 14276 s, respectively, for the coatings having initial

thickness of 206 µm, 215 µm, 192 µm, and 946 µm, respectively and then plateaus off. This coating is also following the same trend as in case of Figure 3.10b. The final concentration of PEG in layer 1, layer 2, layer 3, and single thick layer coatings were 0.249 g cm^{-3}, 0.213 g cm^{-3}, 0.217 g cm^{-3}, and 0.255 g cm^{-3} for the coatings having initial concentration 0.055 g cm^{-3}, 0.055 g cm^{-3}, 0.055 g cm^{-3}, and 0.055 g cm^{-3}, respectively.

Figure 3.17 shows the percentage residual CLB with time in PS-PEG-CLB coatings having PS (10.06%), PEG (5.13%), and CLB (84.81%) of a 75 µl solution of each layer, and a single thick layer of 225 µl. The linear decrease in the dried layer 1, 2, 3, and single thick layer is upto 7042 s, 5497 s, 8703 s, and 17061 s and by that time 88.09%, 76.07%, 83%, and 86.88% of solvent has been removed, respectively. The ultimate residual solvent left in the layer 1, 2, 3 and single thick layer are 5.46%, 13.76%, 13.68%, and 9.36% respectively.

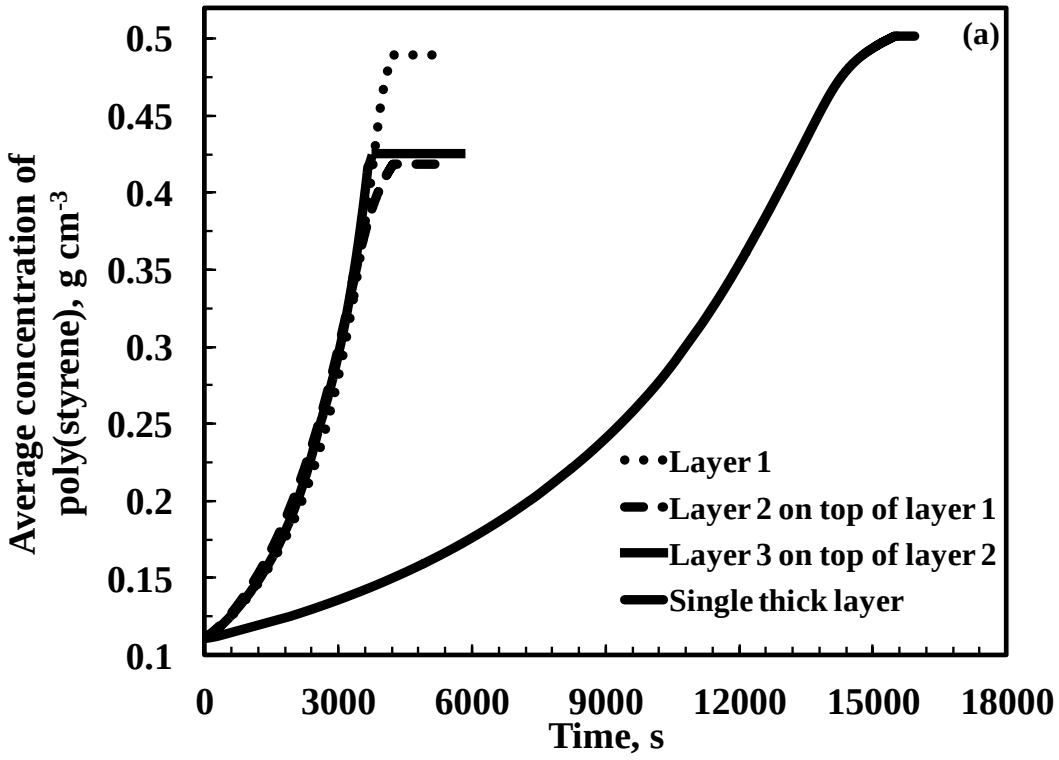

Figure 3.16(a): Average concentration of poly(styrene) with time in poly(styrene)-poly(ethylene glycol)-chlorobenzene: 10.06 wt%, 5.31 wt% and 84.81 wt%, respectively of 50 µl injected volume at 8 °C.

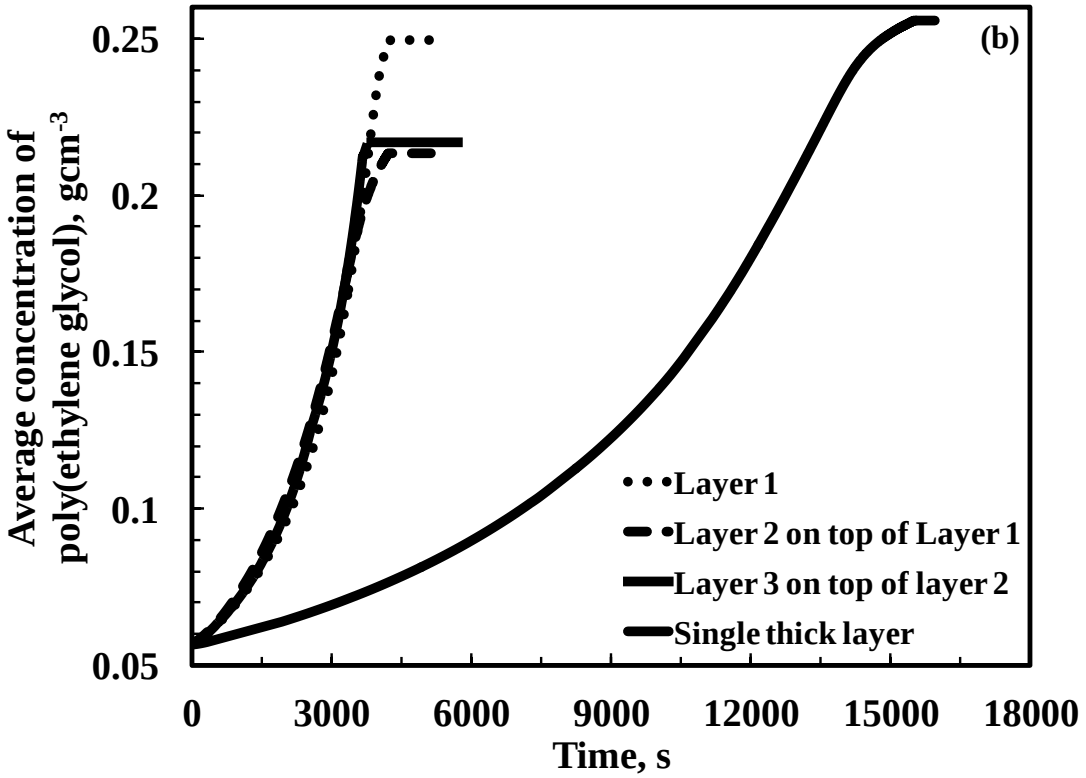

Figure 3.16(b): Average concentration of poly(ethylene glycol) with time in poly(styrene)- poly(ethylene glycol)-chlorobenzene: 10.06 wt%, 5.31 wt% and 84.81 wt%, respectively of 50 µl injected volume at 8 °C.

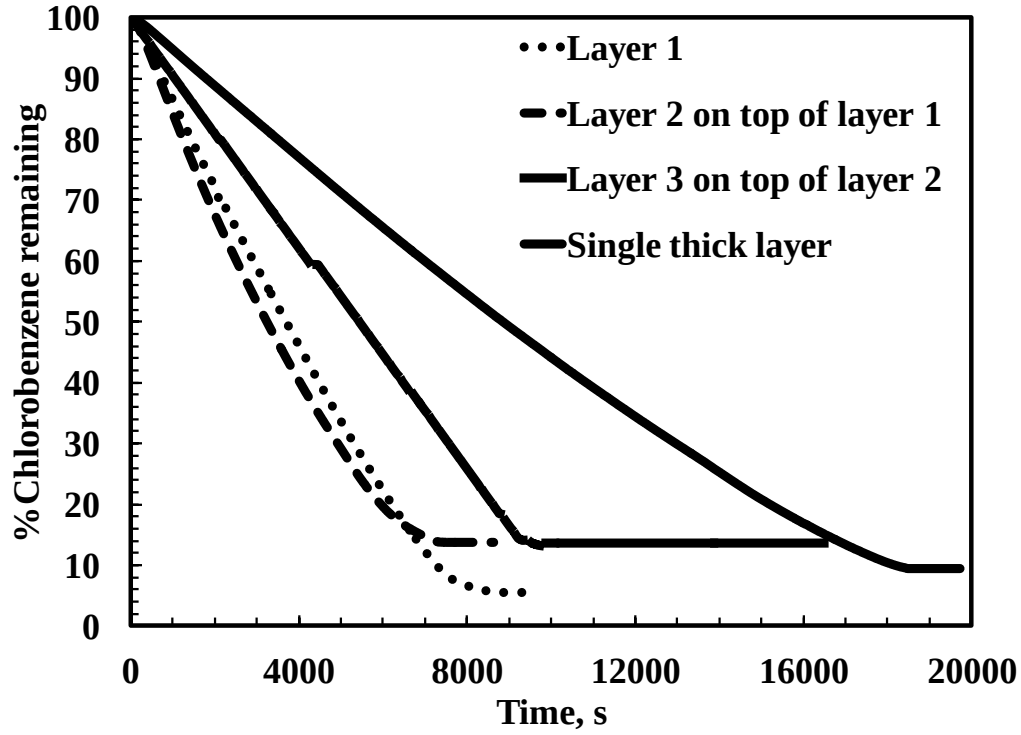

Figure 3.17: Percentage residual chlorobenzene with time in coating having poly(styrene), poly(ethylene glycol) and chlorobenzene: 10.06 wt%, 5.31 wt% and 84.81 wt%, respectively of 75 µl injected volume at 8 °C.

Figure 3.18a and 3.18b show the evolution of the coating thickness and non-dimensional coating thickness of layer-by-layer coating and single thick layer of PS-PEG-CLB having PS (10.06%), PEG (5.13%), and CLB (84.81%) of a 75µl solution of each layer, and a single thick layer of 225 µl. Single coating thickness of 225 µl is reduced to 280 µm in 40187 s from its initial thickness of 1204 µm. Layer 1, layer 2, layer 3 in LBL assembly are reduced to 82 µm, 88 µm, 71 µm from their initial thicknesses of 412 µm, 328 µm, and 264 µm in 9572 s, 8632 s, and 19501 s, respectively.

Figure 3.19a shows the average concentration of poly(styrene) with time. It represents that the polymer concentration start increasing with time due to the evaporation of chlorobenzene from coating. In layer 1, layer 2, layer 3, and single thick layer coatings, the concentration of the polymer increases exponentially up to 8337 s, 6412 s, 9123 s, and 18162 s respectively, for the coatings having initial thickness of 412 µm, 328 µm, 264 µm, and 1204 µm respectively, and then plateaus off. The final concentration of PS in layer 1, layer 2, layer 3, and single thick layer coatings were 0.559 g cm^{-3}, 0.413 g cm^{-3}, 0.414 g cm^{-3}, and 0.479 g cm^{-3} for the coatings having initial concentration 0.11 g cm^{-3}, 0.11 g cm^{-3}, 0.11 g cm^{-3}, and 0.11 g cm^{-3}, respectively.

Figure 3.19b shows the average concentration of poly(ethylene glycol) with time. It represents that the polymer concentration start increasing with time due to the evaporation of chlorobenzene from coating. In layer 1, layer 2, layer 3, and single thick layer coatings, the concentration of the polymer increases exponentially up to 8277 s, 6467 s, 9158 s, and 18297 s respectively for the coatings having initial thickness of 412 µm, 328 µm, 264 µm, and 1204 µm respectively and then plateaus off. The final concentration of PEG in layer 1, layer 2, layer 3, and single thick layer coatings were 0.285 g cm^{-3}, 0.210 g cm^{-3}, 0.211 g cm^{-3}, and 0.244 g $cm^{-3}$for the coatings having initial concentration 0.055 g cm^{-3}, 0.055 g cm^{-3}, 0.055 g cm^{-3}, and 0.055 g cm^{-3}, respectively.

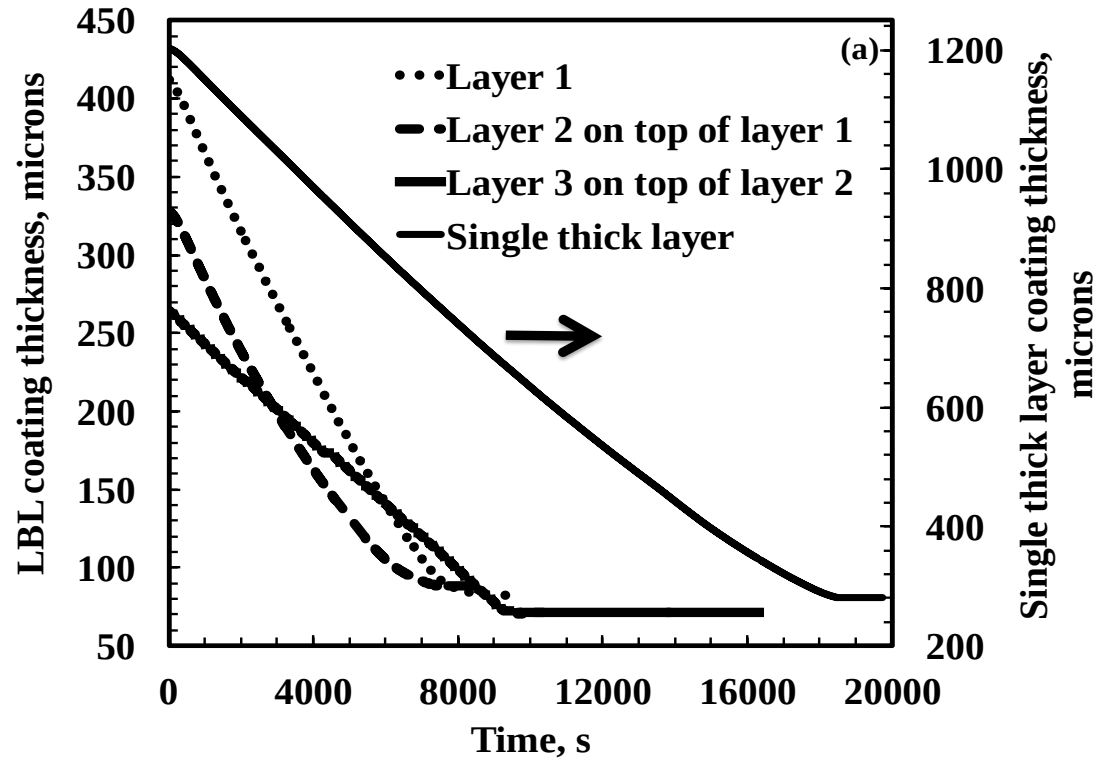

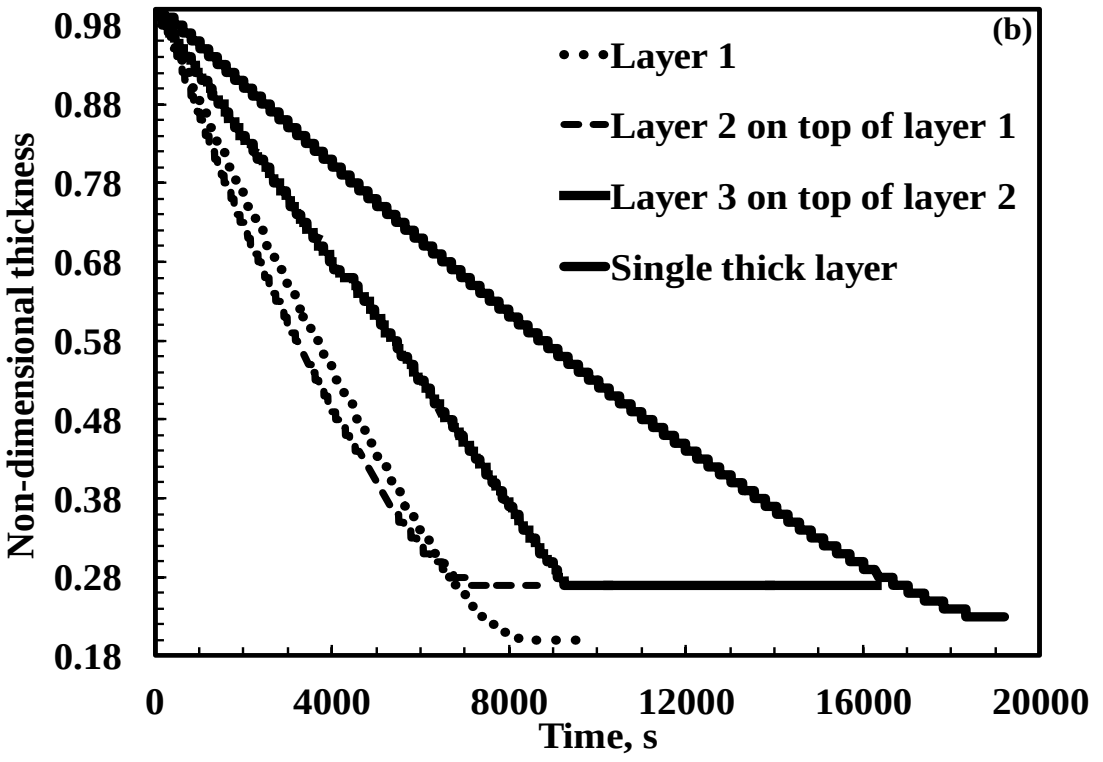

Figure 3.18 (a): Layer-by-layer coating thickness and single-layer coating thickness with time. **(b).** Non-dimensional coating thickness with time in poly(styrene), poly(ethylene glycol) and chlorobenzene: 10.06 wt%, 5.31 wt% and 84.81 wt%, respectively of 75 µl injected volume at 8 °C.

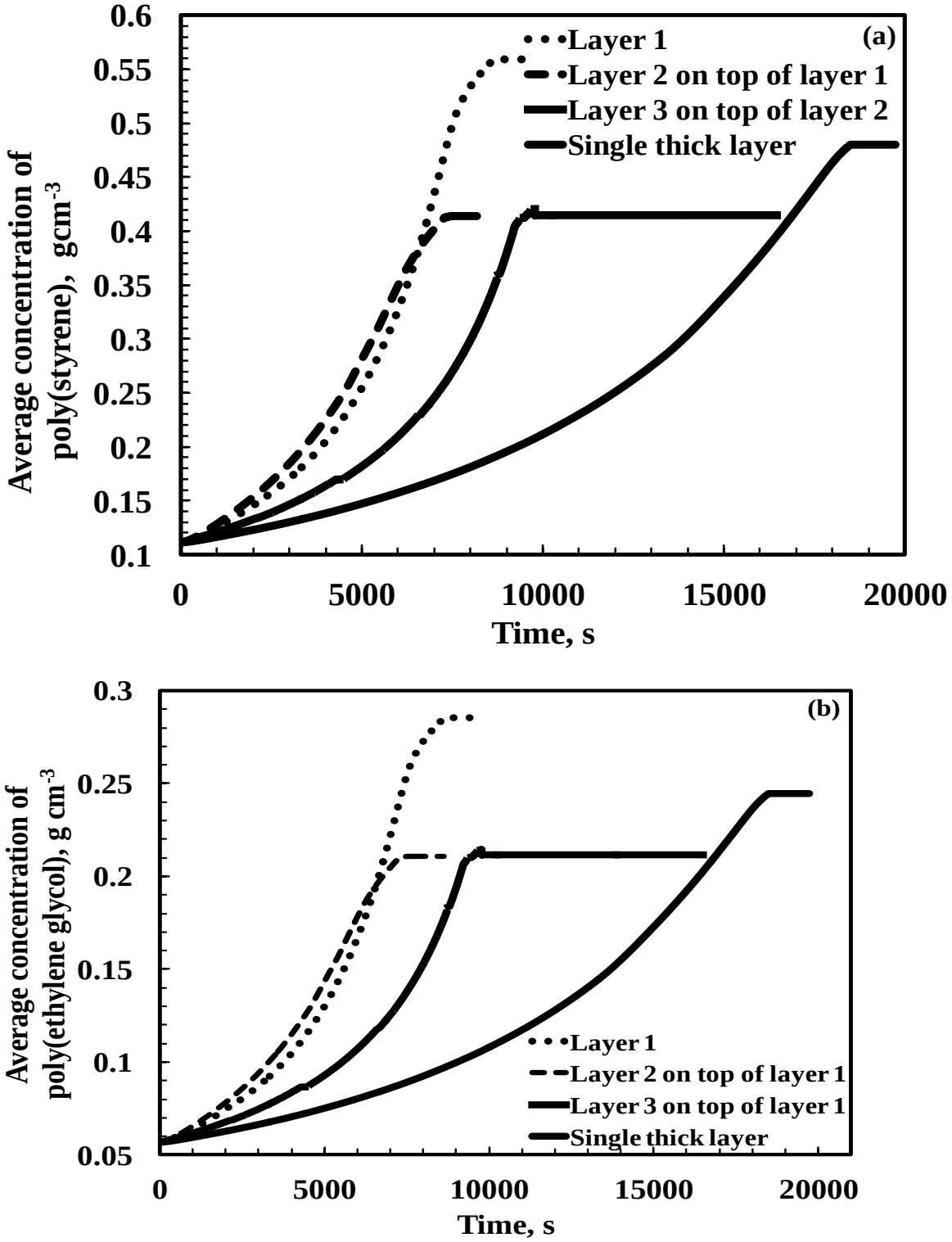

Figure 3.19(a): Average concentration of poly(styrene) with time. **(b).** Average concentration of poly(ethylene glycol) with time in poly(styrene)- poly(ethylene glycol)-chlorobenzene: 10.06 wt%, 5.31 wt% and 84.81 wt%, respectively of 75 µl injected volume at 8 °C.

3.3.4 PS (10.02%) - PEG (9.96%) - CLB (80.02%) Coatings

Figure 3.20 shows the percentage residual CLB with time in PS-PEG-CLB coatings having PS (10.02%), PEG (9.96%), and CLB (80.02%) of a 50µl solution of each layer, and a single thick layer of 150µl. The linear decrease trend in the dried layer 1, 2, 3, and single thick layer is upto 3901 s, 5231 s, 4836 s and 8833 s and by that time 81.29%, 89.58%, 90.39%, and 76.18% of solvent has been removed, respectively. The ultimate residual solvent left in the layer 1, 2, 3, and single thick are 10.99%, 5.86%, 5.88%, and 9.88% respectively.

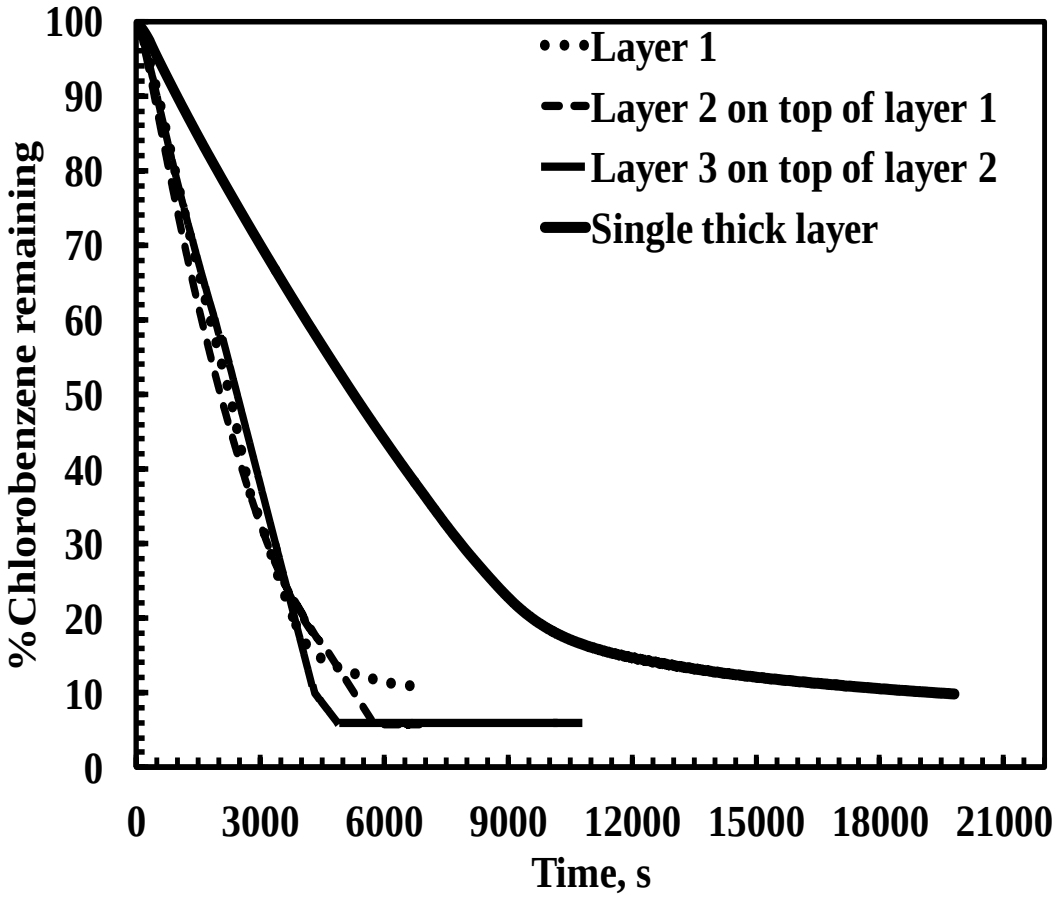

Figure 3.20: Percentage residual chlorobenzene with time in coating having poly(styrene), poly(ethylene glycol) and chlorobenzene: 10.02 wt%, 9.96 wt% and 80.02 wt%, respectively of 50 µl injected volume at 8 °C.

Figure 3.21a and 3.21b shows the coating thickness and non-dimensional coating thickness of layer-by-layer coating and single thick layer of PS-PEG-CLB having PS (10.02%), PEG (9.96%), and CLB (80.02%) of a 50µl solution of each layer, and a single thick layer of 150 µl. Single coating thickness of 150 µl is reduced to 251 µm in 19816 s from its initial thickness of 901 µm. Layer 1, layer 2, layer 3 in

LBL assembly are reduced to 107 µm, 54 µm, 65 µm from their initial thicknesses of 359 µm, 220 µm, and 265 µm, in 6967 s, 6851 s, and 10794s, respectively.

Figure 3.22a shows the average concentration of poly(styrene) with time. It represents that the polymer concentration start increasing with time due to the evaporation of chlorobenzene from coating. In layer 1, layer 2, layer 3, and single thick layer coatings, the concentration of the polymer increases exponentially up to 4466 s, 5681 s, 4791 s, and 9603 s respectively, for the coatings having initial thickness of 359 µm, 220 µm, 265 µm, and 901 µm respectively, and then plateaus off. The final concentration of PS in layer 1, layer 2, layer 3 and single thick layer coatings were 0.398 g cm^{-3}, 0.454 g cm^{-3}, 0.453 g cm^{-3}, and 0.402 g cm^{-3} for the coatings having initial concentration 0.11 g cm^{-3}, 0.11 g cm^{-3}, 0.11 g cm^{-3}, and 0.11 g cm^{-3}, respectively.

Figure 3.22b shows the average concentration of poly(ethylene glycol) with time. It represents that the polymer concentration start increasing with time due to the evaporation of chlorobenzene from coating. In layer 1, layer 2, layer 3 and single thick layer coatings, the concentration of the polymer increases exponentially up to 4421 s, 5656 s, 4811 s, and 9808 s respectively, for the coatings having initial thickness of 359 µm, 220 µm, 265 µm, and 901 µm respectively, and then plateaus off. This is also following the same trend as in case of Figure 10b and Figure 16b. The final concentration of PEG in layer 1, layer 2, layer 3, and single thick layer coatings were 0.395 g cm^{-3}, 0.451 g cm^{-3}, 0.451 g cm^{-3}, and 0.400 g cm^{-3}, for the coatings having initial concentration 0.11 g cm^{-3}, 0.11 g cm^{-3}, 0.11 g cm^{-3}, and 0.11 g cm^{-3}, respectively.

Figure 3.23 shows the percentage residual CLB with time in PS-PEG-CLB coatings having PS (10.02%), PEG (9.96%), and CLB (80.02%) of a 75 µl solution of each layer, and a single thick layer of 225 µl. The linear falling trend in the dried layer 1, 2, 3, and single thick layer is upto 4887 s, 4235 s, 5442 s, and 13564 s and by that time solvent removed are 77.55%, 84.21%, 86.31%, and 68.37%, respectively. The ultimate residual solvent left in the layer 1, 2, 3, and single thick layer are 14.48%, 10.44%, 8.27%, and 13.89%, respectively.

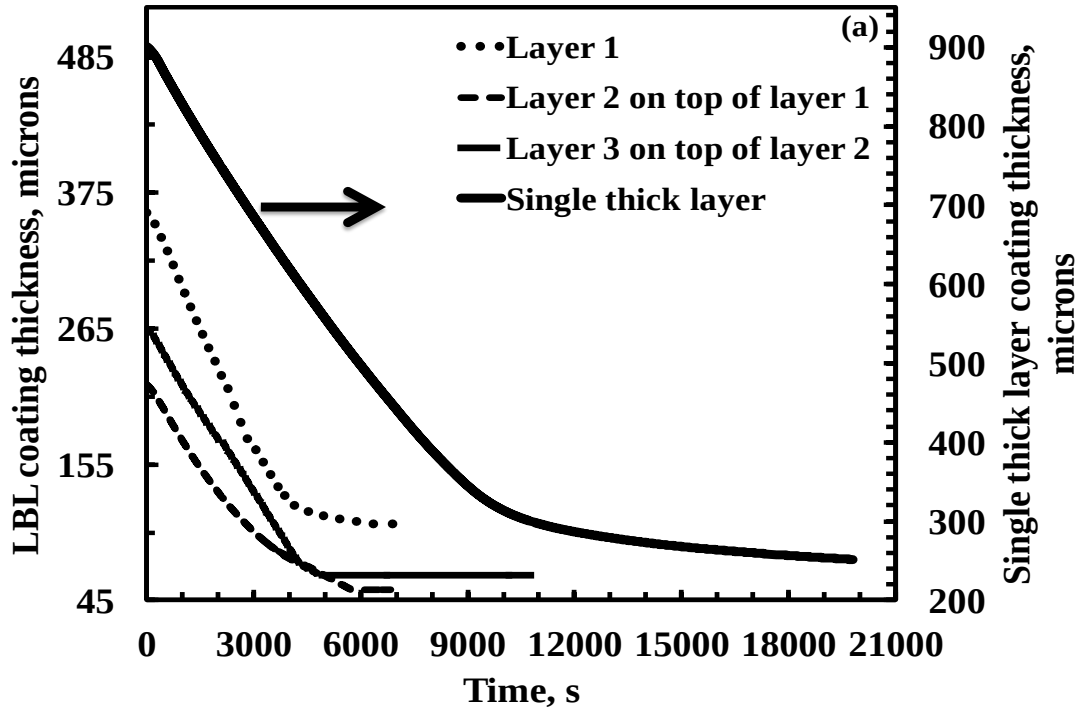

Figure 3.21 (a): Layer-by-layer coating thickness and single-layer coating thickness with time in poly(styrene), poly(ethylene glycol) and chlorobenzene: 10.02 wt%, 9.96 wt% and 80.02 wt%, respectively of 50 µl injected volume at 8 °C.

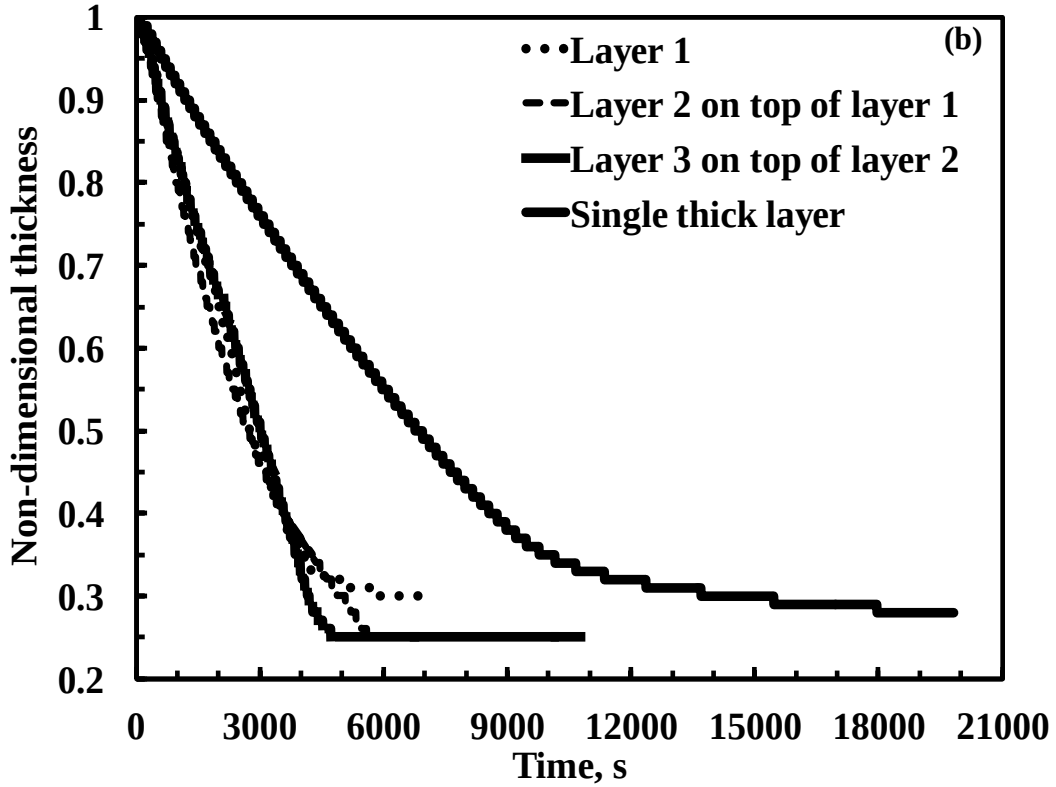

Figure 3.21 (b). Non-dimensional coating thickness with time in poly(styrene), poly(ethylene glycol) and chlorobenzene: 10.02 wt%, 9.96 wt% and 80.02 wt%, respectively of 50 µl injected volume at 8 °C.

Figure 3.24a and 3.24b shows the evolution of the coating thickness and non-dimensional coating thickness of layer-by-layer coating and single thick layer of PS-PEG-CLB having PS (10.02%), PEG (9.96%), and CLB (80.02%) of a 75 µl solution of each layer and a single thick layer of 225 µl. Single coating thickness of 225 µl is reduced to 533 µm in 40819 s from its initial thickness of 1721 µm. Layer 1, layer 2, layer 3 in the LBL assembly are reduced to 152 µm, 77 µm, 148 µm from their initial thickness of 484 µm, 273 µm, and 559 µm, respectively, in 13726 s, 7740 s, and 11104 s, respectively. The residual solvent in layer-by-layer case is much higher than the single thick layer.

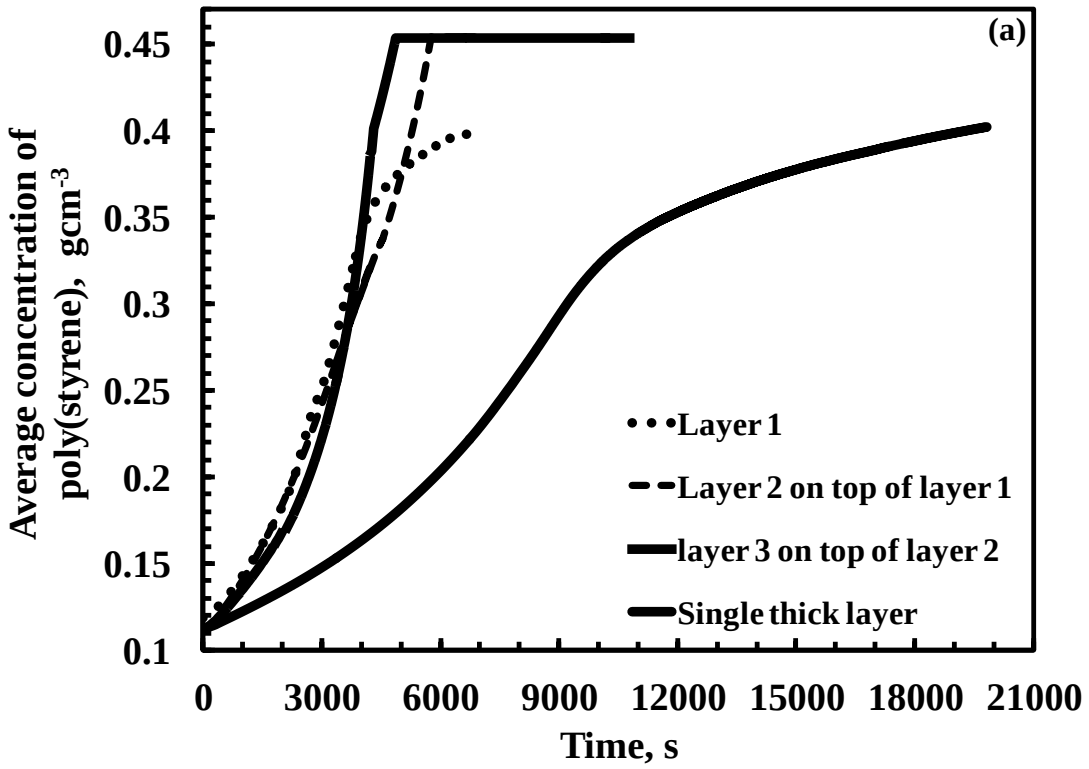

Figure 3.22 (a): Average concentration of poly(styrene) with time poly(ethylene glycol)- poly(ethylene glycol)-chlorobenzene: 10.02 wt%, 9.96 wt% and 80.02 wt%, respectively of 50 µl injected volume at 8 °C.

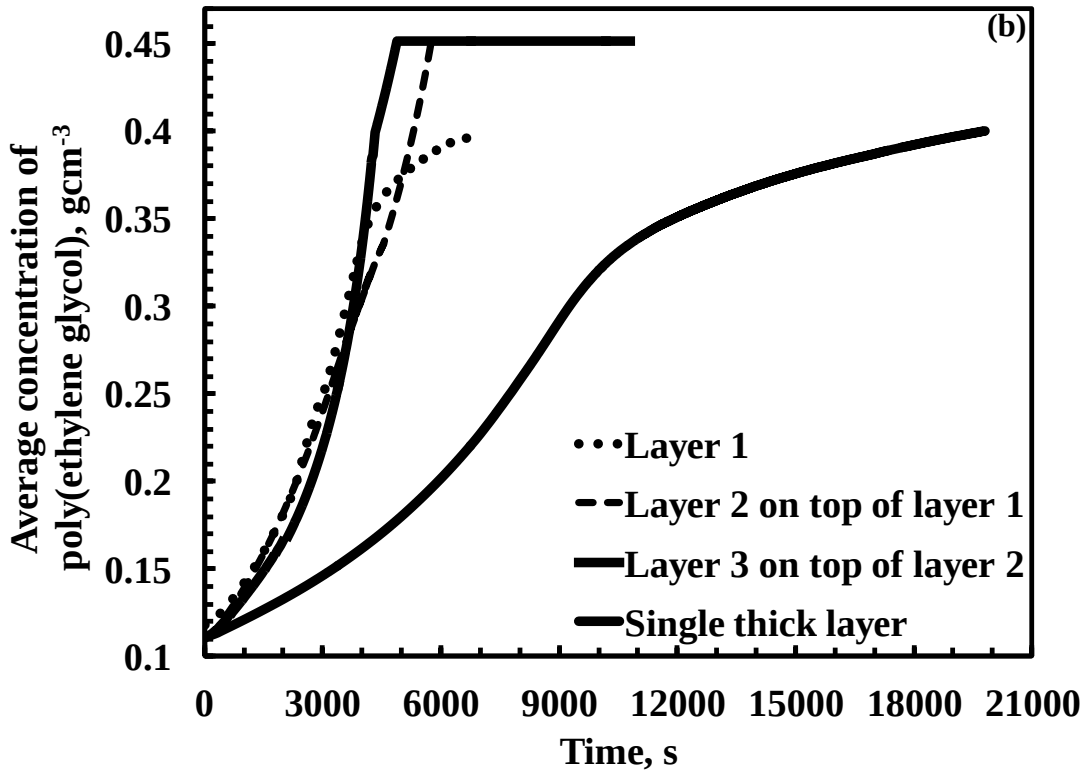

Figure 3.22 (b): Average concentration of poly(ethylene glycol) with time in poly(ethylene glycol)- poly(ethylene glycol)-chlorobenzene: 10.02 wt%, 9.96 wt% and 80.02 wt%, respectively of 50 µl injected volume at 8 °C.

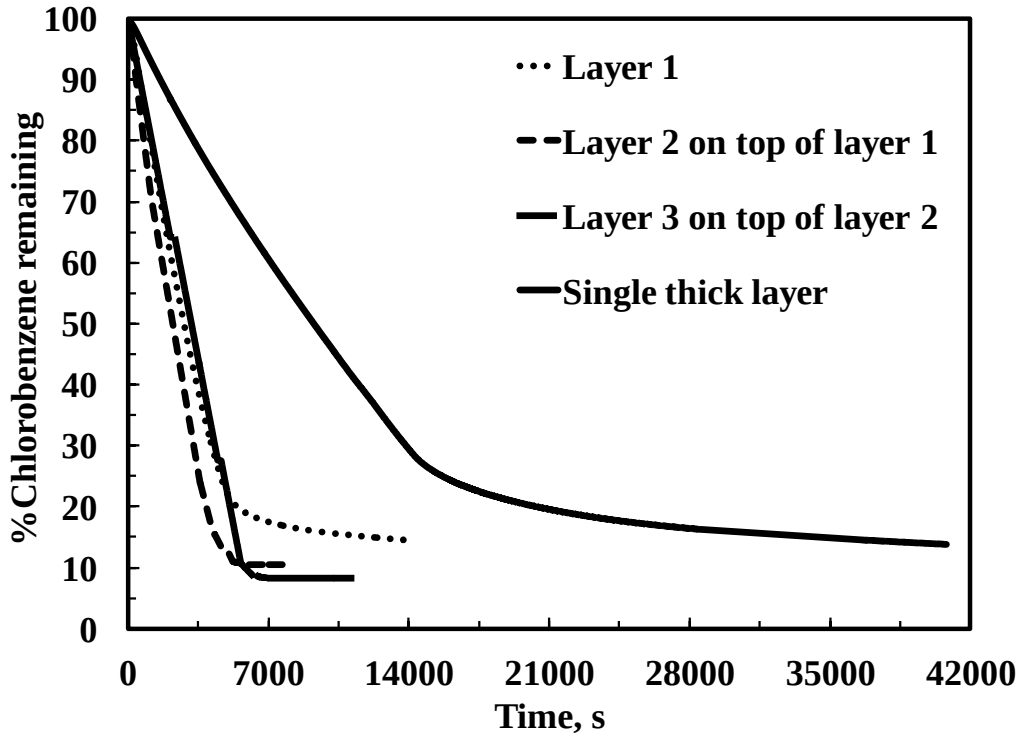

Figure 3.23: Percentage residual chlorobenzene with time in coating having poly(styrene), poly(ethylene glycol) and chlorobenzene: 10.02 wt%, 9.96 wt% and 80.02 wt%, respectively of 75 µl injected volume at 8°C.

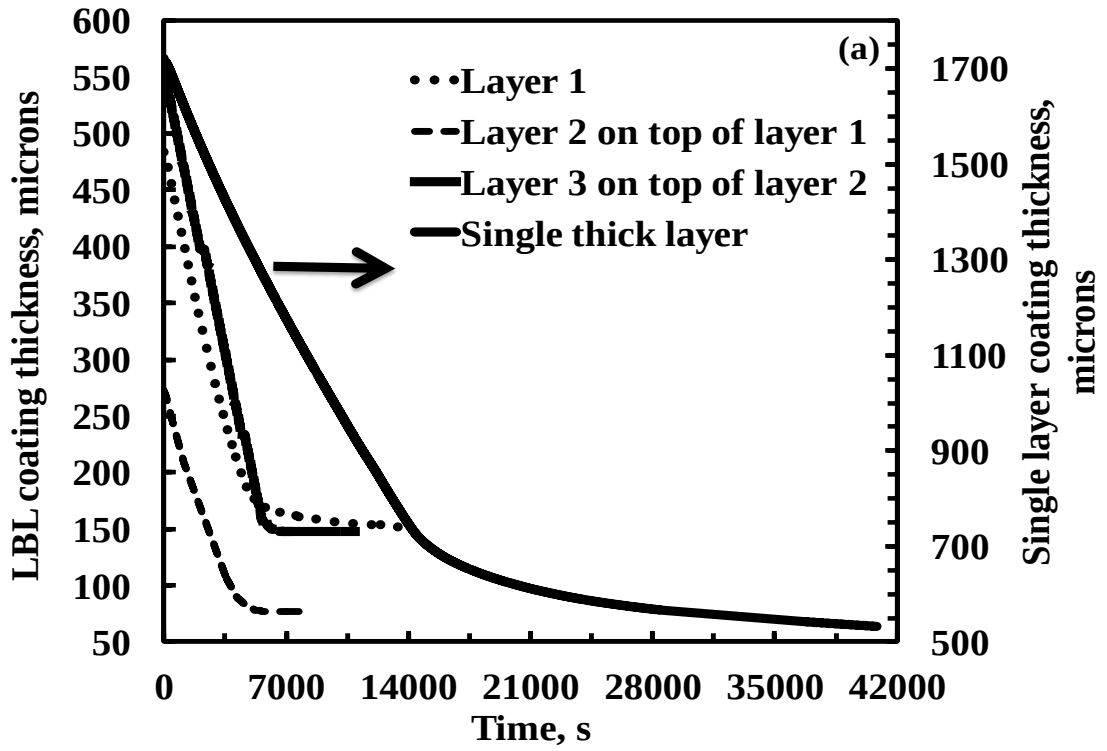

Figure 3.24(a): Layer-by-layer coating thickness and single-layer coating thickness with time in poly(styrene), poly(ethylene glycol) and chlorobenzene: 10.02 wt%, 9.96 wt% and 80.02 wt%, respectively of 75 µl injected volume at 8 °C.

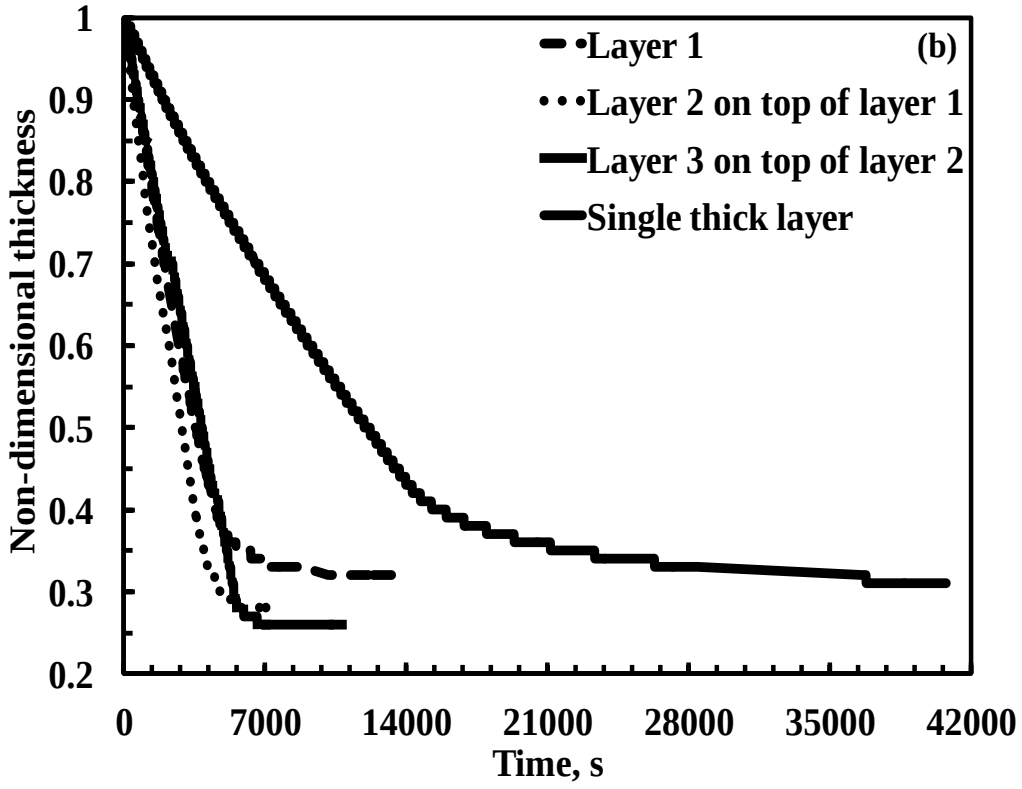

Figure 3.24(b): Layer-by-layer coating thickness and single-layer coating thickness with time in poly(styrene), poly(ethylene glycol) and chlorobenzene: 10.02 wt%, 9.96 wt% and 80.02 wt%, respectively of 75 µl injected volume at 8 °C.

Figure 3.25a shows the average concentration of poly(styrene) with time. It represents that the polymer concentration start increasing with time due to the evaporation of chlorobenzene from coating. In layer 1, layer 2, layer 3, and single thick layer coatings, the concentration of the polymer increases exponentially up to 5662 s, 4615 s, 5982 s, and 14624 s, respectively, for the coatings having initial thickness of 484 µm, 273 µm, 559 µm, and 1721 µm, respectively, and then plateaus off. The final concentration of PS in layer 1, layer 2, layer 3, and single thick layer coating were 0.354 g cm^{-3}, 0.395 g cm^{-3}, 0.420 g cm^{-3}, and 0.359 g cm^{-3} for coatings having initial concentration 0.11 g cm^{-3}, 0.11 g cm^{-3}, 0.11 g cm^{-3}, and 0.11 g cm^{-3}, respectively.

Figure 3.25b shows the average concentration of poly(ethylene glycol) with time. It represents that the polymer concentration start increasing with time due to the evaporation of chlorobenzene from coating. In layer 1, layer 2, layer 3, and single thick layer coatings, the concentration of the polymer increases exponentially up to 5558 s, 4675 s, 6002 s, and 14564 s, respectively, for the coatings having initial thickness of 484 µm, 273 µm, 559 µm, and 1721 µm, respectively, and then plateaus off. The final concentration of PEG in layer 1, layer 2, layer 3, and single thick layer coating were 0.352 g cm-3, 0.329 g cm-3, 0.418 g cm-3, and 0.357 g cm-3 for the coatings having initial concentration 0.11 g cm^{-3}, 0.11 g cm^{-3}, 0.11 g cm^{-3}, and 0.11 g cm^{-3}, respectively. Figure 3.25a and Figure 3.25b also follow the same trend as in the case of Figure 3.10b, Figure 3.16b and Figure 3.22b.

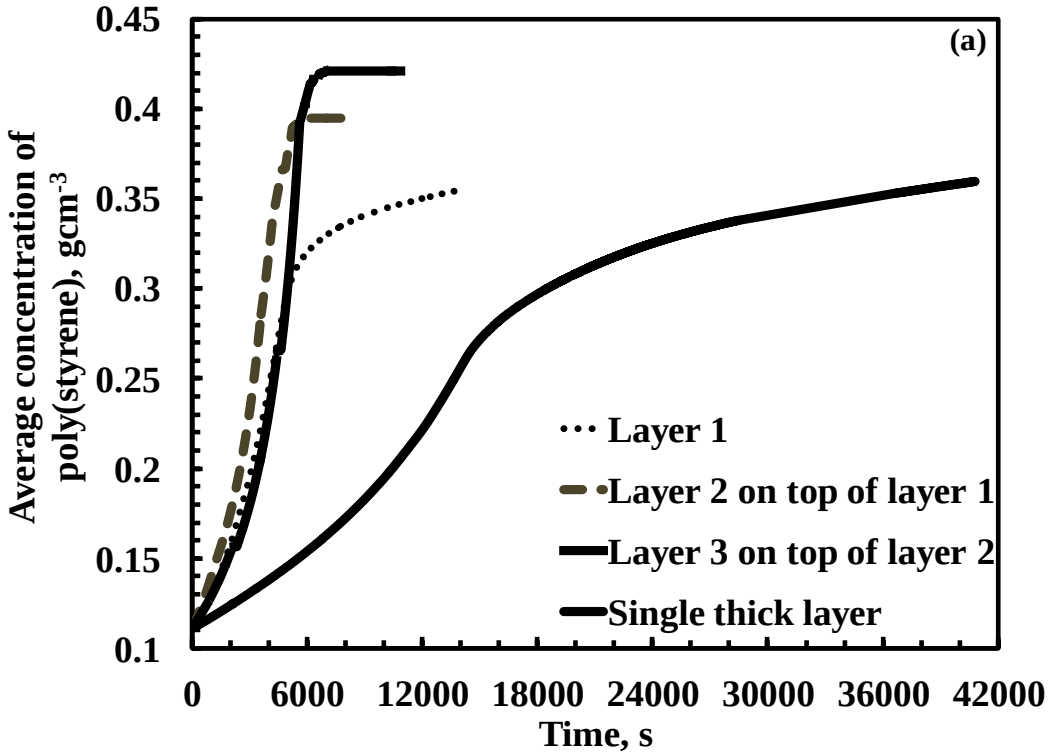

Figure 3.25(a): Average concentration of poly(styrene) with time in poly(ethylene glycol)- poly(ethylene glycol)-chlorobenzene: 10.02 wt%, 9.96 wt% and 80.02 wt%, respectively of 75 µl injected volume at 8 °C.

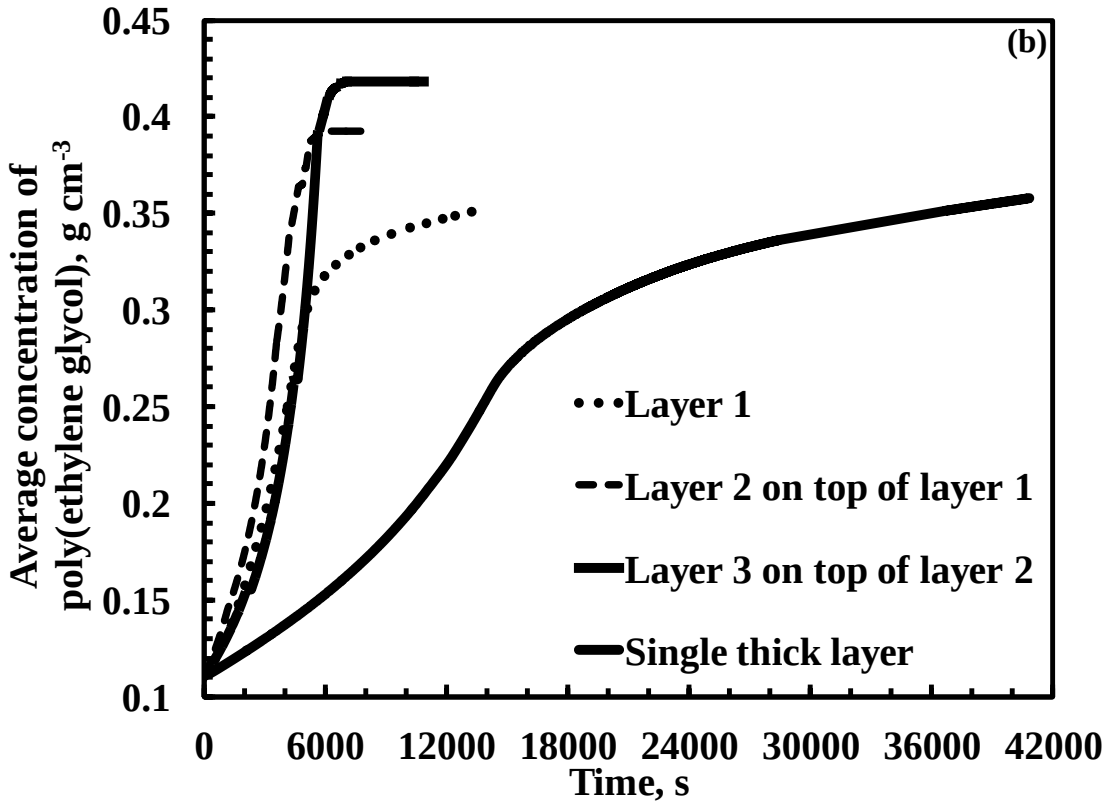

Figure 3.25(b): Average concentration of poly(ethylene glycol) with time in poly(ethylene glycol)- poly(ethylene glycol)-chlorobenzene: 10.02 wt%, 9.96 wt% and 80.02 wt%, respectively of 75 µl injected volume at 8 °C.

A comprehensive summary of the data obtained is presented in Table 3.1. Doubling the PEG from 5% to 10% has significantly increased the residual solvent as can be seen in Table 3.1, that is, from 19% to 23.03% for 50 µl injected volume initial volume, and from 34.87% to 29.8% for 75 µl of injected volume. PS (5.05%)- PEG (4.98%)- CLB (89.97%) is taken as a base shown in row 1. The residual solvent entrapped increases from 19% to 23.03% with the increase in the injected volume. With doubling of PEG as shown in row 3, there is a decrease in the residual solvent that is from 12.8% to 9.83% in the case of single thick layer coating. As PEG is an amorphous polymer, it will have better diffusion of the solvent. In the case of LBL, each layer will turn to glassy at the end of drying. The percentage of solvent for the glassy layer is system specific, that is, for the PS-CLB system it would be a specific value as mentioned in the literature [20]. Hence, more amount of solvent got trapped in the coating as shown in row 3, for the 50 µl injected volume of each layer. This also follows for the 75 µl of the injected volume in doubling the PEG from 5% to 10% as shown in row 4.

Now, doubling of PS increases the residual solvent drastically from 19% to 34.58% as shown in row 5, for the LBL technique. PS has a higher glass transition temperature than PEG. Glass transition is a strong function of the weight fraction. Now, doubling the concentrations of both PS and PEG increases the residual solvent from 19% to 22.73% due to the more viscous polymeric solution as shown in rows 7 and 8 in Table 3.1 for the 50 µl injected volume. There is a slight decrease in the residual solvent percentage in the 75 µl injected volume, that is, from 34.87% to 33.19% in row 8, for the LBL technique as compared to the base case, row 1, of the LBL technique. While preparing coatings, there is some amount of residual solvent remained trapped in the coatings. In the case of LBL technique, the coatings were prepared in layers, so the solvent in the top coating will diffuse in the previous coatings also, which makes it difficult to come out from the coating, resulting in the higher amount of residual solvent left in the LBL coatings as compared to the single thick layer coating. Elucidating in terms of interaction parameter, the polymer and solvent might have reached a parameter value that is not a further function of the concentration. This could be due to the non-dependency of solution thermodynamics beyond a particular value of the polymer mass fraction. As the polymer concentration increases, the amount of solution poured into the sample holder decreases due to an

increased viscosity. The average concentrations of both the polymers have increased at a slow rate with the addition of more amount of polymer, which shows that the coatings are rubbery for a longer time with a slow diffusion rate, which is nearly equal to the rate of evaporation of the solvent from the top.

Table 3.1: Summary of drying data of LBL coatings and single thick layer PS-PEG-CLB coatings.

S. No	Composition	Injected Volume, µL	Initial thickness (µm)	Final thickness (µm)	Drying time (s)		Residual Solvent%	Ultimate Residual Solvent (%)
					Falling rate time (s)	Constant rate time (s)		
1.	PS: 5.05 %, PEG :4.98 % CLB: 89.97	Layer 1 : 50	377	51	0-5072	5072-6882	3.97	19
		Layer 2 : 50	407	71	0-4952	4952-7297	8.3	
		Layer 3 : 50	326	49	0-4317	4317-5752	6.73	
		Single thick layer: 150	**1260**	**271**	0-18091	18091-20706	**12.8**	**12.8**
2.	PS: 5.05 %, PEG :4.98 % CLB: 89.97	Layer 1 : 75	678	109	0-6132	6231-8728	6.75	34.87
		Layer 2 : 75	570	119	0-4158	4158-6489	12.22	
		Layer 3 : 75	503	122	0-4358	4358-6489	15.9	
		Single thick layer: 225	**1349**	**276**	0-19748	19748-21568	**11.69**	**11.69**
3.	PS: 5.05%, **PEG:10.04%** CLB:84.91%	Layer 1 : 50	406	93	0-5157	5157-6117	9.72	23.03
		Layer 2 : 50	462	94	0-6868	6868-8418	6.73	
		Layer 3 : 50	459	93	0-5806	5806-7592	6.58	
		Single thick layer: 150	**613**	**141**	0-10279	10279-11929	**9.83**	**9.83**
4.	PS: 5.05%, **PEG:10.04%** CLB:84.91%	Layer 1 : 75	416	103	0-6102	6102-8558	11.89	29.8
		Layer 2 : 75	402	87	0-6983	6983-9674	8.1	
		Layer 3 : 75	468	108	0-7058	7058-8793	9.81	
		Single thick layer: 225	**1327**	**318**	0-19246	19246-21956	**10.88**	**10.88**
5.	**PS: 10.06%,** PEG: 5.13%, CLB:84.81%	Layer 1 : 50	206	47	0-3937	3937-5237	8.33	34.58
		Layer 2 : 50	215	57	0-3516	3516-5437	13.39	
		Layer 3 : 50	192	50	0-3732	3732-5888	12.86	
		Single thick layer: 150	**946**	**209**	0-12761	12761-15941	**8.1**	**8.1**
6.	**PS: 10.06%,** PEG: 5.13%, CLB:84.81%	Layer 1 : 75	412	82	0-7042	7042-9572	5.46	32.9
		Layer 2 : 75	328	88	0-5497	5497-8632	13.76	
		Layer 3 : 75	264	71	0-8703	8703-16501	13.68	
		Single thick layer: 225	**1204**	**280**	0-17061	17061-19727	**9.36**	**9.36**
7.	**PS: 10.01%, PEG: 9.95%,** CLB: 80.02%	Layer 1 : 50	359	107	0-3901	3901-6467	10.99	22.73
		Layer 2 : 50	220	54	0-5231	5231-6851	5.86	
		Layer 3 : 50	265	65	0-4838	4838-10794	5.88	
		Single thick layer: 150	**901**	**251**	0-8833	8833-19816	**9.88**	**9.88**
8.	**PS: 10.01%, PEG: 9.95%,** CLB: 80.02%	Layer 1 : 75	484	152	0-4887	4887-13726	14.48	33.19
		Layer 2 : 75	273	77	0-4235	4235-7740	10.44	
		Layer 3 : 75	559	148	0-5442	5442-11104	8.27	
		Single thick layer: 225	**1721**	**533**	0-13564	13564-40819	**13.89**	**13.89**

3.4 Conclusions

The residual solvent content in the poly(strene)-poly(ethylene glycol)-chlorobenzene coatings of the LBL assembly has more percentage of solvent trapped in the coating as compared to the single thick layer coatings. More viscous solution has more solvent remaining in the coating. The solution should be diluted to reduce the residual solvent.

References

[1] H. Levine, L. Slade, Influences of the glassy and rubbery states on the thermal, mechanical, and structural properties of doughs and baked products, in: Dough rheology and baked product texture, Springer, Boston, MA, 1990, 157-330.

[2] M. Eriksson, H. Goossens, T. Peijs, Influence of drying procedure on glass transition temperature of PMMA based nanocomposites, Nanocomposites, 1 (2015) 36-45.

[3] B.J. Briscoe, E. Pelillo, S.K. Sinha, Scratch hardness and deformation maps for polycarbonate and polyethylene, Polymer Engineering & Science, 36 (1996) 2996-3005.

[4] J. Sharma, R.K. Arya, S. Ahuja, C.K. Bhargava, Residual solvent study in polymer− polymer—solvent coatings: Poly (styrene)—poly (methyl methacrylate)—tetrahydrofuran coatings, Progress in Organic Coatings, 113 (2017) 200-206.

[5] D. Wang, L. Nie, X. Shao, H. Yu, Exposure profile of volatile organic compounds receptor associated with paints consumption, Science of The Total Environment, 603 (2017) 57-65.

[6] A. Cheng, R. Swaminathan, Layer By Layer (Lbl) Self-Assembly Strategy And Its Applications, Nanotechnology Engineering, University of Waterloo, 1-5.

[7] T. Pham, X. Cheng, S. Kumar, Drying of multicomponent thin films on substrates with topography, Journal of Polymer Science Part B: Polymer Physics, 55 (2017) 1681-1691.

[8] R.K. Arya, M. Vinjamur, Near-optimization of operating conditions and residence times in multizone dryers for polymer coatings, Industrial & Engineering Chemistry Research, 48 (2009) 10504-10514.

[9] L. Francis, A. McCormick, D. Vaessen, J. Payne, Development and measurement of stress in polymer coatings, Journal of Materials Science, 37 (2002) 4717-4731.

[10] S.-T. Hsu, Y.L. Yao, Effect of Film Formation Method and Annealing on Morphology and Crystal Structure of Poly (L-Lactic Acid) Films, Journal of Manufacturing Science and Engineering, 136 (2014) 1-9.

[11] C.K. Bhargava, R.K. Arya, Design of Binary Polymeric Coatings for Minimizing the Residual Solvent, Part I: Experimentation, Drying Technology, 33 (2015) 92-102.

[12] K. Ute, N. Miyatake, K. Hatada, Glass transition temperature and melting temperature of uniform isotactic and syndiotactic poly (methyl methacrylate) s from 13mer to 50mer, Polymer, 36 (1995) 1415-1419.

[13] A. Pathania, J. Sharma, R.K. Arya, S. Ahuja, Effect of crosslinked polymer content on drying of binary polymer—solvent coatings, Progress in Organic Coatings, 114 (2018) 78-89.

[14] R.K. Arya, Measurement of concentration profiles in thin film binary polymer-solvent coatings using confocal Raman spectroscopy: Free volume model validation, Drying Technology, 32 (2014) 992-1002.

[15] D. Siebel, P. Scharfer, W. Schabel, Determination of Concentration-Dependent Diffusion Coefficients in Polymer–Solvent Systems: Analysis of Concentration Profiles Measured by Raman Spectroscopy during Single Drying Experiments Excluding Boundary Conditions and Phase Equilibrium, Macromolecules, 48 (2015) 8608-8614.

[16] J. Sharma, K. Tewari, R.K. Arya, Diffusion in polymeric systems–A review on free volume theory, Progress in Organic Coatings, 111 (2017) 83-92.

[17] R.K. Arya, K. Tewari, S. Shukla, Non-Fickian drying of binary polymeric coatings: Depth profiling study using confocal Raman spectroscopy, Progress in Organic Coatings, 95 (2016) 8-19.

[18] S.P. Velaga, D. Nikjoo, P.R. Vuddanda, Experimental Studies and Modeling of the Drying Kinetics of Multicomponent Polymer Films, AAPS PharmSciTech, 19 (2018) 425-435.

[19] H. Yan, L. Zhao, Z. Fang, H. Wang, Construction of multilayer coatings for flame retardancy of ramie fabric using layer-by-layer assembly, Journal of Applied Polymer Science, 134 (2017), 1-11.

[20] T. Chow, Molecular interpretation of the glass transition temperature of polymer-diluent systems, Macromolecules, 13 (1980) 362-364.

Chapter 4

Morphological Studies of Poly(styrene)-Poly(ethylene glycol)-Chlorobenzene System

This chapter includes the morphological behavior of the prepared coating of the PS-PEG-CLB system using scanning electron microscopy (SEM). The coatings prepared from single thick layer and layer-by-layer assembly was analyzed by SEM. The outcomes from the drying induced phase separated coatings are discussed in this chapter.

4.1 Introduction

Polymeric membranes are used for the separation, chemical sensors, chromatography, and solid phase extraction [1]. Porous polymeric coatings have received much interest, due to their high porosity and their ability to be manufactured from phase separation of polymeric solution. In this, Porosity is seen as an important property to understand the nature and to create advanced structures. These coatings have huge advantages because of their high surface area and well-defined porosity and their ability to be molded into thin films and monolithic forms [2].

Polymers such as linear homopolymers [3], coil-coil block polymers [4], copolymers [5], etc have been reported to form microporous structures. Phase separation method is used for making membranes. Portraying the broad range of physical appearances and the type of material they are made from, the synthetic membrane can be of symmetric (isotropic) or asymmetric (anisotropic) nature. Asymmetric membranes include different structure with large to fine pore size,

forming the skin on top of the membrane [6]. Hence they have various industrial applications such as ultrafilteration, reverse osmosis, and gas separation [7].

Dense polymeric membranes can be prepared from the evaporation of solvent by different methods such as solution casting, dry casting, thermally induced phase separation, and vapor induced phase separation. If the drying rate is higher than the phase separation rate, then a dense top layer is formed due to high solvent evaporation rate [8]. Physical and chemical study in the field of binary polymeric coatings has been very well documented in the literature [9-12].

The structural analysis of the coating is now applicable in the field of polymeric films. Porous polymeric films are used in many fields such as photonics [13], tissue engineering [14] etc. Marongoni convection is one of the possible principles leading to the formation of highly ordered hexagonal array [15-17]. The complete evaporation of the solvent results in 3D or 2D arrays of hexagonally ordered pores [3]. The phase separation of a polymer-solvent-non solvent system by vapor phase is studied in the literature [18]. Polystyrene (PS) and its derivatives containing polar groups are well studied commercial polymers. The linear PS is known to be the best for making porous polymeric films and ordered structures. The very first honeycomb structure contained solid films with hexagonal 2D arrangement of holes of 1-5 μm diameter by Francois et al. [19] from poly(styrene) solutions on glass platelets. The substrate and the solvent play a key role in making an ordered homogeneous hexagonal pore arrangement, their dimensions and degree of their orderliness in the film.

Ghannam et al. [20] reported highly ordered self-assembled honeycomb structures of poly(styrene) with cationic end group that formed star like arrangement with carbon disulfide. The prepared films were spread on inorganic support (mica and glass) and organic support (PVC sheets). The scanning electron microscopy (SEM) analysis of the films showed that the hexagonal structures were of homogeneously pore size of 4 μm on mica substrate. But on glass substrate, less ordered structures with much greater pore polydispersity were formed. On PVC sheets, the homogeneous pores were 1.5 μm in size.

Nicho et al. [21] studied the morphology of poly(styrene) (PS)-poly(3-octylthiophene) (P3OT)-toluene thin films with atomic force microscope (AFM). The study showed that PS-P3OT had lamellar structure along with pit formation. The pit depth varied from 46nm-70nm for 20% to 40% of P3OT in PS, and reached upto 74nm at nearly 60% of P3OT in PS.

Zareh et al. [22] studied a conductive polymer system of poly(aniline) (PANI)-starch-Polystyrene –THF composites. UV, FTIR, SEM, DSC analysis were done, and their biodegradability tests were performed to check the conductivity of the composites and the effect of the concentration of PANI on the composites. The size of PANI played a major role in granular structure of PANI/starch blends. Nanoscale PANI favored high conductivity in PANI/starch blends. All the characterizations favored the PANI/starch blend as compared to pure starch and provided the higher conductivity as compared to pure starch.

Ferrari et al. [23] studied the effect of solvents in making so-called breath figures from the linear poly(styrene) solutions. The solvents studied by them were acetone, cabon disulfide, cholorform, ethyl acetate, methyl ethyl ketone, dichloromethane, tetrahydrofuran, and toluene. The solvents were chosen in such a way that they have partial miscibility or immiscibility with water and have lower or higher density than water. Irregular or poor ordered breath figures were obtained from acetone, ethyl acetate, tetrahydrofuran, and acetone. Dicholomethane, chloroform and carbon disulfide resulted into highly ordered breath figures due to their low energy differences.

The ternary coatings made two polymer and one solvent is a promising field in the polymer films [24-27]. The researchers have used only single polymer along with solvent and non-solvent. In this work a novel method is introduced to prepare the polymeric membrane using multipolymer solvent system. Poly(styrene)-poly(ethylene glycol)-chlorobenzene system is selected to study the drying induced phase separation. The morphological studies of the PS-PEG-CLB coating at different initial concentrations and initial film thicknesses by using SEM are investigated in the present study.

4.2 Experimental

4.2.1 Materials and methods

Poly(ethylene glycol)-6000 **(**density: 1.2 g cm^{-3}, Molecular weight: 5000-7000,) and Poly(styrene) (molecular weight: 192000,density: 1.05 g cm^{-3},) was supplied by Sigma Aldrich, Germany. Chlorobenzene (Molecular weight: 112 g/mol, density: 1.11 g cm^{-3}) was supplied by Spectrochem, India. All chemicals are used without any further purification. Solution casting method was used to get uniform and thin films. Several homogeneous films of poly(styrene)-poly(ethylene glycol)-chlorobenzene **(**PS-PEG-CLB) were prepared. The solution was transferred by means of micropipette into the stainless steel sample holder of diameters (12.24 mm and 14.65 mm) and depth (2000 µm and 4000 µm). PS-PEG-CLB solutions were prepared of concentration having 5.05 wt% (PS)- 4.98 wt% (PEG)- 89.97 wt% (CLB), 5.05 wt% (PS)-10.04 wt%(PEG) -84.91 wt% (CLB), 10.06 wt% (PS)- 5.13 wt% (PEG)-84.81 wt% (CLB) and 10.01 wt% (PS)- 9.96 wt% (PEG)- 80.02 wt% (CLB).

4.2.2 Preparation of membranes

Films were prepared by using layer-by-layer and single thick layer techniques. In LBL technique, 50 µl and 75 µl of four different concentrations were poured into the sample holder and its solvent weight loss data was recorded as a function of time by using semi micro analytical weighing balance (Precisa ES225SM-DR) having an accuracy of ±0.0001g. Data were recorded till no further significant change in the mass was observed with respect to time. All experiments were performed at 8 □C without any air flow. The film was then kept for 1-2 weeks for any further removal of solvent and taken as the ultimate dried film. The layer 2 and layer 3 of same volume were also prepared in the same manner on top of previous one. In the single thick layer film, the total amount of the entire three layers was poured at once and dried.

4.2.3 Characterization

Morphological studies of the PS-PEG-CLB coatings of four different concentrations had been examined by SEM (JEOL JSM-6510LV, TIET, Patiala-Punjab, India). The pores dimensions and circularity were evaluated by using the freeware images analysis software called ImageJ. The mean average and the standard deviations of the pore size were also calculated for the better understanding. The standard deviation was calculated by the equation:

$$S = \sqrt{\frac{\sum_{i=1}\left(x_i - \bar{x}\right)^2}{n-1}} \tag{4.1}$$

where s is the standard deviation, x_i is the diameter of the one hole, $\bar{x}$ is the mean of diameter of the holes in the coating, n is the number of holes. The schematic diagram of the mechanism of formation of holes is shown in Figure 4.1.

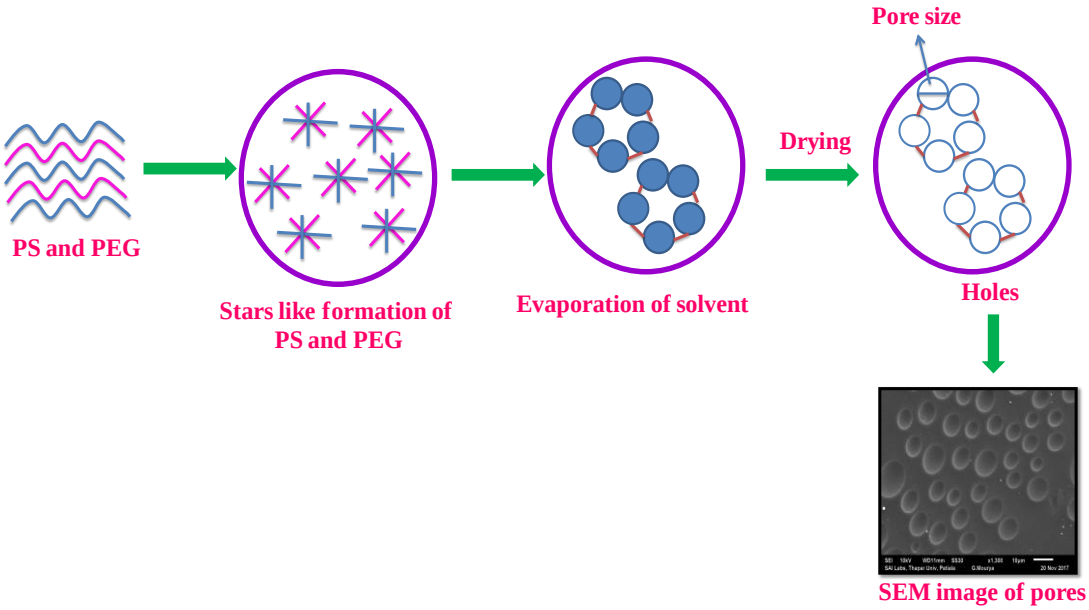

Figure 4.1: The schematic diagram of formation of holes.

4.3 Results and Discussion

Figure 4.2 (a and b) shows the top and bottom surface morphology of membranes prepared from poly(styrene)-poly(ethylene glycol)-chlorobenzene (5.05%-4.98%-89.97%) of 50 µl of LBL assembly. The initial thicknesses of layer 1, layer 2, and layer 3 were 377 µm, 407 µm, and 326 µm, respectively and final thicknesses were 51 µm, 71 µm, and 49 µm, respectively. The ultimate residual solvent percentage left in this coating was 19%. Figure 4.2 (c) represents the average area of the holes with respect to the diameters of the holes present in the coating. Highly ordered structure is observed in this coating with greater polydispersity in the size of the holes. The pores have a circular geometry. The average diameter of the circular holes is about 7.68 µm. Films are porous on the top and dense at the bottom. This could be due to the phase separation on the top side. This clearly indicates the formation of asymmetric membranes. The values of average size, average area of holes, and their standard deviation values were summarized in the Table 4.1.

Figure 4.3 (a and b) shows the top and bottom surface morphology of membranes prepared from poly(styrene)-poly(ethylene glycol)-chlorobenzene (5.05%-4.98%-89.97%) of 150 µl of single thick layer coating. The initial thickness and final thicknesses were 1260 µm and 271 µm, respectively. The residual solvent left in this coating was 12.8%. Figure 4.3 (c) represents the average area of the holes with respect to the diameters of the holes present in the coating. The average diameter of the holes is 9.61 µm which is higher than the 50 µl of injected volume in the layer-by-layer technique. In this case also the bottom side has a dense surface and forms the asymmetrical membrane.

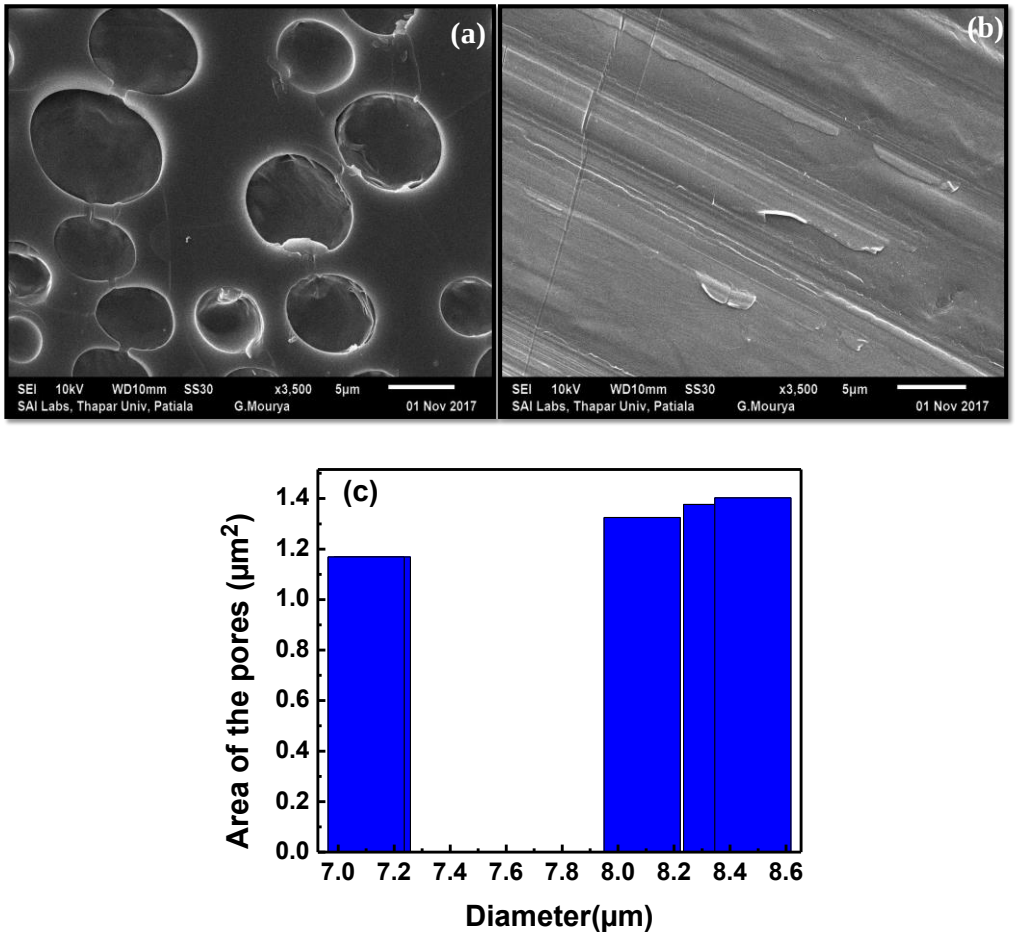

Figure 4.2 (a and b). SEM image showing top and bottom surface image of percentage having poly(styrene)-poly(ethylene glycol)-6000-chlorobenzene (5.05%-4.98%-89.97%) of 50 µl of LBL assembly and **(c)** the area of the number of pores present in the film.

Figure 4.4 (a and b) shows the top and bottom surface morphology of membranes prepared from poly(styrene)-poly(ethylene glycol)-chlorobenzene (5.05%-4.98%-89.97%) of 75 µl of LBL assembly. The initial thicknesses of layer 1, layer 2, and layer 3 were 678 µm, 570 µm, and 503 µm, respectively, and final thicknesses were 109 µm, 119 µm and 122 µm, respectively. The ultimate residual solvent percentage left in this coating was 34.87%. Figure 4.4 (c) represents the average area of the holes with respect to the diameters of the holes present in the coating. The average pore size is 8.53 µm and also shows the linkage of pores with each other. The bottom surface also seems to be porous without any specific type of pore geometry. The bigger size and higher value of standard deviation because of higher amount of residual solvent present in the coating i.e, 34.87%.

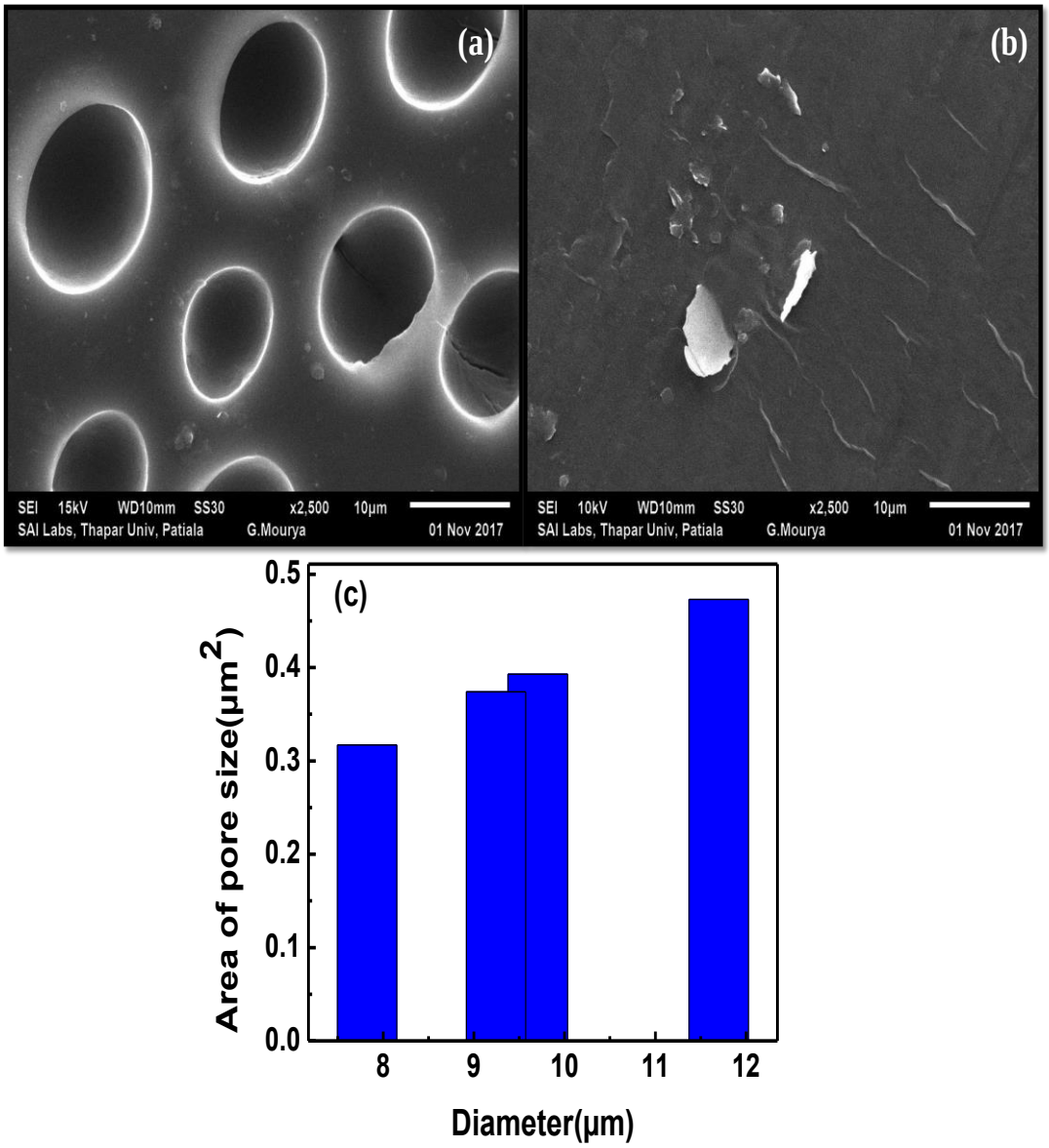

Figure 4.3 (a and b): SEM images showing top and bottom surface of poly(styrene)-poly(ethylene glycol)-6000-chlorobenzene (5.05%-4.98%-89.97%) of 150 µl of Single thick layer film and **(c)** the area of the different pores present in the film.

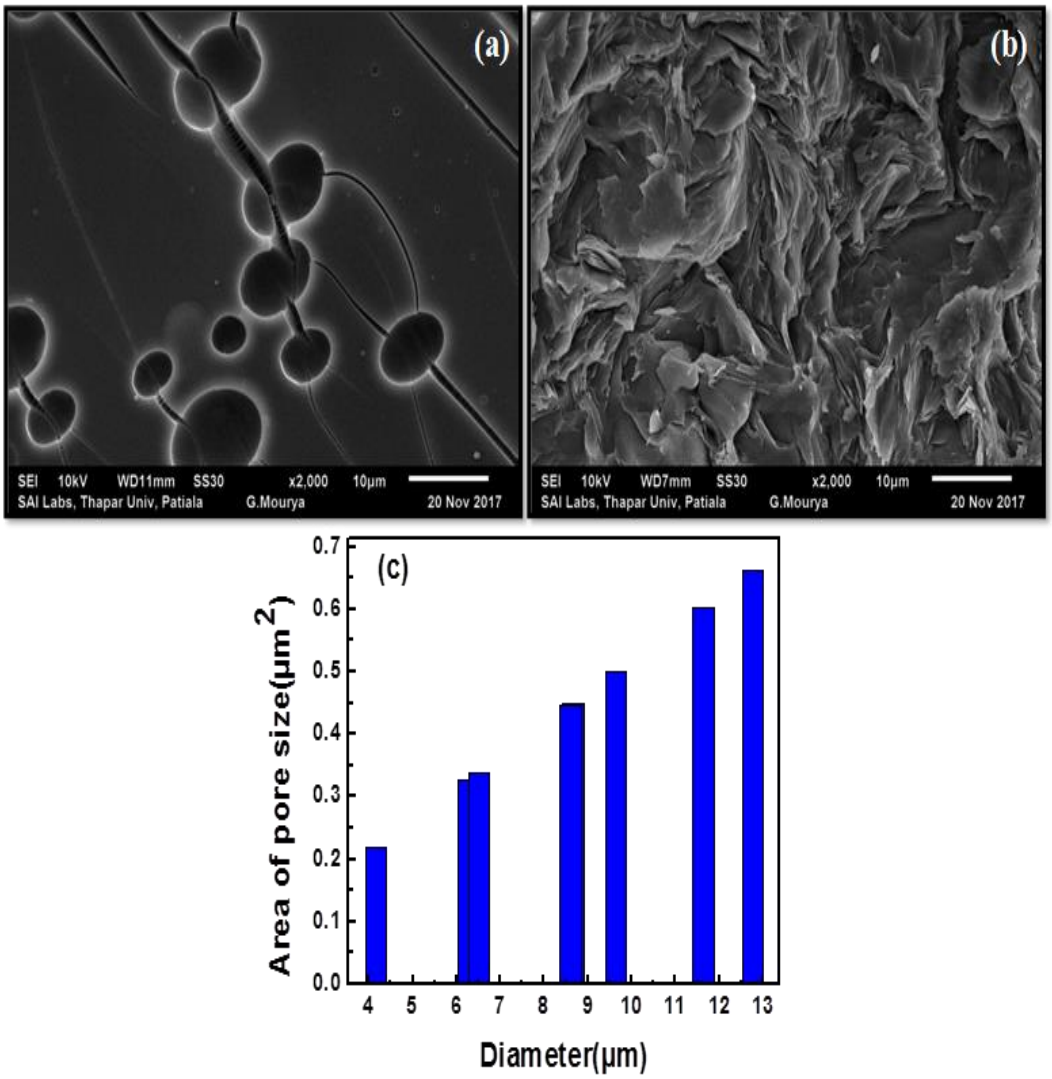

Figure 4.4 (a and b): SEM images showing top and bottom surface images of poly(styrene)-poly(ethylene glycol)-6000-chlorobenzene (5.05%-4.98%-89.97%) of 75 µl of LBL films and **(c)** the area of the different pores present in the film.

Figure 4.5 (a and b) shows the top and bottom surface morphology of the membranes prepared from poly(styrene)-poly(ethylene glycol)-chlorobenzene (5.05%-4.98%-89.97%) of 225 µl of single thick layer coating. The initial thickness and final thicknesses were 1349 µm and 276 µm, respectively. The residual solvent percentage left in this coating was 11.69%. Figure 4.5 (c) represents the average area of the holes with respect to the diameters of the holes present in the film. The average diameter of the pore size in this coating is 13.04 µm which is nearly double than the 50 µl of injected volume in LBL technique of the same concentration. This could be due to the higher percentage of solution casted into the substrate. The bottom side is also porous without any specific types of pore geometry.

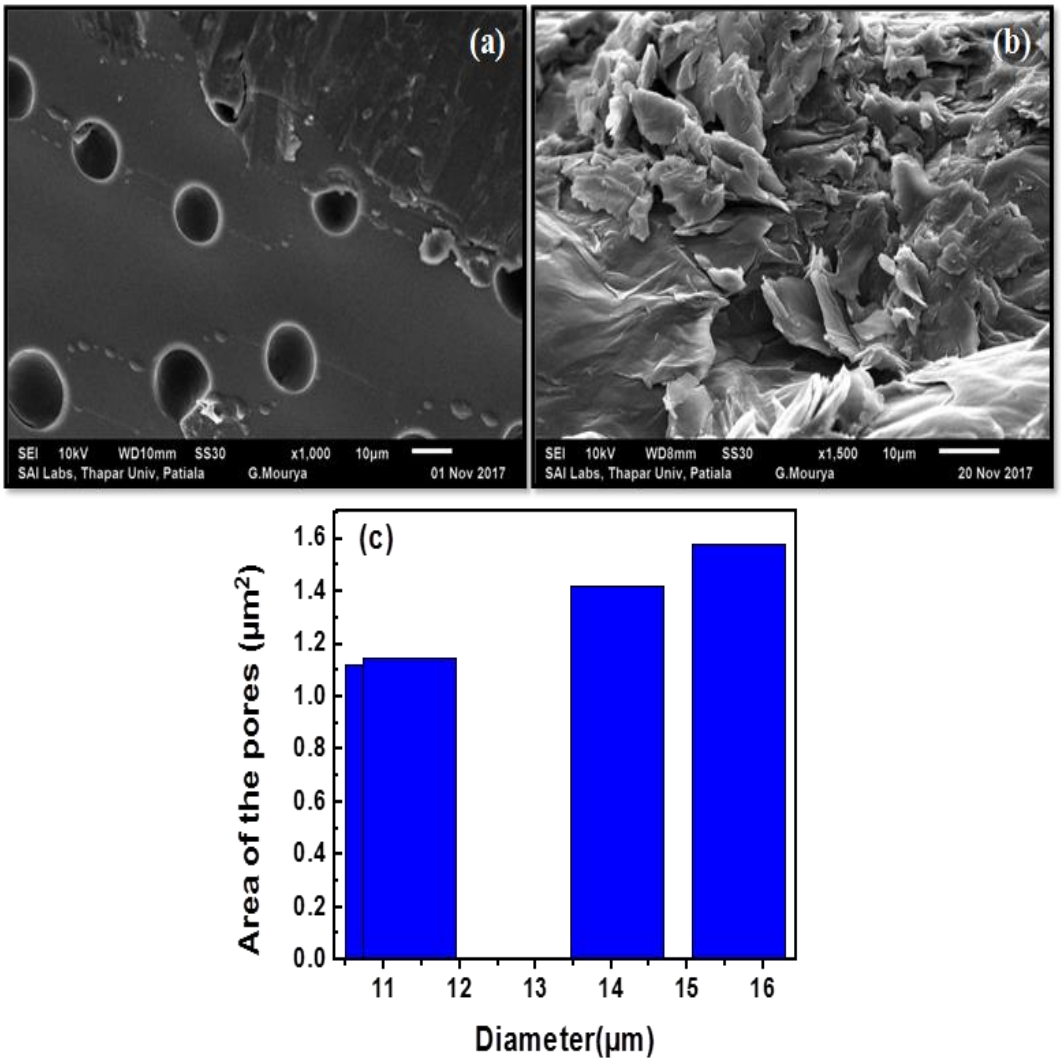

Figure 4.5 (a and b): SEM images showing top surface images of poly(styrene)-poly(ethylene glycol)-6000-chlorobenzene (5.05%-4.98%-89.97%) of 225 µl of single thick layer film and **(c)** the area of the different pores present in the film.

Figure 4.6(a and b) shows the top and bottom surface morphology of membranes prepared from poly(styrene)-poly(ethylene glycol)-chlorobenzene (10.06%-5.13%-84.81%) of 50 µl of LBL coatings. Figure 4.6 (c) represents the average area of the holes with respect to the diameters of the holes present in the coating. The initial thicknesses of layer 1, layer 2, and layer 3 were 206 µm, 215 µm, and 192 µm, respectively and final thicknesses were 47 µm, 57 µm, and 50 µm respectively. The ultimate residual solvent percentage left in this coating was 34.58%. With the increase in the concentration of PS from 5% to 10%, the average diameter of the hole is 4.89 µm which is smaller than the 7.68 µm of 50 µl of injected volume of poly(styrene)-poly(ethylene glycol)-chlorobenzene (5.05%-4.98%-89.97%). The smaller pore size has more advantages than the higher pore size as it is easily used for

separation due to high flux and can be used for gaseous separation. In this case, membranes are asymmetric but pore geometry is different on top and bottom. On top side, pores are circular and the bottom side has dense nature.

Figure 4.7 (a and b) shows the top and bottom surface morphology of membranes prepared from poly(styrene)-poly(ethylene glycol)-chlorobenzene (10.06%-5.13%-84.81%) of 75 µl of LBL coatings. Figure 4.7 (c) represents the average area of the holes with respect to the diameters of the holes present in the coating. The initial thicknesses of layer 1, layer 2, and layer 3 were 412 µm, 328 µm, and 264 µm, respectively, and final thicknesses were 82 µm, 88 µm, and 71 µm respectively. The ultimate residual solvent percentage left in this coating was 32.9%. The average diameter of the pore size in this coating is 4.02 µm which is nearly double than the 75 µl of injected volume of poly(styrene)-poly(ethylene glycol)-chlorobenzene (5.05%-4.98%-89.97). The bottom side has no pores. In this case also the pore diameter has decreased drastically due to high amount of polymer.

Figure 4.8 (a and b) shows the top and bottom surface morphology of membranes prepared from poly(styrene)-poly(ethylene glycol)-chlorobenzene (10.06%-5.13%-84.81%) of 150 µl of single thick layer coating. Figure 4.8 (c) represents the average area of the holes with respect to the diameters of the holes present in the coating. The initial thickness and final thicknesses were 946 µm and 209 µm respectively. The residual solvent percentage left in this coating was 8.1%. The average pore diameter in this case is 7.07 µm and average pore area is 0.53 μm^2. This also has less average diameter than injected volume of 150 µl of single thick layer coating of concentration having poly(styrene)-poly(ethylene glycol)-chlorobenzene (5.05%-4.98%-89.97%). The excellent distribution and uniformity of pore size has been observed on the top side. However, no trend has been found on the bottom side.

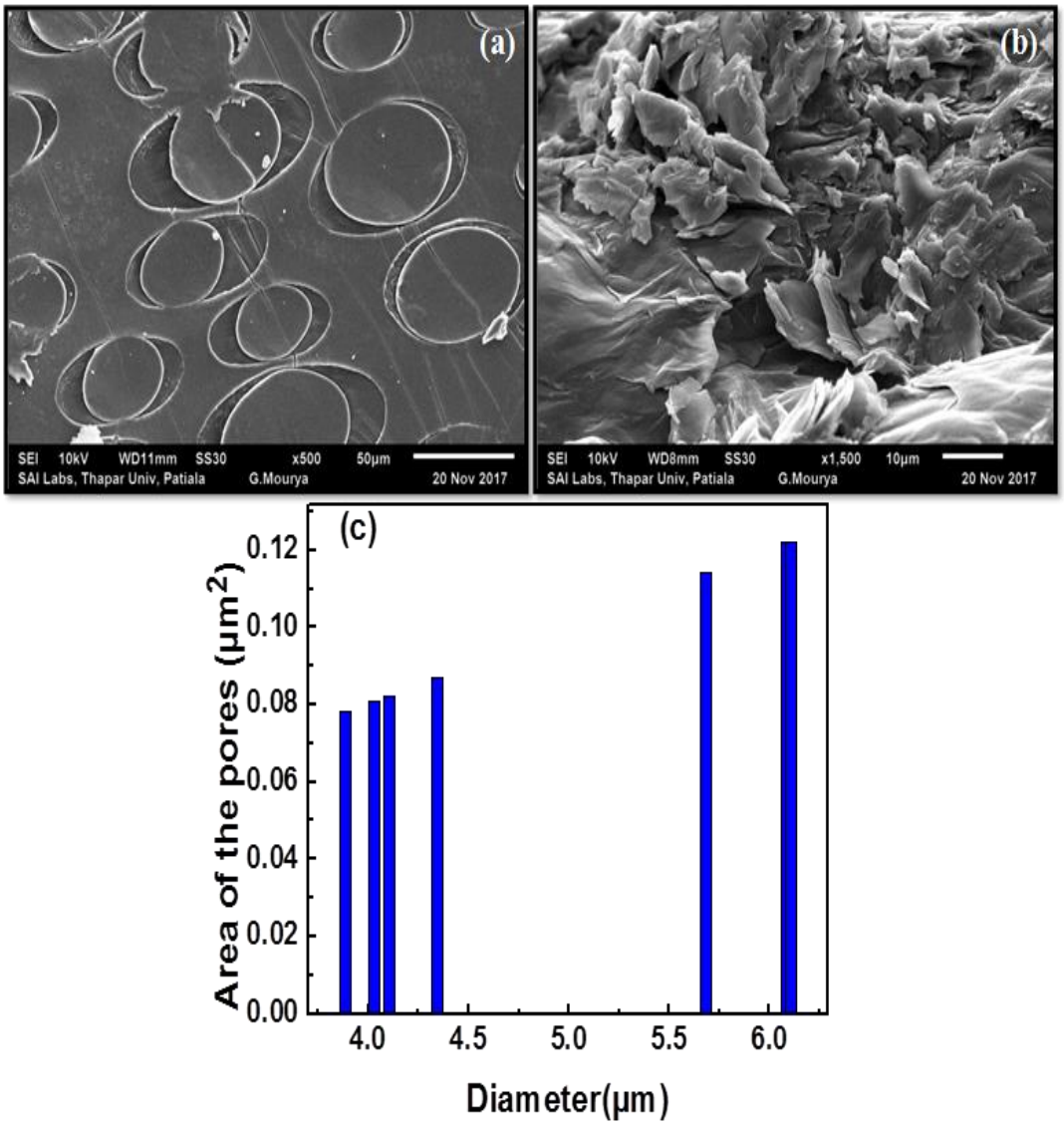

Figure 4.6 (a and b): SEM images showing top and bottom surface images of poly(styrene)-poly(ethylene glycol)-6000-chlorobenzene (10.06%-5.13%-84.81%) of 50 µl of LBL films and **(c)** the area of the different pores present in the film.

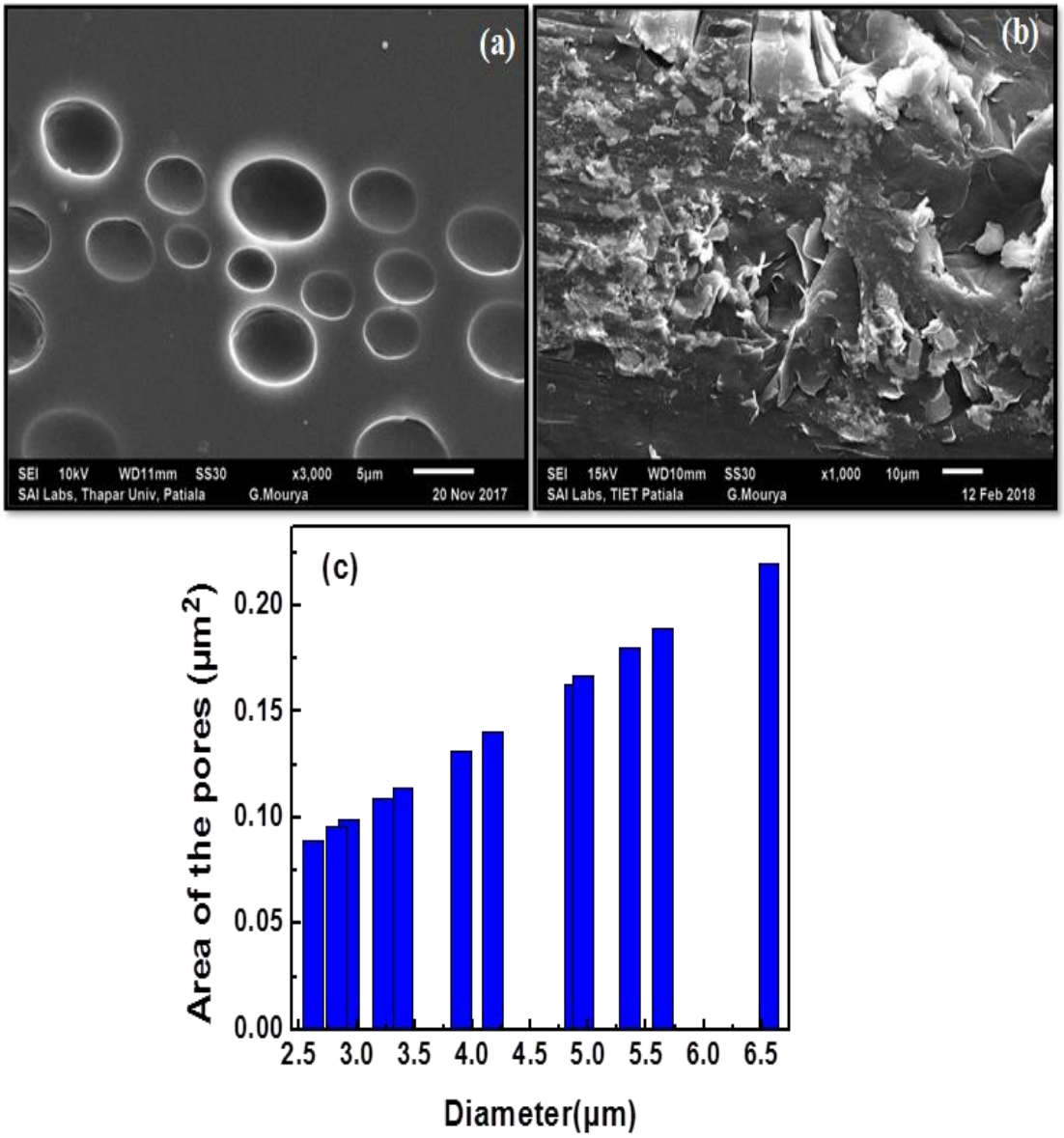

Figure 4.7 (a and b): SEM images showing top and bottom surface images of poly(styrene)-poly(ethylene glycol)-6000-chlorobenzene (10.06%-5.13%-84.81%) of 75 µl of LBL films and **(c)** the area of the different pores present in the film.

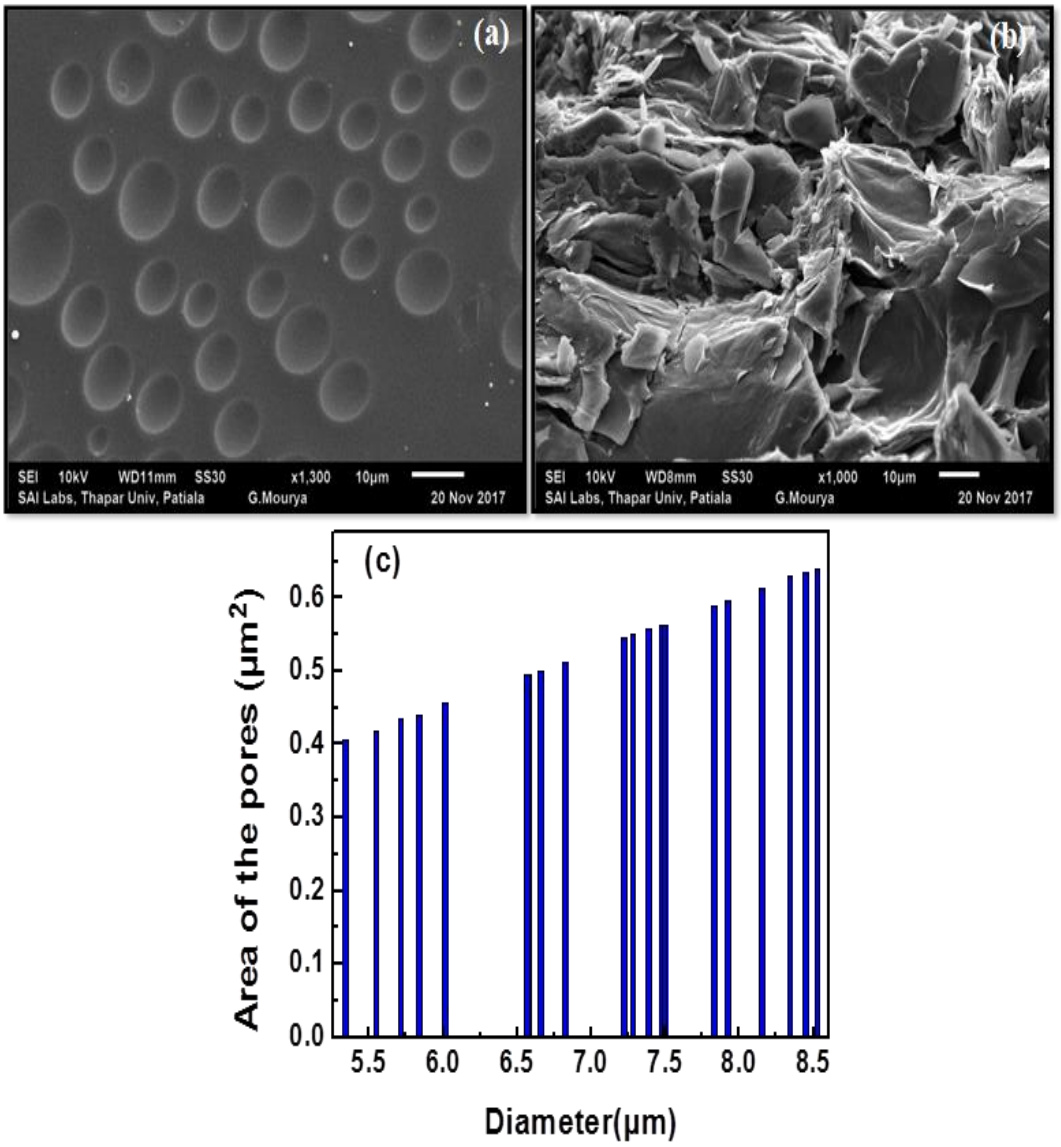

Figure 4.8 (a and b): SEM images showing top and bottom surface images of poly(styrene)-poly(ethylene glycol)-6000-chlorobenzene (10.06%-5.13%-84.81%) of 150 µl of single thick layer film and **(c)** the area of the different pores present in the film.

Figure 4.9 (a and b) shows the top and bottom surface morphology of membranes prepared from poly(styrene)-poly(ethylene glycol)-chlorobenzene (10.06%-5.13%-84.81%) of 225 µl of single thick layer coating. The initial thickness and final thicknesses were 1204 µm and 280 µm respectively. The residual solvent percentage left in this coating was 9.36%. Figure 4.9 (c) represents the average area of the holes with respect to the diameters of the holes present in the coating. The average pore diameter in this case is 4.63 µm and average pore area is 0.43 μm^2. This also has less average diameter than injected volume of 225 µl of single thick layer coating of

concentration having poly(styrene)-poly(ethylene glycol)-chlorobenzene (5.05%-4.98%-89.97%). Pores are very uniform in size and can be used for selective separation. Bottom side is completely non porous in nature.

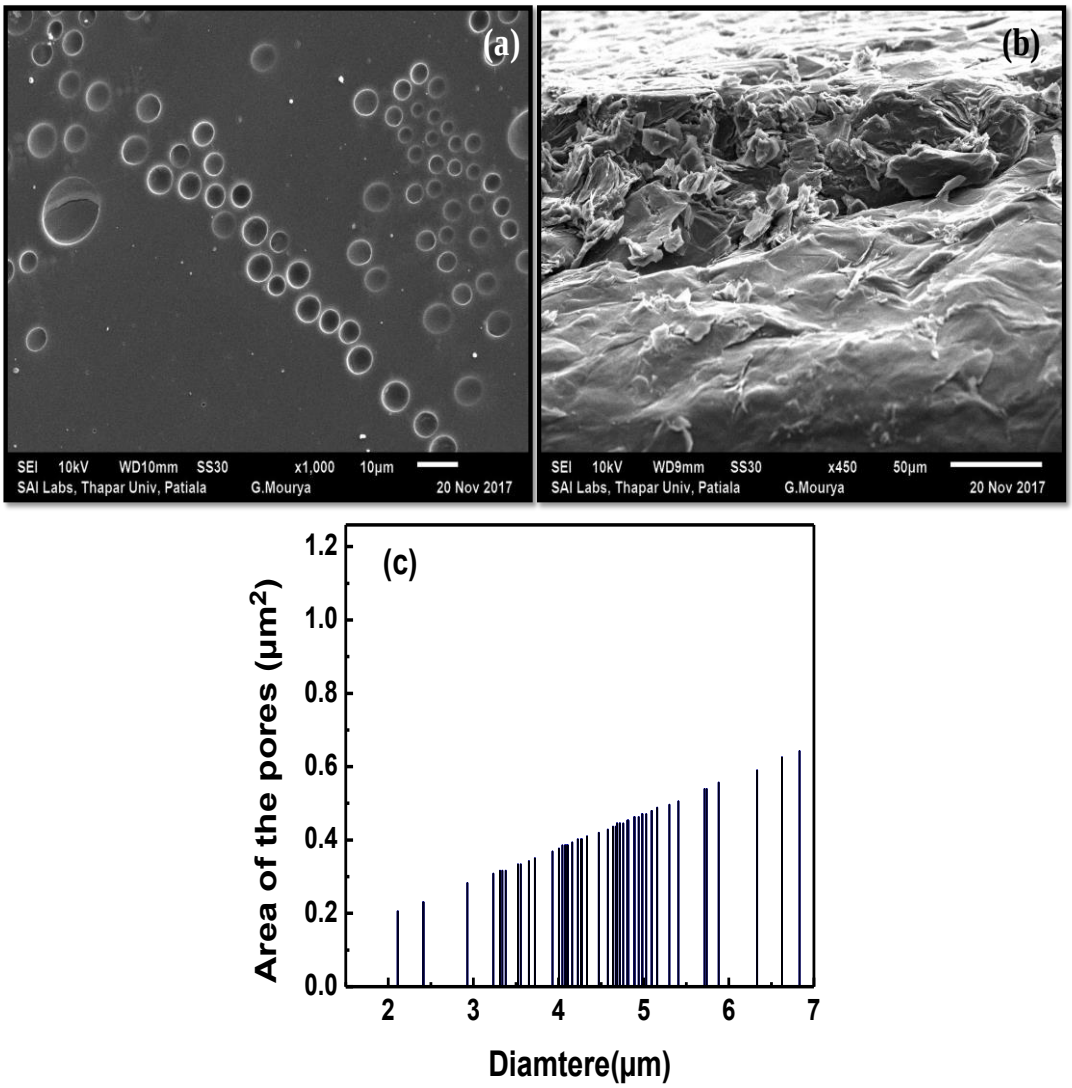

Figure 4.9 (a and b): SEM images showing top and bottom surface images of poly(styrene)-poly(ethylene glycol)-6000-chlorobenzene (10.06%-5.13%-84.81%) of 225 µl of single thick layer film and **(c)** the area of the different pores present in the film.

Figure 4.10 (a and b) shows the top and bottom surface morphology of membranes prepared from poly(styrene)-poly(ethylene glycol)-chlorobenzene (5.05%-10.04%-84.91%) of 50 µl of LBL coatings. Figure 4.10 (c) represents the average area of the holes with respect to the diameters of the holes present in the coating. The initial thicknesses of layer 1, layer 2 and layer 3 were 406 µm, 462 µm and 459 µm respectively and final thicknesses were 93 µm, 94 µm and 93 µm

respectively. The ultimate residual solvent percentage left in this coating was 23.03%. In this case, the concentration of PEG has been doubled from 5% to 10%, and the pore size is decreased from 7.68 µm to 4.66 µm and indicates higher uniformity of the holes as compared to Figure 4.2 (a). The highly porous membranes are formed with circular pores on the top and zig zag structure on bottom side.

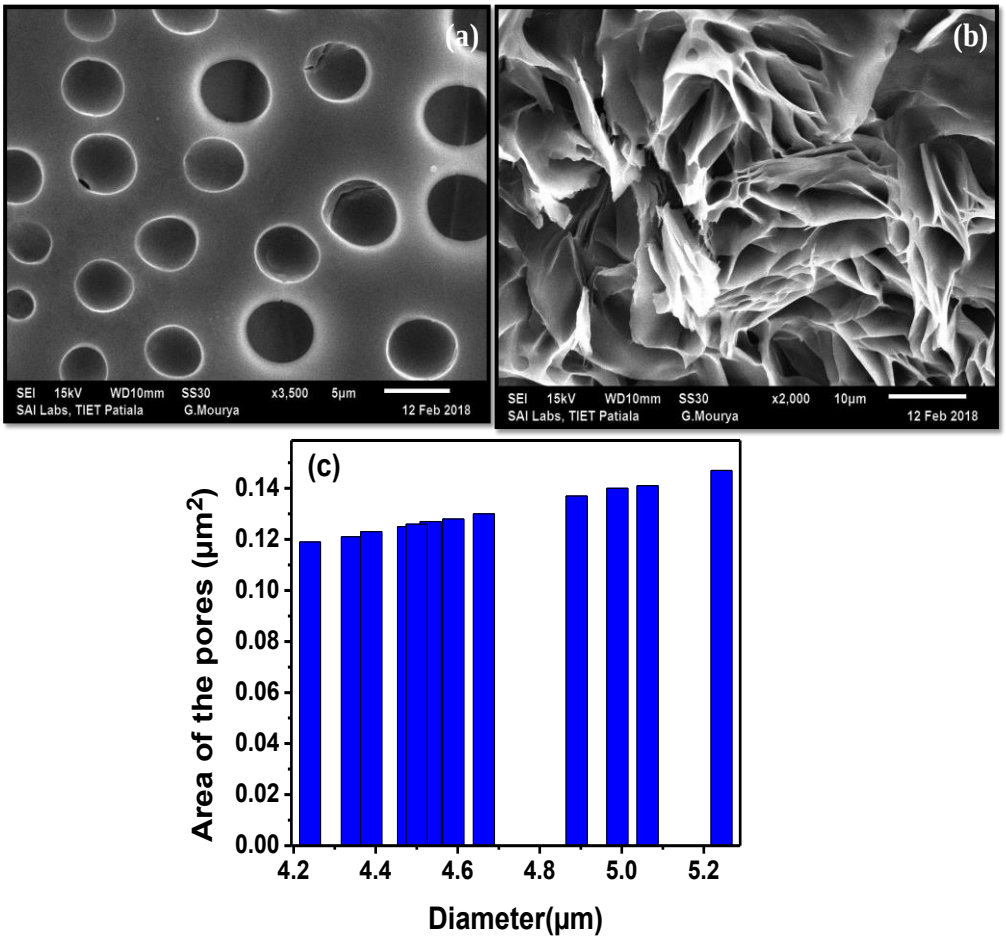

Figure 4.10 (a and b): SEM images showing top and bottom surface images of poly(styrene)-poly(ethylene glycol)-6000-chlorobenzene (5.05%-10.04%-84.91%) of 50 µl of LBL films and **(c)** the area of the different pores present in the film.

Figure 4.11(a and b) shows the top and bottom surface morphology of membranes prepared from poly(styrene)-poly(ethylene glycol)-chlorobenzene (5.05%-10.04%-84.91%) of 75 µl of LBL coatings. . The initial thicknesses of layer 1, layer 2 and layer 3 were 416 µm, 402 µm and 468 µm respectively and final thicknesses were 103 µm, 87 µm and 108 µm respectively. The ultimate residual solvent percentage left in this coating was 29.8%. Figure 4.11c represents the average area of the holes with respect to the diameters of the holes present in the coating. The average pore diameter in this coating is 4.27 µm, which is also lower than 8.53 µm With the increase in PEG concentration, the diameter of pore has decreased, this

could be due to the amorphous nature of PEG and more and more evaporation of solvent takes place from this coating. Even the residual solvent content is also low as compared to other concentration of the system. These membranes are porous on the top and non porous on the bottom side due to less amount of solvent left in bottom side resulting in dense films.

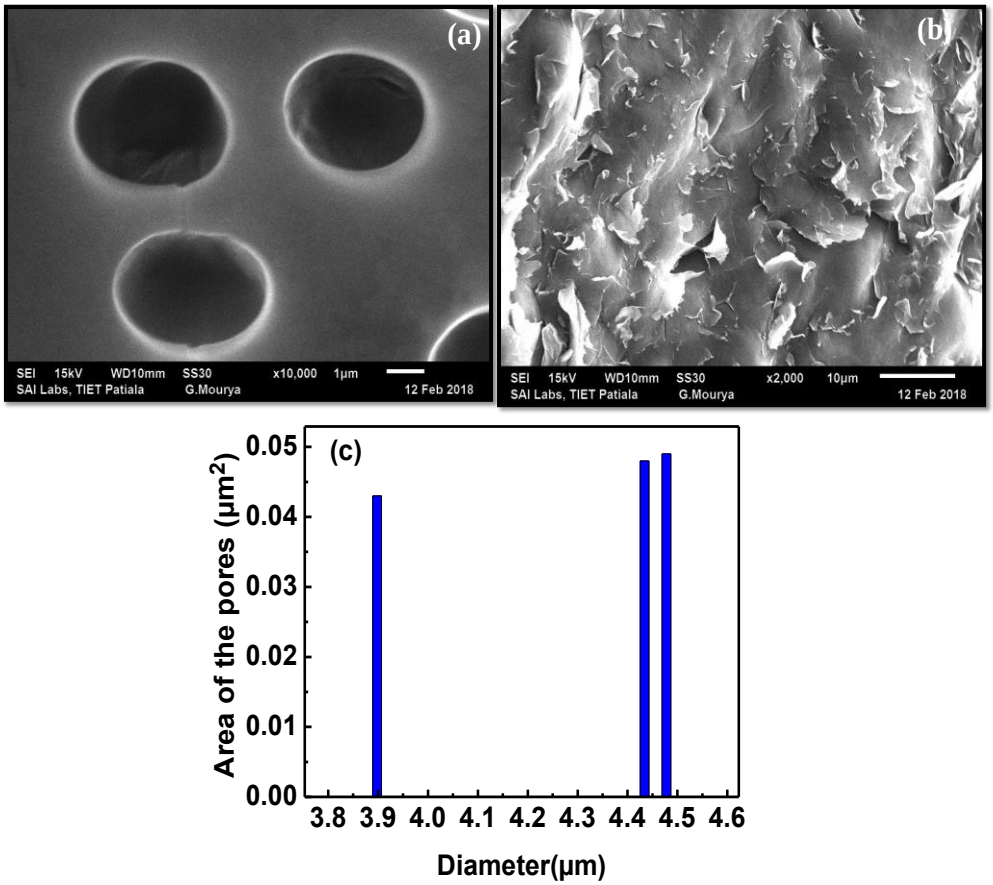

Figure 4.11 (a and b): SEM images showing top and bottom surface images of poly(styrene)-poly(ethylene glycol)-6000-chlorobenzene (5.05%-10.04%-84.91%) of 75 µl of LBL films and **(c)** the area of the different pores present in the film.

Figure 4.12 (a and b) shows the top and bottom surface morphology of membranes prepared from poly(styrene)-poly(ethylene glycol)-chlorobenzene (5.05%-10.04%-84.91%) of 150 µl of single thick coatings. Figure 4.12 (c) represents the average area of the holes with respect to the diameters of the holes present in the coating. The initial thickness and final thicknesses were 613 µm and 141 µm respectively. The residual solvent percentage left in this coating was 9.83%. in this coating of single layer the average pore diameter of the coating is 5.76 µm and is nearly same as that for the injected volume of 50 µl of the same composition of LBL

assembly. This image also shows some linkages among the holes. This crosslinking will impart additional strength to these membranes. The bottom surface has no pores.

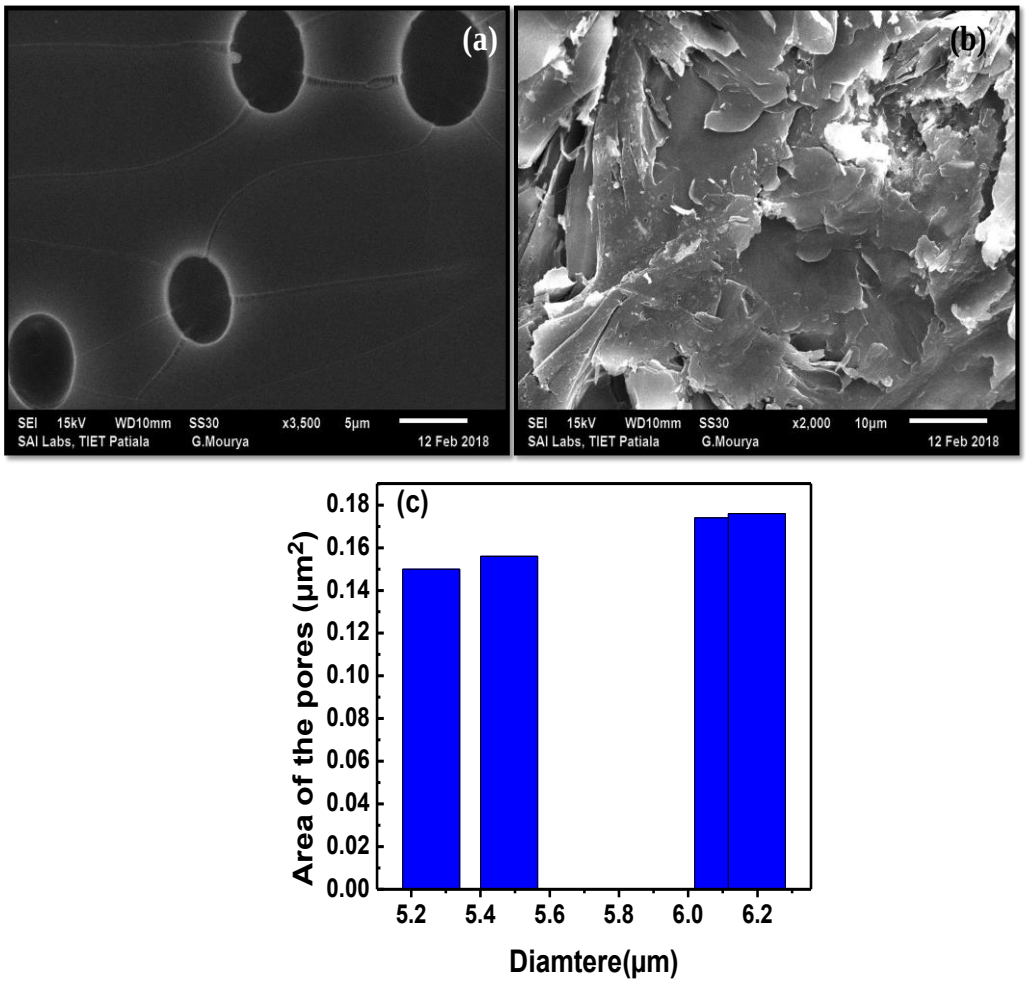

Figure 4.12 (a and b): SEM images showing top and bottom surface images of poly(styrene)-poly(ethylene glycol)-6000-chlorobenzene (5.05%-10.04%-84.91%) of 150 µl of single thick layer film and **(c)** the area of the different pores present in the film.

Figure 4.13 (a and b) shows the top and bottom surface morphology of membranes prepared from poly(styrene)-poly(ethylene glycol)-chlorobenzene (5.05%-10.04%-84.91%) of 225 µl of single thick layer coating. The initial thickness and final thicknesses were 1327 µm and 318 µm respectively. The residual solvent percentage left in this coating was 10.88%. Figure 4.13 (c) represents the average area of the holes with respect to the diameters of the holes present in the coating. The average pore diameter in this case is 10.01 µm which is less than the injected volume of 225 µl of single thick layer coating of concentration having poly(styrene)-

poly(ethylene glycol)-chlorobenzene (5.05%-4.98%-89.97%). Some degree of porosity is also observed in bottom side without any proper shape and size.

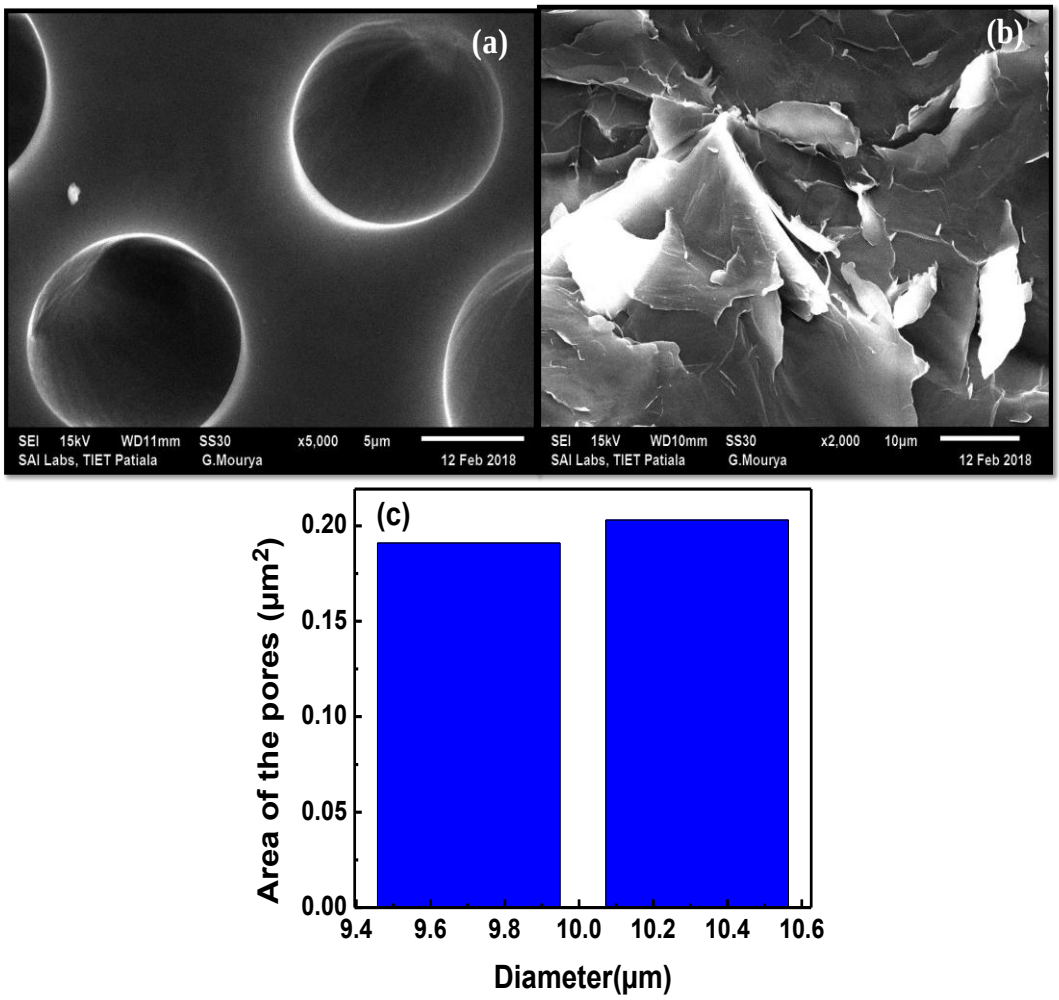

Figure 4.13 (a and b): SEM images showing top and bottom surface images of poly(styrene)-poly(ethylene glycol)-6000-chlorobenzene (5.05%-10.04%-84.91%) of 225 µl of single thick layer film and **(c)** the area of the different pores present in the film.

Figure 4.14 (a and b) shows the top and bottom surface morphology of membranes prepared from poly(styrene)-poly(ethylene glycol)-chlorobenzene ((10.02%-9.96%-80.46%) of 50 µl of LBL coatings. The initial thicknesses of layer 1, layer 2 and layer 3 were 359 µm, 220 µm and 265 µm respectively and final thicknesses were 107 µm, 54 µm and 65 µm respectively. The ultimate residual solvent percentage left in this coating was 22.73%. Figure 4.14 (c) represents the average area of the holes with respect to the diameters of the holes present in the coating. Now the concentration of both the polymers PS and PEG have doubled to

check the pore diameter of the holes. With the doubling of both the polymers the average pore diameter has significantly decreased from 7.68 µm of 50 µl of injected volume of concentration having PS-PEG-CLB (5.05%-4.98%-89.97%) to 3.74 µm of membranes prepared from PS-PEG-CLB (10.02%-9.96%-80.46%) of 50 µl of LBL coatings. The porosity at the bottom side has also improved significantly as compared to the Figure 4.13 (b).

Figure 4.15 (a and b) shows the top and bottom surface morphology of membranes prepared from poly(styrene)-poly(ethylene glycol)-chlorobenzene (10.02%-9.96%-80.46%) of 75 µl of LBL coatings. Figure 4.15 (c) represents the average area of the holes with respect to the diameters of the holes present in the coating. The initial thicknesses of layer 1, layer 2 and layer 3 were 484 µm, 273µm and 559 µm respectively and final thicknesses were 152 µm, 77 µm and 148 µm respectively. The ultimate residual solvent percentage left in this coating was 33.19%. The average pore diameter in this case is 5.25 µm and favors the lesser pore diameter with the increase in polymer content with non uniform geometry and pores on bottom side.

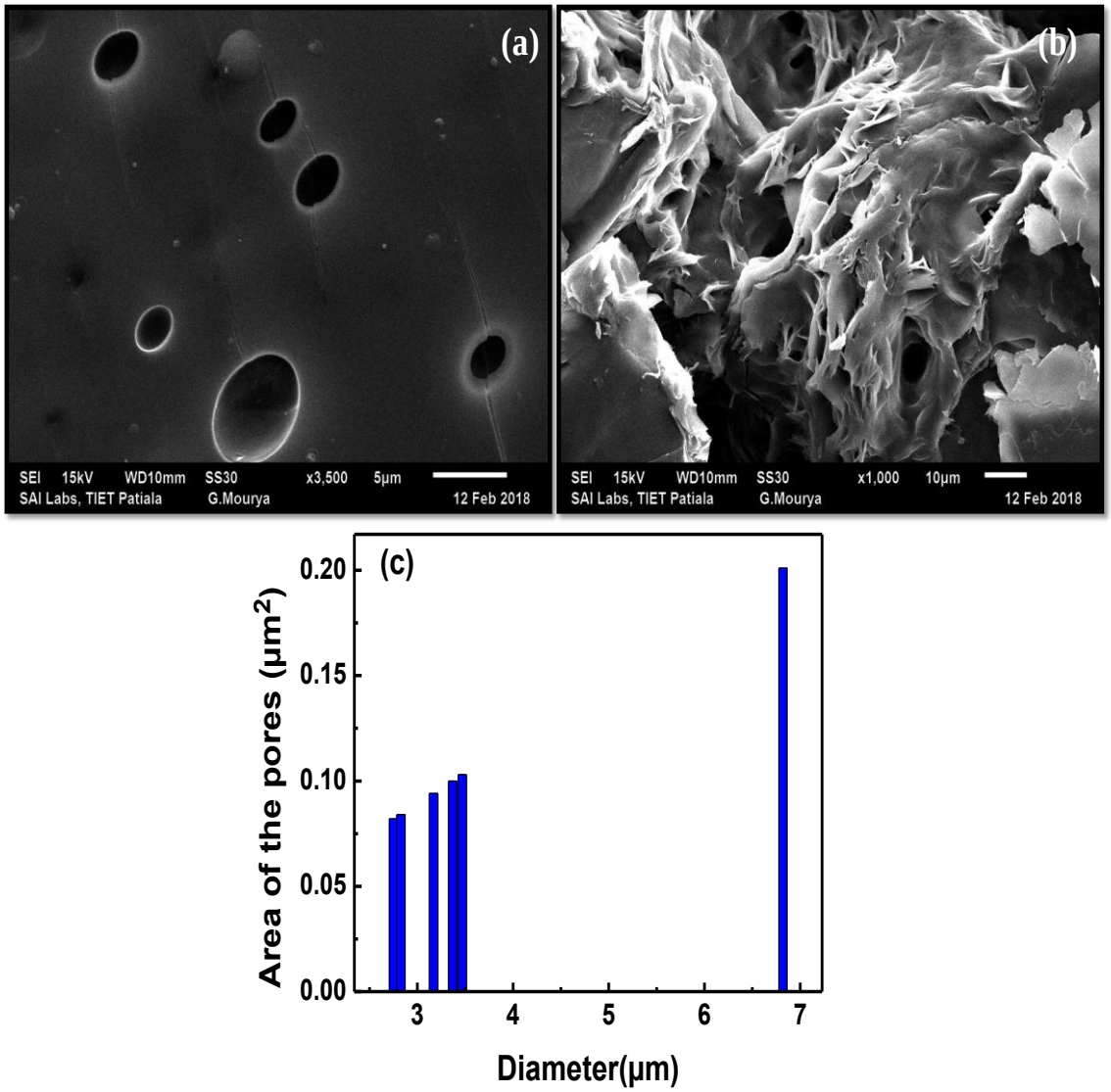

Figure 4.14 (a and b): SEM images showing top and bottom surface images of poly(styrene)-poly(ethylene glycol)-6000-chlorobenzene (10.02%-9.96%-80.46%) of 50 µl of LBL films and **(c)** the area of the different pores present in the film.

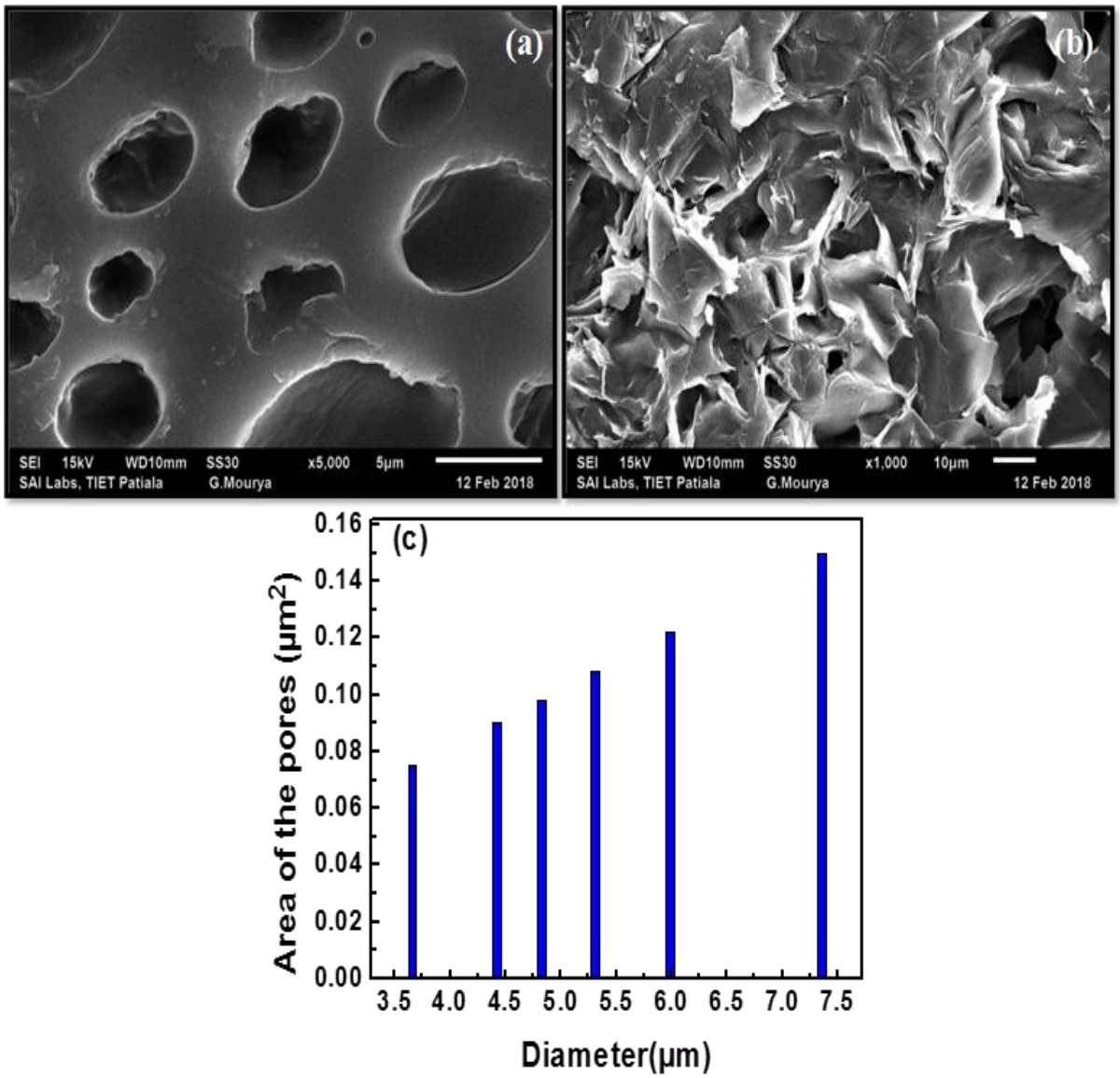

Figure 4.15 (a and b): SEM images showing top and bottom surface images of poly(styrene)-poly(ethylene glycol)-6000-chlorobenzene (10.02%-9.96%-80.46%) of 75 µl of LBL films and **(c)** the area of the different pores present in the film.

Figure 4.16 (a and b) shows the top and bottom surface morphology of membranes prepared from poly(styrene)-poly(ethylene glycol)-chlorobenzene (10.02%-9.96%-80.46%) of 150 µl of single thick layer coating. The initial thickness and final thicknesses were 901 µm and 255 µm respectively. The residual solvent percentage left in this coating was 9.88%. Figure 4.16 (c) represents the average area of the holes with respect to the diameters of the holes present in the coating. The average pore diameter in this case is 4.69 µm and favors the lesser pore diameter with the increase in polymer content. Excellent porous nature with great uniformity on porous side and completely dense on the bottom side.

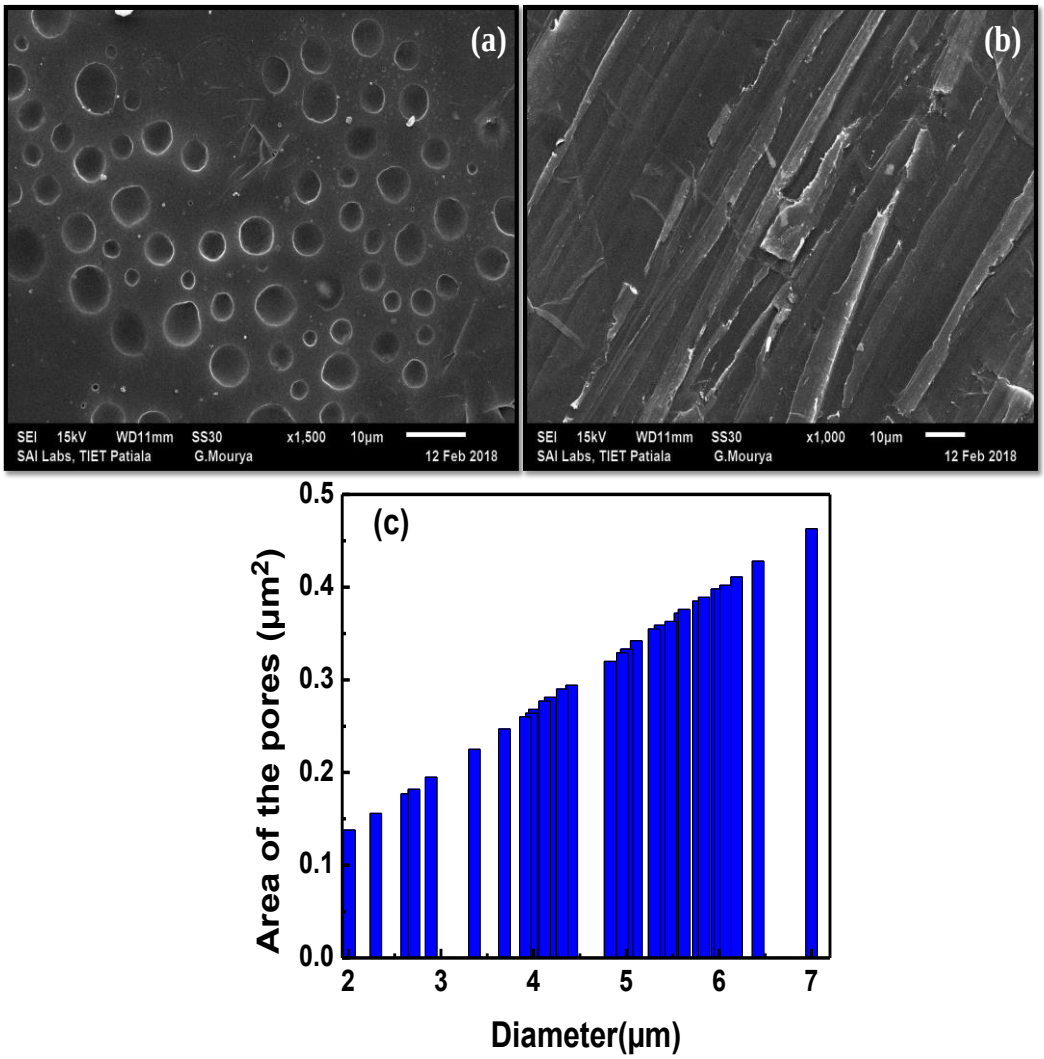

Figure 4.16 (a and b): SEM images showing top and bottom surface images of poly(styrene)-poly(ethylene glycol)-6000-chlorobenzene (10.02%-9.96%-80.46%) of 150 µl of LBL films and **(c)** the area of the different pores present in the film.

Figure 4.17 (a and b) shows the top and bottom surface morphology of membranes prepared from poly(styrene)-poly(ethylene glycol)-chlorobenzene (10.02%-9.96%-80.46%) of 225 µl of single thick layer coating. The initial thickness and final thicknesses were 1721 µm and 533 µm respectively. The residual solvent percentage left in this coating was 13.89%. Figure 4.17 (c) represents the average area of the holes with respect to the diameters of the holes present in the coating. The average pore diameter in this case is 6.52 µm and favors the lesser pore diameter with the increase in polymer content. The shape of pores is lightly oval in this case with good uniformity. The bottom side is also completely dense in this case.

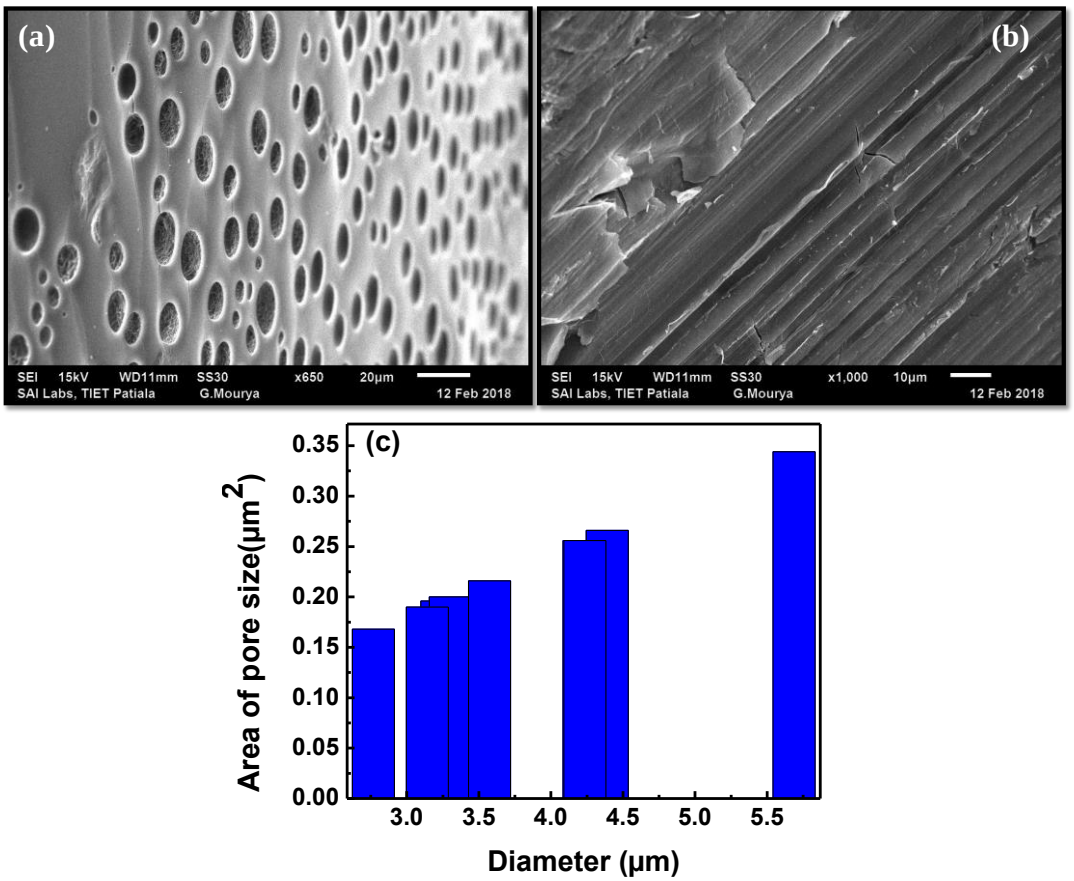

Figure 4.17(a and b). SEM image showing top and bottom surface image respectively of percentage having poly(styrene)-poly(ethylene glycol)-6000-chlorobenzene (10.02%-9.96%-80.46%) of 225 µl of LBL films and **(c)** the area of the number of pores present in the film.

The change in average diameter and its area is summarized in Table 4.1. The average diameter of 5% of both the PS and PEG is 7.68 µm as seen in row 1 which is taken as base. With the increase in PS from 5% to 10% the average diameter is 4.89 µm in case of 50 µl of injected volume seen in row 3. In the next case with the doubling of PEG from 5% to 10%, the average diameter is decreased from 7.68 µm to 4.66 µm seen in row 5. With the doubling of both the polymers PS and PEG also decreased the pore size very significantly from 7.68 µm to 3.74 µm. The decrease in pore size exhibits higher surface area. The increase in polymer content affects the porosity of the membrane and decreased the pore size which may be due to the lesser amount of solvent is being left in the film and which is required for phase separation.

Table 4.1: Summarized values of the pores present in coatings of different concentrations.

S.No	Composition	Injected volume	Average pore diameter (µm) (A_d)	Average area of the pores (µm^2) (A_a)	Standard deviation of pores diameter (S_d)	Ultimate residual solvent (%)	Figure No.
1.	PS: 5.05 %, PEG :4.98% CLB:89.97%	Layer 1: 50 µl	7.68	0.232	3.18	19	4.2
		Layer 2: 50 µl					
		Layer 3: 50 µl					
		Single thick layer (150µl)	9.61	0.389	2.56	12.8	4.3
2.	PS: 5.05 %, PEG :4.98% CLB:89.97%	Layer 1: 75 µl	8.53	0.442	8.14	34.87	4.4
		Layer 2: 75 µl					
		Layer 3: 75 µl					
		Single thick layer (225µl)	13.04	1.31	4.88	11.69	4.5
3.	PS: 10.06 %, PEG :5.13% CLB:84.81%	Layer 1: 50 µl	4.89	0.098	1.03	23.03	4.6
		Layer 2: 50 µl					
		Layer 3: 50 µl					
		Single thick layer (150µl)	7.07	0.53	0.96	9.83	4.8
4.	PS: 10.06 %, PEG :5.13% CLB:84.81%	Layer 1: 75 µl	4.20	0.14	1.60	29.8	4.7
		Layer 2: 75µl					
		Layer 3: 75 µl					
		Single thick layer (225µl)	4.63	0.43	2.19	10.88	4.9
5.	PS: 5.05 %, PEG :10.04% CLB:84.91%	Layer 1: 50 µl	4.66	0.13	0.099	34.58	4.10
		Layer 2: 50µl					
		Layer 3: 50 µl					
		Single thick layer (150µl)	5.76	0.164	0.212	8.1	4.12
6.	PS: 5.05 %, PEG :10.04% CLB:84.91%	Layer 1: 75 µl	4.27	0.46	0.104	32.9	4.11
		Layer 2: 75µl					
		Layer 3: 75 µl					
		Single thick layer (225µl)	10.01	0.197	0.189	9.36	4.13
7.	PS: 10.02 %, PEG :9.96% CLB:80.46%	Layer 1: 50 µl	3.74	0.11	2.36	22.73	4.14
		Layer 2: 50µl					
		Layer 3: 50 µl					
		Single thick layer (150µl)	4.69	0.31	1.61	9.88	4.16
8.	PS: 10.02 %, PEG :9.96% CLB:80.46%	Layer 1: 75 µl	5.25	0.107	1.39	33.19	4.15
		Layer 2: 75 µl					
		Layer 3: 75 µl					
		Single thick layer (225µl)	4.3	1.07	1.30	13.89	4.17

4.4 Conclusions

PS-PEG-CLB is the excellent multipolymer solvent system to get homogeneous symmetric and asymmetric membranes. Medium thick films are giving the symmetric films. However, asymmetric films are formed in case of thicker one having high amount of total polymer content. The size of pore can be controlled by increasing the polymer content to a large extent. With the increase in the polymer content there is decrease in the pore diameter of the holes present in the coating. Even the doubling of one of the polymer also favors in the lower pore diameter of the holes.

References

[1] A. Mirmohseni, A. Oladegaragoze, Construction of a sensor for determination of ammonia and aliphatic amines using polyvinylpyrrolidone coated quartz crystal microbalance, Sensors and Actuators B: Chemical, 89 (2003) 164-172.

[2] D. Wu, F. Xu, B. Sun, R. Fu, H. He, K. Matyjaszewski, Design and preparation of porous polymers, Chemical Reviews, 112 (2012) 3959-4015.

[3] O. Pitois, B. Francois, Formation of ordered micro-porous membranes, The European Physical Journal B-Condensed Matter and Complex Systems, 8 (1999) 225-231.

[4] G. Widawski, M. Rawiso, B. François, Self-organized honeycomb morphology of star-polymer polystyrene films, Nature, 369 (1994) 387.

[5] B. Francois, Y. Ederle, C. Mathis, Honeycomb membranes made from C60 (PS) 6, Synthetic Metals, 103 (1999) 2362-2363.

[6] B. Ladewig, M.N.Z. Al-Shaeli, Fundamentals of Membrane Processes, Fundamentals of Membrane Bioreactors, Springer, 2017, pp. 13-37.

[7] D. Vaessen, A. McCormick, L. Francis, Effects of phase separation on stress development in polymeric coatings, Polymer, 43 (2002) 2267-2277.

[8] R.K. Arya, Phase separation in multicomponent polymer-solvent-nonsolvent coatings, South African Journal of Chemical Engineering, 18 (2013) 30-40.

[9] S.-T. Hsu, Y.L. Yao, Effect of Film Formation Method and Annealing on Morphology and Crystal Structure of Poly (L-Lactic Acid) Films, Journal of Manufacturing Science and Engineering, 136 (2014) 021006.

[10] R.K. Arya, Calibration curves to measure concentrations in multicomponent polymeric coatings using confocal Raman spectroscopy, International Journal of Chemical Engineering and Applications, 2 (2011) 421.

[11] J. Sharma, R.K. Arya, S. Ahuja, C.K. Bhargava, Residual solvent study in polymer− polymer—solvent coatings: Poly (styrene)—poly (methyl methacrylate)—tetrahydrofuran coatings, Progress in Organic Coatings, 113 (2017) 200-206.

[12] J. Sharma, K. Tewari, R.K. Arya, Diffusion in polymeric systems–A review on free volume theory, Progress in Organic Coatings, 111 (2017) 83-92.

[13] H. Yabu, M. Takebayashi, M. Tanaka, M. Shimomura, Superhydrophobic and lipophobic properties of self-organized honeycomb and pincushion structures, Langmuir, 21 (2005) 3235-3237.

[14] M. Srinivasarao, D. Collings, A. Philips, S. Patel, Three-dimensionally ordered array of air bubbles in a polymer film, Science, 292 (2001) 79-83.

[15] O. Karthaus, N. Maruyama, X. Cieren, M. Shimomura, H. Hasegawa, T. Hashimoto, Water-assisted formation of micrometer-size honeycomb patterns of polymers, Langmuir, 16 (2000) 6071-6076.

[16] B. de Boer, U. Stalmach, H. Nijland, G. Hadziioannou, Microporous Honeycomb-Structured Films of Semiconducting Block Copolymers and Their Use as Patterned Templates, Advanced Materials, 12 (2000) 1581-1583.

[17] H. Yabu, M. Tanaka, K. Ijiro, M. Shimomura, Preparation of honeycomb-patterned polyimide films by self-organization, Langmuir, 19 (2003) 6297-6300.

[18] H. Matsuyama, M. Nishiguchi, Y. Kitamura, Phase separation mechanism during membrane formation by dry-cast process, Journal of Applied Polymer Science, 77 (2000) 776-783.

[19] B. François, O. Pitois, J. François, Polymer films with a self-organized honeycomb morphology, Advanced Materials, 7 (1995) 1041-1044.

[20] L. Ghannam, M. Manguian, J. François, L. Billon, A versatile route to functional biomimetic coatings: ionomers for honeycomb-like structures, Soft Matter, 3 (2007) 1492-1499.

[21] M. Nicho, D. Peña-Salgado, P. Altuzar-Coello, Morphological and physicochemical properties of spin-coated poly (3-octylthiophene)/polystyrene composite thin films, Thin Solid Films, 518 (2010) 1799-1803.

[22] I. Sharifian, Conductive and biodegradable polyaniline/starch blends and their composites with polystyrene, Iranian Polymer Journal, 20 (2011) 319-328.

[23] E. Ferrari, P. Fabbri, F. Pilati, Solvent and substrate contributions to the formation of breath figure patterns in polystyrene films, Langmuir, 27 (2011) 1874-1881.

[24] C. Panayiotou, J. Vera, Thermodynamics of polymer–polymer–solvent and block copolymer–solvent systems I. Experimental measurements, Polymer Journal, 16 (1984) 89-102.

[25] C. Panayiotou, J. Vera, Thermodynamics of Polymer–Polymer–Solvent and Block Copolymer–Solvent Systems II. Theoretical Treatment of Data with the Nonrandom New Flory Theory, Polymer Journal, 16 (1984) 103-112.

[26] A. Clark, Direct analysis of experimental tie line data (two polymer–one solvent systems) using Flory–Huggins theory, Carbohydrate Polymers, 42 (2000) 337-351.

[27] P.E. Price, I.H. Romdhane, Multicomponent diffusion theory and its applications to polymer-solvent systems, AIChE Journal, 49 (2003) 309-322.

Chapter 5

Effect of Molecular Weight on Residual Solvent

This chapter provides a detailed discussion about another selected system that is poly(styrene)-poly(methyl methacrylate)-ethylbenzene. The effect of molecular weight of both the polymers on the drying behavior of polymeric coatings has been discussed in this chapter.

5.1 Introduction

Diverse improvements in materials used in daily life have now become an important research field today. Polymeric materials have their dominance in the field of packaging, building and construction markets. In the case of fencing, automotive fuel and park benches, the thermosetting and thermoplastic polymers act as the replacement of metals due to their high strength and protection providing ability to corrosion [1]. Polymeric coatings, having durable and non durable applications are attracting much interest in industrial and technological advances. The multi component system of polymer-solvent helps in rheological properties [2] and also affects the solubility of the solution. These multi component films have applications in coating [3] and printing [4]. More than one component in the polymeric coating involves mass and heat transport operation, for polymerization reactions, membrane manufacturing, and coating processing. The transport phenomenon helps in regulating the temperature profile and determining the composition dependent material properties such as viscosity and surface tension [5].

Coatings can be prepared by polymers, surfactants, and colloidal particles through a process in which all the volatile components are evaporated and a polymeric film is obtained. These coatings are dried under normal conditions with or

without air flow [6]. Drying of coatings converts its rubbery state into a glassy state, and, hence, is considered as the last and controlling step. A well controlled drying process helps to reduce the possible defects like cracks, blisters, etc.

The confinement of polymers in coatings results in change of their properties [7]. It was reported that in a blend film of high molecular-weight PS and low-molecular-weight PMMA, the latter can be stable at the blend surface as result of reduced conformational entropic penalty [8]. Multicomponent mixtures of high molecular weight polymers are of considerable commercial interest since their material properties can be controlled by the blending of several constituents components. It is not only the molecular weight that affects the morphology but solvents used for making the films, and annealing that impacts the morphology of PS/PMMA films [9]. Furthermore, the end groups and film thickness affects the surface segregation and morphology. It has been found that due to the lower surface energy, poly(methyl methacryalte) and poly(styrene) molecules segregates at the free surface under equilibrium conditions [8]. Polystyrene and poly(methyl methacrylate) are widely studied and discussed polymers as model systems for thin film preparation, polymer-polymer interactions, phase separation, and diffusion studies [10, 11]. Small molecular diffusion in a polymer solution is important for processes like drying of coatings [12], drug delivery [13], and polymerization kinetics [14].

Earlier, Vrentas and Duda [15] studied the dependency of diffusion coefficients in binary solutions and interpreted the data using free volume theory [16], Flory Huggins theory [17], and Bueche's entanglement theory [18] for a wide range of polymer concentrations for the poly(styrene)-ethylbenzene system. They observed that at lower concentration of the polymer, the diffusion coefficient changed significantly with the molecular weight. At high concentration of polymer, the diffusion coefficient of all ranges of polymer molecular weight was indistinguishable.

Waggoner et al. [13] also studied the impact of molecular weight on solvent diffusion in the binary systems of poly(styrene) and poly(methyl methacrylate) in toluene, ethylbenzene, cumene, choloroform, methyl ethyl ketone and tert- butyl acetate. They changed the polymer concentration between 0-50 wt%. They used free volume theory and kinetic theory to fit their data. They concluded that with the

increase in the weight fraction of both the polymers, the diffusion coefficient decreased. The solvent self diffusion coefficient also decreased with the increase in molecular size of solvent and polymer.

Spangler et al. [19] studied the effect of molecular weight of polymer and interaction between polymer and solvent on the film thickness and surface topography. They used poly(methyl methacrylate) and poly(styrene) as polymers and toluene, ethyl acetate, and dichloromethane as solvents. They used polydisperse as well as monodisperse poly(methyl methacrylate) and poly(styrene) with different molecular weights. The molecular weight of poly(styrene) and poly(methyl methacrylate) (1.20×10^5, 1.86×10^5, 7.75×10^5, 1.26×10^5) and (1.75×10^4 , 2.3×10^4 , 4.75×10^4 , 9×10^4) respectively. The higher molecular weight of the polymers increased the viscosity of the solution and resulted in the thickening of the film.

Burns and kim [20] studied the blends of poly(styrene) and poly(methyl methacrylate) in methylene chloride. They characterized the blends using scanning electron microscopy and differential scanning electron microscopy. They varied the molecular weight of poly(methyl methacrylate) from 39300 to 56900 by keeping the molecular weight of poly(styrene) constant, i.e, 24500. The micrographs showed that the higher molecular weight of poly(methyl methacrylate) had lower immiscibility than the lower molecular weight of poly(methyl methacrylate) with poly(styrene). They observed fall in the glass transition temperature with decrement in the molecular weight and it was highest in case of PMMA coatings.

As per the literature, the molecular weight of polymers has significant effect on coatings. Earlier researchers [21, 22] have studied these in binary coatings only. In the present work, the effect of molecular weight on the residual solvent in multi-polymer solvent coating has been investigated. The effect of molecular weight of both the polymers involved has been investigated respectively. Their effect on coating thickness is also investigated. Hence, this study allows us to choose better polymeric combination with appropriate molecular weight for minimizing the residual solvent, so that minimum solvent remains in the coating and perfect glassy films are obtained at the end of drying.

5.2 Materials and Methods

All the chemicals were used as supplied and their specifications are given in Table 5.1.

Table 5.1: List of chemicals used in the experimentation.

S.No	Component	Molecular Weight	Density	Supplier
1.	Poly(styrene)	35000	1.06	Sigma Aldrich, Germany
		192000	1.04	Sigma Aldrich, Germany
		350000	1.04	Sigma Aldrich, Germany
		280000	1.04	Sigma Aldrich, Germany
2.	Poly(methyl methacrylate)	120000	1.18	Sigma Aldrich, Germany
		350000	1.17	Sigma Aldrich, Germany
		996000	1.17	Sigma Aldrich, Germany
3.	Ethylbenzene	106.17	0.866	Spectrochem.Pvt.Ltd.

The required amount of PS and PMMA were taken in leach proof Schott duran bottles. These bottles were mechanically shaken for two days, followed by manual shaking for about 15 minutes, 4 to 5 times a day for one week period in order to get homogeneous solutions. Thin films of these solutions were prepared using solution casting technique by pouring required amount of polymeric solution in a stainless steel circular holder of depth 4000 µm and 14.65 mm diameter. Several combinations of PS-PMMA-EB were prepared using different molecular weights. The prepared solutions are listed in Table 5.2.

Three different volumes that is (200 µl, 400 µl, and 600 µl) of polymeric solutions were transferred into the sample holder. The mass loss data with respect to time was measured by using semi micro analytical weighing balance (Precisa ES225SM-DR) having an accuracy of ±0.0001g under natural convection without air flow and heating.

Table 5.2: Coating solutions of different PS / PMMA molecular weights.

S. No	Solution combination	Sample name
1.	PS(35,000)-PMMA(1,20,000)-EB (4.97%- 4.94% - 90.09 %)	PSPM-1
2.	PS(2,80,000)-PMMA(1,20,000)-EB (5.11%- 4.97% - 89.92 %)	PSPM-2
3.	PS(3,50,00)-PMMA(120000)-EB (4.98%- 4.95% - 90.07 %)	PSPM-3
4.	PS(1,92,000)-PMMA(3,50,000)-EB (5.02%- 5.02% - 89.96 %)	PSPM-4
5.	PS(1,92,000)-PMMA(9,96,000)-EB (5.01%- 5.04% - 89.95 %)	PSPM-5

5.3 Results and Discussion

5.3.1 Drying of PS-PMMA-EB coating of nearly 1000 µm

Figure 5.1 shows the change in residual solvent with respect to time in PS-PMMA-EB coatings of different molecular weights. In the case of PSPM-1, the linearly falling trend up to 9467 is due to the evaporation of the solvent and 91.79% of solvent has been evaporated from the coating. This indicates that convection mass transfer is dominating, and the drying is externally controlled. The remaining 8.21% of the solvent decreases very slowly. The diffusion then slows down in the coating resulting in slow mass transfer from coating to air. The data was recorded until it plateus off. At the end of drying, 7.42% of solvent has been permanently trapped in the coating. In PSPM-2, the molecular weight of PS has been increased from 35000 to 280000 and PMMA molecular weight is kept constant at 120000. The linearly falling rate period decreases upto 9537 s, and by that time, 94.26% of the solvent has been removed, which is higher than PSPM-1, and the remaining 5.74% of the solvent is decreasing very slowly up to 12238 s, and 4.88% of the ultimate residual solvent has been permanently trapped in the coating. In the case of PSPM-3, again the molecular weight of PS is increased to 350000 without any change in the PMMA molecular weight. The decrease in residual solvent linearly falls up to 10479 s, and 94.38% of the solvent has been evaporated from the coating. Thereafter, residual solvent is decreasing very slowly, and 3.01% solvent is left in the coating after 12450s.

In PSPM-4, the molecular weight of PS and PMMA are 192000 and 350000, respectively. The linear decrease in residual solvent in this case is up to 11140 s, and 93.94% of the solvent has been removed from the coating. The ultimate residual solvent left in the coating is 4.93% after 12475 s. In the case of PSPM-5, the molecular weight of PS is kept constant at 192000, and the molecular weight of PMMA is increased to 996000. The linear trend of residual solvent decrease is up to 10409 s, and by that time, 90.12% of the solvent has been removed. The ultimate residual solvent left in this coating is 8.92% after 12390 s. The results shows that the residual solvent left in the coatings is decreasing with increase in PS molecular weight as far as the molecular weight of PS is higher than PMMA.

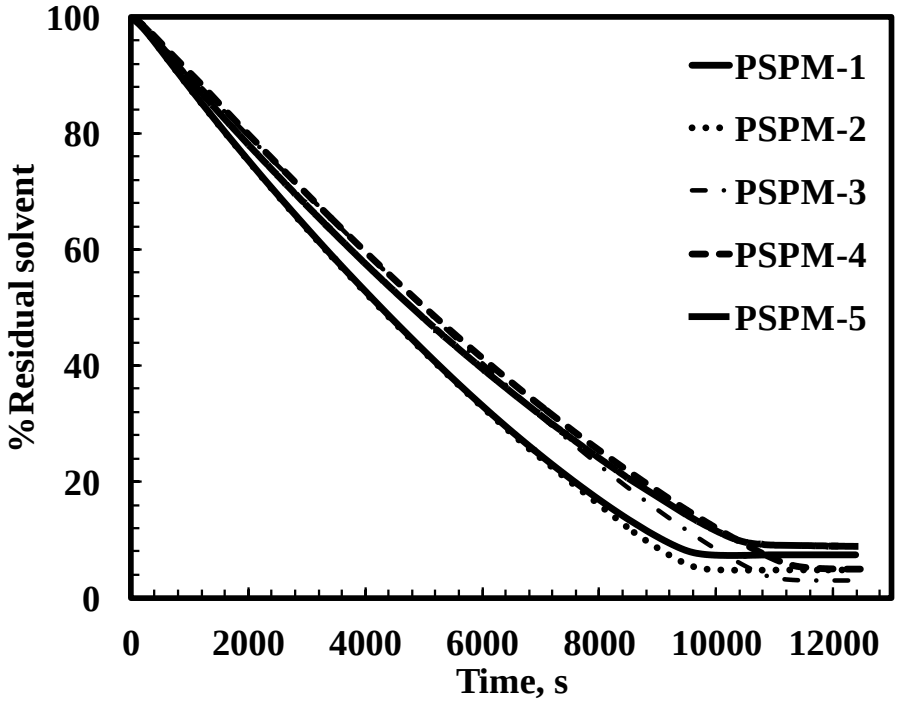

Figure 5.1: Residual solvent as a function of time in PS-PMMA-EB with different molecular weight of nearly 1000 microns coating thickness at 25 °C.

Figure 5.2 shows the change in coating thickness and non dimensional thickness with respect to time in PS-PMMA-EB coatings with different molecular weight of both the polymers. Figure 2 shows that in PSPM-1, the initial coating thicknesses is 998 µm, which decreases due to the evaporation of solvent and linearly decreases up to 154 µm in 9467 s, and slowly decreases further up to 12378 s. The final coating thickness of PSPM-1 coating is 146 µm. In PSPM-2, the initial coating thicknesses is 991 µm, which linearly decreases up to 132 µm in 9537 s and slowly

decreases further up to 12238 s. The final coating thickness of PSPM-2 coating is 124 µm. In PSPM-3, the initial coating thickness is 1024 µm linearly decrease up to 134 µm in 10479 s and slowly decreases further up to 12450 s. The final coating thickness of PSPM-3 coating is 110 µm. The final coating thickness is decreases from PSPM-1 to PSPM-3 due to the less residual solvent present in the coating. In case of higher molecular weight of PMMA than PS i.e, PSPM-4, the initial coating thickness is 1097 µm linearly decrease up to 148 µm in 11140 s, and slowly decreases further up to 12475 s. The final coating thickness of PSPM-4 coating is 137 µm. The final coating has little increase from the previous cases due to the higher amount of residual solvent present in the coating. In case of PSPM-5, the initial coating thickness is 1075 µm, which linearly decreases up to 183 µm in 10409 s, and slowly decreases further up to 12390 s. The final coating thickness of PSPM-5 coating is 174 µm. The final coating thickness also affected by the molecular weight of PS and PMMA. The higher molecular weight of PS has less coating thickness due to less percentage of residual solvent present in the coating. Therefore PSPM-3 has least coating thickness of 110 µm as compared to other prepared coatings. Non- dimensional thickness graphs shows that upto 8400 s, PSPM-1 and PSPM-2 has exactly same mass transfer process. However PSPM-3, PSPM-4 and PSPM-5 also have same mass transfer process but faster than PSPM-1 and PSPM-2. At later stage of drying every coating is left with a different value due to diffusion controlled regime.

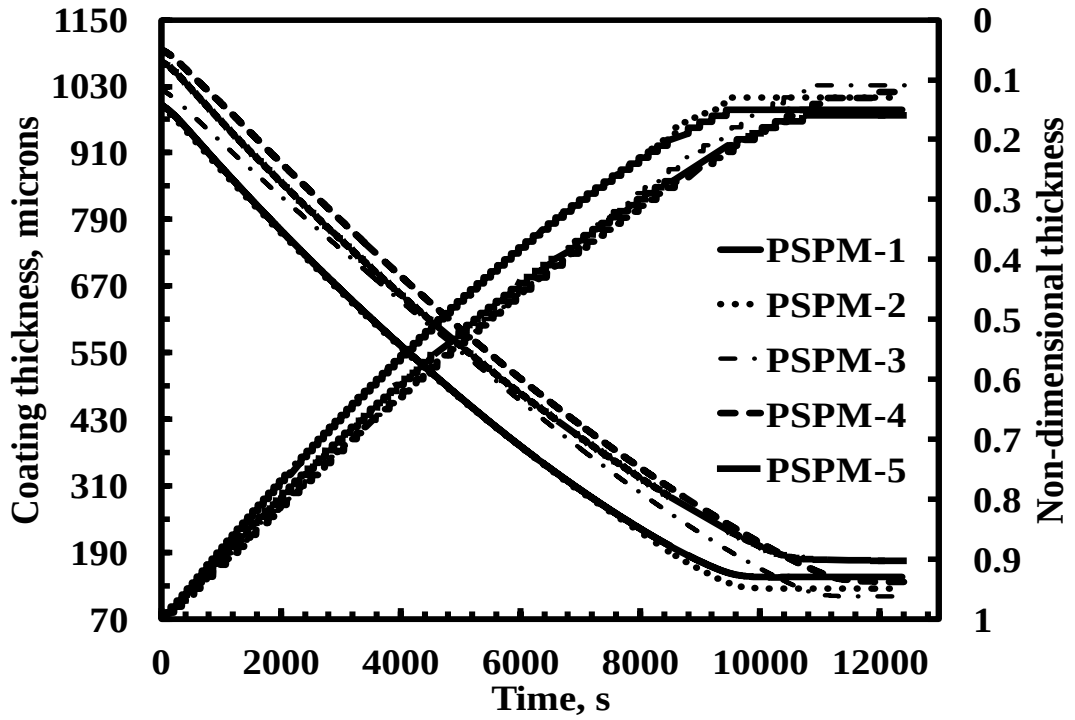

Figure 5.2: Change in coating thickness and Non-dimensional thickness as a function of time in PS-PMMA-EB with different molecular weight of nearly 1000 microns coating thickness at 25 °C.

Figure 5.3(a) and 5.3(b) shows the average concentration of poly(styrene) and poly(methyl methacrylate) with time. The polymer concentration gets increased with time due to the evaporation of ethylbenzene from coating. In ternary multi polymeric system, PSPM-1, PSPM-2, PSPM-3, PSPM-4 and PSPM-5, the concentration of the polymer increases exponentially up to 9467 s, 9537 s, 10479 s, 11140 s, and 10409 s, respectively of coatings having initial thickness of 998 µm, 991 µm, 1024 µm, 1097 µm, and 1075 µm respectively, and then leveled off. The final concentration of PS in PSPM-1, PSPM-2, PSPM-3, PSPM-4 and PSPM-5 were 0.30 g cm-3, 0.361 g cm^{-3}, 0.412 g cm^{-3}, 0.356 g cm^{-3}, and 0.32 g cm^{-3} for coatings having initial concentration 0.044 g cm^{-3}, 0.044 g cm^{-3}, 0.044 g cm-3, 0.044 g cm^{-3}, and 0.044g cm^{-3} respectively. Figure 3 (b) shows the PMMA concentration as a function of time. The final concentration of PMMA in PSPM-1, PSPM-2, PSPM-3, PSPM-4 and PSPM-5 were 0.298 g cm^{-3}, 0.351 g cm^{-3}, 0.409 g cm^{-3}, 0.356 g cm^{-3} and 0.276 g cm^{-3}, for coatings having initial concentration 0.043 g cm^{-3}, 0.044 g cm^{-3}, 0.043 g cm^{-3}, 0.044 g cm^{-3} and 0.044g cm^{-3} respectively.

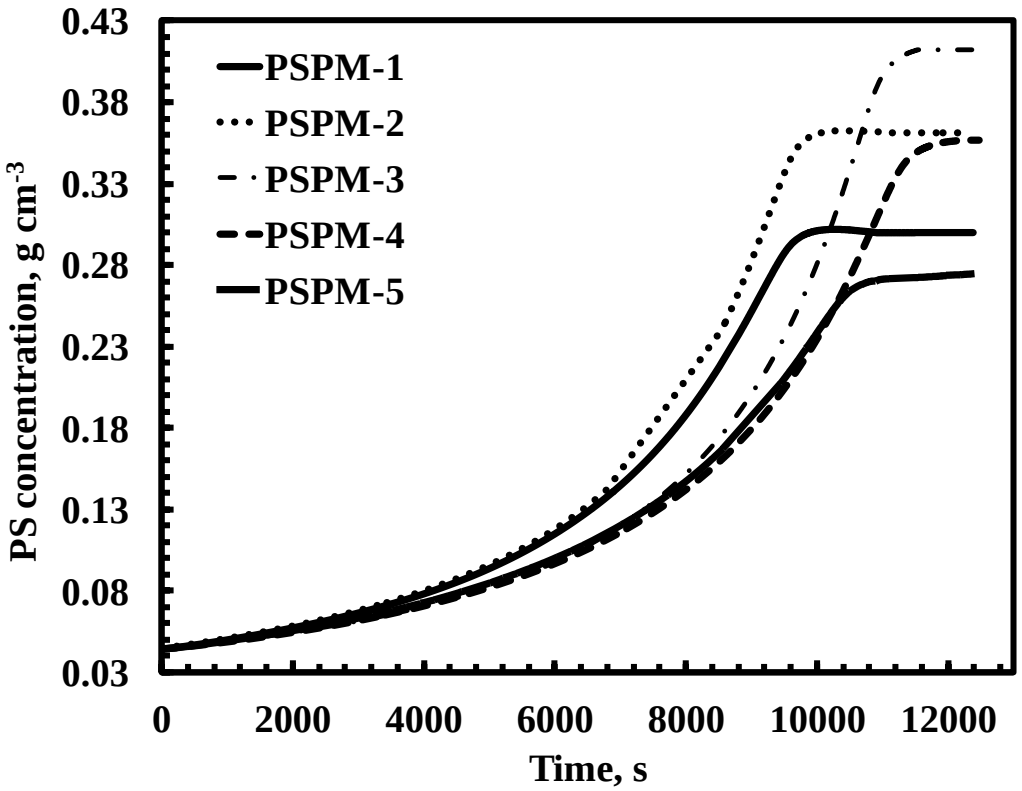

Figure 5.3(a): Poly(styrene) concentration as a function of time in PS-PMMA-EB with different molecular weight of nearly 1000 microns coating thickness at 25 °C.

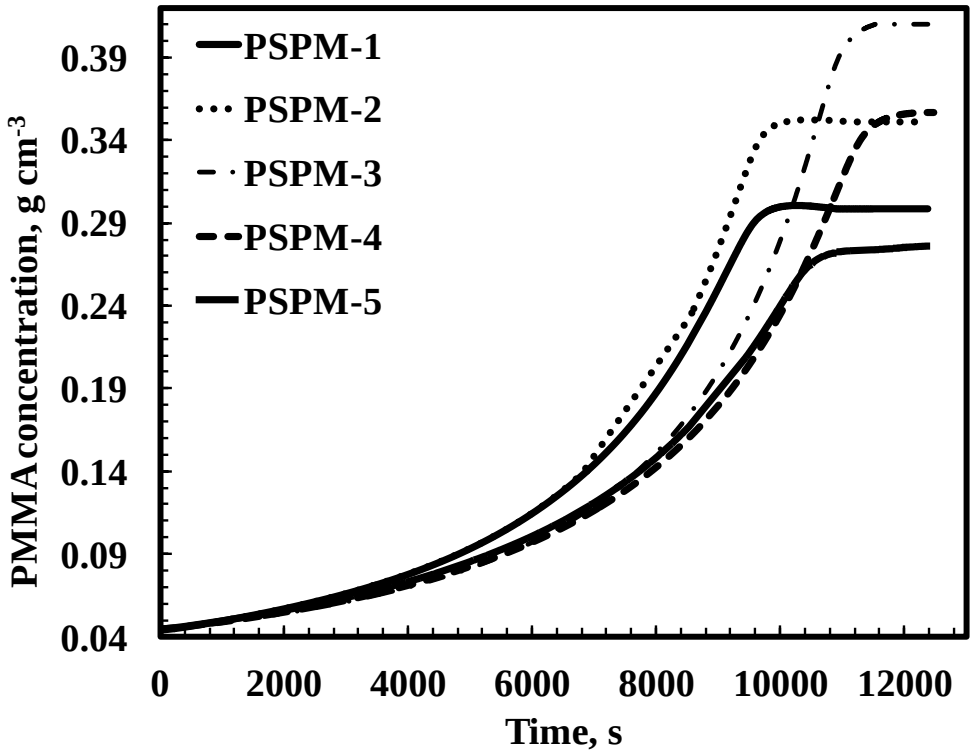

Figure 5.3(b): Poly(methyl methacrylate) concentration as a function of time in PS-PMMA-EB with different molecular weight of nearly 1000 microns coating thickness at 25 °C.

Figure 5.4 shows the average concentration of ethylbenzene with time. The EB concentration is decreasing with time due to the evaporation of ethylbenzene from coating. In ternary multi polymeric system, PSPM-1, PSPM-2, PSPM-3, PSPM-4 and PSPM-5 the concentration of the EB decreases exponentially up to 9467 s, 9537 s, 10479 s, 11140 s and 10409 s respectively of coatings having initial thickness of 998 µm, 991 µm, 1024 µm, 1097 µm and 1075 µm respectively and then leveled off. The final concentration of EB in PSPM-1, PSPM-2, PSPM-3, PSPM-4, and PSPM-5 were 0.403 g cm^{-3}, 0.31 g cm^{-3}, 0.224 g cm^{-3}, 0.314 g cm^{-3} and 0.43 g cm^{-3} for coatings having initial concentration 0.79 g cm^{-3}, 0.798 g cm^{-3}, 0.798 g cm^{-3}, 0.799 g cm^{-3} and 0.79 g cm^{-3} respectively. The least concentration of solvent is present in PSPM-3 which has higher molecular weight of PS and has the least residual solvent percentage as compared to other prepared system.

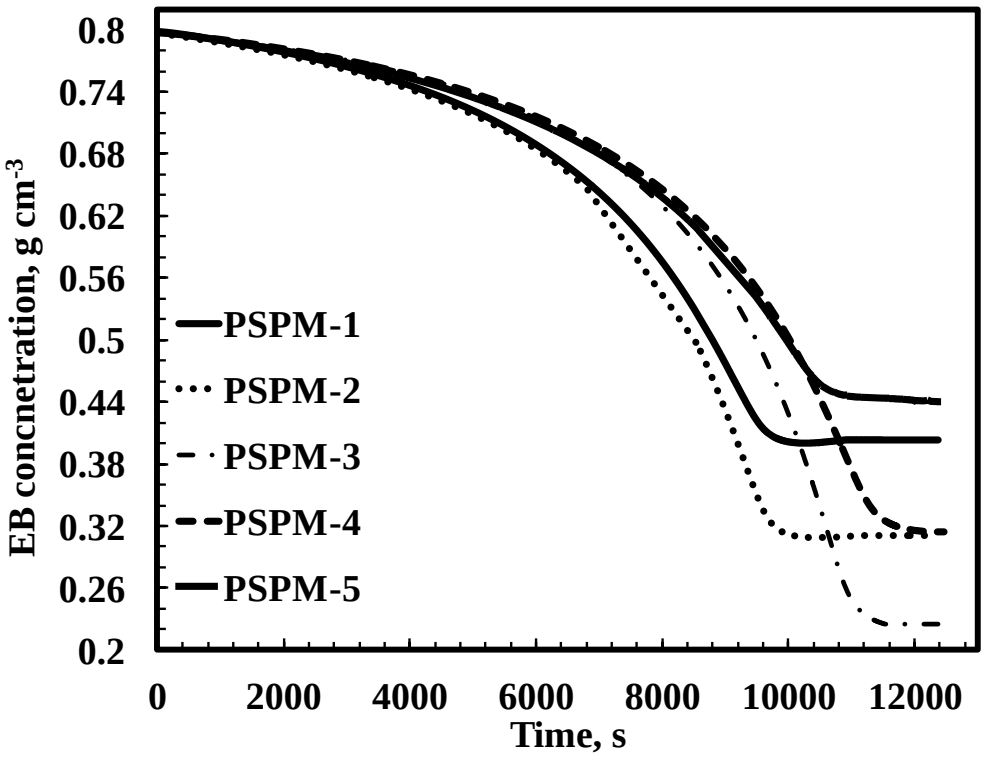

Figure 5.4: Ethylbenzene concentration as a function of time in PS-PMMA-EB with different molecular weight of nearly 1000 microns coating thickness at 25 °C.

5.3.2 Drying of PS-PMMA-EB coating of nearly 1750 µm

Figure 5.5 shows the change in residual solvent with respect to increase in time in PS-PMMA-EB coating with different molecular weight of nearly 1750 µm initial thickness. The solvent removal trends are nearly same in PSPM-1, PSPM-2, PSPM-4 and PSPM-5 as compared to PSPM-3. The residual solvent left in the PSPM-1, PSPM-2, PSPM-4, PSPM-3 and PSPM-5 are 5.22%, 5.03%, 4.12%, 6.06% and 6.5% respectively. The residual solvent left in the PSPM-3 is also lower in this case as compared to other coatings. In case of 1000 µm coating thickness, the residual solvent removal trends were different for each sample coatings. It may be due to skinning phenomena in thin coatings as can be seen in Figure 1 and Figure 5.

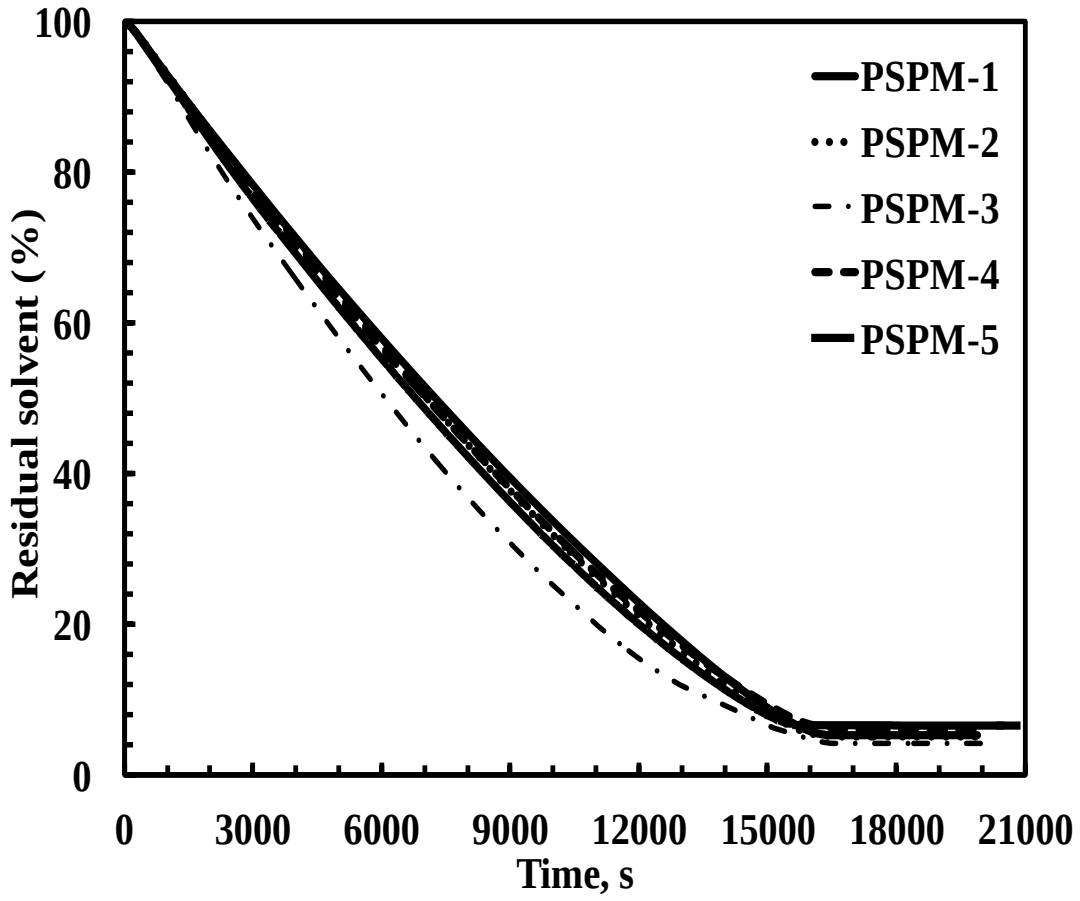

Figure 5.5: Residual solvent as a function of time in PS-PMMA-EB with different molecular weight of nearly 1750 microns coating thickness at 25 °C.

Figure 5.6 shows the change in coating thickness with respect to increase in time in PS-PMMA-EB coating with different molecular weight of nearly 1750 µm initial thickness. The decrease in coating thickness followed the same trend in PSPM-1, PSPM-2, PSPM-4 and PSPM-5 as compared to PSPM-3. The final coating thickness left in the PSPM-1, PSPM-2, PSPM-4, PSPM-3 and PSPM-5 are 223 µm, 219 µm, 200 µm, 261 µm and 262 µm respectively. The final coating thickness in the PSPM-3 is also lower in this case as compared to other coatings.

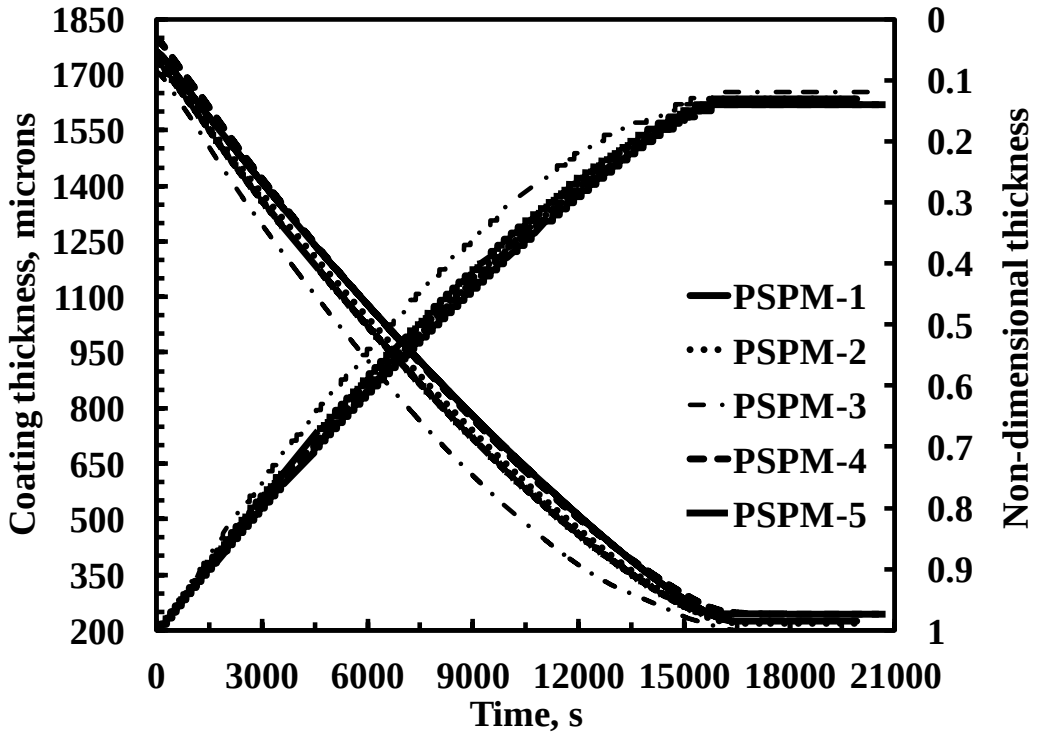

Figure 5.6: Change in coating thickness and Non-dimensional thickness as a function of time in PS-PMMA-EB with different molecular weight of nearly 1750 microns coating thickness at 25 °C.

Figure 5.7 (a) and 5.7 (b) shows the average concentration of poly(styrene) and poly(methyl methacrylate) with time. The final concentration of PS in PSPM-1, PSPM-2, PSPM-3, PSPM-4 and PSPM-5 were 0.34 g cm^{-3}, 0.35 g cm^{-3}, 0.37 g cm^{-3}, 0.32 g cm^{-3}, and 0.31 g cm^{-3} for coatings having initial concentration 0.044 g cm^{-3}, 0.044 g cm^{-3}, 0.044 g cm^{-3}, 0.044 g cm^{-3} and 0.044g cm^{-3} respectively. Figure 5.7 (b) shows the PMMA concentration as a function of time. The final concentration of PMMA in PSPM-1, PSPM-2, PSPM-3, PSPM-4 and PSPM-5 were 0.34 g cm-3, 0.34 g cm^{-3}, 0.37 g cm^{-3}, 0.356 g $cm^{-3}$and 0.32 g cm^{-3} for coatings having initial concentration 0.044 g cm^{-3}, 0.044 g cm^{-3}, 0.043 g cm^{-3}, 0.044 g $cm^{-3}$and 0.044g cm^{-3}, respectively.

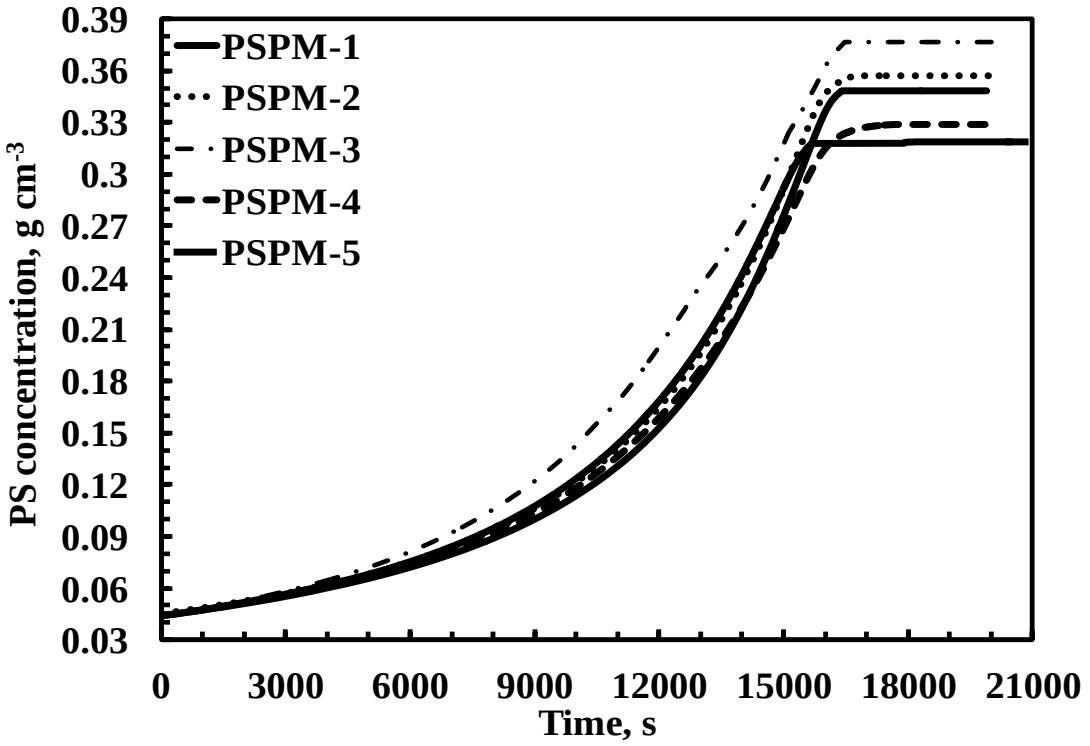

Figure 5.7(a): Poly(styrene) concentration as a function of time in PS-PMMA-EB with different molecular weight of nearly 1750 microns coating thickness at 25 °C.

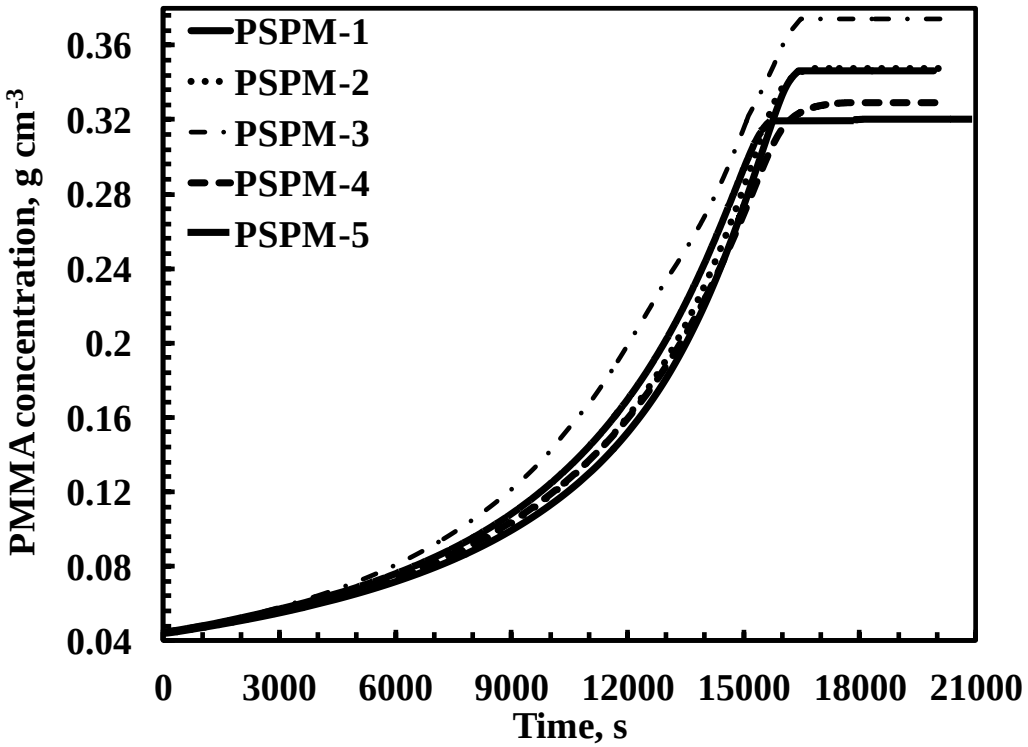

Figure 5.7(b): Poly(methyl methacrylate) concentration as a function of time in PS-PMMA-EB with different molecular weight of nearly 1750 microns coating thickness at 25 °C.

Figure 5.8 shows the average concentration of ethylbenzene with time. The final concentrations of EB in PSPM-1, PSPM-2, PSPM-3, PSPM-4 and PSPM-5 were 0.32 g cm^{-3}, 0.31 g cm^{-3}, 0.28 g cm^{-3}, 0.35 g $cm^{-3}$and 0.37 g cm^{-3} for coatings having initial concentration 0.79 g cm^{-3}, 0.798 g cm^{-3}, 0.798 g cm^{-3}, 0.799 g $cm^{-3}$and 0.79 g cm^{-3} respectively.

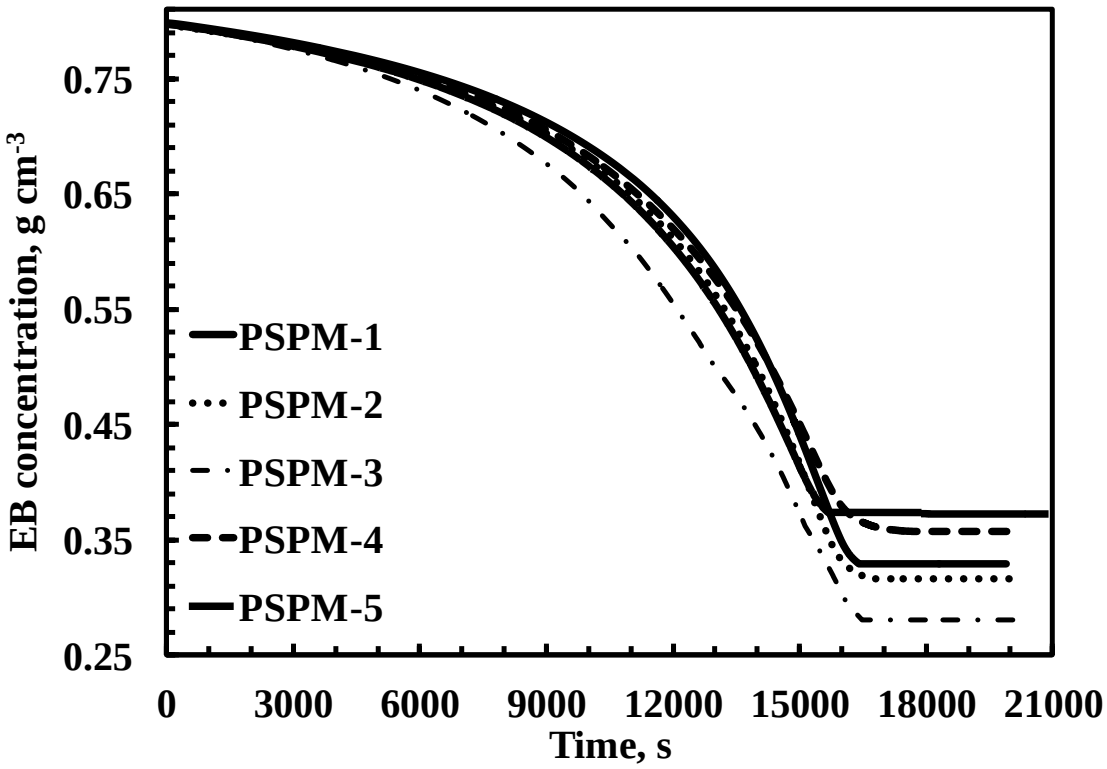

Figure 5.8: Ethylbenzene concentration as a function of time in PS-PMMA-EB with different molecular weight of nearly 1700 microns coating thickness at 25 °C.

5.3.3 Drying of PS-PMMA-EB coating of nearly 3500 µm

Figure 5.9 shows the change in residual solvent with respect to increase in time in PS-PMMA-EB coating with different molecular weight of nearly 3500 µm initial thickness. The residual solvent left in the PSPM-1, PSPM-2, PSPM-4, PSPM-3 and PSPM-5 are 7.84%, 5.5%, 3.87%, 7.27% and 11.27% respectively. The residual solvent left in the PSPM-3 is also lower in this case as compared to other coatings.

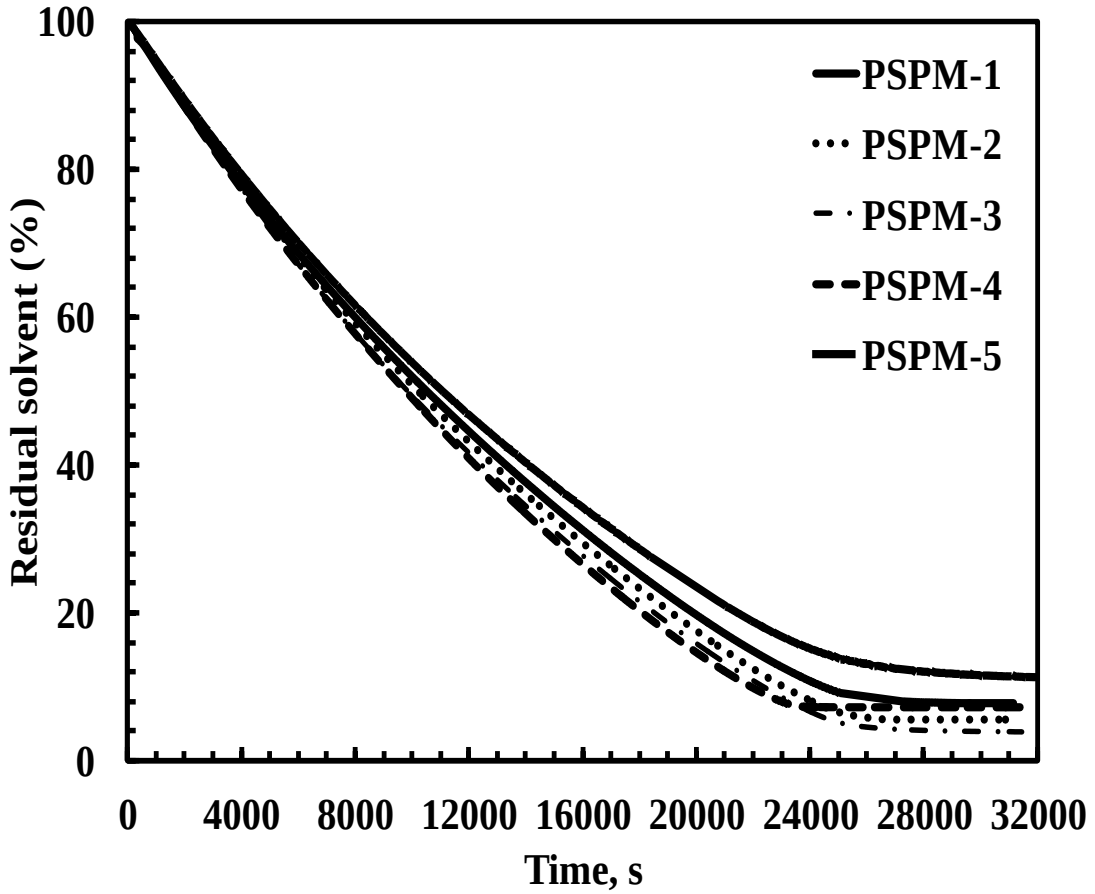

Figure 5.9: Residual solvent as a function of time in PS-PMMA-EB with different molecular weight of nearly 3500 microns coating thickness at 25 °C.

Figure 5.10 shows the change in coating thickness with respect to increase in time in PS-PMMA-EB coating with different molecular weight of nearly 3500 µm initial thickness. The decrease in coating thickness followed the same trend in PSPM-1, PSPM-2, PSPM-4 and PSPM-5 as compared to PSPM-3. The final coating thickness left in the PSPM-1, PSPM-2, PSPM-4, PSPM-3 and PSPM-5 are 534 µm, 466 µm, 418 µm, 511 µm and 642 µm respectively. The final coating thickness in the PSPM-3 is also lower in this case as compared to other coatings.

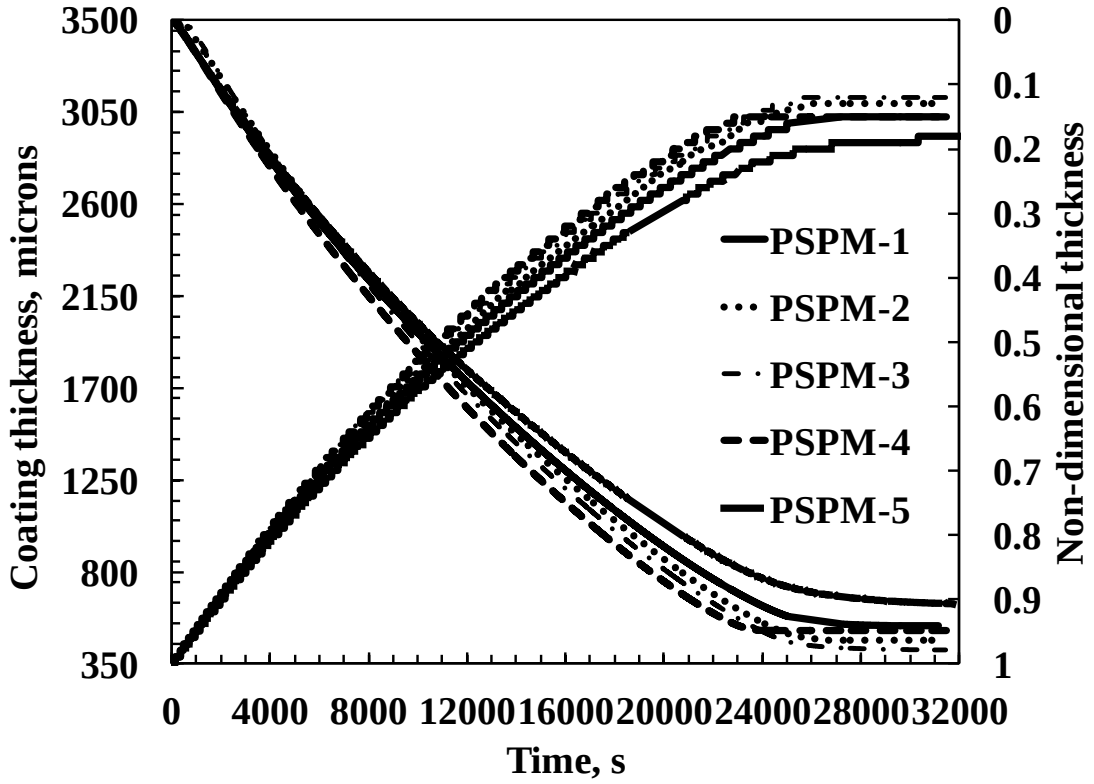

Figure 5.10: Change in coating thickness and Non dimensional thickness as a function of time in PS-PMMA-EB with different molecular weight of nearly 3500 microns coating thickness at 25 °C.

Figure 5.11(a) and 5.11(b) shows the average concentration of poly(styrene) and poly(methyl methacrylate) with time. The final concentration of PS in PSPM-1, PSPM-2, PSPM-3, PSPM-4 and PSPM-5 were 0.30 g cm^{-3}, 0.361 g cm^{-3}, 0.412 g cm^{-3}, 0.356 g $cm^{-3}$and 0.32 g cm^{-3} for coatings having initial concentration 0.044 g cm^{-3}, 0.044 g cm^{-3}, 0.044 g cm^{-3}, 0.044 g cm^{-3} and 0.044g cm^{-3} respectively. The final concentration of PMMA in PSPM-1, PSPM-2, PSPM-3, PSPM-4 and PSPM-5 were 0.298 g cm^{-3}, 0.351 g cm^{-3}, 0.409 g cm^{-3}, 0.356 g $cm^{-3}$and 0.276 g cm^{-3} for coatings having initial concentration 0.043 g cm^{-3}, 0.044 g cm^{-3}, 0.043 g cm^{-3}, 0.044 g $cm^{-3}$and 0.044g cm^{-3} respectively.

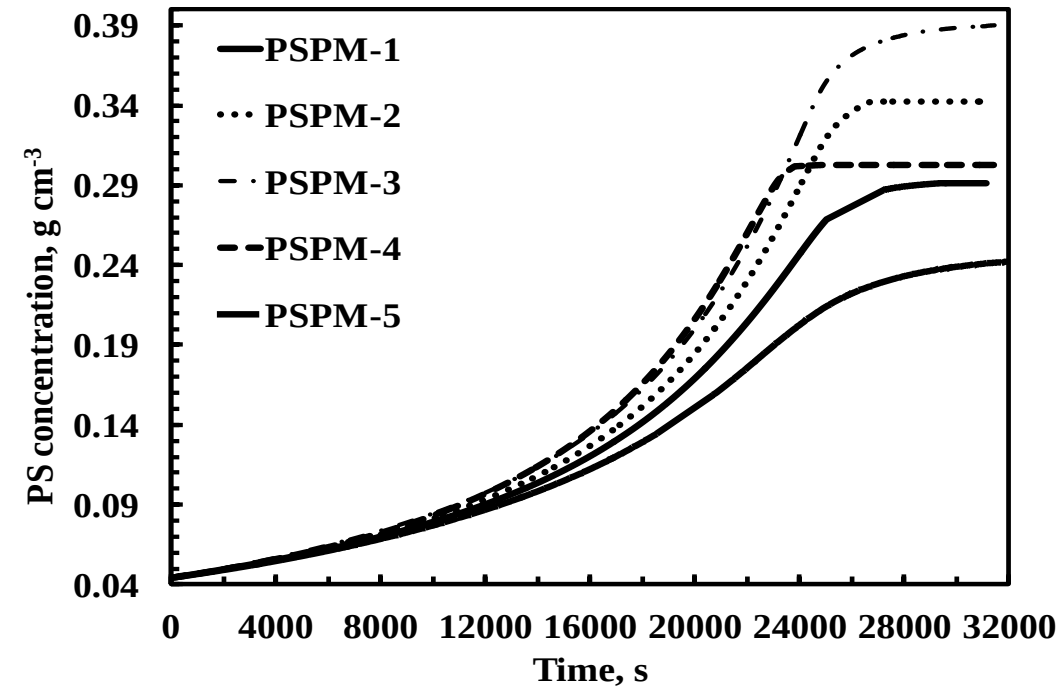

Figure 5.11(a): Poly(styrene) concentration as a function of time in PS-PMMA-EB with different molecular weight of nearly 3500 microns coating thickness at 25 °C.

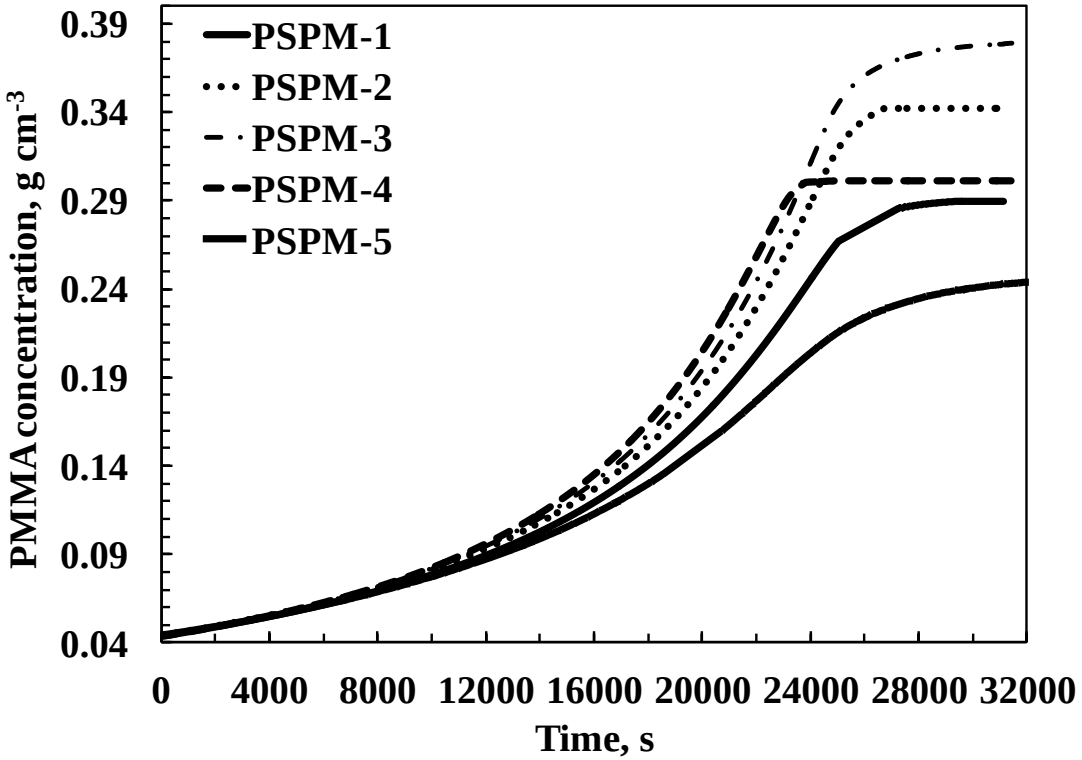

Figure 5.11(b): Poly(methyl methacrylate) concentration as a function of time in PS-PMMA-EB with different molecular weight of nearly 3500 microns coating thickness at 25 °C.

Figure 5.12 shows the average concentration of ethylbenzene with time. The final concentration of EB in PSPM-1, PSPM-2, PSPM-3, PSPM-4 and PSPM-5 were 0.403 g cm^{-3}, 0.31 g cm^{-3}, 0.224 g cm^{-3}, 0.314 g $cm^{-3}$and 0.43 g cm^{-3} for coatings having initial concentration 0.79 g cm^{-3}, 0.798 g cm^{-3}, 0.798 g cm^{-3}, 0.799 g $cm^{-3}$and 0.79 g cm^{-3}respectively. The least concentration of solvent is present in PSPM-3 which has higher molecular weight of PS has the least residual solvent percentage as compared to other prepared system.

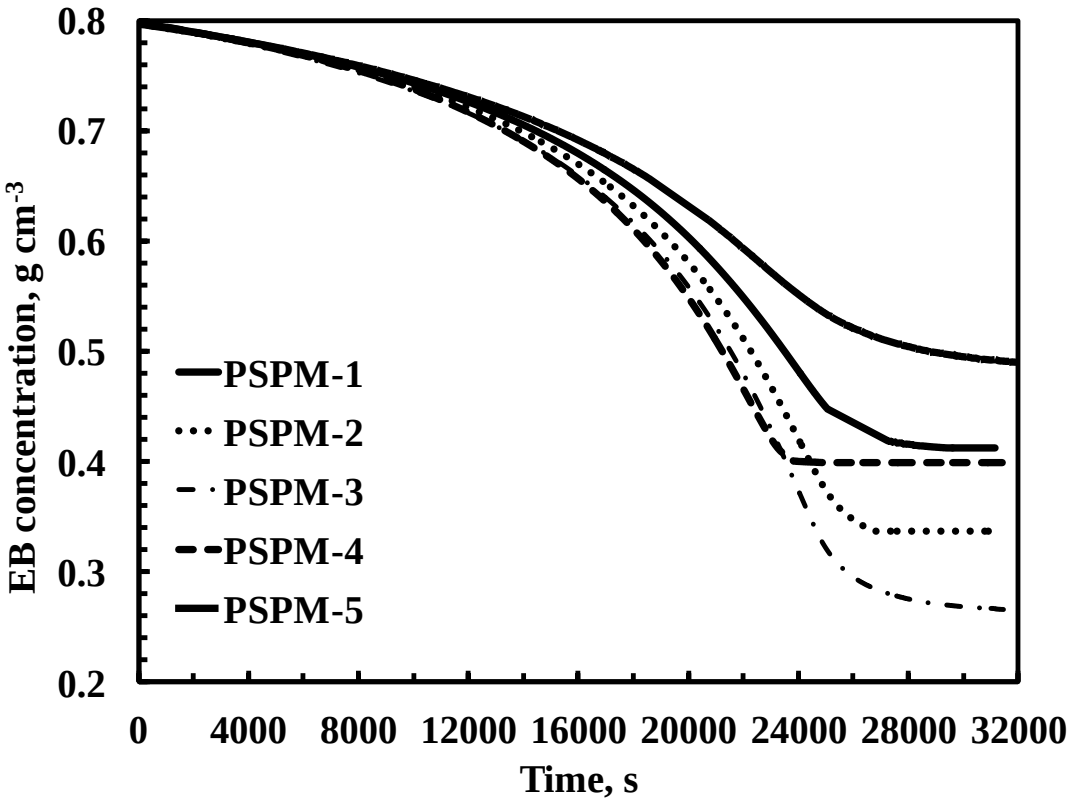

Figure 5.12: Ethylbenzene concentration as a function of time in PS-PMMA-EB with different molecular weight of nearly 3500 microns coating thickness at 25 °C.

Table 5.3 represents the summary of drying data of the coatings of PS-PMMA-EB with different molecular weight of PS and PMMA. The initial thicknesses were changed to get the better comparison between the coatings. In initial thickness of around 1000 µm, the coatings which has higher molecular weight of PS shows better results in residual solvent percentage as can be seen in row 3 i.e, PSPM-3. The further change in initial thickness of approximately 1700 µm, the results show the same similarity and hence show least residual solvent percentage in the case of PSPM-3. The doubled in initial thickness proved that molecular weight of PS

decrease the residual solvent to a significant extent. The increase in PMMA molecular weight increased the residual solvent percentage as seen in row 5.

Similar results were obtained in the case of 1750 µm thickness coatings. The least and highest residual solvent was 4.12% in case of PSPM-3 row 8, and 6.5% in PSPM-5 row 10, respectively. In the case of 3500 µm thickness coatings, PSPM-3 has less residual solvent i.e, 3.87% as can be seen in row 13, and PSPM-5 still has the highest residual solvent, i.e, 11.27 % as seen in row 15.

Table 5.3: Summary of drying data of different PS-PMMA-EB coatings.

S. No	Sample name	Injected volume, µL	Initial coating thickness, µm	Drying Time (s)		Final coating thickness, µm	Ultimate residual solvent (%)
				Falling rate time, s	Constant rate time, s		
1.	PSPM-1	200	998	0-9467	9467-12378	146	7.42
2.	PSPM-2		991	0-9537	9537-12238	124	4.88
3.	**PSPM-3**		**1024**	**0-10479**	**10479-12450**	**110**	**3.01**
4.	PSPM-4		1097	0-11140	11140-12475	137	4.93
5.	**PSPM-5**		**1075**	**0-10409**	**10409-12390**	**174**	**8.92**
6.	PSPM-1	400	1763	0-15597	15597-19907	223	5.22
7.	PSPM-2		1731	0-15660	15660-20116	219	5.03
8.	**PSPM-3**		**1708**	**0-15788**	**15788-20253**	**200**	**4.12**
9.	PSPM-4		1797	0-15780	15780-20050	261	6.06
10.	**PSPM-5**		**1737**	**0-15051**	**15051-20817**	**262**	**6.5**
11.	PSPM-1	600	3527	0-24984	24984-31150	534	7.84
12.	PSPM-2		3582	0-24459	24459-30971	466	5.5
13.	**PSPM-3**		**3598**	**0-25083**	**25083-31464**	**418**	**3.87**
14.	PSPM-4		3514	0-22599	22599-31540	511	7.27
15.	**PSPM-5**		**3503**	**0-24932**	**24932-31934**	**642**	**11.27**

5.4 Conclusions

The gravimetric studies of change of molecular weight of PS and PMMA in EB as a solvent were studied. The results clearly indicate that by increasing the molecular weight of PS, the residual solvent percentage gets reduced as compared to the higher molecular weight of PMMA. Therefore the thermodynamic of this system is a strong function of PS molecular weight.

References

[1] K.D. Weiss, Paint and coatings: a mature industry in transition, Progress in Polymer Science, 22 (1997) 203-245.

[2] M. Dabral, L. Francis, L. Scriven, Drying process paths of ternary polymer solution coating, AIChE Journal, 48 (2002) 25-37.

[3] C.M. Cardinal, Y.D. Jung, K.H. Ahn, L. Francis, Drying regime maps for particulate coatings, AIChE Journal, 56 (2010) 2769-2780.

[4] J. Wang, Z. Zheng, H. Li, W. Huck, H. Sirringhaus, Dewetting of conducting polymer inkjet droplets on patterned surfaces, Nature Materials, 3 (2004) 171-176.

[5] T. Pham, X. Cheng, S. Kumar, Drying of multicomponent thin films on substrates with topography, Journal of Polymer Science Part B: Polymer Physics, 55 (2017) 1681-1691.

[6] R.K. Arya, M. Vinjamur, Near-optimization of operating conditions and residence times in multizone dryers for polymer coatings, Industrial & Engineering Chemistry Research, 48 (2009) 10504-10514.

[7] K. Binder, S. Puri, S.K. Das, J. Horbach, Phase separation in confined geometries, Journal of Statistical Physics, 138 (2010) 51-84.

[8] T. Tanaka, R. Nakatsuru, Y. Kagari, N. Saito, M. Okubo, Effect of molecular weight on the morphology of polystyrene/poly (methyl methacrylate) composite particles prepared by the solvent evaporation method, Langmuir, 24 (2008) 12267-12271.

[9] D. Borah, R. Senthamaraikannan, S. Rasappa, B. Kosmala, J.D. Holmes, M.A. Morris, Swift nanopattern formation of PS-b-PMMA and PS-b-PDMS block

copolymer films using a microwave assisted technique, ACS Nano, 7 (2013) 6583-6596.

[10] H. Ade, A. Smith, S. Qu, S. Ge, J. Sokolov, M. Rafailovich, Phase segregation in polymer thin films: Elucidations by X-ray and scanning force microscopy, EPL (Europhysics Letters), 45 (1999) 526.

[11] D.A. Winesett, H. Ade, J. Sokolov, M. Rafailovich, S. Zhu, Substrate dependence of morphology in thin film polymer blends of polystyrene and poly (methyl methacrylate), Polymer International, 49 (2000) 458-462.

[12] J. Sharma, R.K. Arya, S. Ahuja, C.K. Bhargava, Residual solvent study in polymer− polymer—solvent coatings: Poly (styrene)—poly (methyl methacrylate)—tetrahydrofuran coatings, Progress in Organic Coatings, 113 (2017) 200-206.

[13] R.A. Waggoner, F.D. Blum, J. MacElroy, Dependence of the solvent diffusion coefficient on concentration in polymer solutions, Macromolecules, 26 (1993) 6841-6848.

[14] M.A. Freedman, J.S. Becker, S. Sibener, Effects of film thickness and molecular weight on the interfacial dynamics of atactic poly (methyl methacrylate), The Journal of Physical Chemistry B, 112 (2008) 16090-16096.

[15] J. Vrentas, J. Duda, Diffusion in polymer–solvent systems. II. A predictive theory for the dependence of diffusion coefficients on temperature, concentration, and molecular weight, Journal of Polymer Science: Polymer Physics Edition, 15 (1977) 417-439.

[16] J. Vrentas, J. Duda, Diffusion in polymer—solvent systems. I. Reexamination of the free-volume theory, Journal of Polymer Science Part B: Polymer Physics, 15 (1977) 403-416.

[17] P.J. Flory, Fifteenth spiers memorial lecture. Thermodynamics of polymer solutions, Discussions of the Faraday Society, 49 (1970) 7-29.

[18] W.W. Graessley, Molecular entanglement theory of flow behavior in amorphous polymers, The Journal of Chemical Physics, 43 (1965) 2696-2703.

[19] L.L. Spangler, J.M. Torkelson, J.S. Royal, Influence of solvent and molecular weight on thickness and surface topography of spin-coated polymer films, Polymer Engineering & Science, 30 (1990) 644-653.

[20] C.M. Burns, W.N. Kim, Solution blending of polystyrene and poly (methyl methacrylate), Polymer Engineering & Science, 28 (1988) 1362-1372.

[21] C.K. Bhargava, R.K. Arya, Design of Binary Polymeric Coatings for Minimizing the Residual Solvent, Part I: Experimentation, Drying Technology, 33 (2015) 92-102.

[22] R.K. Arya, K. Tewari, S. Shukla, Non-Fickian drying of binary polymeric coatings: Depth profiling study using confocal Raman spectroscopy, Progress in Organic Coatings, 95 (2016) 8-19.

Chapter 6

Effect of Molecular Weight on Morphology and Thermal Properties

This chapter discussed about the effect of molecular weight of the polymers on the morphological behavior, and the calorimetric studies of coatings.

6.1 Introduction

6.1.1 Effect of molecular weight on the thermal properties of coatings

The studies on physical properties and morphology of polymeric coatings are attracting much interest due to their use in the field of membranes, microelectronic coatings and adhesive, photo resists for semiconductor microlithography, and optical fibers [1]. However, the physical properties of polymeric films are different from the bulk materials. Glass transition temperature is a characteristic of polymers that marks their transition from glassy to rubbery state.

Glass transition temperature (T_g) is considered a main parameter to check the applicability of the polymeric films and thus has attracted extensive attention [2]. It gives immense information about the change in physical properties such as the rate of diffusion of solvent through the polymer, coefficient of thermal expansion, mechanical modulus, melting and crystallization point. The glass transition temperature is closely linked to the concept of free volume space in the molecules also, and thus occurs when there is appropriate free volume to allow molecules in the polymer backbone to move relative to one another. For example, below T_g, the molecular motion seizes due to very low free volume, and the molecules oscillate around a fixed position and behave like solid. Above T_g, molecules produce more free volume due to more oscillations and vibrations of the chain segments [3]. The

dependence of glass transition temperature on the film thickness is getting more attention in the field of polymeric coatings.

The glass transition of polymeric films can easily be calculated from differential scanning calorimetry (DSC), ellipsometry, local Atomic force microscopy (AFM) thermal probes, AFM lateral force methods, positron annihilation, and Brillouin light scattering (BLS) [4]. Out of these methods, calorimetry marked its special position due to its simplicity and universal behavior. Physical properties such as heat capacity, enthalpy, and its integral over temperature can easily be calculated using DSC. There is very limited study of the depression in T_g of thin films. Their glass transition temperature substantially deviates from that of the bulk polymer. The glass transition temperature is very much dependent on the substrate used to make the polymeric coatings. It decreases with the decrease in the coating thickness for freely standing films. It increases with decrease in the coating thickness for the substrate supported films due to strong attractive substrate interactions. The enhancement in the T_g is caused due to the interaction between the polymer and the substrate [5, 6].

The effect of film thickness on the glass transition temperature has been well-elucidated in the literature. The very first depression of T_g in the nanoconfined materials was found by Jackson and Mckenna [7] and further verified by Jonas and co workers [8]. Yung et al. [9] measured the absolute heat capacity and glass transition temperature of the unsupported poly(styrene) ultrathin films with a step scan method. They used the polystyrene-toluene system for their study and the films were prepared by means of the spin coating technique on mica substrate. They also prepared a triple layered of poly(isobutylene)-polystyrene-poly(isobutylene). Their study stated that the absolute heat capacity and glass transition temperature of glass and liquid decreased with the decrease in the film thickness.

Porter and Blum [1] studied the thermal behavior of thin films of poly(methyl methacrylate) adsorbed onto silica using modulated differential scanning calorimetry. The glass transition temperature of the film increased from 108 ^{o}C to 136 ^{o}C for poly(methyl methacrylate) adsorbed on silica from toluene. Even for the poly(methyl methacrylate)-toluene-benzene system, the glass transition temperature increased

further upto 167 ^{o}C due to the increase in the polarity which made the solvents thermodynamically compatible with poly(methyl methacrylate).

Efremov et al. [10] studied differential scanning calorimetry of the ultrathin polymeric films (< 10nm) of poly(styrene) and poly(methyl methacrylate) in toluene and poly(2-vinyl pyridine) in n-butanol on the platinum surface prepared using the spin coating technique. They also studied the thickness dependence of T_g. At low thickness of around 1-3 nm, a pronounced depression in T_g was seen as compared to the thickness of hundreds of nanometers.

The glass transition temperature not only depends on the substrate but also on the molecular weight of the polymer. Generally, the glass transition temperature of the polymers increases with the increase in molecular weight. On a moderate range of molecular weight there is no visible dependence on T_g [11] . There are several theories and equations for the dependence of molecular weight on T_g such as Chow [12], who designed an empirical equation for the glass transition temperature of the polymer-diluent systems. He expressed T_g in terms of the concentration of diluent, molecular and interaction parameters, the transition isobaric specific heat increment. The number of diluent molecules (N), and the number of lattice sites ($N+L$) are defined by:

$$\ln\frac{T_g}{T_{g0}} = \beta\left\{(1-\theta)\ln(1-\theta) + \theta\ln\theta - \chi_s(1-\theta)\right\} \tag{6.1}$$

where $\beta = k(N+L)/\Delta C_p$: T_g: glass transition temperature, $\theta = \frac{N}{N+L}$, χ_s: interaction parameter

$$N = m_d N_A / M_d \tag{6.2}$$

$$N + L = z m_p N_A / M_p \tag{6.3}$$

where N_A: Avogadro's number, m: mass, M_w: molecular weight, M_p: Molecular weight of monomer; d and p are subscript for diluents and polymer.

For bulk polymer, Flory-Fox equation [13] relates the molecular weight and T_g as follows

$$T_g^{bulk}(M_n) = T_{g\infty} - \frac{K}{M_n} \tag{6.4}$$

where, $T_{g\infty}$ and K: fitting parameters, M_n: Molecuar weight of the polymer, T_g^{bulk}: Glass transition temperature of the bulk polymer.

The effects of molecular weight of polymer and thickness on T_g were investigated by Singh and coworkers [14]. They studied the binary system, polystyrene (M_w; 212400, 560900, 1571000)- toluene. The effect of molecular weight and thickness on T_g is more pronounced at high molecular weight and thickness values. They developed an equation in which the molecular weight and thickness were related with the glass transition temperature as follows:

$$T_g = f(M_w) \times f\left(\frac{h}{\langle s^2 \rangle^{1/2}}\right) \tag{6.5}$$

where T_g; glass transition temperature, h: thickness of the film, M_w: molecular weight of the polymer and $\langle s^2 \rangle^{1/2}$: unperturbed root mean square radius of gyration.

Xia et al. [15] studied the effect of molecular weight of freely standing poly(methyl methacrylate) films. They related the molecular weight with the free volume space between the films. They concluded that at nanoscale thickness, the low molecular weight of PMMA showed more deviation from their bulk behavior and thus exhibited lower T_g due to less chain end segments and more interfacial free volume space.

More recently, Kun and Tsui [5] studied the glass transition temperature of the supported poly(methyl methacrylate) films on silica at two molecular weights of 2.5 and 5 kg/mol and syndiotacticities (59 and 69%) by ellipsometry. The tacticity, substrate, and molecular weight of the polymers affected the T_g. Their study showed that the syndiotactic PMMA had depressed the T_g more and had stronger substrate effect than the atactic PMMA in the case of higher molecular weight of 5 kg/mol. At lower molecular weight of 2.5 kg/mol, the effect of the free surface became ineffective in syndiotactic PMMA.

6.1.2 Effect of molecular weight on the surface morphology of coatings

Membranes can be isotropic and anisotropic in shape. Asymmetric films have attracted much interest due to their potential applications as well as fundamental studies. These are mostly used in the gas and liquid separations since the top layer provides a barrier to the external materials and the small pores provide the good mechanical strength [16]. There are techniques such as phase inversion and solution casting, which lead to the formation of asymmetric membranes. The surface composition can be changed or controlled by molecular weight, surface free energy, change in concentration, and architecture. The control of molecular weight is very helpful in the industrial applications like desorption, adsorption, coatings, modifiers, and adhesives [17, 18]

The morphology of the poly(styrene) (PS) /poly(methyl methacrylate) (PMMA) films were also investigated by scanning electron microscopy. These coatings can be better understood by the morphological studies, which help us to understand the core depth and behavior of any particle, materials, and coatings. For example, Tanaka et al. [19] studied the effect of molecular weight on the morphology of the poly(styrene)-poly(methyl methacrylate) blend by the solvent evaporation method using toluene as a solvent. They conducted the gel permeation chromatography to check the molecular weight distributions, observed the composite in the optical micrographs, scanning electron microscope, (SEM) and transmission electron microscopy (TEM), and measured the interfacial tension using pendant drop method. They concluded through the SEM images that the degree of protrusion increased with increasing molecular weight and had a snowman like structure. The TEM micrographs showed that with the increase in the molecular weight the

interfacial tension decreased and had a janus like morphology. The phase separation only occurred at higher molecular weight of the polymer and with lower weight percentage.

Burns and Kim [20] studied the blends of poly(styrene) and poly(methyl methacrylate) in methylene chloride made from the solution casting method. They characterized the blends using SEM and DSC. They varied the molecular weight of poly(methyl methacrylate) from 39300 to 56900 by keeping the molecular weight of poly(styrene) constant at 24500. The micrographs showed that the PMMA of a higher molecular weight had lower immiscibility with poly(styrene) than the poly(methyl methacrylate) of a lower molecular weight . A decrease in the glass transition temperature was observed but the highest decrease was in the case of lower molecular weight PMMA.

Borah et al. [21] studied the morphology of the block co-polymer thin films of polystyrene-b-poly(methyl methacrylate) (PS-b-PMMA) and polystyrene-b-polydimethyl siloxane (PS-b-PDMS) in toluene. The coatings were prepared using spin coating technique. They used the microwave assisted annealing without using any solvent and observed the micro-phase separation in PS-b-PMMA and PS-b-PDMS. They varied the molecular weight of the block polymers from 5000 to 104000. The SEM analysis showed that with the increase in the annealing time in the low molecular weight PS-b PMMA, there were disordered patterns and more defected sites. The thermal annealing at low temperatures showed the micro phase separation in the high molecular weight of the PS-b-PMMA and PS-b-PDMS.

The effect of the molecular weight on the polymeric films is somewhat unpredictable because the glass transition temperature is a phase change phenomenon. It depends on many factors and is very sensitive to a change of polymer composition, fraction of chain ends, concentration, chain length, thickness, etc. Moreover, the morphological study also helps to understand the coating behavior.

For the present study, the main goal is to see the effect of molecular weight of the polymers on the morphological and glass transition of the PS-PMMA-EB coatings. The coating thicknesses were kept constant for better understanding of the dependency of molecular weight on the glass transition temperature. The calorimetric

and the morphological behavior of the system were analyzed by means of differential scanning calorimetry and scanning electron microscopy, respectively.

6.2 Materials and Methods

All the chemicals were used as supplied. Polystyrene (PS) and poly(methyl methacrylate) (PMMA) with molecular weight (35000, 120000, 350000) and (120000, 350000, 996000) respectively were purchased from Sigma Aldrich, Germany. Ethylbenzene (EB) was purchased from Spectrochem Pvt. Ltd, India. The required amount of PS and PMMA were taken in leach proof Schott duran bottles. These solutions were homogenized in mechanical shaker for 5 days. Films were prepared using solution casting technique by pouring required amount of polymeric solution in stainless steel circular holders of depth 4000 µm and 14.65 mm diameter. Different solutions of PS-PMMA-EB were prepared using the polymers of different molecular weights. The prepared solutions are listed in Table 6.1.

Table 6.1: Coating solutions of different PS/PMMA molecular weights.

S. No	Solution combination	Sample name
1.	PS(35,000)-PMMA(1,20,000)-EB (4.97%- 4.94% - 90.09 %)	PSPM-1
2.	PS(2,80,000)-PMMA(1,20,000)-EB (5.11%- 4.97% - 89.92 %)	PSPM-2
3.	PS(3,50,00)-PMMA(120000)-EB (4.98%- 4.95% - 90.07 %)	PSPM-3
4.	PS(1,92,000)-PMMA(3,50,000)-EB (5.02%- 5.02% - 89.96 %)	PSPM-4
5.	PS(1,92,000)-PMMA(9,96,000)-EB (5.01%- 5.04% - 89.95 %)	PSPM-5

Glass transition temperature (T_g) of the pure polymers used and the prepared coatings were analyzed by DSC 131 evo, Setaram, France, at the heating and cooling rates of 20 K/min, in nitrogen environment. For DSC analysis, ~30 mg of the sample was taken in a 120 µL aluminium pan. The reference was kept blank. All the samples were pretreated for 10 min at 25 ^{o}C inside the chamber, before proceeding for the analysis. The morphological study of the prepared coatings was investigated using scanning electron microscopy (SEM) (JEOL JSM-6510LV, TIET, Patiala-Punjab, India).

6.3 Results and Discussion

6.3.1 Effect of molecular weight on T_g

Figure 6.1 (a-c) show the profiles of the heat flow with the increase in temperature for the pure PS (M_w: 35000), pure PMMA (M_w: 120000), and their blend, PSPM-1 coating. The T_g values of the pure PS (35000) and PMMA (120000) computed from these profiles was 76^{o}C and 105^{o}C respectively. PMMA has two values of T_g as seen in Figure 6.1(b). Table 6.2 presents T_g values of different bulk and blended polymers.

In the case of coatings prepared by adding these two polymers, a single T_g value is exhibited between the T_g values of the mixed components. The T_g value of the PSPM-1 coating comes around 72^{o}C, which is lower than that of the bulk polymers as shown in Figure 6.1(c). The more chain end segments from the low molecular weight polymer, and higher segmental mobility may result in the depression of the T_g of the coating. Also, the addition of the solvent could also be responsible for the decrease in T_g due to plasticization [22].

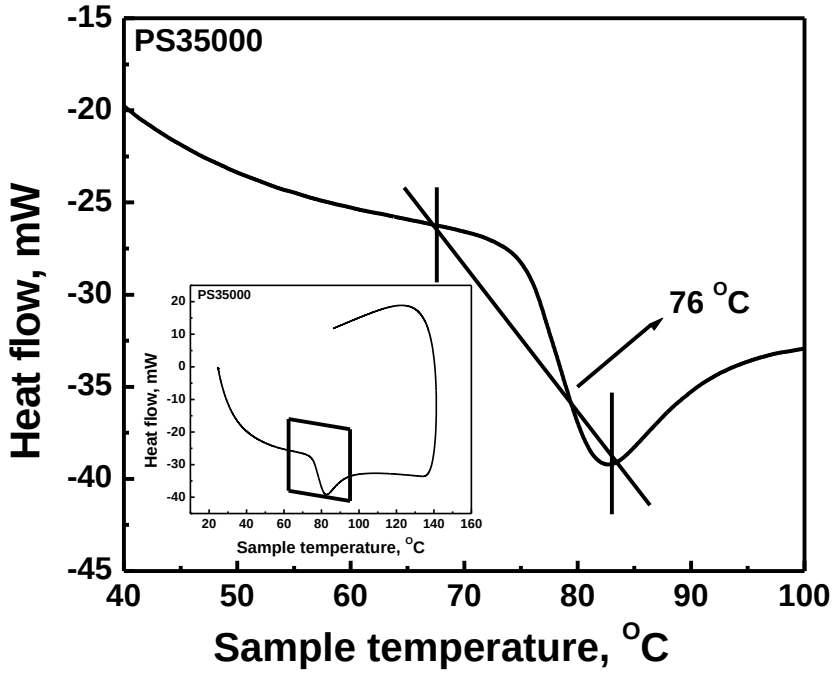

Figure 6.1(a): Heat flow as a function of sample temperature of pure poly(styrene) of molecular weight 35000.

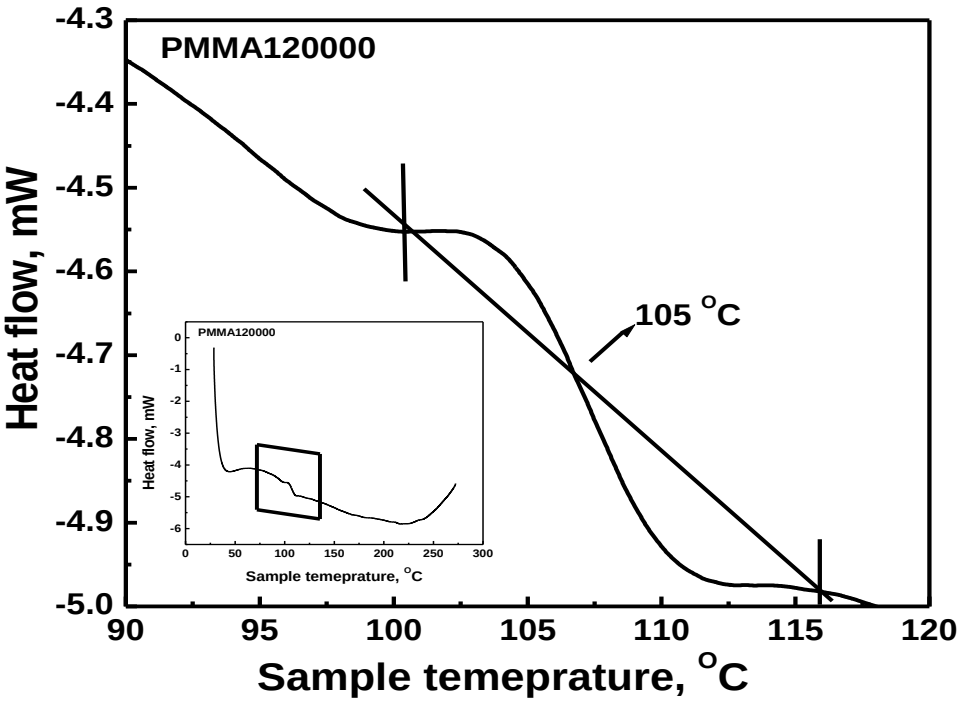

Figure 6.1(b): Heat flow as a function of sample temperature of pure poly(methyl methacrlate) of molecular weight 120000.

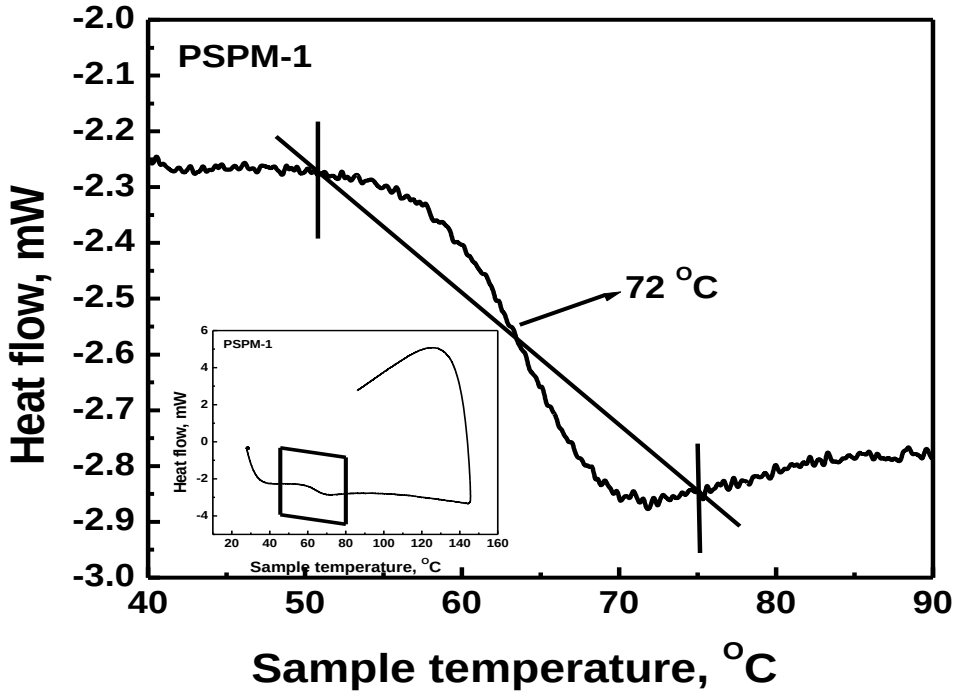

Figure 6.1(c): Heat flow as a function of sample temperature of PSPM-1.

Figure 6.2(a) and 6.2(b) show the profiles of the heat flow with the increase in temperature for the bulk PS (M_w: 280000) and PSPM-2 coating, respectively. In this case, the PSPM-2 coating was prepared by PS of molecular weight 280000 without changing the molecular weight of PMMA. PSPM-2 coating has a T_g of 68 ^oC, and PSPM-1 coating has a T_g of 72 ^oC as seen in Table 6.2. The lower T_g indicates an increase in the free volume and more chain end segments of the polymers.

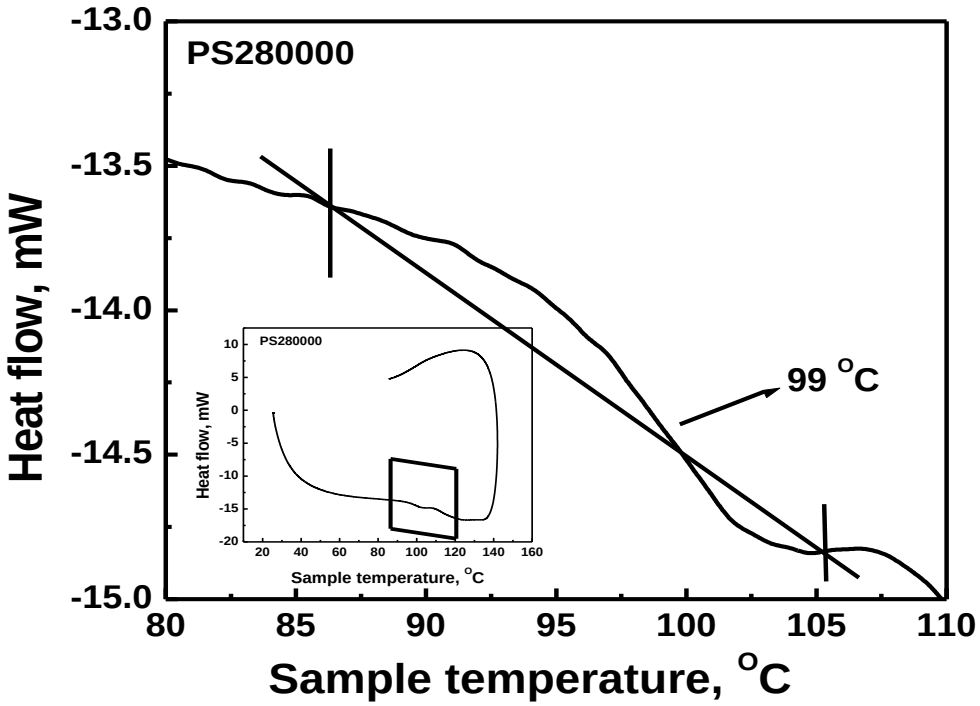

Figure 6.2(a): Heat flow as a function of sample temperature of pure poly(styrene) of molecular weight 280000.

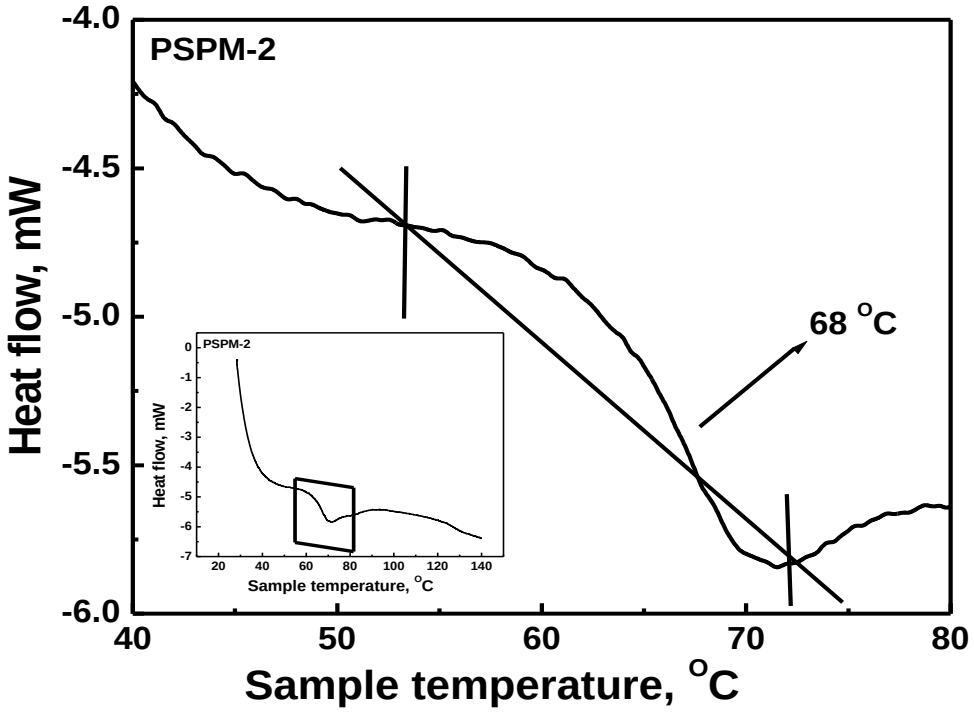

Figure 6.2(b): Heat flow as a function of sample temperature of PSPM-2.

Figures 6.3(a) show the profiles of the heat flow with the increase in temperature for the pure PS (M_w: 350000). Figure 6.3(b) shows the profiles of the coating prepared using PS (350000) and PMMA (120000). The glass transition temperature of the dried film comes out to be 77 ^oC which is again in between the two polymers. The PSPM-3 coating has a little increase in the T_g as compared to the previous PSPM-1 and PSPM-2 coatings. The high M_w of the polymers have less chain end segments which decreases the free volume and hence there is little enhancement of the T_g in this case.

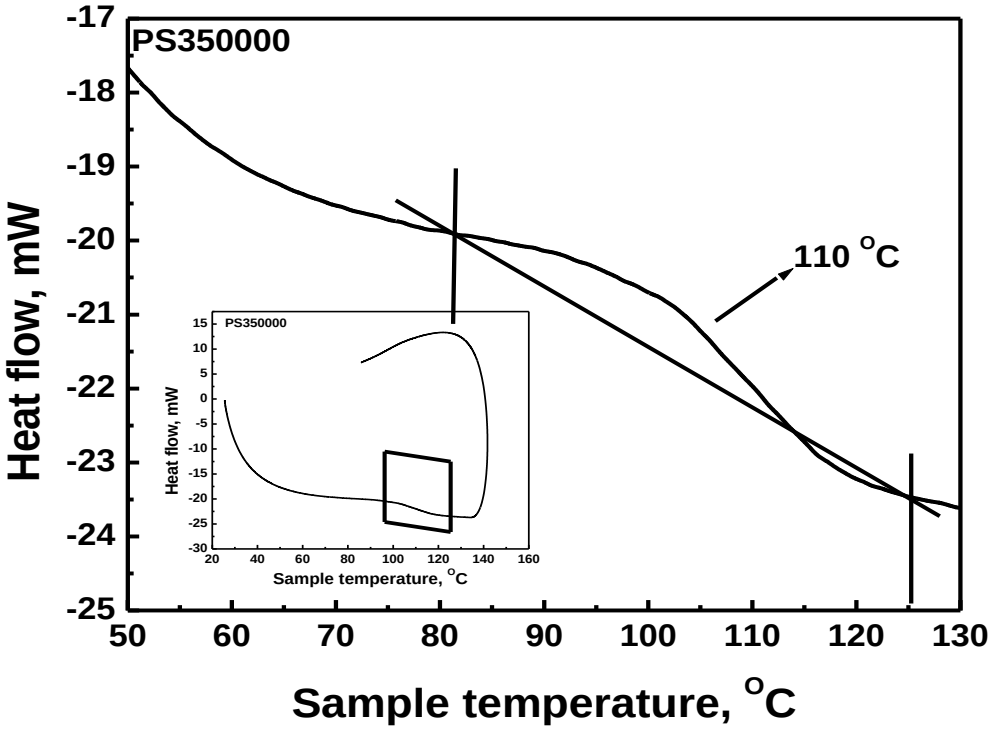

Figure 6.3(a): Heat flow as a function of sample temperature of pure poly(styrene) of molecular weight 350000.

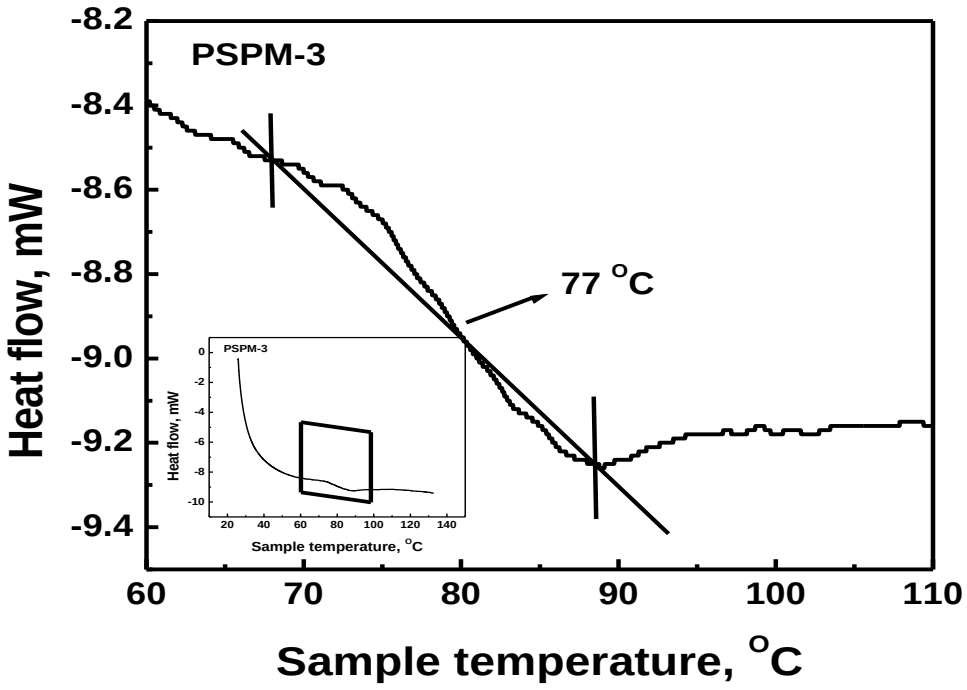

Figure 6.3(b): Heat flow as a function of sample temperature of PSPM-3.

Figure 6.4(a-c) show the profiles between heat flow with the increase in temperature of pure PS (M_w: 192000), pure PMMA (350000), and dried coating prepared using these polymers, respectively. The T_g of the pure PS (192000), and PMMA (350000) were 104 ^oC and 130 ^oC, respectively. The T_g of the coating prepared using these two polymers comes out to be 105 ^oC. The T_g of this coating is also in between the pure polymers. The T_g of this film is very close to the pure PS (M_w: 192000). PSPM-4 has the highest T_g among all the previously prepared coatings. This could be due to the higher degree of entanglement of the polymers of high M_w used, which requires more energy to break or loosen the entangled chains. The higher M_w of the polymers made the solution viscous and the coatings became harder and remained glassy to a great extent of temperature. The coatings having high T_g are harder, have high strength, and have better utilization.

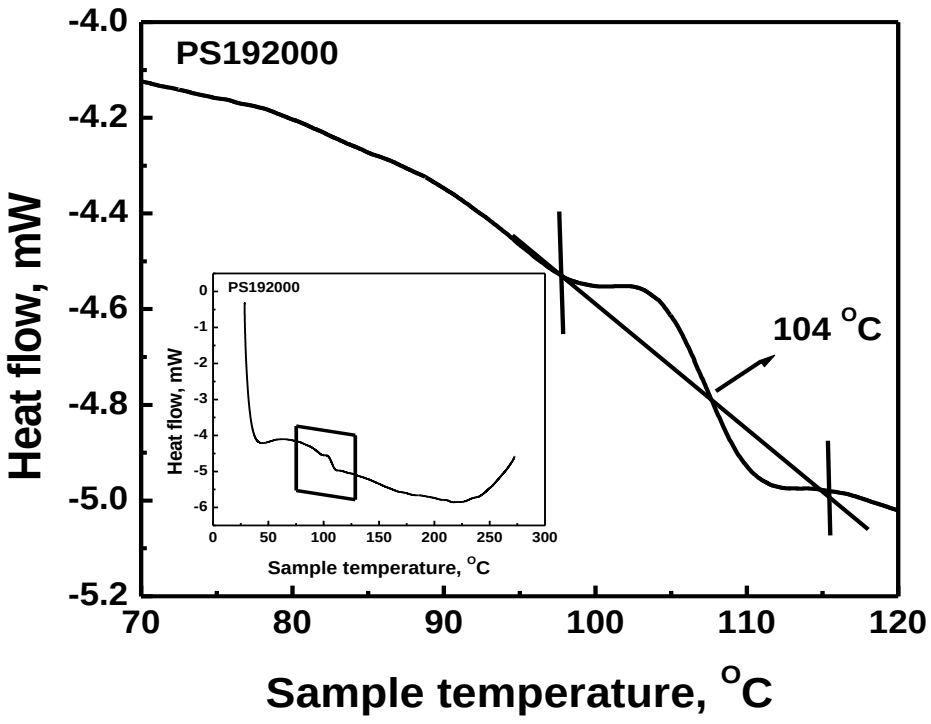

Figure 6.4(a): Heat flow as a function of sample temperature of pure poly(styrene) of molecular weight 192000.

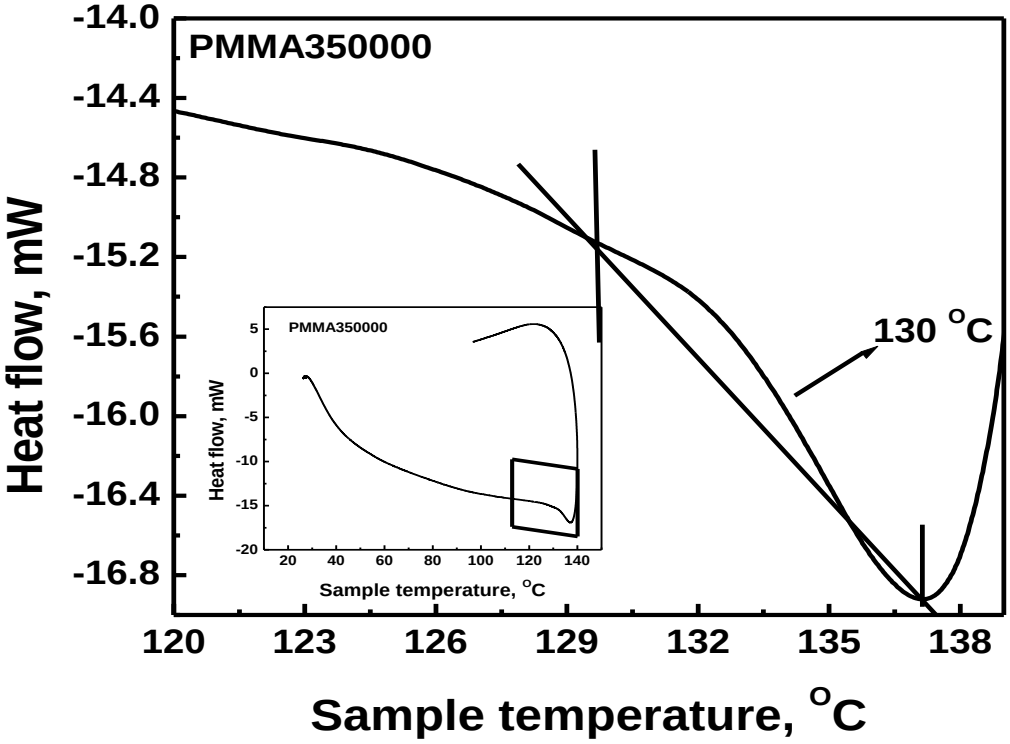

Figure 6.4(b): Heat flow as a function of sample temperature of pure poly(methyl methacrylate) of molecular weight 350000.

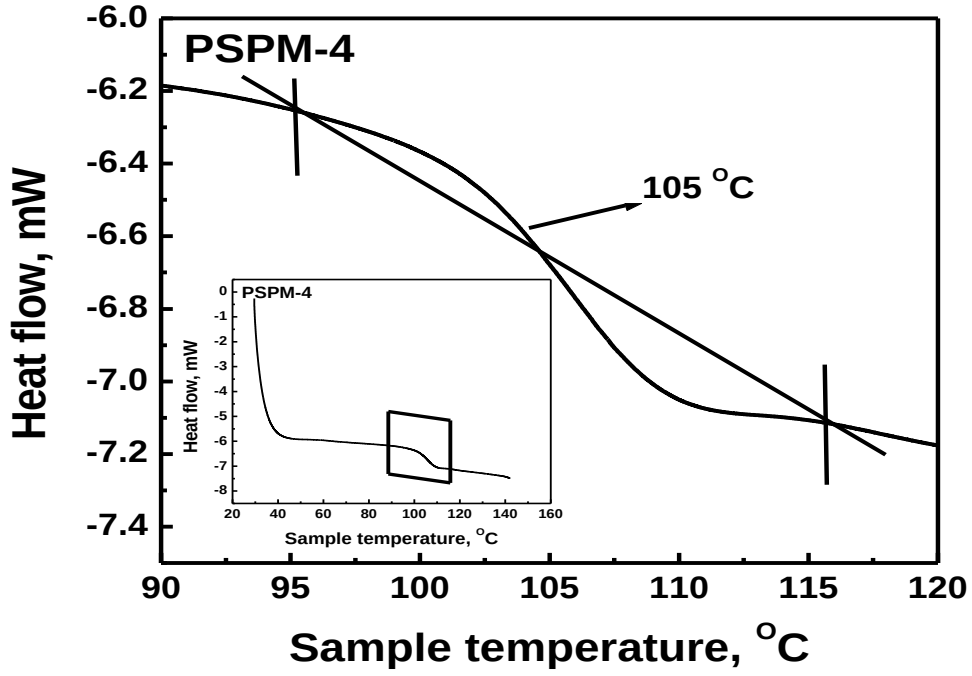

Figure 6.4(c): Heat flow as a function of sample temperature of PSPM-4.

Figure 6.5(a) and 6.5(b) shows the profiles between heat flow with the increase in temperature of the bulk PMMA (M_w: 996000), and PSPM-5, respectively. Pure PMMA of molecular weight 996000 shows two glass transition temperatures in this case. The glass transition temperature of the pure PMMA was at 120 ^oC. As can be seen in Figure 6.5(b) the glass transition temperature of the coating prepared using PS (192000) and PMMA (996000) came out to be 66 ^oC. The effect of molecular weight on the glass transition temperature occurs within a certain limit of M_w, after which T_g is independent of M_w. In this case, the M_w of PMMA is so high that it exceeds the critical molecular weight, and thus does not affect the T_g. Only the M_w of PS has effect on the T_g, and thus lowers the T_g to a great extent. The PS is a non-polar polymer, hence it is weakly interacted with the solvents and thus shows a pronounced decrease in the T_g [23].

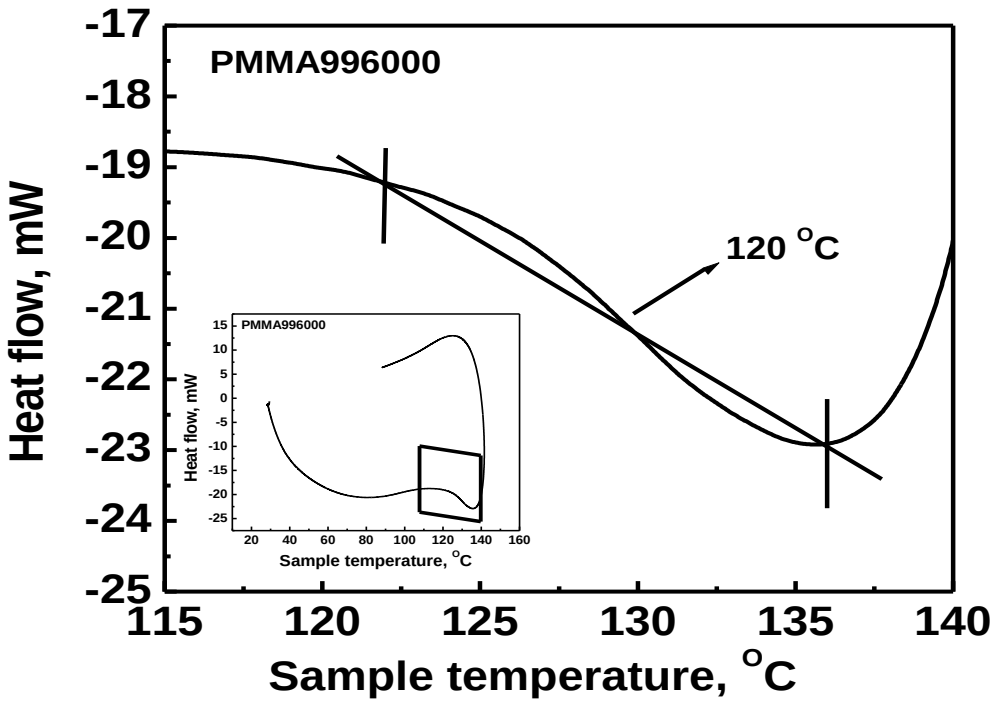

Figure 6.5(a): Heat flow as a function of sample temperature of pure poly(methyl methacrylate) of molecular weight 996000.

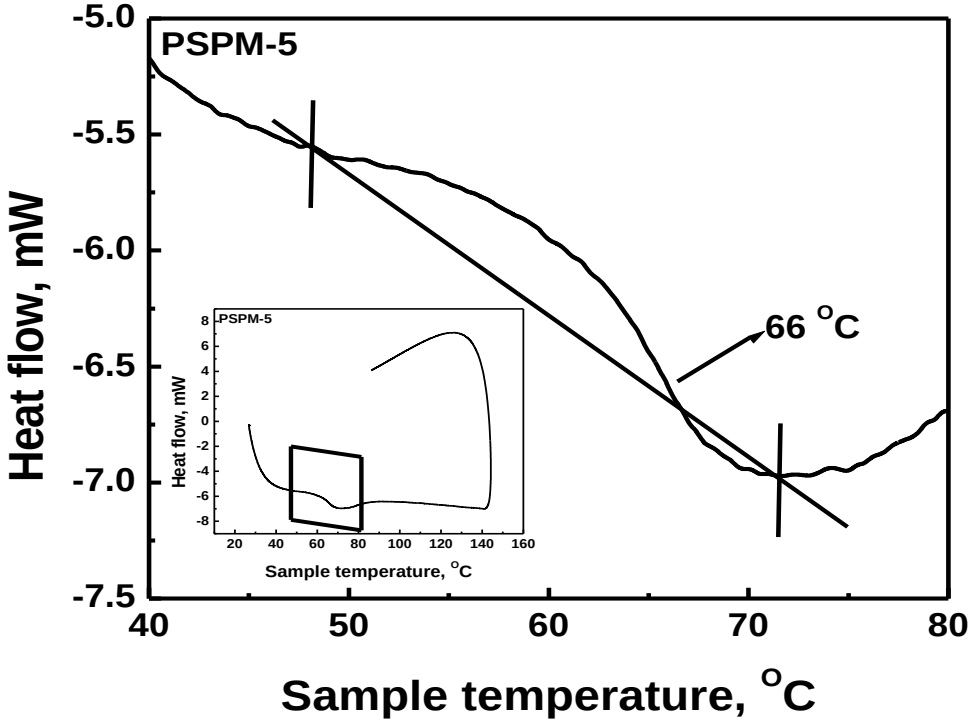

Figure 6.5 (b): Heat flow as a function of sample temperature of PSPM-5.

Table 6.2: Glass transition temperature of the bulk polymers and prepared coatings.

S.No	PS (M_w)	T_g (^oC)	PMMA (M_w)	T_g (^oC)	Coatings	T_g (^oC)	Initial coating thickness (microns)
1.	35000	76	120000	105	PSPM-1	72	998
2.	280000	99	120000	105	PSPM-2	68	991
3.	350000	110	120000	105	PSPM-3	77	1024
4.	192000	104	350000	130	PSPM-4	105	1097
5.	192000	104	996000	120	PSPM-5	66	1075

6.3.2 Effect of molecular weight on morphology

Figures 6.6 (a and b) show the top and bottom surfaces of PSPM-1, respectively. The initial coating thickness of the film is 998 microns and is dried at 25 ^oC for 12378 s. The top surface has undistributed phase separation. The semi

circular particles or voids are visible indicating the low phase separation in the coating. The film is little non porous in this case. The bottom surface has a dense nature.

Figures 6.7 (a and b) show the top and bottom surfaces of PSPM-2, respectively. The initial coating thickness of the film is 991 microns and is dried at 25 ^{o}C for 12238 s. Dense polymeric films are formed in this case. Top surface shows the precipitation of polymer.

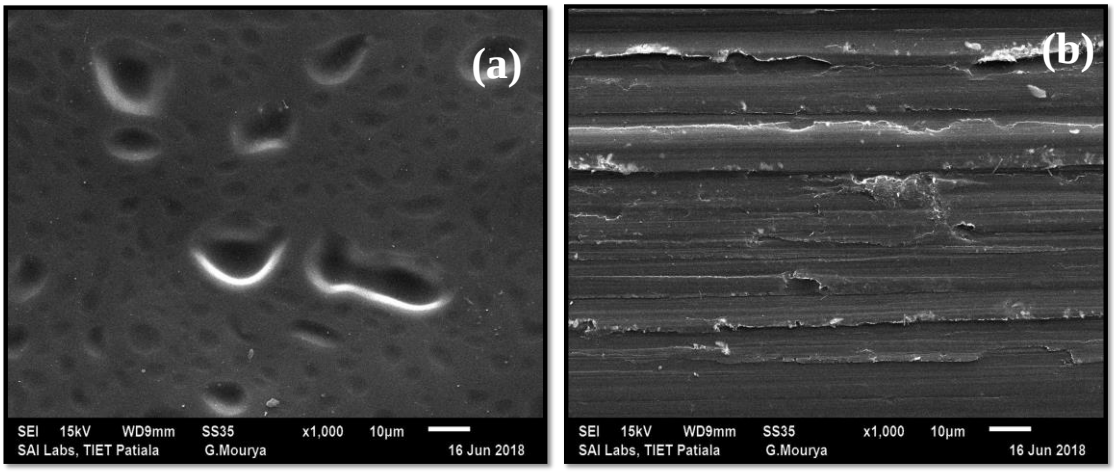

Figure 6.6: SEM image showing (a) top and (b) bottom surface image of PSPM-1 coating.

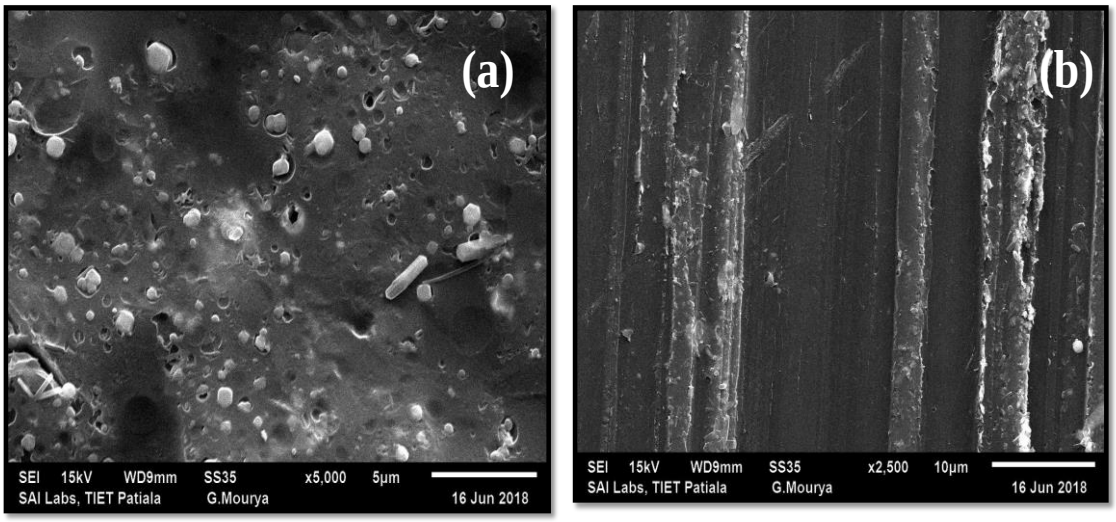

Figure 6.7: SEM image showing (a) top and (b) bottom surface image of PSPM-2 coating.

Figures 6.8 (a and b) show the top and bottom surfaces of PSPM-3 respectively. The initial coating thickness of the film is 1024 microns and is dried at 25 ^{o}C for 12450 s. The molecular weight of the PS is higher in this case than PMMA. Therefore, the precipitation of one polymer takes place in the film. There are some dusts particles also present at the coating surface which may occur while scratching the film from the substrate. Dense non porous films are formed in this case.

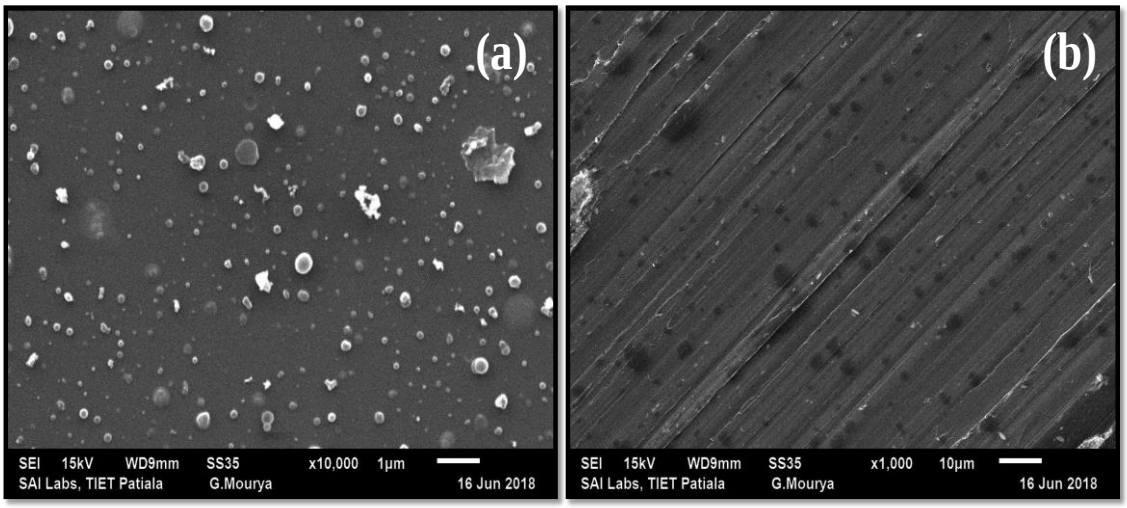

Figure 6.8: SEM image showing (a) top and (b) bottom surface image of PSPM-3 coating.

Figures 6.9 (a and b) show the top and bottom surfaces of PSPM-4, respectively. The initial coating thickness of the film is 1097 microns and is dried at 25 ^{o}C for 12475 s. Proper phase separation can be seen in this film with porous structure at the top side of the membrane. Intermediate molecular weights of the polymers lead to a better phase separation.

Figures 6.10 (a and b) show the top and bottom surfaces of PSPM-5, respectively. The initial coating thickness of the film is 1075 and is dried at 25 ^{o}C for 12390 s. The molecular weight of PMMA was taken higher than PS. The precipitates of the higher molecular weight of PMMA were visible. The immiscibility of different molecular weight of the PS/PMMA is easily seen in this case. The bottom surface is dense with no pores.

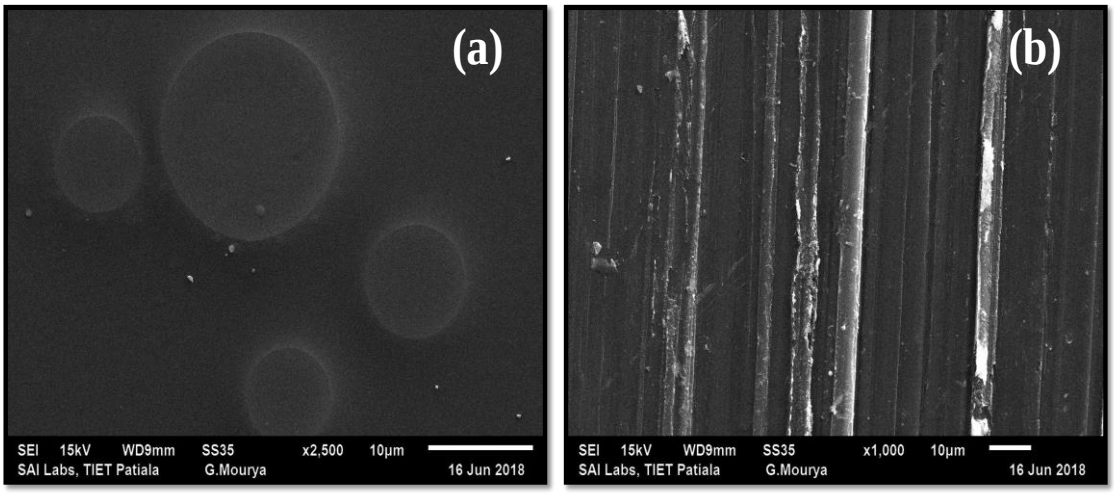

Figure 6.9: SEM image showing (a) top and (b) bottom surface image of PSPM-4 coating.

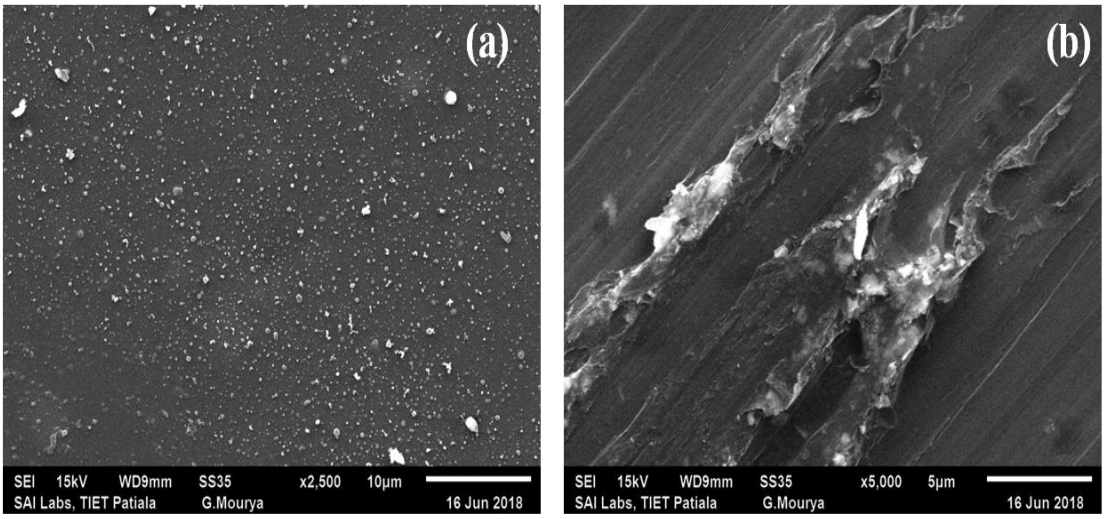

Figure 6.10: SEM images showing (a) top and (b) bottom surface image of PSPM-5 coating.

6.4 Conclusion

The effect of molecular weight on the glass transition temperature as well as the morphological behavior of multi-polymer polymer solvent PS-PMMA-EB coatings was thoroughly investigated. PSPM-4 showed the higher glass transition temperature out of all the other prepared coatings. Phase separated membranes are also formed in the case of PSPM-1 and PSPM-4. High amount of precipiatation was observed in case of PSPM-2 and PSPM-5. There is some precipitation in the case of PSPM-3 also. In the case of PSPM-3, in which PS molecular weight was highest

along with moderate molecular weight of PMMA, the membrane is completely dense on the top and bottom sides. They also exhibited a phase separated coating. The low molecular weight polymeric coating reduced the T_g to a great extent and forms dense and symmetric polymeric films.

The T_g values of PSPM-2 and PSPM-5 are exceptionally lower. As the molecular weight of PS increases from PSPM-1 to PSPM-2, there is increase in polar attraction between PS and PMMA, which reduces the cohesive forces between the PMMA polymer chains and increases the segmental mobility, thereby reducing the T_g value of the coating. Another reason could be the structure of PMMA. There are two conflicting factors at work. First, the CH_3 group in PMMA is an impediment to the free rotation around C-C bond of the chain backbone, thus obstructing the chain mobility. This could be the cause of the increase of T_g value from PSPM-3 to PSPM-4, when PMMA molecular weight was increased. However, another factor dominates in PSPM-5, when the PMMA molecular weight is increased drastically to ten times than PSPM-3. The C-C and C-O linkages in PMMA are themselves supple. As the chain length increases, the flexibility of the chain increases their segmental mobility, which should decrease the T_g. In multicomponent system , the friction factor among the species will be the controlling factor along with jumping units. Either a unit or combination of the units can be which will greatly affect the glass transition temperature.

Earlier researcher also studied the molecular weight affects on the compatibility, that one with smaller molecular weight enhances the miscibility of polymer blend causing in a decreased size of microdomains [18]. For a low molecular weight polymer, the difference in surface energy between main chain groups and chain end groups caused a particular influence on the phase separated structure. The molecular weight affects the movement of polymer chains and hence the morphology of phase separation. High molecular weight polymer increased the porosity of the membrane [19]. This confirms the phase separated as well as the porosity of the PSPM-4 coatings. Hence, PSPM-4 shows the better phase separation.

References

[1] C.E. Porter, F.D. Blum, Thermal characterization of PMMA thin films using modulated differential scanning calorimetry, Macromolecules, 33 (2000) 7016-7020.

[2] H. Levine, L. Slade, Influences of the glassy and rubbery states on the thermal, mechanical, and structural properties of doughs and baked products, in: Dough rheology and baked product texture, Springer, 1990, 157-330.

[3] B.E. Mattioni, P.C. Jurs, Prediction of glass transition temperatures from monomer and repeat unit structure using computational neural networks, Journal of chemical information and computer sciences, 42 (2002) 232-240.

[4] J.H. Kim, J. Jang, W.-C. Zin, Estimation of the thickness dependence of the glass transition temperature in various thin polymer films, Langmuir, 16 (2000) 4064-4067.

[5] K. Geng, O.K. Tsui, Effects of polymer tacticity and molecular weight on the glass transition temperature of poly (methyl methacrylate) films on silica, Macromolecules, 49 (2016) 2671-2678.

[6] Y. Grohens, L. Hamon, G. Reiter, A. Soldera, Y. Holl, Some relevant parameters affecting the glass transition of supported ultra-thin polymer films, The European Physical Journal E, 8 (2002) 217-224.

[7] C.L. Jackson, G.B. McKenna, The glass transition of organic liquids confined to small pores, Journal of Non-Crystalline Solids, 131 (1991) 221-224.

[8] J. Zhang, G. Liu, J. Jonas, Effects of confinement on the glass transition temperature of molecular liquids, The Journal of Physical Chemistry, 96 (1992) 3478-3480.

[9] Y.P. Koh, G.B. McKenna, S.L. Simon, Calorimetric glass transition temperature and absolute heat capacity of polystyrene ultrathin films, Journal of Polymer Science Part B: Polymer Physics, 44 (2006) 3518-3527.

[10] M.Y. Efremov, E.A. Olson, M. Zhang, Z. Zhang, L.H. Allen, Glass transition in ultrathin polymer films: calorimetric study, Physical Review Letters, 91 (2003) 085703.

[11] P. De Gennes, Glass transitions in thin polymer films, The European Physical Journal E, 2 (2000) 201-205.

[12] T. Chow, Glass transition temperature of polymer-diluent systems, Ferroelectrics, 30 (1980) 139-145.

[13] K. Ute, N. Miyatake, K. Hatada, Glass transition temperature and melting temperature of uniform isotactic and syndiotactic poly (methyl methacrylate) s from 13mer to 50mer, Polymer, 36 (1995) 1415-1419.

[14] L. Singh, P.J. Ludovice, C.L. Henderson, Influence of molecular weight and film thickness on the glass transition temperature and coefficient of thermal expansion of supported ultrathin polymer films, Thin solid films, 449 (2004) 231-241.

[15] W. Xia, D.D. Hsu, S. Keten, Molecular weight effects on the glass transition and confinement behavior of polymer thin films, Macromolecular rapid communications, 36 (2015) 1422-1427.

[16] B. Jung, J.K. Yoon, B. Kim, H.-W. Rhee, Effect of molecular weight of polymeric additives on formation, permeation properties and hypochlorite treatment of asymmetric polyacrylonitrile membranes, Journal of membrane science, 243 (2004) 45-57.

[17] Y. Liu, M.C. Messmer, Surface structures and segregation of polystyrene/poly (methyl methacrylate) blends studied by sum-frequency (SF) spectroscopy, The Journal of Physical Chemistry B, 107 (2003) 9774-9779.

[18] L. Qian, H. Zhang, Controlled freezing and freeze drying: a versatile route for porous and micro-/nano-structured materials, Journal of Chemical Technology & Biotechnology, 86 (2011) 172-184.

[19] T. Tanaka, R. Nakatsuru, Y. Kagari, N. Saito, M. Okubo, Effect of molecular weight on the morphology of polystyrene/poly (methyl methacrylate) composite particles prepared by the solvent evaporation method, Langmuir, 24 (2008) 12267-12271.

[20] C.M. Burns, W.N. Kim, Solution blending of polystyrene and poly (methyl methacrylate), Polymer Engineering & Science, 28 (1988) 1362-1372.

[21] D. Borah, R. Senthamaraikannan, S. Rasappa, B. Kosmala, J.D. Holmes, M.A. Morris, Swift nanopattern formation of PS-b-PMMA and PS-b-PDMS block copolymer films using a microwave assisted technique, Acs Nano, 7 (2013) 6583-6596.

[22] N.R. Jadhav, V.L. Gaikwad, K.J. Nair, H.M. Kadam, Glass transition temperature: Basics and application in pharmaceutical sector, Asian Journal of Pharmaceutics (AJP): Free full text articles from Asian J Pharm, 3 (2014).

[23] M. Eriksson, H. Goossens, T. Peijs, Influence of drying procedure on glass transition temperature of PMMA based nanocomposites, Nanocomposites, 1 (2015) 36-45.

Chapter 7

Depth Profile Study of Poly(styrene) – Poly(methyl methacrylate) – Tetrahydrofuran Coatings

In the previous chapters, residual solvent studies, morphological studies, and thermal analysis of various multi-polymer solvent coatings have been reported. This chapter deals with the depth dependent concentration measurement of the polymers and solvent in the dried PS-PMMA-THF coating.

7.1 Introduction

In polymer-solvent solution, the diffusion plays an important role and its study is of key interest in the ongoing research. The study of the depth dependent concentration helps us to understand the processes like diffusion, corrosion, oxidation, ion implantation, and interface segregation [1]. The factors such as the penetrant, concentration, temperature, and nature of the polymer and solvent affects the dynamics of the diffusion as well as the overall drying behavior of the coatings [2]. The diffusion coefficient is known to decrease with decreasing solvent content by several orders of magnitude.

Earlier, the depth profiling of the coating was being studied with the help of Fourier transform infrared spectroscopy [3, 4], and this technique was limited upto few μm. Now-a-days, confocal Raman microscopy is gaining much interest since it analyzes the sample without any deformation of the sample. Confocal Raman microscopy is widely used to image, map, and analyze physical and chemical properties in three dimensions. Raman spectra can be obtained at different positions in the same sample by just placing the sample in an automated *x, y,* and *z* mapping stages. This helps in getting the full Raman spectra throughout the sample. Due to its very good spatial resolution in lateral as well as optical axis of the microscope, confocal Raman spectroscopy helps in various applications. A few applications are the study of thin layers that are buried in a matrix of another material, and multilayer

foils or fiber composite materials. This also helps in the study of properties of the material as a function of depth within the material of the film. Confocal Raman spectroscopy is efficient in depth profiling of laminates, coatings, membranes, and composites [5].

Everall [6] derived the expression for predicting the spatial depth, shape, and position of the Raman response along the *z*-axis of poly(ethylene terephtalate) coated with UV cured acrylate-based coating. He concluded that the depth of focus changed with the point of focus, and, hence, linearly increased with the depth. This indicated that the least the breadth of an interface, the deeper the interface was buried in the sample. In another communication [7], he discussed about the depth resolution problem due to the mismatch of the refractive index of the air and coating. Due to the mismatch the actual depth penetration would be more than the set depth, and the depth resolution can be calculated by following equation:

$$\text{Depth of Resolution} = d\left[\sqrt{\left(\frac{NA^2(\beta^2-1)}{(1-NA^2)}+\beta^2\right)}-\beta\right] \tag{7.1}$$

where d is depth of focus within the sample from surface of the sample, NA is numerical aperture of the objective used. β is defined as:

$$\beta = \frac{\text{Refractive index of the sample}}{\text{Refractive index of medium between sample and lens}} \tag{7.2}$$

Siebel et al. [2] measured the concentration-dependent diffusion coefficients directly from the spectroscopic data of single film drying experiments. They studied the poly(vinyl acetate)-methanol and poly(vinyl acetate)-toluene systems. They calculated the diffusion coefficients by means of the Fick's law from the quantitative data of concentration profiles measured from the inverse micro Raman spectroscopy. The results are independent of the boundary conditions in the gas phase. They observed that the diffusion coefficient varied at high solvent mass fractions (> 0.3), and showed significant drop at low solvent mass fractions (< 0.1). The calculated

diffusion coefficients showed good agreement with the literature data from the gravimetric sorption experiments.

Arya et al. [8] measured the concentration profiles of dried binary coatings of the poly(methyl methacrylate)-ethylbenzene and poly(styrene)-*p*-xylene systems using confocal Raman spectroscopy. They also demonstrated that the profiles are sigmoid in shape in the case of binary polymer-solvent system as they went through the glass transition. The coatings had high concentration of polymer near the top and low concentration near the substrate.

Arya [9] also studied the concentration profiles of the wet polymeric coatings of poly(styrene)-tetrahydrofuran, poly(methyl methacrylate)-tetrahydrofuran, and poly(styrene)-*p*-xylene systems. The concentrations profiles were measured using confocal Raman spectroscopy. He regressed the free volume theory parameters from the measured concentration data. He concluded that the predicted concentration profiles from the model were in good agreement with the measured profiles in the case of a highly volatile solvent, that is in poly(styrene)-tetrahydrofuran and poly(methyl methacrylate)-tetrahydrofuran systems. However, the free volume model was not able to predict the entire measured profiles in the case of less volatile solvent in poly(styrene)-*p*-xylene system.

Arya and Vinjamur [10] measured the concentration profiles in two ternary polymer-solvent using confocal Raman spectroscopy in poly(styrene)-tetrahydrofuran-*p*-xylene and poly(methyl methacrylate)-ethylbenzene-tetrahydrofuran systems. They correlated their experimental mass loss data of the ternary system with the predicted models. The models that had cross term diffusion coefficients [11] were in more agreement as compared to the models that do not have cross term diffusion coefficients. They also concluded that for both the systems, the models were conservative as they predicted a high concentration of the less volatile solvent, and, thus, predicted a higher value of the residual solvent.

Recently, Siebel et al. [12] studied the drying of quaternary coatings of poly(vinyl acetate)-toluene-methanol-dichloromethane. Their results showed that the initial coating composition affected the drying behavior and the thickness was more in the case of equal loading as compared that for the varying solvent loading. They

measured the concentration with respect to depth using confocal Raman spectroscopy. They also developed a diffusion model to predict the drying behavior in the quaternary system, and validated it using the depth profile data.

Confocal Raman spectroscopy has been used to measure the concentration profiles in dried and wet coatings of rubbery [2, 9, 10, 12-15] as well as glassy nature [8]. In the present work confocal Raman spectroscopy is used to measure the concentration profiles in the dried coating of multi-polymer solvent system in order to check the distribution of polymers during the course of drying.

7.2 Materials and Methods

7.2.1 Experimental procedures

Gravimetric study

Poly(styrene) having density 1.05 g cm^{-3} and molecular weight 192000 (Sigma Aldrich, Germany), tetrahydrofuran (Spectrochem, India) having density 0.8892 g cm^{-3}, and molecular weight 72.11, poly(methyl methacrylate (Sigma Aldrich, Germany) having density 1.18 g cm^{-3}, and molecular weight 120000. Single thin coatings were prepared using solution casting technique. A measured amount of solution was transferred using micropipette into stainless steel circular sample holder having the depth of 2000 μm and diameter of 12.24 mm. The mass of film was recorded as a function of time by means of Precisa analytical weighing balance having the accuracy of ± 0.0001 g. The mass loss data was recorded till no further appreciable change was observed in two consecutive readings for sufficiently long time (i.e, 20 min). The drying graphs are given in Section 2.3 of Chapter 2.

Depth profile study

Figure 7.1 shows the schematic of the confocal Raman spectroscopy [9, 14]. The laser beam is focused through the objective lens on a point within the sample at z plane marked as red. In addition, a pinhole diaphragm is located at the focal length of the objective to make a confocal arrangement. The solid lined z plane represents the

depth at which the laser is focused, while the dashed lined planes represent the out of focus planes. The beams that are reflected from the focal plane travel through the pinhole aperture, and are collected by the detector. The confocal arrangement cuts of the signals from the out of focal planes, and provides the Raman signals purely from the point of focus.

The focal plane can be moved up and down manually or with the help of z motor with a resolution of 1 μm. The Raman spectrometer was supplied by Jobin Yvon Horiba (Horiba Pvt Ltd., Bangalore India, model: HR 800UV, excitation wavelength 514.5 nm Argon gas). The base of the coating was located by looking at the picture of the substrate by adjusting the position of platform up and down. The Raman spectra of substrate must be noisy to make sure that the actual focus of the laser beam is on the substrate. The platform is further moved up by 1μm to recheck the spectra if its shows any Raman signal which confirms that the previous position was at substrate and the laser is focused within the sample. The platform was further lowered by 10 micron to move further up into the coating, and this was continued till no Raman signal was observed, which confirmed that laser is focused out of the film. In this study, 20X dry lens was used which has a numerical aperture of 0.4. The depth of resolution was calculated using Eq. (7.1). As needed in the calculations, the refractive index of poly(styrene), poly(methyl methacrylate) and tetrahydrofuran are 1.46, 1.497 and 1.407, and that of the air is 1.0003. The amount of poly(styrene), PMMA and THF left after drying are 0.0053 g, 0.0063 g and 0.0065 g, respectively, in Chapter 2. The average refractive index of the dried coating comes out to be 1.303. Based on this, the calculated β value is 1.3026. The calculated depth resolution at 10 microns from top using Eq 7.1 comes out to be 0.5 microns. Table 7.1 shows the depth of focus and depth of resolution data of the PS-PMMA-THF system. In this work, the platform is moved from bottom to top. Therefore, depth of resolution will not play any role in the measurements.

Table 7.1: Variation of depth of resolution with depth of focus.

Depth from top, microns	Depth of resolution, µm	Upper limit of depth, µm
0	0	0
10	0.5	11
20	1	21
30	1.5	32
40	2	42
50	2.5	53
60	3	63
70	3.5	74
80	4	84
90	4.5	95
100	5	105
110	5.5	116
120	6	126
130	6.5	137

DSC Study

The T_g of the prepared coatings were analysed by DSC 131 evo, Setaram, France, at the heating and cooling rates of 20 K/min, in nitrogen environment. For DSC analysis, ~30 mg of the sample was taken in a 120 µL aluminium pan. All the samples were pretreated for 10 min at 25 ^{o}C inside the chamber, before proceeding for the analysis.

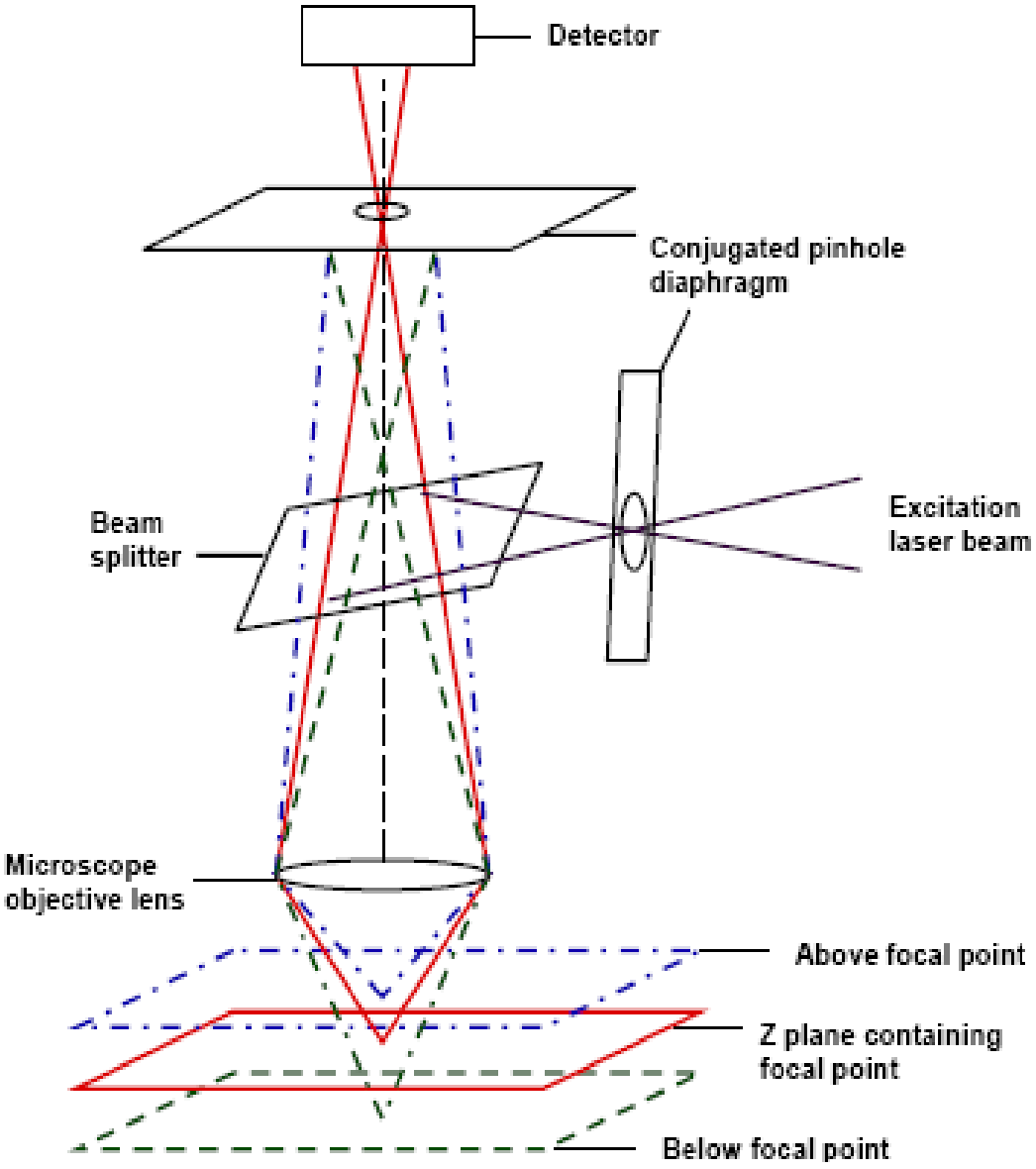

Figure 7.1: Schematic representation of the confocal Raman spectrometer

7.2.2 Calibration curves

The quantification of the Raman intensities into the concentrations by means of calibration curves is carried out. Several samples of binary poly(styrene)-tetrahydrofuran and poly(methyl methacrylate)- tetrahydrofuran were prepared in varying composition in sealed quartz vials as per the guidelines available in the literature [14, 16]. Sufficient time was given to equilibrate these vials, and the spectra were taken at several positions to check the homogeneity of the solution by checking the constant ratios of Raman intensities. The Raman spectra of pure PS, PMMA, and THF are given in Chapter 1 as Figures 1.2, 1.3, and 1.5, respectively. There are several Raman peaks in each constituent, out of which, three distinguished peaks were selected for their identification and characterization. The peak intensities of their distinguished Raman peaks considered were 1002.15 cm^{-1}, 814.545 cm^{-1}, and 914.113 cm^{-1} for PS, PMMA, and THF, respectively.

Calibration plots of the ratios of intensities of the polymer to the solvent versus the ratio of mass fraction of the polymer to the solvent generated. Binary calibration plots were used to the calculate concentration of solvents and polymer in ternary systems. The binary calibrations are shown in Figures 7.2 and 7.3.

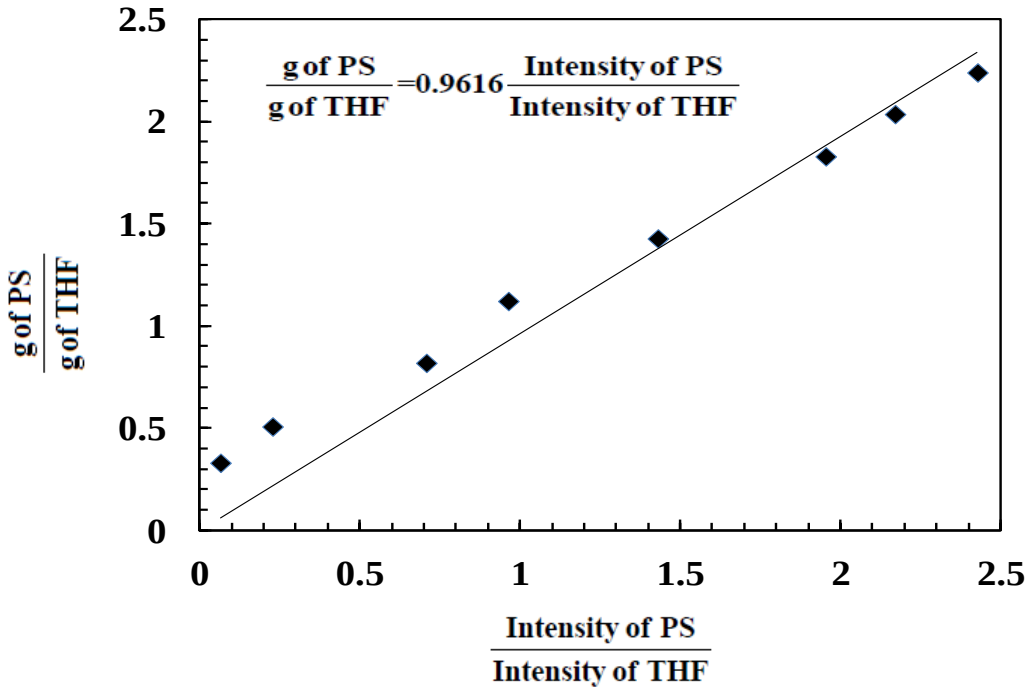

Figure 7.2: Calibration plot for poly(styrene)-tetrahydrofuran system

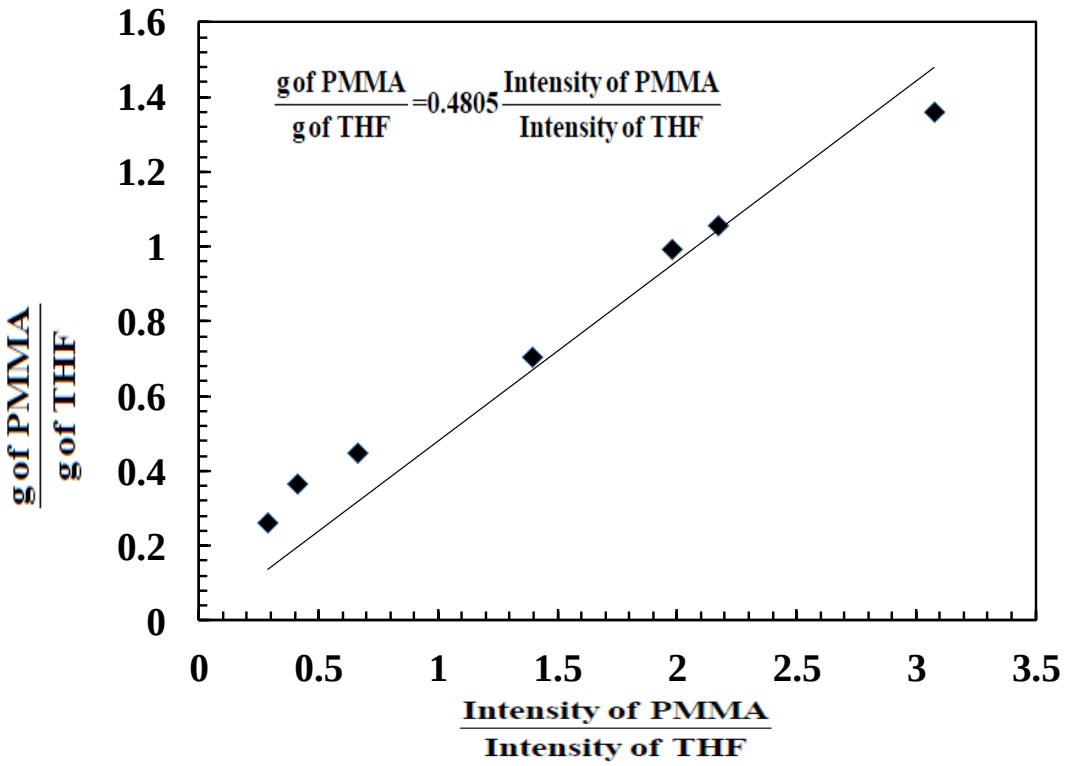

Figure 7.3: Calibration plot for poly(methyl methacrylate)-tetrahydrofuran system

The applicability of these binary calibration curves for multi-polymer solvent system was then checked by making several samples of different concentrations of PS-PMMA-THF in sealed vials. The Raman intensities in these samples were recorded, and are given in Table 7.2. Binary calibration plots give the relation between the ratio of intensity of polymer to intensity of solvent, and amount of polymer to amount of solvent. Regression coefficients of calibration curves in Figure 7.2 and 7.3 are 0.998 and 0.995, respectively. For illustration purposes, the calculation for row 1 is shown as follows:

Let the amount of THF be 1 g as common specie in both the system. The amount of PS and PMMA are then calculated using the binary relationships obtained for PS-THF and PMMA-THF systems in Figures 7.2 and 7.3, respectively. These relationships are as follows:

$$\frac{\text{g of PS}}{\text{g of THF}} = 0.9616 \times \frac{\text{Intensity of PS}}{\text{Intensity of THF}} \tag{7.3}$$

$$\frac{\text{g of PMMA}}{\text{g of THF}} = 0.4805 \times \frac{\text{Intensity of PMMA}}{\text{Intensity of THF}} \tag{7.4}$$

By substituting the values of THF weight and Raman intensities in the above equations, equations 7.3 and 7.4 are rewritten as:

$$\frac{\text{g of PS}}{1} = 0.9616 \times \frac{115.304}{930.79} \Rightarrow \text{PS} = 0.1191\text{g} \tag{7.5}$$

$$\frac{\text{g of PMMA}}{1} = 0.4805 \times \frac{450.22}{930.79} \Rightarrow \text{PMMA} = 0.2324\,\text{g} \tag{7.6}$$

The weight percentage of PS, PMMA and THF comes out to be 8.81, 17.19, and 73.99, respectively. Subsequently, these weight percentages are checked by the weight percentages of PS, PMMA, and THF in the prepared ternary vials. Table 7.2 shows good agreement between the actual and those calculated from the binary calibration plots for the PS-PMMA-THF system. This clearly indicates that the binary calibration plots can be used to calculate the concentration of the multi-polymer-solvent system. The concentration of PS, PMMA and THF were calculated and plotted as a function of positions.

Table 7.2: Comparison of the wt% of polymers and solvent calculated from binary calibration plots and those of the prepared ternary polymer-polymer-solvent system.

Sample number	Prepared ternary solution						Calculated from binary calibration (%)		
	PS (wt%)	PS intensity	PMMA (wt%)	PMMA intensity	THF (wt%)	THF, intensity	PS	PMMA	THF
1	8.42	115.304	16.54	450.22	75.02	930.79	8.81	17.19	73.99
2	16.23	120.711	8.5	126.233	75.27	520.64	16.59	8.68	74.72
3	11.15	134.36	5.43	130.711	83.04	938.85	11.46	5.72	82.81
4	10.59	160.6	10.24	290.83	79.16	937.46	10.44	11.61	77.94

7.3 Results and Discussion

Raman spectra were recorded at several positions in the dried coating of PS-PMMA-THF system. These species are then transformed into concentration as per the procedure provided in Section 7.2.2.

Figure 7.4 shows the depth profile of THF in the dried PS-PMMA-THF coating of initial thickness 935 microns that was dried without air flow for 1 h 56 min at 25 °C. The concentration of THF at the base is high, that is, 0.388 g cm^{-3}, which exponentially decreases to a value of 0.298 g cm^{-3} corresponding to 30 microns from base. Thereafter, a very less change is observed in the concentration until 30 microns from the surface. Again, there is a relatively fast decrease in the concentration until the surface comes, and the surface has the concentration of 0.197 g cm^{-3}. The mass percentages of THF at the surface and bottom are 19.73 and 38.66, respectively.

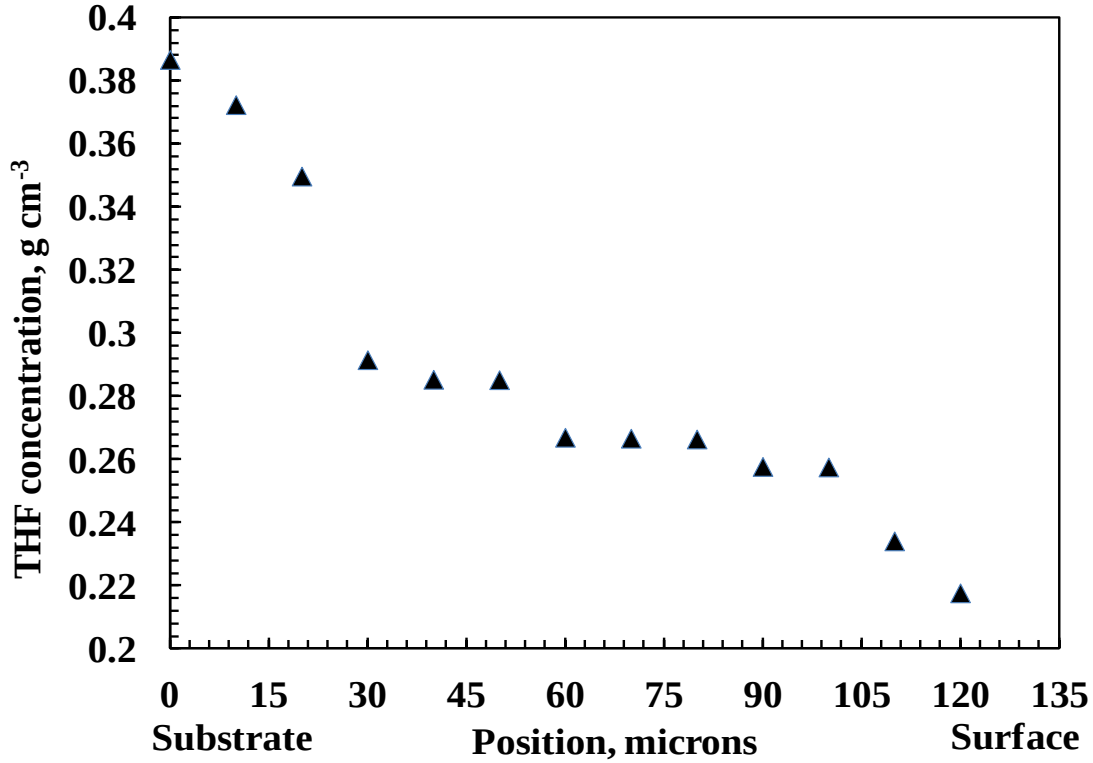

Figure 7.4: Tetrahydrofuran concentration profile in the PS-PMMA-THF system having initial percentages 5.2%, 6.25%, and 88.55%, respectively. Initial coating thickness was 935 microns. Drying temperature was 25 ° C.

Figure 7.5 shows the depth profile of PS in the dried PS-PMMA-THF coating. The concentration of PS at the bottom is low, that is, 0.360 g cm^{-3}, which increases to a value of 0.42 g cm^{-3} corresponding to 30 microns from base. Thereafter, a very less change is observed in the concentration until 30 microns from the surface. Again, there is a relatively fast decrease in the concentration until the surface comes, and the surface has the concentration of 0.502 g cm^{-3}.

Figure 7.6 shows the depth profile of PMMA in the dried PS-PMMA-THF coating. The concentration of PMMA at the bottom is low, that is, 0.255 g cm^{-3}, which increases to a value of 0.29 g cm^{-3} corresponding to 30 microns from base. Thereafter, a very less change is observed in the concentration until 30 microns from the surface. Again, there is a relatively fast decrease in the concentration until the surface comes, and the surface has the concentration of 0.336 g cm^{-3}.

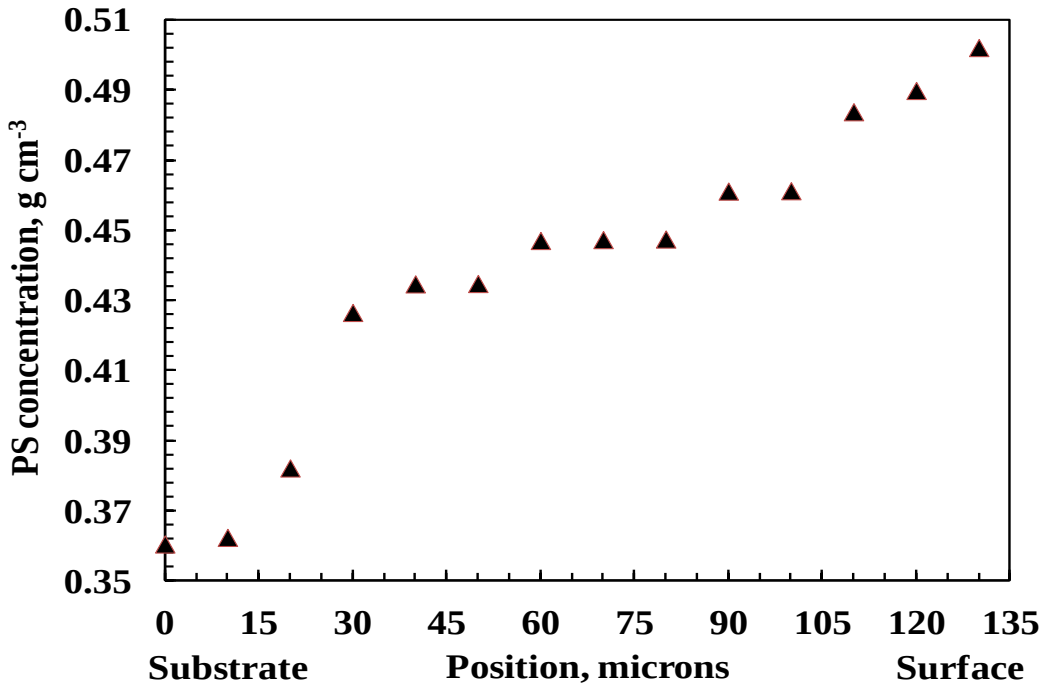

Figure 7.5: Poly(styrene) concentration profile in the PS-PMMA-THF system having initial percentages 5.2 %, 6.25%, and 88.55%, respectively. Initial coating thickness was 935 microns. Drying temperature was 25 °C.

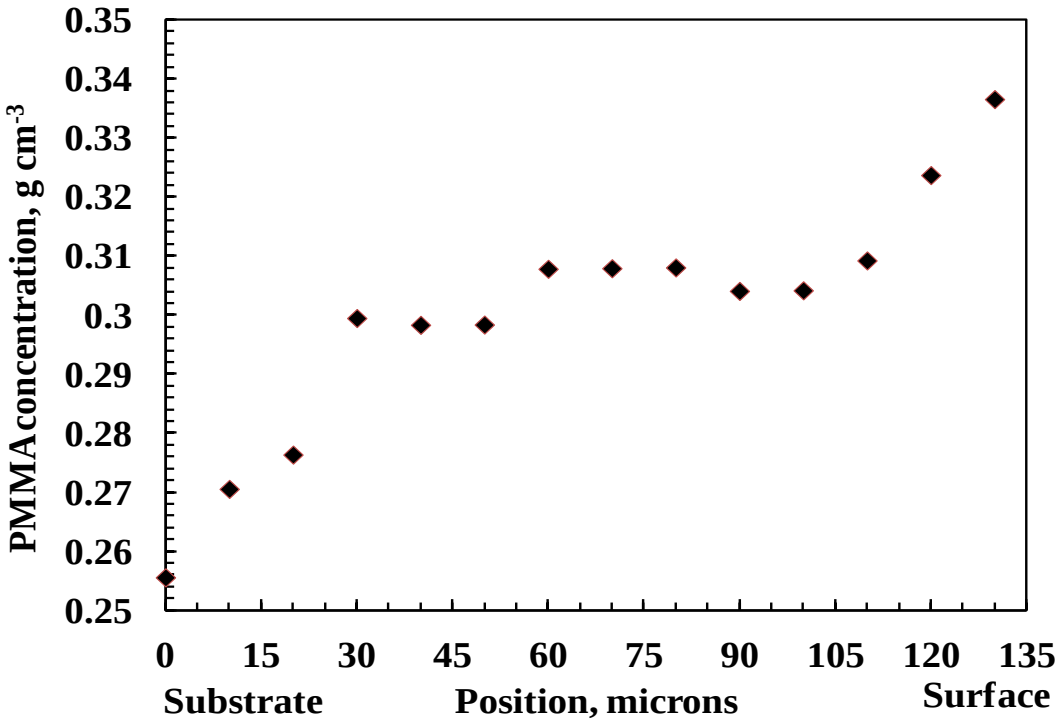

Figure 7.6: Poly(methyl methacrylate) concentration profile in the PS-PMMA-THF system having initial percentages 5.2 %, 6.25%, and 88.55%, respectively. Initial coating thickness was 935 microns. Drying temperature was 25 ° C.

The concentration of THF is decreasing from the substrate to surface of the coating. The mass fraction of THF at the surface and near the substrate is 0.19 and 0.39, respectively. The solvent mass fraction helps us to understand the glassy and rubbery region of the coating. The glass transition temperature of the coating depends on the solvent concentration in the polymer and is a strong function of the solvent concentration. The solvent reduces the glass transition temperature significantly [17]. The glass transition temperatures of PS and PMMA are ~100 °C and ~110 °C, respectively.

Chow [17] showed that the glass transition temperature of poly(styrene)–*p*-xylene system was depressed to about 85 °C at a concentration of 0.115 g cm^{-3}. Further, Verros [18] had found that the glass transition temperature of poly(methyl methacrylate)–toluene film was nearly equal to 23 °C at toluene mass fraction < 0.19. Arya et al. [8] also analyzed the glassy region of the coating at a solvent mass fraction much lower than 0.19. The glass transition temperature of PS-EB system at 0.1 mass fraction of EB was found to be 40 °C [19]. For PMMA-toluene system it was 25 ˚C at 0.12 mass fraction of toluene [20].

Figure 7.7 shows the thermographs of the dried PS-PMMA-THF coating. The glass transition temperature of the coating comes out to be 69˚C. The heating and cooling rate was 20K/min, and the purging gas was nitrogen. Figure 7.8 shows the mass fraction of polymers and solvent with position. The average mass fraction of the THF based on the gravimetric data is 0.36. These results show that at room temperature, this coating will be glassy at THF mass fraction 0.36 or less than it. However, the actual mass fraction of THF at the bottom is 0.39. However, since the coatings were dried at the room temperature that is considerably less than 69 ˚C, the entire coating would be glassy. As reported by earlier researcher for similar polymer the mass fraction for glassy region is in between of 0.12 to 0.19 for different solvent having slight differences in molecular weight. The molecular weights of EB, toluene and THF are 106.17 g/mol, 92.14 g/mol, and 72.61g/mol, respectively. The variation in glass transition temperature and mass fraction of solvent may also occur due to thermodynamic interaction of multi-polymer solvent system.

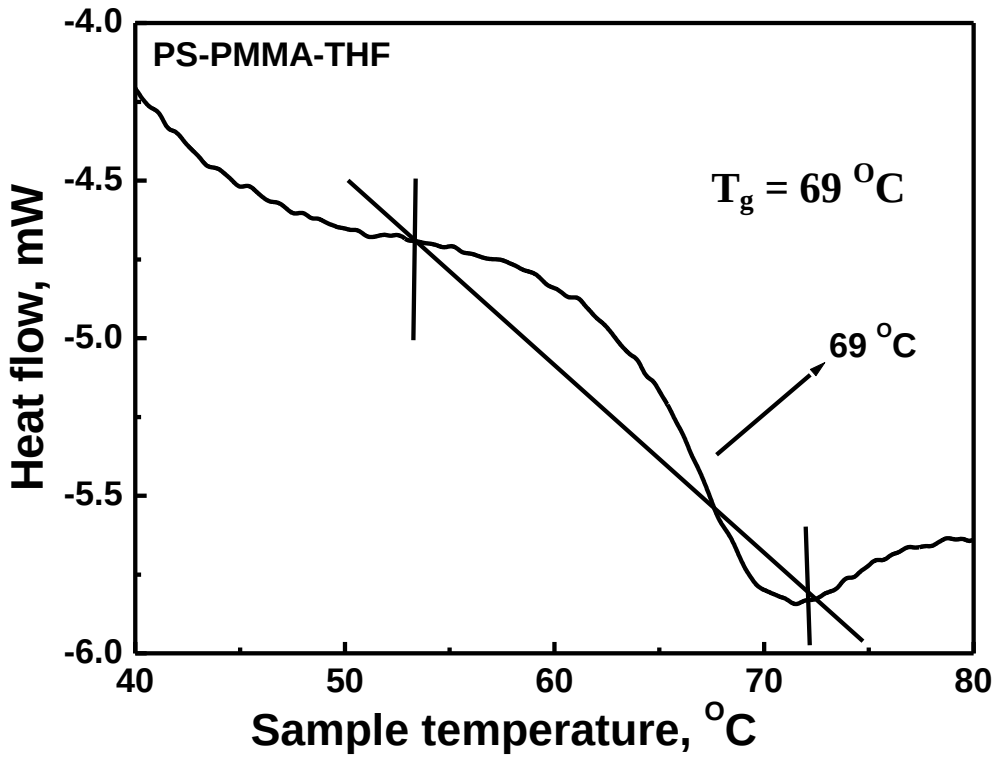

Figure 7.7: Heat flow as a function of sample temperature of PS-PMMA-THF coating.

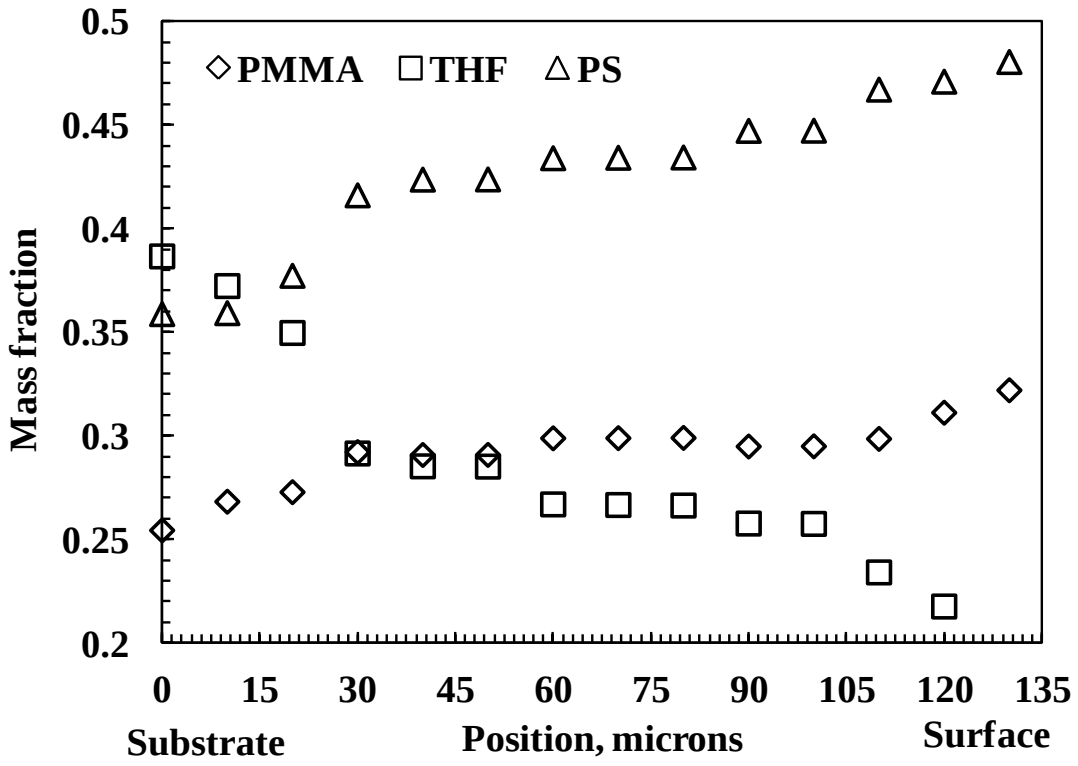

Figure 7.8: Mass fraction of coating constituents with position.

7.4 Conclusions

Binary calibration curves are successfully used to calculate the concentrations in ternary PS-PMMA-THF system with very good agreement. Confocal Raman spectroscopy has been successfully used to measure the depth profiles of the dried coating. The results showed that these dried coating will turn to glassy due to very low amount of solvent mass fraction. The measured profiles of poly(styrene) and poly(methyl methacrylate) in tetrahydrofuran exhibited an increase in concentration from the substrate to the surface.

References

[1] S. Hofmann, Evaluation of concentration-depth profiles by sputtering in SIMS and AES, Applied Physics, 9 (1976) 59-66.

[2] D. Siebel, P. Scharfer, W. Schabel, Determination of concentration-dependent diffusion coefficients in Polymer–Solvent systems: analysis of concentration profiles measured by raman spectroscopy during single drying experiments excluding boundary conditions and phase equilibrium, Macromolecules, 48 (2015) 8608-8614.

[3] R. Saure, V. Gnielinski, Moisture Measurement by FT-IR-Spectroscopy, Drying Technology, 12 (1994) 1427-1444.

[4] R. Saure, G. Wagner, E.-U. Schlünder, Drying of solvent-borne polymeric coatings: I. Modeling the drying process, Surface and Coatings Technology, 99 (1998) 253-256.

[5] K. Williams, G. Pitt, D. Batchelder, B. Kip, Confocal Raman microspectroscopy using a stigmatic spectrograph and CCD detector, Applied Spectroscopy, 48 (1994) 232-235.

[6] N.J. Everall, Modeling and measuring the effect of refraction on the depth resolution of confocal Raman microscopy, Applied Spectroscopy, 54 (2000) 773-782.

[7] N. Everall, Depth profiling with confocal Raman microscopy, Part I, Spectroscopy, 19 (2004) 22-33.

[8] R.K. Arya, K. Tewari, S. Shukla, Non-Fickian drying of binary polymeric coatings: Depth profiling study using confocal Raman spectroscopy, Progress in Organic Coatings, 95 (2016) 8-19.

[9] R.K. Arya, Measurement of concentration profiles in thin film binary polymer-solvent coatings using confocal Raman spectroscopy: Free volume model validation, Drying Technology, 32 (2014) 992-1002.

[10] R.K. Arya, M. Vinjamur, Measurement of concentration profiles using confocal Raman spectroscopy in multicomponent polymeric coatings—model validation, Journal of Applied Polymer Science, 128 (2013) 3906-3918.

[11] J.M. Zielinski, B.F. Hanley, Practical friction-based approach to modeling multicomponent diffusion, AIChE Journal, 45 (1999) 1-12.

[12] D. Siebel, W. Schabel, P. Scharfer, Diffusion in quaternary polymer solutions—Model development and validation, Progress in Organic Coatings, 110 (2017) 187-194.

[13] W. Schabel, P. Scharfer, M. Muller, I. Ludwig, M. Kind, Measurement and simulation of concentration profiles in the drying of binary polymer solutions, Chemie Ingenieur Technik, 75 (2003) 1336-1344.

[14] W. Schabel, I. Ludwig, M. Kind, Measurements of concentration profiles in polymeric solvent coatings by means of an inverse confocal micro Raman spectrometer—Initial results, Drying Technology, 22 (2004) 285-294.

[15] W. Schabel, P. Scharfer, M. Kind, Measurement and simulation of concentration profiles during drying of thin films with help of confocal-Micro-Raman spectroscopy, Chemie Ingenieur Technik, 75 (2003) 1105-1106.

[16] R.K. Arya, Calibration curves to measure concentrations in multicomponent polymeric coatings using confocal Raman spectroscopy, International Journal of Chemical Engineering and Applications, 2 (2011) 421-424.

[17] T. Chow, Molecular interpretation of the glass transition temperature of polymer-diluent systems, Macromolecules, 13 (1980) 362-364.

[18] G.D. Verros, Application of irreversible thermodynamics to the solvent diffusion in an amorphous glassy polymer: A comprehensive model for drying of toluene-poly (methyl methacrylate) coatings, The Canadian Journal of Chemical Engineering, 93 (2015) 2298-2306.

[19] G. Billovits, C. Durning, Linear viscoelastic diffusion in the poly (styrene)-ethylbenzene system: comparison between theory and experiment, Macromolecules, 27 (1994) 7630-7644.

[20] A. Dubreuil, F. Doumenc, B. Guerrier, C. Allain, Drying of polymer varnishes: Solvent diffusion in glassy polymer films, Heat Transfer, 3 (2002) 105-110.

Chapter 8

Conclusions and Future Work

Residual solvent study of PS-PMMA-THF, PS-PMMA-TOL, PS-PMMA-EB, and PS-PEG-CLB systems have been carried out. The results show that the amount of residual solvent left in the case of single thick layer is always lower than the coatings prepared using the layer-by-layer technique. The high amount of glassy polymer that is PS, results in more residual solvent. However, the high amount of amorphous polymer, that is, PEG, results in very long drying time, but has reasonably low residual solvent as compared to glassy polymers.

The effect of molecular weight on residual solvent has been studied. The results show that the equal percentage of nearly same molecular weight polymers results in low residual solvent. However, no exact trend was observed for very low as well as high molecular weight of polymers. The high molecular weight PMMA is resulting in more drying time as compared to PS, but is retaining less residual solvent. In case of PS-PEG-CLB system, the coatings were porous in nature in the case of layer-by-layer assembly with uniform pore distribution. The single thick layer was relatively dense as compared to the layer-by-layer coatings.

The glass transition temperatures of the prepared multi-polymer solvent coatings are higher as compared to their individual binary coatings. The glass transition temperatures of the prepared coatings are around 60 ˚C or higher. These coatings can be used in hot climate where surrounding temperature is reasonably high.

The confocal Raman spectroscopy has been used to measure the depth dependent concentration in dried PS-PMMA-THF coating. The depth profiles are Fickian in nature from the substrate to a reasonable thickness. However, the solvent profile is flat near the surface, but the polymer profiles are completely in exponential

form. The distribution of the polymers is not equal in the entire coating. The PS mass fraction is higher in the top layer as compared to PMMA.

These experimental studies will be useful in developing the mathematical diffusion model to predict the drying behavior of multi-polymer solvent coatings. The mathematical model will be helpful in the design of the coatings and industrial dryers to avoid the drying induced defects. The future work may include the thermal properties and morphological behavior of the PS-PMMA-THF, PS-PMMA-TOL, PS-PMMA-EB. The comparison of PS(192000)-PMMA(120000)-EB may also be studied for better understandings of effect of molecular weight on morphological, thermal behavior and residual solvent.